VOLUME 39 AUGUST 1961 NUMBER 8

Canadian Journal of Physics

Published by THE NATIONAL RESEARCH COUNCIL

OTTAWA CANADA

CANADIAN JOURNAL OF PHYSICS

Under the authority of the Chairman of the Committee of the Privy Council on Scientific and Industrial Research, the National Research Council issues THE CANADIAN JOURNAL OF PHYSICS and five other journals devoted to the publication, in English or French, of the results of original scientific research. Matters of general policy concerning these journals are the responsibility of a joint Editorial Board consisting of: members representing the National Research Council of Canada; the Editors of the Journals; and members representing the Royal Society of Canada and four other scientific societies.

EDITORIAL BOARD

Representatives of the National Research Council

I. McT. Cowan (Chairman), *University of British Columbia*
Léo Marion, *National Research Council*
H. G. Thode, *McMaster University*
D. L. Thomson, *McGill University*

Editors of the Journals

D. L. Bailey, *University of Toronto*
T. W. M. Cameron, *Macdonald College*
F. E. Chase, *Ontario Agricultural College*
H. E. Duckworth, *McMaster University*
Léo Marion, *National Research Council*
J. F. Morgan, *Department of National Health and Welfare, Ottawa*
J. A. F. Stevenson, *University of Western Ontario*

Representatives of the Societies

D. L. Bailey, *University of Toronto*
Royal Society of Canada
T. W. M. Cameron, *Macdonald College*
Royal Society of Canada
H. E. Duckworth, *McMaster University*
Royal Society of Canada
Canadian Association of Physicists
P. R. Gendron, *University of Ottawa*
Chemical Institute of Canada
D. J. Le Roy, *University of Toronto*
Royal Society of Canada
J. F. Morgan, *Department of National Health and Welfare, Ottawa*
Canadian Biochemical Society
R. G. E. Murray, *University of Western Ontario*
Canadian Society of Microbiologists
J. A. F. Stevenson, *University of Western Ontario*
Canadian Physiological Society

Ex officio

Léo Marion (Editor-in-Chief), *National Research Council*
J. B. Marshall (Administration and Awards), *National Research Council*

Manuscripts for publication should be submitted to Dr. H. E. Duckworth, Editor, Canadian Journal of Physics, Hamilton College, McMaster University, Hamilton, Ontario.
For instructions on preparation of copy, see **NOTES TO CONTRIBUTORS** (back cover).

Proof, correspondence concerning proof, and orders for reprints should be sent to the Manager, Editorial Office (Research Journals), Division of Administration and Awards, National Research Council, Ottawa 2, Canada.

Subscriptions, renewals, requests for single or back numbers, and all remittances should be sent to Division of Administration and Awards, National Research Council, Ottawa 2, Canada. Remittances should be made payable to the Receiver General of Canada, credit National Research Council.

The journals published, frequency of publication, and subscription prices are:

Canadian Journal of Biochemistry and Physiology	Monthly	$9.00 a year
Canadian Journal of Botany	Bimonthly	$6.00 a year
Canadian Journal of Chemistry	Monthly	$12.00 a year
Canadian Journal of Microbiology	Bimonthly	$6.00 a year
Canadian Journal of Physics	Monthly	$9.00 a year
Canadian Journal of Zoology	Bimonthly	$5.00 a year

The price of regular single numbers of all journals is $2.00.

Canadian Journal of Physics

Issued by THE NATIONAL RESEARCH COUNCIL OF CANADA

VOLUME 39 AUGUST 1961 NUMBER 8

PROTON SPIN–LATTICE RELAXATION IN POLYATOMIC GASES[1]

M. BLOOM, M. LIPSICAS,[2] AND B. H. MULLER[3]

ABSTRACT

The proton spin–lattice relaxation time T_1 has been measured in gaseous samples of methane, ethylene, and ethane as a function of pressure at room temperature and also at 193° K for methane. In the pure gases T_1 is proportional to density, ρ, at low densities indicating that *intra*molecular interactions couple the spin systems to the lattice, as is the case in hydrogen gas. T_1/ρ at low densities gives information on the mean square angle through which the molecules are rotated per collision. Relaxation due to paramagnetic O_2 is observed at higher densities when oxygen gas is added as an impurity. The relaxation probability per collision with an oxygen molecule is about 5 times larger for the ethylene–oxygen system than for the other two systems studied. This anomaly is discussed in terms of the theory of Oppenheim and Bloom. It is shown that a study of the temperature dependence of T_1 due to O_2 impurities provides a new way of obtaining detailed information on the Lennard–Jones parameters for the interaction between O_2 and the solvent molecules.

1. INTRODUCTION

It has been shown in an earlier paper (Lipsicas and Bloom 1961) that measurements of the proton spin–lattice relaxation time, T_1, in H_2 gas are capable of giving unique information about the anisotropic part of the H_2–H_2 interaction. This is so because, unlike monatomic spin systems such as He^3, the principal mechanism enabling the nuclear spin system in H_2 gas to exchange energy with the translational degrees of freedom of the gas, and hence establish thermal equilibrium at the temperature T of the gas, involves those intermolecular interactions which cause transitions between the rotational substates of the H_2 molecules. The experimental results reported here of T_1 in CH_4, C_2H_4, and C_2H_6 gases as functions of temperature and pressure demonstrate that the main spin–lattice relaxation mechanism in polyatomic gases is basically of the same sort as in H_2. Just as in H_2, there is an *intra*molecular dipole–dipole interaction between the magnetic moments of the protons on each molecule. Collisions between molecules cause molecular reorientation

[1]Manuscript received May 1, 1961.
Contribution from the Department of Physics, University of British Columbia, Vancouver, B.C. This research was supported by the National Research Council of Canada.
[2]Present address: Department of Physics, Rutgers University, New Brunswick, N.J.
[3]Department of Physics, University of Wyoming, Laramie, Wyoming. Work performed while holding National Science Foundation Faculty Fellowship on leave of absence from University of Wyoming.

and a consequent modulation of the *intra*molecular interaction. If the *intra*molecular interactions are all known, one can, in principle, relate T_1 to those anisotropic intermolecular interactions which produce transitions between the rotational substates of the molecules.

The mechanism for T_1 in polyatomic molecules mentioned above was first introduced to interpret T_1 in liquids (Bloembergen, Purcell, and Pound 1948). The time dependence of the *intra*molecular interactions was calculated in terms of a model of the molecule as a sphere undergoing a rotational random walk in a viscous medium and T_1 was related to the viscosity of the liquid. More rigorous treatments of the rotational random walk model have recently been carried out by Furry (1957) and Favro (1960) for spherical and non-spherical molecules respectively. Hubbard (1958) has incorporated some of these recent results in a careful treatment of the polyatomic spin system using Redfield's (1957) density matrix formulation of relaxation theory. Hubbard relates T_1 to the rotational diffusion coefficient D which appears in Furry's theory. The rotational random walk model is thus on a fairly firm theoretical foundation. It is difficult, however, within the scope of the model itself to answer questions regarding its validity for different classes of liquids. Also, even if it is valid, the relationship of D to intermolecular interactions is not at all obvious.

In the experiments reported here T_1 is studied in polyatomic gases both at low densities, where only two-body collisions are important, and as a function of density up to liquidlike densities. It may, therefore, be possible eventually to answer the questions formulated above by a detailed analysis of our results and further study of relaxation in gases. We make a start in this direction for the low density gases, where the mean time between successive steps in the rotational random walk is simply the mean time between collisions as calculated from the transport properties of the gas. We are able to show from our T_1 values that although the rotational random walk model may be applicable in CH_4 gas it is inapplicable to C_2H_4 or C_2H_6 gas, because our results can only be understood if each collision between pairs of these latter molecules causes a very large molecular reorientation.

Before proceeding to a detailed discussion of our results it will be useful to outline some of those basic differences between H_2 and the polyatomic molecules studied here which are important from the point of view of nuclear spin relaxation theory.

The *intra*molecular interactions which contribute to T_1 in H_2 are of two types, a dipole–dipole interaction between the magnetic moments of the two protons and a spin rotational interaction between the proton magnetic moments and the rotational magnetic moment of the molecule. The orders of magnitude of these two interactions are comparable with one another in H_2, each of them producing a magnetic field at each proton of order 30 gauss (Kellogg *et al.* 1939). Very few direct measurements of the *intra*molecular interactions have been made in polyatomic molecules, but it is expected that the spin rotational interaction will be much smaller than for H_2, and should produce negligible relaxation effects as compared with the dipole–dipole inter-

action. Some recent measurements on C_2H_2 (Anderson and Ramsey 1960), where the rotational contribution to the magnetic field at the protons is of the order of 1 gauss, seem to bear this out.

Hydrogen has two modifications, *ortho* and *para*, corresponding to total nuclear spins $I = 1$ and 0 respectively. Resonance is only observed due to the *ortho*-H_2 molecules. Only odd rotational states ($J = 1, 3, \ldots$) are allowed for *ortho*-H_2 molecules, and because of the small moment of inertia of the H_2 molecule, the excited rotational states ($J > 1$) are not sufficiently populated to produce appreciable T_1 contributions even at temperatures up to room temperature (Lipsicas and Bloom 1961; Needler and Opechowski 1961). Measurements of T_1 in H_2 may be related directly to mean lifetimes of the molecules in each of the three magnetic substates of the $J = 1$ state.

The differences between H_2 and the polyatomic molecules are illustrated by the case of CH_4, which has three modifications, two of which have non-vanishing nuclear spin. They are *meta* ($I = 2$), *ortho* ($I = 1$), and *para* ($I = 0$), which have statistical weights 5:9:2 respectively. Since the rotational states allowed for each modification are determined by symmetry considerations, and since transitions between different modifications are highly forbidden, one might expect, in general, to observe a relaxation curve described by the sum of two exponentials, one each from the *ortho* and *meta* molecules. In all the experimental results to be described, we always report, within experimental error, only a single exponential recovery of the magnetization towards equilibrium. This is explained by examination of the expressions for the relative populations (Q_2, Q_1) of the $I = 2$ and $I = 1$ modifications, respectively, at a temperature T (Maue 1937).

$$
\begin{aligned}
Q_2 &= 5\,[1+7\exp(-12a)+9\exp(-20a)+\ldots], \\
Q_1 &= 9\exp(-2a)+15\exp(-6a)+42\exp(-12a) \\
&\qquad +54\exp(-20a)+99\exp(-30a)+\ldots,
\end{aligned} \tag{1}
$$

where $a = \hbar^2/2I_0kT = 7.68/T$,

I_0 = moment of inertia of the CH_4 molecule.

Thus, the rotational states allowed for *meta*- and *ortho*-CH_4 are

meta: $J = 0, 3, 4, \ldots$,

ortho: $J = 1, 2, 3, 4, 5, \ldots$.

At room temperature the value of J which we obtain by equating the rotational energy of the J state, $J(J+1)\hbar^2/2I_0$, to kT is approximately $J = 6$. Thus, very high values of J are appreciably populated at the temperatures where our experiments have been done. Examination of (1) shows that the *ortho* and *meta* modifications share the same higher rotational states. Although there will be two time constants the difference between them will be small at high temperatures and difficult to resolve. As we shall discuss later, an additional reason for anticipating more than one exponential arises from Hubbard's (1958) analysis, but there, too, it turns out to be difficult to resolve the two exponentials experimentally.

Because the high rotational states are appreciably populated by the polyatomic gas molecules, they may be pictured as approximately classical molecules as far as their angular momentum properties are concerned. Thus, the rotational random walk model often used to describe molecular reorientation due to collisions with other molecules has some chance of success, since the molecules can, in principle, undergo very small reorientations.

2. EXPERIMENTAL METHODS

All the T_1 measurements were made using the pulse technique. The procedure used for most of the measurements here was a slight modification of the usual pulse technique, convenient for the measurement of long relaxation times. A succession or train of pulses was applied in a time short compared with T_1. This train ensured that the magnetization at the end of the train was close to zero. At a time t later a similar train of pulses was applied and the height $A(t)$ of the first echo due to this train was measured. T_1 was deduced from the usual relation

$$A(t) = A(\infty)[1-\exp(-t/T_1)] \tag{2}$$

where $A(\infty)$ is the value of $A(t)$ for $t \gg T_1$. Usually we waited a time $t \gtrsim 10T_1$ to obtain $A(\infty)$. In some experiments t was measured using a stop watch, while in others we used a system of decade counters.

For details of the electronics, high pressure system and low temperature system, the reader is referred to the paper by Lipsicas and Bloom (1961).

The samples of methane, ethane, and ethylene gas used here were Research Grade ($\gtrsim$99.6% pure) or Pure Grade ($\gtrsim$99% pure) obtained from Phillips Petroleum Co. The impurities listed by the supplier were other hydrocarbons whose influence on T_1 is negligible in these quantities.

In some of the experiments to be described later oxygen gas was added purposely as an impurity. This was done originally to ensure that the experimental results, especially in the low density region, really were characteristic of the pure gas and not affected by paramagnetic impurities. Later we found that the influence of paramagnetic impurities on T_1 was of interest for its own sake. The actual measurements of impurity concentration were done very crudely, however, and it is difficult to assign experimental errors to this important quantity. In practice we simply filled our high pressure bomb to a certain measured pressure of O_2. We then added the gas being studied to the highest available pressure, usually less than 100 atmospheres. The ratio of O_2 concentration to solvent concentration was then calculated from the measured pressures and the known compressibility factors for the gases. The pressure dependence of T_1 was measured by releasing small quantities of the mixture.

Only in the case of CH_4 did we obtain an independent estimate of the O_2 concentration. This was obtained by measuring T_1 in the liquid where the relationship between T_1 and O_2 concentration is accurately known (Sandhu, Lees, and Bloom 1960).

3. THEORY

T_1 may be expressed in terms of Fourier transforms of the correlation functions of those interactions which enable energy to be exchanged between the nuclear spin system and the other degrees of freedom (lattice) of the material in which the spins are located. As we have pointed out in the Introduction, the nuclear spin-molecular rotational interaction may be neglected for polyatomic molecules, so that only correlation functions associated with dipole–dipole interactions need be considered. Then, for a system of identical nuclei of spin I and gyromagnetic ratio γ, Bloembergen, Purcell, and Pound (1948) and Kubo and Tomita (1954) have derived the formula

$$\frac{1}{T_1} = \frac{3}{2}\gamma^4\hbar^2 I(I+1)[J_1(\omega_0)+J_2(2\omega_0)], \tag{3}$$

$$J_k(\omega) = \int_{-\infty}^{\infty} \langle F_k(t)F_k^*(t+\tau)\rangle \exp(i\omega\tau)d\tau, \qquad k = 1, 2, \tag{4}$$

$$F_1(t) = \sqrt{\frac{8}{15}} \sum_j Y_{21}(\theta_{ij}, \phi_{ij})/r_{ij}^3 , \tag{5a}$$

$$F_2(t) = \sqrt{\frac{32}{15}} \sum_j Y_{22}(\theta_{ij}, \phi_{ij})/r_{ij}^3 , \tag{5b}$$

where the external magnetic field $\mathbf{H}_0$ is oriented along the z-axis and the vector $\mathbf{r}_{ij}$ joining the ith and jth nuclei has polar and azimuthal angles θ_{ij} and ϕ_{ij} respectively. $Y_{21}(\theta,\phi)$ and $Y_{22}(\theta,\phi)$ are spherical harmonics. $\omega_0 = \gamma H_0$ is the Larmor frequency of the nuclei. The bracket $\langle\ \rangle$ indicates an average over the equilibrium ensemble for the lattice.

The sum over j includes all those nuclei on the same molecule as the ith nucleus as well as those on neighboring nuclei. Contributions to T_1 due to interactions between nuclear spins on different molecules are inversely proportional to density and hence negligible in low density gases. At liquidlike densities their contributions may be comparable to those of the *intra*molecular interactions. The evaluation of the intermolecular dipole–dipole terms in equation (3) in terms of molecular properties of dense gases or liquids has been discussed elsewhere (Bloembergen, Purcell, and Pound 1948; Torrey 1953; Oppenheim and Bloom 1959, 1961). Here, we shall only discuss *intra*molecular interactions so that the sum over j in (5) includes only other nuclear spins on a single molecule. In the following paragraphs we shall first consider the case of rigid molecules and then attempt to allow for the effect of internal degrees of freedom.

A. Rigid Molecules

Usually correlation functions in (4) may be approximated by

$$\langle F_k(t)F_k^*(t+\tau)\rangle = \langle F_k(t)F_k^*(t)\rangle e^{-\tau/\tau_c} \tag{6}$$

where τ_c, the correlation time, usually satisfies the inequality $\omega_0^2\tau_c^2 \ll 1$ for

gases and liquids. If this assumption and equation (6) are satisfied then T_1 for rigid molecules can be written down using equation (3) and the facts that r_{ij} is time independent and $\langle |Y_{lm}|^2 \rangle = 1/4\pi$

$$\frac{1}{T_1} = 2\gamma^4\hbar^2 I(I+1)\tau_c \sum_j r_{ij}^{-6}. \tag{7}$$

For a molecule containing N protons ($I = \frac{1}{2}$) equidistant from one another so that $r_{ij} = r_0$

$$T_1 = \frac{2}{3(N-1)} T_0 = \frac{2}{3(N-1)} \frac{r_0^6}{\gamma^4\hbar^2\tau_c}. \tag{8}$$

Hubbard (1958) has recalculated the relaxation of the nuclear spin magnetization for rigid molecules having three or four identical nuclei of spin $\frac{1}{2}$ equidistant from one another using Redfield's theory (1957) which takes into account off-diagonal terms in the density matrix for nuclear spins. He finds that the relaxation is governed by two exponentials in each case so that, strictly speaking, one cannot define a unique T_1. For the 4-spin case, CH_4, the z-component of magnetization $M(t)$ was found to have the following time dependence as it relaxed towards its equilibrium value M_0.

$$M_0 - M(t) = \{M_0 - M(0)\}\left\{\left(\frac{92-13(46)^{1/2}}{184}\right)\exp\left[-\frac{3}{40}(73+2(46)^{1/2})\frac{t}{T_0}\right] + \left(\frac{92+13(46)^{1/2}}{184}\right)\exp\left[-\frac{3}{40}(73-2(46)^{1/2})\frac{t}{T_0}\right]\right\}. \tag{9}$$

The coefficients of the two exponential terms are in the ratio 1/50. It is thus extremely difficult to separate the two exponentials experimentally. Our signal/noise was not sufficiently great to resolve two such terms and we always observed only a single time constant. If we assume that one measures a single time constant given by the time constant of the exponential with the larger coefficient, then

$$T_1 = 0.225\ T_0 \quad \text{for } CH_4.$$

This differs by less than 1% from $T_1 = \frac{2}{9}T_0$ obtained from equation (8), putting $N = 4$.

Similar arguments lead to $T_1 = 0.332\ T_0$ for a 3-spin system using Hubbard's theory while the usual (diagonal density matrix) theory gives $T_1 = \frac{1}{3}T_0$.

Hubbard (1958) has pointed out that if the off-diagonal terms in the density matrix are neglected, the result for T_1 depends on the representation used. Here we have found close agreement between his result and T_1 calculated assuming a diagonal density matrix in a representation in which I_z for each proton is diagonalized. Hubbard's calculation becomes complicated for a 4-spin system such as C_2H_4 where the protons are not equidistant; thus we shall take the above result as justification for relating T_1 to τ_c for C_2H_4, and also for more complicated polyatomic molecules, using equations (3)–(7).

For CH_4, where $r_0 = 1.78 \times 10^{-8}$ cm, we have

$$T_1\tau_c = 1.24\times10^{-11}\ \text{sec}^2\ (CH_4) \tag{10}$$

while for C_2H_4, where the known structure of the C_2H_4 molecule (American Institute of Physics Handbook 1957) gives 1.86 Å, 2.42 Å, and 3.05 Å for the interproton distances in equation (7)

$$T_1\tau_c = 3.85\times10^{-11}\ \text{sec}^2\ (C_2H_4). \tag{11}$$

In treating C_2H_6 as a rigid molecule, one overestimates T_1 by less than 10% by considering it as a composite of two identical 3-spin systems, since the protons on different methyl groups are comparatively far from each other. Then, one obtains

$$T_1\tau_c \cong 1.86\times10^{-11}\ \text{sec}^2\ (C_2H_6). \tag{12}$$

Thus, within the scope of the above theory, measurements of T_1 may be used to evaluate τ_c as defined by equation (6). Furry (1957) has shown that if the molecule is assumed to undergo a rotational random walk, then $\tau_c = 1/6D$, where D is the "rotational diffusion coefficient". In the model of a molecule behaving as a classical sphere of radius b in a medium of viscosity

$$\tau_c = \frac{4\pi\eta b^3}{3kT}. \tag{13}$$

It is not expected that equation (13) would be applicable to dilute gases, but it will be interesting to apply it to the dense gas. For the dilute gas, one can to a reasonable approximation define the mean time between collisions τ from the measured transport properties of the gas. For a hard-sphere gas (Hirschfelder 1954)

$$\frac{1}{\tau} = 4a^2\rho\left(\frac{\pi kT}{m}\right)^{1/2} \tag{14}$$

where a is the diameter of the molecule, m is the mass of the molecule, and ρ is the number of molecules per cm^3.

Since the anisotropic interactions which produce molecular reorientation are short range one can picture the orientation of a molecule as changing only as a result of collisions whose frequency is defined by the usual kinetic theory cross sections. One can then, quite precisely, define two opposite limiting cases.

Case 1. Weak Coupling Approximation

The mean square angle of rotation per collision $\langle\alpha^2\rangle$ is assumed small. Then, the theory of Furry (1957) would hold and with the additional assumption that τ is the mean time between successive rotations in the rotational random walk, one obtains

$$\frac{\tau}{\tau_c} = \langle\alpha^2\rangle \ll 1. \tag{15}$$

Thus, to test whether the rotational random walk theory holds, for the dilute gas one only has to examine the order of magnitude of τ/τ_c. If it does hold τ/τ_c gives a measure of $\langle\alpha^2\rangle$.

Case 2. Strong Coupling Approximation

Each collision leaves the molecule randomly oriented. In this case it is easily shown that $\tau = \tau_c$.

B. Non-rigid Molecules

In a non-rigid molecule such as C_2H_6, there is the possibility of each of the two CH_3 groups undergoing rotations about the C—C axis of the molecule in addition to the rotation of the molecule as a whole. The activation energy for CH_3 rotation in C_2H_6 is approximately 3000 cal/mole (Kemp and Pitzer 1937) so that at sufficiently high temperatures this rotation would be taking place to an appreciable degree even between collisions. There is also the possibility of collisions occurring which cause an appreciable reorientation of a CH_3 group but not of the molecule as a whole. A complete theory of T_1 in gases should, therefore, be formulated in terms of a complete description of the internal degrees of freedom of the molecules. Such a theory might follow the lines of the detailed treatment of the H_2 molecule by Needler and Opechowski (1961), for example.

In the absence of such a theory we can at least draw some conclusions about the limiting case that the motions associated with internal degrees of freedom are much faster than the reorientational motions of the molecule as a whole. If τ_{int} is a characteristic time associated with the internal motions, Muller (1954) has pointed out that for the case $\tau_{int} \ll \tau_c$, and also $\omega_0\tau_c \ll 1$, the Hamiltonian describing the intramolecular dipole–dipole interactions may be replaced by its average over the internal motions and T_1 calculated in the usual way using this new effective Hamiltonian. One always obtains a longer T_1 than for the rigid molecule. For rapid rotation of a CH_3 group around its symmetry axis, it is found that T_1 is multiplied by a factor 4 (Muller 1954) so that for ethane we find, using equation (12)

$$T_1\tau_c \cong 7.4\times10^{-11} \text{ sec}^2 \quad (C_2H_6 \text{ with rapid internal } CH_3 \text{ rotations}). \tag{16}$$

Relaxation by Paramagnetic Impurities

The presence of O_2 or other paramagnetic impurities often provides a potent mechanism for T_1, since the magnetic moments of paramagnetic atoms or molecules are about 1000 times as large as those of nuclei. In polyatomic gases at sufficiently low densities, however, the effect of a small amount of paramagnetic impurity should be negligible. The reason for this is that, for relaxation by paramagnetic impurities, T_1 should be inversely proportional to density, while for the pure gas $T_1 \propto 1/\tau_c \propto$ density.

For the gas, the contribution of a paramagnetic impurity to T_1 may be shown to be (Bloembergen *et al.* 1948; Oppenheim and Bloom 1961)

$$\frac{1}{T_1} = \frac{8\pi}{3}\frac{\gamma_n^2\langle\mu_p^2\rangle N_p}{a^2}\left[\frac{\pi(M_p+m)}{2kT}\right]^{1/2}\int_0^\infty F(y)dy \qquad \text{gas.} \tag{17}$$

The corresponding formula for the dense gas or liquid is

$$\frac{1}{T_1} = \frac{16\pi}{3} \frac{\gamma_n^2 \langle \mu_p^2 \rangle N_p}{(D_p + D_H)a} \int_0^\infty \frac{F(y)}{y} dy \qquad \text{liquid,} \tag{18}$$

where γ_n is the nuclear gyromagnetic ratio, $\langle \mu_p^2 \rangle$ is the mean square value of the magnetic moment operator for the paramagnetic molecule, N_p is the number of paramagnetic molecules per cm^3, M_p and m are the masses of the paramagnetic molecule and the hydrocarbon molecule respectively, D_p and D_H are the diffusion constants of the paramagnetic molecule and the hydrocarbon molecule respectively, and a is a characteristic length for the molecular interaction such as the Lennard–Jones parameter.

$$F(y) = \left[\int_0^\infty \frac{[g(x)]^{1/2} J_{5/2}(xy)}{x^{3/2}} dx \right]^2; \tag{19}$$

$g(x)$ is the radial distribution function of the paramagnetic molecule and hydrocarbon molecule system, where x is the separation of a pair of molecules expressed in units of the characteristic length a.

$$g(x) = \exp\left[-\frac{V(x)}{kT} \right] \tag{20}$$

where $V(x)$ is the potential energy of a pair of molecules separated by a distance xa. For a liquid or dense gas, $g(x)$ is more complicated (Oppenheilm and Bloom 1961).

Evaluation of the integral in equation (18) using a realistic intermolecular potential such as the Lennard–Jones potential must be done numerically. Results of such calculations are not yet available. We give here the result for $\int_0^\infty F(y)dy$ assuming a square well potential for the intermolecular potentia and using equation (20) for the radial distribution function of the dilute gas. For best agreement with the Lennard–Jones potential in fitting second virial coefficients of gases, the parameters of the square well are as follows (Hirschfelder *et al.* 1954):

$$\begin{aligned} V(x) &= \infty && x < 1 \\ V(x) &= V_0 = 0.56\epsilon && 1 < x < 1.8 \\ V(x) &= 0 && x > 1.8 \end{aligned} \tag{21}$$

where ϵ is the Lennard–Jones energy parameter.

For this case, equation (17) becomes

$$\frac{1}{T_1} = \frac{4}{3} \frac{\gamma_n^2 \langle \mu_p^2 \rangle N_p}{a^2} \left[\frac{\pi(M_p + m)}{2kT} \right]^{1/2} f\left(\frac{V_0}{kT} \right) \tag{22}$$

where

$$f(x) = e^x + 0.31(e^{x/2} - 1)^2 - 0.72\, e^{x/2}(e^{x/2} - 1); \tag{23}$$

$f(x)$ is plotted in Fig. 1.

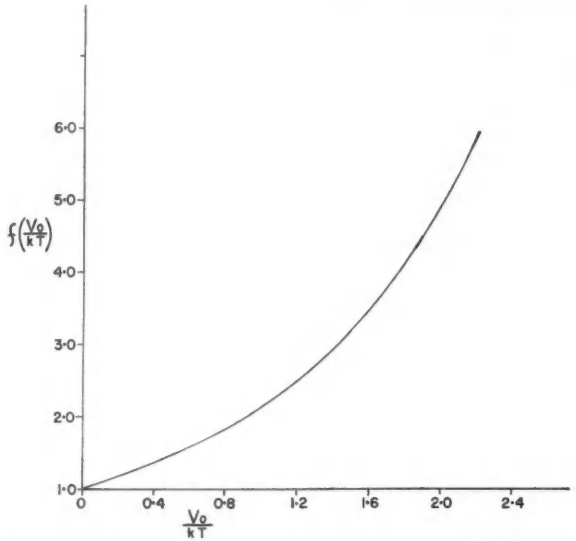

FIG. 1. Plot of $f(V_0/kT)$ versus V_0/kT. The function $f(V_0/kT)$ is defined by equation (23).

4. EXPERIMENTAL RESULTS AND DISCUSSION

Methane (CH_4) Gas

Measurements of T_1 in methane were made at two temperatures, 193° K and 293° K. The former temperature is only 2 Kelvin degrees above the critical temperature. The results for T_1 are shown in Figs. 2 and 4 as functions of density. Figure 3 shows the density as a function of pressure for the lower temperature to indicate the effect of three-body and higher-order collisions on the equation of state for the gas. The density measurements were made using the amplitudes of the nuclear magnetic resonance signal as described elsewhere (Lipsicas, Bloom, and Muller 1961).

The main qualitative features of our results may be summarized as follows:

(*a*) T_1 is proportional to the density ρ in the low density gas. This confirms the over-all picture we have presented earlier of the relaxation being due to *intra*molecular interactions which are modulated by those collisions between pairs of molecules which cause molecular reorientation.

(*b*) T_1/ρ for low density CH_4 gas is about 200 times as large as for H_2. This partially reflects the fact that $T_1\tau_c$, which is about 1.24×10^{-11} sec^2 for CH_4 according to equation (10), is about 35 times as large as the corresponding value for H_2 (Bloembergen *et al.* 1948). As has been discussed in the Introduction, however, τ_c has a somewhat different significance for the two cases.

(*c*) The addition of paramagnetic impurities in the form of O_2 gas does not influence the very low density results at all but does influence the higher density measurements. Thus, in the samples containing a relatively large amount of O_2, T_1 goes through a maximum value when plotted as a function of density. It is likely that, at the highest densities in the measurements at

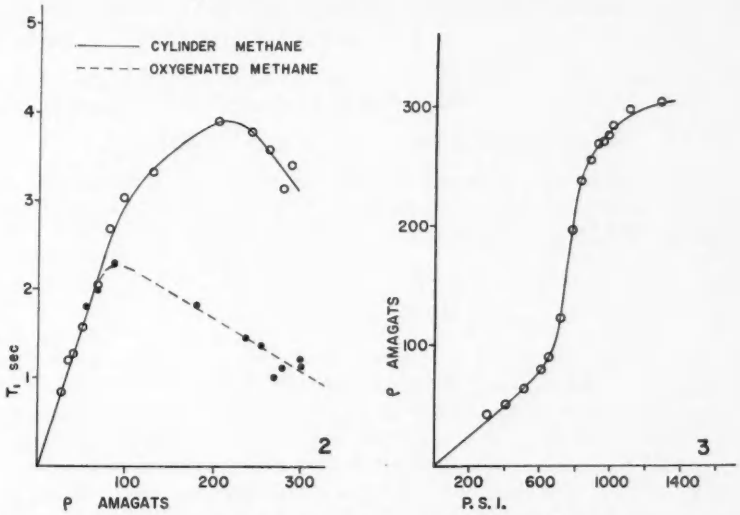

FIG. 2. Plot of T_1 versus density for CH_4 gas at 193° K; closed circles are measurements for samples containing 0.1% O_2.
FIG. 3. Plot of density versus pressure for CH_4 gas at 193° K.

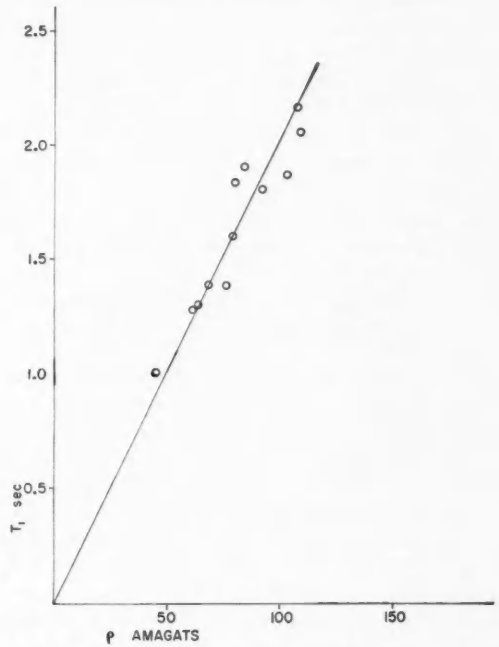

FIG. 4. Plot of T_1 versus density for CH_4 gas at 293° K.

193° K, paramagnetic impurities are playing a role even in our purest sample.

The slopes of the straight lines drawn through the low density T_1 values in Figs. 2 and 4 give:

$$\begin{aligned} T_1/\rho &= 3\times10^{-2}\ \text{sec/Amagat}, \qquad T = 193°\ \text{K}, \\ T_1/\rho &= 2.05\times10^{-2}\ \text{sec/Amagat}, \qquad T = 293°\ \text{K}. \end{aligned} \tag{24}$$

Using equation (10) to obtain τ_c from the results of equation (24) and evaluating τ from equation (14) using $a = 3.8\times10^{-8}$ cm, the Lennard–Jones parameter for CH_4 (Hirschfelder *et al.* 1954), we obtain

$$\begin{aligned} \tau/\tau_c &= 0.27, \qquad T = 193°\ \text{K}, \\ \tau/\tau_c &= 0.15, \qquad T = 293°\ \text{K}. \end{aligned} \tag{25}$$

Thus the inequality (15) is not really satisfied, especially at the lower temperature, and it is not clear whether one can interpret the values of τ/τ_c in equations (25) as giving the mean square angle of rotation per collision $\langle\alpha^2\rangle$. However, the fact that τ/τ_c at 193° K is approximately twice as large as τ/τ_c at 293° K is consistent with what one would anticipate under the approximation $\langle\alpha^2\rangle \ll 1$. For this case, the angle of rotation of a molecule due to a collision with another having relative velocity V is proportional to $1/V$. Thus $\langle\alpha^2\rangle \propto \langle(1/V)^2\rangle \propto T^{-1}$; (293/193) is equal to 1.52 as compared with $\langle\alpha^2\rangle_{193°\,K}/\langle\alpha^2\rangle_{293°\,K} \approx 1.8$. It would be interesting, therefore, to generalize Furry's random walk treatment of the molecular rotations to include the case $\langle\alpha^2\rangle$ not necessarily much smaller than unity. As we shall see below, the C_2H_4 and C_2H_6 gases most certainly do not satisfy the condition $\langle\alpha^2\rangle \ll 1$.

Measurements of rotational dispersion by means of ultrasonic absorption experiments (Kelly 1957) indicate that "the number of collisions required to excite the rotational mode in methane lies between 14 and 17". The fact that fewer collisions are required to reorient the CH_4 molecules according to our measurements indicates, as one might expect from energy conservation, that collisions which reorient the molecules without causing a change in the J quantum number are (about 2 times) more frequent at room temperature than collisions which cause a change in J.

Turning now to relaxation of CH_4 by O_2 impurities, the results for a sample containing 0.1% O_2 impurity are given in Fig. 2. As mentioned earlier, the amount of O_2 was determined by measuring T_1 in the liquid where the relationship between T_1 and N_p is known experimentally (Sandhu, Lees, and Bloom 1960). At the higher densities where the impurity relaxation predominates, $T_1\rho$ is approximately constant and equal to 350 Amagat-sec. Since there are 0.1% O_2 molecules this gives $T_1N_p = 0.35$ Amagat-sec for O_2 in CH_4 gas.

The theoretical value for T_1N_p may be found by evaluating equation (22). In fact, if $\langle\mu_p^2\rangle$ was known accurately, this experiment could be used to evaluate the parameters a, V_0 associated with the O_2–CH_4 intermolecular interaction. If one takes $\langle\mu_p^2\rangle = \gamma(O_2)^2\hbar^2S(S+1) = 0.67\times10^{-39}$ e.m.u. (American Institute of Physics Handbook 1957) and using $\gamma_n = 2.67\times10^4$, $T = 193°$ K, $T_1N_p = 0.35$ Amagat-sec and the known masses of O_2 and CH_4 molecules, equation (22) gives

$$\frac{f(V_0/kT)}{a(\text{Å})^2} = 0.24. \tag{26}$$

The Lennard–Jones force constants for O_2 and CH_4 from second virial coefficients are (Hirschfelder *et al.* 1954)

$$\epsilon/k = 148.2° \text{ K}, \quad a = 3.817 \text{ Å}, \quad CH_4,$$

$$\epsilon/k = 118° \text{ K}, \quad a = 3.46 \text{ Å}, \quad O_2.$$

We approximate the force constants of the O_2–CH_4 interaction using the *empirical combining laws.*

$$\epsilon_{12} = (\epsilon_1\epsilon_2)^{1/2}, \quad a_{12} = \tfrac{1}{2}(a_1+a_2), \tag{27}$$

which gives

$$\epsilon/k = 132° \text{ K}, \quad a = 3.64 \text{ Å}, \quad CH_4\text{–}O_2. \tag{28}$$

Using equations (21) and (28) we get $V_0/kT = 0.38$ at 193° K corresponding to $f(x) = 1.29$. Thus, we estimate

$$\frac{f(V_0/kT)}{a(\text{Å})^2} = \frac{1.29}{(3.64)^2} = 0.098 \tag{29}$$

in good agreement with the result obtained from T_1 measurements and given in equation (26) considering the crudeness of the square well model and the use of the *empirical combining laws.*

It will be interesting to see whether the agreement is improved after the integration in equation (17) has been carried out using a more realistic potential. Also of interest will be a comparison of the theory with T_1 measurements carried out over a wide range of temperature.

Ethylene (C_2H_4) Gas

Measurements of T_1 in ethylene gas at 293° K are shown in Fig. 5 for the purest sample available and for a sample with 0.35% O_2 added. The main features of the results are that T_1 is again proportional to density in the low density region with a slope about 10 times greater than for CH_4, and that oxygen seems to be much more effective in shortening T_1 than for CH_4 gas.

From the linear region in the T_1 versus ρ curve for the pure gas we obtain

$$T_1/\rho = 0.25 \text{ sec/Amagat}, \quad T = 293° \text{ K}. \tag{30}$$

We follow the same procedure as used to interpret the methane results, using equation (11) to obtain τ_c from the T_1 measurements and equation (14) to obtain τ. In equation (14) we take the hard-sphere diameter of the C_2H_4 molecules to be 4.2 Å. We then obtain

$$\frac{\tau}{\tau_c} = 0.66, \tag{31}$$

which indicates that the molecules are rotated through large angles in each collision.

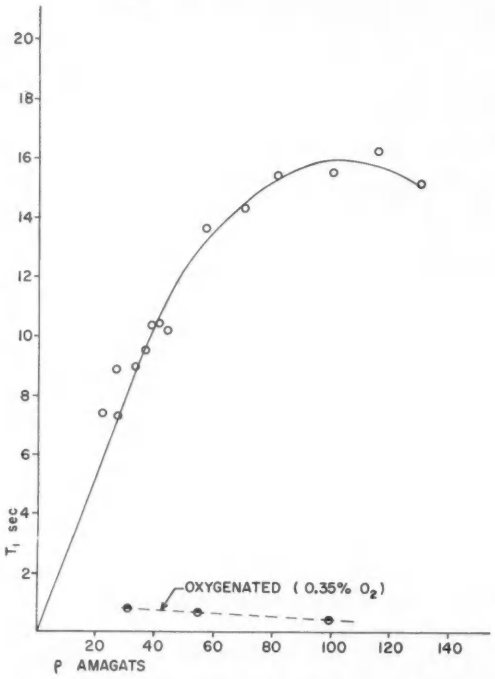

FIG. 5. Plot of T_1 versus density for C_2H_4 gas at 293° K.

When $1/T_1$ is plotted against ρ for the sample containing 0.35% O_2 it gives a straight line with $\rho T_1 = 27$ Amagat-sec. Thus $T_1 N_p = 0.096$ Amagat-sec, which is about 1/4 the value obtained for methane at 193° K. Following the same procedure described in detail in the discussion of methane, we obtain

$$\frac{f(V_0/kT)}{a(\text{Å})^2} = 0.96. \tag{32}$$

If we use the *empirical combining laws* (27) to evaluate the constants for the C_2H_4–O_2 interaction, we obtain from the Lennard–Jones parameters for C_2H_4 (Hirschfelder *et al.* 1954)

$$\begin{aligned} \epsilon/k &= 199° \text{ K}, \qquad a = 4.52 \text{ Å}, \qquad C_2H_4, \\ \epsilon/k &= 153° \text{ K}, \qquad a = 3.99 \text{ Å}, \qquad C_2H_4\text{–}O_2. \end{aligned} \tag{33}$$

This corresponds to $V_0/kT = 0.29$ for $T = 293°$ K and hence, using Fig. 1,

$$\frac{f(V_0/kT)}{a(\text{Å})^2} = \frac{1.22}{(3.99)^2} = 0.08, \tag{34}$$

which is a factor 12 smaller than that given by the interpretation of T_1 in equation (32).

A bold conjecture at this point is to attribute a good part of the factor of 12 difference between (32) and (34) to a drastic breakdown of the *empirical combining laws* given by equation (27) for the case of the C_2H_4–O_2 interaction because C_2H_4 is an unsaturated hydrocarbon.

It may be that the discrepancy by a factor of approximately 2.5 between the f/a^2 values obtained for the CH_4–O_2 interaction from T_1 measurements (26) and the use of the *empirical combining laws* in equations (27), (28), and (29) can be attributed to a systematic error arising from the use of an unrealistic square well potential. Even if that is the case, we are still left with a factor of approximately 5 in f/a^2 to be explained for the C_2H_4–O_2 interaction.

If the range of the interaction given by $a = 3.99$ Å in (33) is assumed to be approximately correct, the factor of 5 mentioned above would indicate that the correct V_0 for the CH_4–O_2 interaction is given by the solution to

$$f(V_0/kT) = 6, \tag{35}$$

which corresponds to $V_0/kT = 2.2$ and hence,

$$V_0/k = 644° \text{ K}, \qquad \epsilon/k = 1150° \text{ K}. \tag{36}$$

On the other hand there is reason to believe, because of the planar structure of C_2H_4, that many collisions between C_2H_4 and O_2 molecules involve a distance of closest approach considerably smaller than the value of a given in equation (33). This would be consistent with the anomalous results obtained.

It does not seem worth while to analyze our results further at this time for several reasons, some of which have been previously discussed. (1) The temperature dependence of $\int_0^\infty F(y)dy$ in equation (17) has not been carried out for a realistic potential. (2) In the derivation of equation (17), the intermolecular potential was assumed to be isotropic (Oppenheim and Bloom 1961) and this is certainly not the case for C_2H_4. (3) $\langle \mu_p^2 \rangle$ may be temperature dependent. (4) The result would indicate a strong temperature dependence for T_1N_p in C_2H_4 with oxygen impurities and no experimental study of this has yet been made.

Ethane (C_2H_6) Gas

The results of T_1 measurements in ethane gas as a function of density at 314° K are shown in Fig. 6. Again, T_1 is proportional to density in the low density region and

$$T_1/\rho = 0.23 \text{ sec/Amagat}. \tag{37}$$

The rigid molecule model (equation 12), taking the hard-sphere diameter of the C_2H_6 molecule as 3.95 Å, leads to

$$\frac{\tau}{\tau_c} = 1.42. \tag{38}$$

On the basis of a model of C_2H_6 having many rotations of the CH_3 groups between collisions, equation (16) gives

$$\frac{\tau}{\tau_c} = 0.35. \tag{39}$$

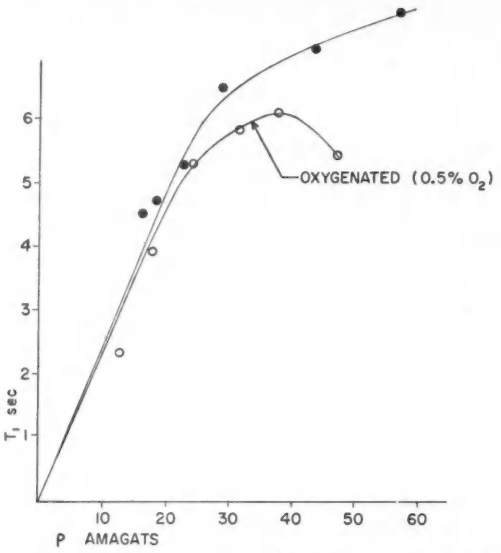

FIG. 6. Plot of T_1 versus density for C_2H_6 gas at 314° K.

It is impossible to make precise statements about whether equation (39) is valid without further experiments, since we may be dealing with the case in which a fraction of the CH_3 groups are rotating between collisions. However, equation (38) would indicate that at least some internal motion is present, since we must always have $\tau_c \gg \tau$.

The influence of O_2 impurities on T_1 seem to be of the same order of magnitude as for CH_4, as indicated by the results for a sample containing 0.5% O_2 shown in Fig. 6.

ACKNOWLEDGMENTS

We wish to thank Dr. R. F. Grant, Dr. J. A. R. Coope, and Dr. R. F. Snyder for some helpful discussions.

REFERENCES

AMERICAN INSTITUTE OF PHYSICS HANDBOOK. 1957. (McGraw-Hill), Tables 5h-28, 7j-15
ANDERSON, C. H. AND RAMSEY, N. F. 1960. Bull. Am. Phys. Soc. **5**, 344.
BLOEMBERGEN, N., PURCELL, E. M., and POUND, R. V. 1948. Phys. Rev. **73**, 679.
FAVRO, L. DALE. 1960. Phys. Rev. **119**, 53.
FURRY, W. H. 1957. Phys. Rev. **107**, 7.
HIRSCHFELDER, J. O., CURTISS, C. F., and BIRD, R. B. 1954. Molecular theory of gases and liquids (Wiley).
HUBBARD, P. S. 1958. Phys. Rev. **109**, 1153. See also Phys. Rev. **111**, 1746 (1958).
KELLOGG, J. M. B., RABI, I. I., RAMSEY, N. F., JR., and ZACHARIAS, J. R. 1939. Phys. Rev. **56**, 728.
KELLY, B. T. 1957. J. Acoust. Soc. Am. **29**, 1055.
KEMP, J. D. and PITZER, K. S. 1937. J. Am. Chem. Soc. **59**, 276.
KUBO, R. and TOMITA, K. 1954. J. Phys. Soc. Japan, **9**, 888.
LIPSICAS, M. and BLOOM, M. 1961. Can. J. Phys. **39**, 881.

LIPSICAS, M., BLOOM, M., and MULLER, B. 1961. J. Chem. Phys. **34**, 1813.
MAUE, A. 1937. Ann. Physik, **30**, 555.
MULLER, B. H. 1954. Ph.D. Thesis. University of Illinois.
NEEDLER, G. T. and OPECHOWSKI, W. 1961. Can. J. Phys. **39**, 870.
OPPENHEIM, I. and BLOOM, M. 1959. Can. J. Phys. **37**, 1324.
——— 1961. Can. J. Phys. **39**, 845.
SANDHU, H. S., LEES, J., and BLOOM, M. 1960. Can. J. Chem. **38**, 493.
TORREY, H. C. 1953. Phys. Rev. **92**, 962.

NOTE ADDED IN PROOF

Since this paper was written, molecular beam experiments on CH_4 have been performed which indicate that our assumption that the spin rotational interaction in methane is negligible as compared with the dipole–dipole interaction may not be justified. This point is discussed by C. S. Johnson, Jr., and J. S. Waugh in a paper closely related to the work reported here, to be published in the Journal of Chemical Physics. We wish to thank Professor Waugh for his interesting correspondence on this point.

OBSERVATION OF THE ($b^1\Sigma_g^+$–$a^1\Delta_g$) TRANSITION IN O_2[1]

J. F. Noxon[2]

ABSTRACT

The Q branch of the (0,0) band of the electric quadrupole ($b^1\Sigma_g^+$–$a^1\Delta_g$) transition in O_2 has been observed at 1.908 μ in the emission spectrum of a discharge through O_2 and He. By a comparison with the (0,0) atmospheric O_2 band ($b^1\Sigma_g^+$–$X^3\Sigma_g^-$), the absolute transition probability for the (b–a) system has been found to be 2.5×10^{-3} sec^{-1}, with an uncertainty of a factor of 2. The (0,0) band of the infrared atmospheric ($a^1\Delta_g$–$X^3\Sigma_g^-$) system of O_2 has also been observed in emission. Using the observed intensity of the (0,1) atmospheric O_2 band in the aurora and airglow one may predict that the (0,0) (b–a) band should be detectable in a strong aurora if observations are made from high altitude.

1. INTRODUCTION

The lowest excited electronic states of O_2 are $a^1\Delta_g$ and $b^1\Sigma_g^+$ (see Herzberg 1950, p. 446) which lie respectively 0.98 ev and 1.63 ev above the $X^3\Sigma_g^-$ ground state. Since transitions between any two of these three states are of the type g–g, they are forbidden by the selection rules for electric dipole radiation and both excited states are consequently metastable.

Spin–orbit interaction leads to a magnetic dipole character for the ($b^1\Sigma_g^+$–$X^3\Sigma_g^-$) and ($a^1\Delta_g$–$X^3\Sigma_g^-$) transitions (Van Vleck 1934), and they give rise to the so-called atmospheric and infrared atmospheric band systems of O_2; the (0,0) bands fall respectively at 7600 Å and 1.27 μ. These systems, as their names imply, appear in the absorption spectrum of the earth's atmosphere and have there been investigated in detail: the infrared atmospheric bands by Herzberg and Herzberg (1947) and the atmospheric bands by Babcock and Herzberg (1948), as well as earlier workers referred to in their paper. The atmospheric O_2 bands are present in the emission from both the aurora and the night airglow (see Chamberlain and Meinel 1954) and have been observed as well in laboratory sources (Kaplan 1947; Kvifte 1951, and references in the latter paper). Quite recently the first observation in emission of the infrared atmospheric system was made by Vallance Jones and Harrison (1958), who found the (0,1) band at 1.58 μ in the twilight airglow spectrum. Owing to reabsorption by O_2 at lower heights the strong (0,0) bands of both systems do not show up in the emission from the upper atmosphere.

The absolute transition probabilities for these two band systems have been determined by absorption studies. Childs and Mecke (1931) found the Einstein A coefficient for spontaneous radiation of the atmospheric bands to be 0.14 sec^{-1}, while Vallance Jones and Harrison (1958) have obtained an A coefficient of 1.9×10^{-4} sec^{-1} for the infrared atmospheric system. Both A coefficients

[1]Manuscript received May 4, 1961.
Contribution from the Physics Department, University of Saskatchewan, Saskatoon, Sask. The research reported in this paper has been sponsored by the Geophysics Research Directorate of the Air Force Cambridge Research Center, Air Research and Development Command, under contract AF 19(604)-7265.
[2]Present address: Pierce Hall, Harvard University, Cambridge, Mass.

refer to emission from $v' = 0$ in the upper electronic state. Since both of these systems correspond to a singlet–triplet intercombination and depend upon spin–orbit interaction, the transition probabilities are considerably lower than for ordinary magnetic dipole radiation for which the probability is around 10^2 or 10^3 sec^{-1} (Van Vleck 1934).

The remaining transition, between the two excited states, $b^1\Sigma_g^+$ and $a^1\Delta_g$, is forbidden as electric dipole by its g–g nature and is also forbidden as magnetic dipole since $\Delta\Lambda = 2$. It does not violate the selection rules for electric quadrupole radiation, however, and is therefore presumably quadrupole in nature. Bands of this system have not hitherto been observed; this is understandable for several reasons. The transition is evidently highly forbidden. The strongest bands all lie at long wavelengths near 2 μ, as will be shown. Finally, the transition does not involve the ground state of O_2 and therefore cannot be conveniently studied in absorption.

The transition probability for emission of the (b–a) system has been estimated by Seaton (1958) to be of the order of 1 sec^{-1}. This estimate, however, was largely conditioned by a requirement that the total probability for radiation from the $O_2(b^1\Sigma_g^+)$ state exceed the probability for emission of the atmospheric bands (b–X) alone, 0.14 sec^{-1}. The requirement arose from other considerations involving the deactivation of metastable oxygen atoms in the upper atmosphere. Seaton's argument has been criticized by Wallace and Chamberlain (1959), who suggested that the transition probability for (b–a) might well be smaller than 1 sec^{-1}.

There appears to be no observation of any other electronic transition in a diatomic molecule which is primarily quadrupole in nature, although such transitions are well known in atoms: for example, the green auroral line of atomic oxygen (see Herzberg 1944). On the other hand, many molecular electronic transitions are permitted both by magnetic dipole and electric quadrupole selection rules; the quadrupole contribution to such transitions is expected to be much weaker than the magnetic dipole contribution, however, and can be detected only by the appearance of weak satellite branches with $\Delta J = \pm 2$. The first observation of such quadrupole satellite branches has recently been reported by Wilkinson and Mulliken (1957), who studied the Lyman–Birge–Hopfield ($a^1\Pi_g$–$X^1\Sigma_g^+$) bands of N_2; they deduce the quadrupole contribution to the total LBH intensity to be about 0.15. In a pure electric quadrupole transition the branches with $\Delta J = \pm 2$ (S and O branches) are expected to be comparable in intensity with branches for which $\Delta J = \pm 1, 0$ (R, P, and Q branches).

It follows that an attempt to observe the (b–a) transition in O_2 is of interest, not only because of the nature of the transition but also because a simultaneous measurement of the intensity of the (b–a) and atmospheric (b–X) bands in emission will permit a determination of the absolute transition probability of the former. This paper reports work along these lines, using a laboratory discharge source, in which the (b–a) transition has been observed and studied, together with bands of both the atmospheric and infrared atmospheric systems of O_2.

EXPERIMENTAL

The discharge was quite similar to one used by Kvifte (1951) in order to study the atmospheric O_2 bands in emission. In order to achieve a high concentration of metastables the cylindrical pyrex discharge tube was of large dimensions, about 80 cm long and 8 cm in diameter, and was filled to about 150 mm Hg pressure with pure helium containing about 0.5% O_2. Aluminum electrodes were placed in side tubes at either end of the large tube and the discharge was operated by a 5000-volt sign transformer at about 60 ma. It was found that a higher oxygen concentration actually led to a reduction in the atmospheric O_2 band intensity, in agreement with the findings of Kvifte (private communication). With a prolonged operation of the discharge the atmospheric bands became weaker, presumably due to cleanup of the O_2. Some residual nitrogen in the helium was found to contaminate the near infrared spectrum with first positive bands. By admitting the oxygen first the nitrogen could be oxidized by applying a Tesla discharge to the helium filling line; the oxides formed were then frozen out in a liquid air trap on the way to the discharge tube.

Most of the observations were made using an infrared scanning spectrometer, equipped with a cooled lead sulphide detector, which had been designed for studies of the spectrum of the night airglow (Noxon, Harrison, and Vallance Jones 1959). With a Corning 7-56 filter to remove higher orders, the 1- to 2-μ region could be examined in the first order; by using a Corning 7-69 filter the 7000-Å to 1-μ range could be studied in the second order, without any other alterations. It was found desirable to use an instrument of greater sensitivity in the near infrared to study the atmospheric O_2 bands in more detail; for this purpose Dr. D. M. Hunten kindly made available his scanning spectrometer equipped with a DuMont K1292 photomultiplier as the detector. Preliminary studies to determine the emission spectrum of the discharge in the 3500-Å to 9000-Å range were made photographically.

In order to measure the relative intensities of the several emission features observed, two low brightness sources, originally designed for auroral and night sky work, were employed (see Harrison and Vallance Jones 1957). One low brightness source had been calibrated against a black body over the range 4000 Å to 1.2 μ while the second had been calibrated over the partially overlapping range 1.0 to 2.0 μ; at 1.2 μ the two sources were found to agree to better than 20%. Wavelengths were determined by using second-, third-, and fourth-order Hg lines.

OBSERVATIONS

A preliminary calculation of the expected positions of bands belonging to the (b–a) system of O_2 showed that the origins of the (0,0), (1,1), and (2,2) bands fall at 1.908 μ, 1.938 μ, and 1.969 μ respectively. Since the potential curves for the two electronic states lie directly above one another, the Franck–Condon principle predicts that bands with $\Delta v = 0$ should be considerably stronger than those with $\Delta v \neq 0$. Consequently, attention was directed to the 1.9-μ region, and the spectrum of the discharge was scanned from 1.85

to 1.95 μ at a spectral slit width of 70 Å. The scanning was carried out very slowly, with an output time constant of 30 seconds, in order to achieve the highest practical signal-to-noise ratio.

Figure 1 shows the resulting spectrum which was consistently found to

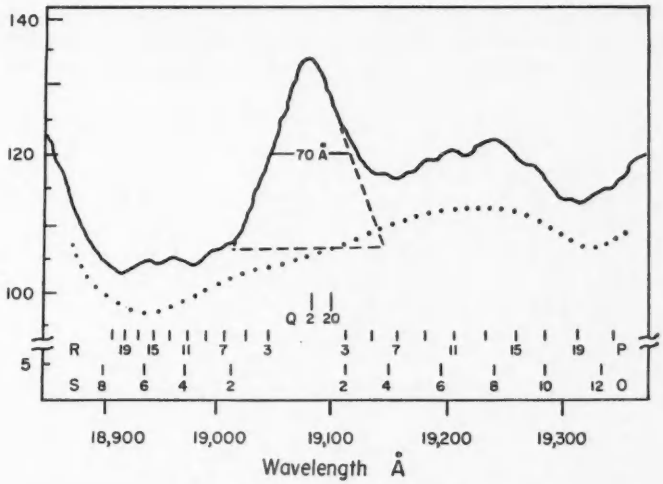

FIG. 1. Solid line: Observed emission spectrum of the discharge through 0.5% O_2 in helium at 150 mm total pressure, showing the peak at 1.908 μ. The spectral slit width was 70 Å.
Dotted line: Illustrating the appearance of the spectrum observed using pure helium at 150 mm pressure.
Dashed line: Assumed contribution of the Q branch of the (0,0) (b–a) O_2 band.
The predicted positions of the rotational lines of the (0,0) band between 1.89 and 1.93 μ are indicated. The numbering corresponds to the quantum number of the lower rotational level (J''). Note the great intensity of the background continuum.

contain the definite peak at 1.908 $\mu \pm 0.003$ μ. This will later be identified as the narrow and relatively intense Q branch of the (0,0) band of the (b–a) system. It will be observed that the peak is superposed upon a strong background. The scans showing the peak at 1.908 μ were all obtained with the O_2–He mixture at high pressure. When the discharge tube was filled to the same total pressure with pure helium the peak was absent, as indicated by the dotted line in Fig. 1; similarly, the peak was also absent in the He–O_2 spectrum when the total pressure was reduced to a few millimeters. The background emission, in particular the maxima near 1.925 μ and 1.935 μ, remained in all cases. It is presumably to be associated with helium.

The peak at 1.908 μ has the shape which would be expected from a narrow emission feature scanned with a spectral slit width of 70 Å, although the long wavelength side of the peak does not stand out in its entirety. In Fig. 1 the emission present only in the high pressure He–O_2 mixture is delineated by a dashed line; this was done by matching the spectrum of pure helium at high pressure with that of the He–O_2 mixture at 1.90 and 1.92 μ and subtracting

the first from the second. When the spectral slit width was reduced to 35 Å the 1.908-μ peak, although weak, appeared to have a width at half height of about 35 Å; the true width of the emission feature responsible can therefore scarcely exceed about 20 Å.

Under conditions where the 1.908-μ peak was strong, a scan in the second order revealed the very much more intense (0,0) band of the (b–X) atmospheric O_2 system, and the neighboring permitted atomic oxygen triplet at 7774 Å. Such a scan is shown in Fig. 2. The same physical slit width was used

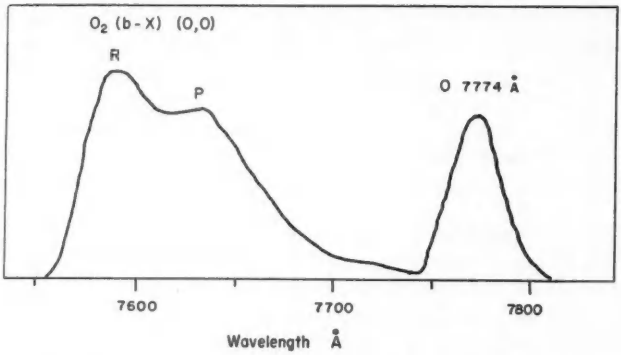

FIG. 2. Spectrum showing the (0,0) atmospheric O_2 band and the allowed atomic oxygen triplet at 7774 Å. 0.5% O_2 in helium at 150 mm total pressure. The spectral slit width was 35 Å.

as in Fig. 1, but the spectral slit width is naturally reduced by a factor of 2. While adequate for a determination of the total intensity of the band, the resolution is not sufficient to separate clearly the P and R branches of the (0,0) band. Both the atomic oxygen line and the atmospheric band were absent in the high pressure discharge through pure helium, as expected; in the low pressure He–O_2 mixture (0.5% O_2) the atomic line was very strong, but the atmospheric O_2 band was either weak or absent entirely. This is to be expected as well, since the band arises from a metastable state which will be effectively quenched by rapid diffusion to the wall at low pressure.

The total intensity of the 1.908-μ peak could be estimated to within about 30% by appropriate subtraction of the helium background, and so could be compared with the total intensity of the (0,0) atmospheric band. It was found that the intensity ratio of the two emissions remained constant to within $\pm$30% over a range of experimental conditions which gave rise to a factor-of-10 variation in the absolute intensity of both emissions. About 20 separate determinations of the ratio were made. The variation of absolute intensity was brought about by changes in total pressure, O_2 concentration, and discharge current. With the help of the calibrated low brightness sources the mean ratio, in photon units, of the intensity of the 1.908-μ peak to the

(0,0) atmospheric band was found to be 0.004; bearing in mind all possible errors involved, the uncertainty in this value is considered to be no more than a factor of 2 either way.

Attention was next directed to the 1.27-μ region in the hope of observing the (0,0) infrared atmospheric band in emission. A strong feature at this wavelength was observed and is shown as the solid line in Fig. 3. Some variation between the intensity of this feature and the (0,0) atmospheric band was

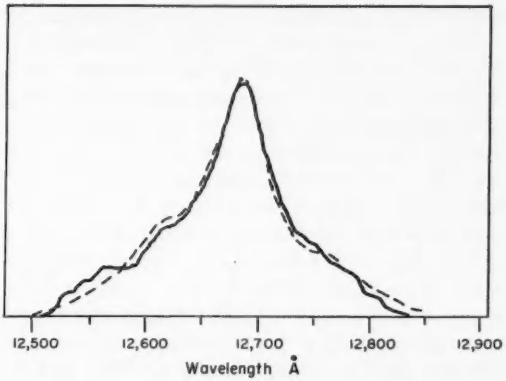

FIG. 3. Solid line: Observed emission at 1.27 μ using a 45-Å spectral slit width; the discharge conditions were similar to those in Figs. 1 and 2.
Dashed line: Synthetic profile of the (0,0) infrared atmospheric O_2 band constructed for 500° K and a 45-Å spectral slit width.

found, but the emission at 1.27 μ was absent both in pure helium at high pressure and in the He–O_2 mixture at low total pressure. The total intensity of the 1.27-μ emission was generally about 5% of the (0,0) atmospheric band.

Finally, the atmospheric O_2 bands were examined at higher resolution using the Hunten scanning spectrometer. With this instrument it was possible to work with a 2-Å spectral slit width and so to resolve the rotational structure in the P branch of the (0,0) atmospheric band. From the value of J' corresponding to the most intense rotational line a rotational temperature of 500° K $\pm$100° K was estimated; because of the long life of the $b^1\Sigma_g^+$ upper state, it is to be expected that this rotational temperature is a good measure of the kinetic temperature in the discharge.

A search was made for other bands belonging to the atmospheric O_2 system. This revealed only the (0,1) band at 8640 Å. From the absence of other bands with $v' > 0$ one may conclude that less than 1 or 2% of the $b^1\Sigma_g^+$ molecules were in $v' > 0$. Kvifte, on the other hand, did observe the (1,1) band in his laboratory discharge, and found it to be about 0.5% of the intensity of the (0,0) band; this indicates a concentration in $v' = 1$ of about 0.6%. These estimates involve the use of the vibrational transition probabilities calculated for the atmospheric bands by Fraser, Jarmain, and Nicholls (1954). In this

connection it may be noted that the present observations give an intensity ratio for the (0,1) to (0,0) band of 0.05 ± 0.01. This agrees well with the ratio of 0.047 predicted by the calculation of Fraser *et al.*, ignoring any possible variation in the electronic transition moment. It is somewhat larger than the value of 0.02 found by Kvifte in his laboratory study of the atmospheric bands.

Apart from the atmospheric O_2 bands, the features at 1.27 and 1.91 μ, which will be identified as the (0,0) band of the (a–X) and (b–a) systems of O_2, and a number of strong permitted atomic oxygen lines, the only other emissions due to oxygen noted between 3500 Å and 20,000 Å were several weak bands of the first negative system of O_2^+ in the 5000-Å to 6000-Å region. No trace appeared of the forbidden atomic oxygen lines at 5577 Å and 6300 Å, nor were any bands observed belonging to the forbidden Herzberg system of O_2. As noted earlier, there is a strong quasi-continuum present at long wavelengths; this became noticeable at about 1.2 μ and appeared to be characteristic of a discharge through helium. Spectroscopic traces of N_2 in the helium were evident by virtue of weak first positive band emission in the visible and near infrared.

DISCUSSION

The ($b^1\Sigma_g^+$–$a^1\Delta_g$) System of O_2

Figure 4 illustrates the rotational levels in the $b^1\Sigma_g^+$ and $a^1\Delta_g$ states and shows the transitions to be expected; because of the apparently quadrupole

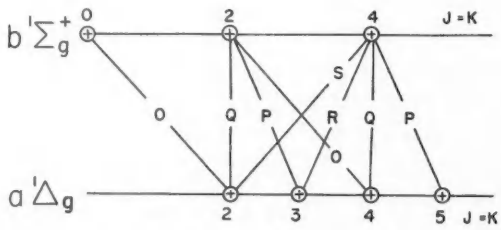

FIG. 4. Rotational levels of the $b^1\Sigma_g^+$ and $a^1\Delta_g$ states of O_2, showing transitions for $\Delta J = 0, \pm 1, \pm 2$.

nature of the electronic transition one may expect the O and S branches, with $\Delta J = \pm 2$, to be comparable in intensity with the P, Q, and R branches. The wavelengths of the rotational lines in the (0,0) band were calculated from the constants for the two electronic states given by Herzberg (1950); for a temperature of 500° K most of the intensity will come from rotational lines with $J' < 20$. Figure 1 shows the predicted positions of a number of the rotational lines expected; the numbering is by J'' in the lower state.The calculation shows that lines in the Q branch with $J' < 20$ all lie between 19,084 and 19,103 Å, a spread of less than 20 Å. Hence, with the resolution employed in the present work, the Q branch will be indistinguishable from a very narrow atomic line; this is a consequence of the nearly identical values for B_0 in the

two electronic states. A second consequence is that the P and R branches lie more or less symmetrically on either side of the Q branch, as do the S and O branches; the spacing of the rotational lines changes very slowly with increasing J. As a result, the lines of the R branch up to $J' = 20$ extend over about 120 Å, those in the P branch over about 200 Å, and those in the S and O branches over about 300 Å and 400 Å respectively. Finally, Fig. 1 shows that within a 70-Å range of 1.908 μ there fall, at shorter wavelengths, only the first two R lines, and, at longer wavelengths, only the first two P and the first O lines. Consequently, the Q branch should not be blended to any extent at a spectral slit width of 70 Å or less.

The appearance of the peak at 1.908 μ, together with the constant ratio of intensity to the (0,0) atmospheric band, makes it highly probable that the feature is in fact the Q branch of the (0,0) band of the (b–a) system. Because the other four branches are broad and unresolvable in the present work, no identification of them can be made in the presence of the strong helium background emission. A spectral slit width of 20 Å might resolve the stronger O branch lines near 1.93 μ; a resolution at least 3 or 4 times greater will be required to untangle the P, R, and S lines. An identification of S or O lines having an intensity comparable with lines of the P, Q, and R branches would be of great interest, and should definitely confirm the electric quadrupole nature of the (b–a) transition. Intensity considerations appear to place such a high resolution beyond the capability of the present spectrometer and discharge.

Since other branches, as well as the helium background, are present in the region on either side of the Q branch, it is clear that a subtraction technique can only approximate the true intensity of the Q branch. This is not expected to yield more than a 30% error, and this has been included in the estimated error of a factor of 2 associated with the ratio of the Q branch to the (0,0) atmospheric band. It will be recalled that this ratio was found to be about 0.004. In order to estimate the absolute transition probability for the (0,0) band of the (b–a) system the assumption is made that the Q branch represents one fifth of the total band intensity. This is approximate, for no attempt has been made to calculate individual line intensities. Recalling that the Einstein A coefficient for the (0,0) atmospheric band is 0.14 sec^{-1}, one finds that the A coefficient for the (0,0) band in the (b–a) system is about 2.5×10^{-3} sec^{-1}, with an uncertainty of a factor of 2.

This probability is far lower than the value of 0.88 sec^{-1} assumed by Seaton (1958), but it is not an unreasonable value for electric quadrupole radiation near 2.0 μ. According to Van Vleck (1934), pure quadrupole emission at about 7500 Å has a transition probability of about 0.1 sec^{-1} (to within a factor of 10 either way). Since the expression for the quadrupole transition probability contains a λ^{-5} term, a factor of 100 reduction is expected for quadrupole radiation near 2.0 μ. The predicted probability is thus of the order of magnitude 10^{-3} sec^{-1}, not too dissimilar to the experimental value found here. Finally, because transitions with $\Delta v \neq 0$ are expected to be of low probability, a negligible error is introduced in equating the A coefficient for the (0,0) band to that for all radiation out of $v' = 0$.

The (0,0) Infrared Atmospheric O_2 Band in Emission

The feature at 1.27 μ shown in Fig. 3, falls at the correct wavelength to be identified with the (0,0) band of the (a–X) infrared atmospheric system of O_2; this band has not previously been observed in emission. In order to confirm the identification, a synthetic profile of the (0,0) band was constructed for a temperature of 500° K, using the wavelengths given by Herzberg and Herzberg (1947) and the line strength factors given by Van Vleck (1934). A triangular slit function was employed to correspond with the 45-Å spectral slit width used in obtaining the spectrum in Fig. 3. Because of the long lifetime of the $a^1\Delta_g$ state, one expects the rotational levels to be in a Boltzmann distribution at about 500° K, similar to those in the $b^1\Sigma_g^+$ state. The resulting synthetic profile is shown in Fig. 3 as a dashed line and appears to agree well with the observed spectrum. This agreement confirms the identification of the 1.27-μ feature as the (0,0) band of the infrared atmospheric system of O_2. Knowing the A coefficients for both the (0,0) (a–X) and (b–X) bands, one may deduce from the relative intensity of the two bands that the concentration of $O_2(a^1\Delta_g)$ in the discharge was about 35 times that of $O_2(b^1\Sigma_g^+)$.

A very crude estimate of the absolute concentration of both metastable states may also be made, since the absolute sensitivity of the spectrometer is known. Assuming that the metastables fill the volume of the discharge uniformly, one finds that the equilibrium concentration of $a^1\Delta_g$ metastables was about 1% of the total amount of O_2 present, and the concentration of $b^1\Sigma_g^+$ about a factor of 35 smaller. The estimate is probably good to within a factor of 10.

Predicted Emission of (b–a) Bands in the Aurora and Night Airglow

The strong $\Delta v = 0$ bands of the (b–a) system all lie between 1.9 and 2.0 μ. In this region atmospheric absorption is complex and nearly complete, due to the presence of H_2O and CO_2 in the earth's atmosphere (Mohler *et al.* 1950). The possibility of observing (b–a) emission from the aurora or night airglow is therefore remote, so long as the observations are made from the ground. On the other hand, observations from a balloon or a high flying aircraft should be little affected by such absorption.

The intensity of (b–a) emission from upper atmospheric sources may be predicted on the basis of the intensity observed for the atmospheric bands, which arise from the same upper electronic state. All but a few per cent of the $O_2(b^1\Sigma_g^+)$ molecules which emit radiation in the aurora and airglow are observed to be in $v' = 0$ (Wallace and Chamberlain 1959). Most of the (b–a) emission should therefore be in the (0,0) band at 1.908 μ. The intensity to be expected must be predicted from the intensity observed for the (0,1) atmospheric band, for the (0,0) atmospheric band is completely reabsorbed by O_2 in the lower atmosphere. From the present work one may deduce that the (0,0) (b–a) band has an intensity equal to $0.02/0.05 = 0.4$ times that of the (0,1) atmospheric band, measured in photon units.

Chamberlain (1954) has shown that a sizeable fraction of the (0,1) intensity observed from the ground may arise from O_2 lying well below the emitting level, as a result of absorption of the (0,0) band and subsequent re-emission as the (0,1) band. But more recent discussion by Wallace and Chamberlain (1959) indicates that the effect is small, presumably because the O_2 at lower

altitude is collisionally deactivated before reradiating. Consequently it will be assumed that the intensity of the (0,1) band as observed from the ground is an accurate measure of the intensity of the band as originally emitted from the aurora or airglow.

The intensity of the (0,1) band in the airglow is observed to be about 1.5 kR (kilorayleigh) in the zenith direction (Dufay 1959) and the corresponding intensity of the (0,0) (b–a) band will be 0.6 kR. This is nearly 100 times smaller than the predicted intensity of the OH vibration–rotation bands in the night airglow at 1.9 μ (Chamberlain and Smith 1959). Consequently, (b–a) emission is not likely to be detected in the night airglow.

In the aurora, on the other hand, the (0,1) atmospheric band has been observed with an intensity as high as 500 kR (Hunten 1958). The corresponding intensity of the (0,0) band in the (b–a) system will be about 200 kR, which should be easily detectable above the OH background if observed near the zenith and from well above the earth's surface.

ACKNOWLEDGMENTS

This investigation was largely dependent upon the scanning spectrometer of high sensitivity designed by Dr. A. Vallance Jones for infrared studies of the aurora and airglow. I wish to thank both Dr. Jones and Dr. D. M. Hunten for making their spectrometers available and for their comments. Dr. Hunten was present during the period when the observations were being carried out, and so was able to offer many useful suggestions concerning the experimental work.

I am most grateful to Dr. G. Herzberg for correspondence concerning the quadrupole nature of the (b–a) transition and to Prof. G. Kvifte for information on his O_2–He discharge. I appreciate the contribution of Mr. E. A. Lytle in obtaining the high resolution spectra of the atmospheric oxygen bands.

REFERENCES

Babcock, H. D. and Herzberg, L. 1948. Astrophys. J. **108**, 167.
Chamberlain, J. W. 1954. Astrophys. J. **119**, 328.
Chamberlain, J. W. and Meinel, A. B. 1954. Earth as a planet (Univ. of Chicago Press), Chap. 11.
Chamberlain, J. W. and Smith, C. A. 1959. J. Geophys. Research, **64**, 611.
Childs, W. H. J. and Mecke, R. 1931. Z. Physik, **68**, 344.
Dufay, M. 1959. Ann. géophys. **15**, 134.
Fraser, P. A., Jarmain, W. R., and Nicholls, R. W. 1954. Astrophys. J. **119**, 286.
Harrison, A. W. and Vallance Jones, A. 1957. J. Atmospheric and Terrest. Phys. **11**, 192.
Herzberg, G. 1944. Atomic spectra and atomic structure (Dover Publications), p. 154ff.
——— 1950. Spectra of diatomic molecules (D. Van Nostrand).
Herzberg, G. and Herzberg, L. 1947. Astrophys. J. **105**, 353.
Hunten, D. M. 1953. Can. J. Phys. **31**, 681.
——— 1958. Ann. géophys. **14**, 167.
Kaplan, J. 1947. Nature, **159**, 673.
Kvifte, G. 1951. Nature, **168**, 741.
Mohler, O. C., Pierce, A. K., McMath, R. R., and Goldberg, L. 1950. Photometric atlas of the near infrared solar spectrum (Univ. of Michigan).
Noxon, J. F., Harrison, A. W., and Vallance Jones, A. 1959. J. Atmospheric and Terrest. Phys. **16**, 246.
Seaton, M. J. 1958. Astrophys. J. **127**, 67.
Vallance Jones, A. and Harrison, A. W. 1958. J. Atmospheric and Terrest. Phys. **13**, 45.
Van Vleck, J. H. 1934. Astrophys. J. **80**, 161.
Wallace, L. and Chamberlain, J. W. 1959. J. Planetary Space Sci. **2**, 60.
Wilkinson, P. G. and Mulliken, R. S. 1957. Astrophys. J. **126**, 10.

A BALLOON-BORNE SPECTROMETER FOR STUDY OF THE AIRGLOW BEYOND 2.0 μ[1]

J. F. Noxon and A. Vallance Jones

ABSTRACT

An account is given of the design, construction, and flight of a balloon-borne infrared spectrometer intended for the study of the night airglow spectrum in the 2.2- to 3.5-μ region. This region is not accessible from the ground because of the strong thermal emission from the lower atmosphere. The spectrometer employed a 64×64 mm plane diffraction grating and a liquid-oxygen-cooled PbS detector. The spectral slit width was 700 Å and the noise-equivalent differential brightness was about 2×10^{-8} watt. cm^{-2}. $sterad^{-1}$. $micron^{-1}$. The observations permitted an upper limit of about 700 kR (kilorayleighs) to be placed on the zenith brightness of the 1–0 OH band; this value is very close to that predicted by Chamberlain and Smith. No emission was observed between 2.3 and 2.7 μ. This establishes an upper limit on the zenith brightness of emission features in this region at 200 kR, for features narrow compared to the spectral slit width, and at about 3000 kR/micron for the differential brightness of any continuous emission. The general design of spectrometers for this wavelength region is considered and a discussion is given of improvements suggested by the results of this experiment.

1. INTRODUCTION

The exploration, from the ground, of the night airglow spectrum in the region beyond 2.0 μ has been attempted by Noxon, Harrison, and Vallance Jones (1959) and by Moroz (1960). In both these investigations it was found that, for wavelengths greater than about 2.5 μ, the thermal emission of the infrared-active molecules of the lower atmosphere completely obscured any emission bands arising from above 50 kilometers; in particular the fundamental sequence of OH vibration–rotation bands in the 3.0-μ region were unobservable. Observations from the ground are also restricted to certain narrow transmission "windows" in the absorption spectrum of the lower atmosphere. Consequently, in 1957, we proposed making observations with an infrared spectrometer flown by balloon to a height above 15 kilometers. This program was carried out as a joint project by the University of Saskatchewan and the Canadian Armament Research and Development Establishment of the Defence Research Board of Canada (CARDE). The University of Saskatchewan was responsible for the design and construction of the spectrometer and its electronics while CARDE was responsible for flying the spectrometer, for the telemetry of the results, for the power supplies of all the air-borne equipment, and for the provision of facilities for preflight testing of the instrument.

The spectrometer, designed for observations between 2.0 and 4.0 μ, was flown on April 27, 1960. Good spectra were obtained up to a height of 7.5 km, but above this height signals received on all the telemetry channels became

[1]Manuscript received April 24, 1961.
Contribution from the Physics Department, University of Saskatchewan, Saskatoon, Sask. The research reported in this paper has been sponsored by the Geophysics Research Directorate of the Air Force Cambridge Research Center, Air Research and Development Command, under contract AF 19(604)-7265.

noisy. While the spectra obtained were of considerable interest, and will be discussed below, the main purpose of this paper will be to describe the spectrometer and the special problems encountered in this wavelength region. The investigation is being continued using a larger spectrometer constructed at CARDE.

2. DESIGN OF SPECTROMETER

In this section a short summary is given of the basic principles controlling the design of infrared spectrometers using photoconductive detectors. When the spectrometer employed in the present work was designed, it was assumed that the weight and size should be held to a minimum, so that it was necessary to consider rather carefully the minimum size of instrument required to detect the $\Delta v = 1$ OH bands. Now that it is possible to fly larger instruments, the relations developed in this section are useful for predicting their performance on the basis of the results obtained in this investigation.

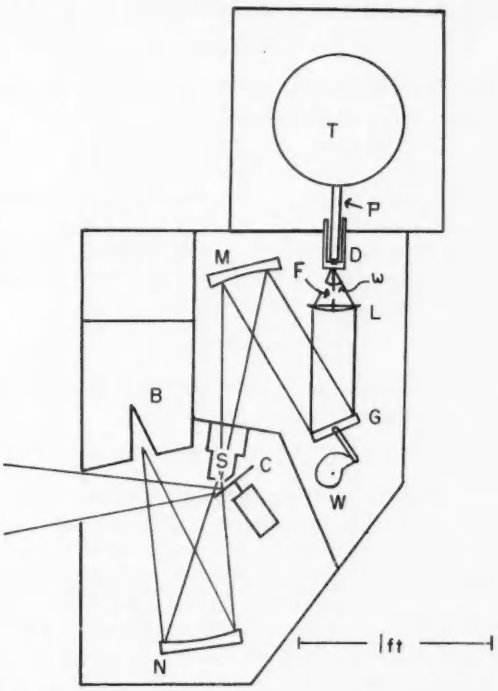

FIG. 1. Scale drawing of balloon-borne spectrometer. The components are labelled in accordance with the description given in Section 3 of the text.

For a spectrometer of the type shown in Fig. 1 the power reaching the detector is given by

$$P = a(B_\lambda \cdot \Delta\lambda) . \omega . t \tag{1}$$

where a is the area of the detector, B_λ is the differential brightness of the source, ω is the solid angle over which the detector receives radiation from the condensing optics, and t is the transmission of the optical system. ($B_\lambda \cdot t \cdot \Delta\lambda$ is the effective brightness of the surface seen by the detector through the spectrometer optics.)

The noise-equivalent power for many detectors is given by the relationship

$$P_n = S.a^{1/2}.(\Delta f/f)^{1/2} = k.a^{1/2} \tag{2}$$

where S is the index of detector performance introduced by R. C. Jones,* Δf is the band width of the amplifying system, f is the modulation frequency of the chopping system, and $k = S.(\Delta f/f)^{1/2}$.

In describing the performance of a spectrometer it is useful to define the quantity, "noise-equivalent brightness", $B_{\lambda N}$. This is the differential brightness of a surface which would give a signal at the output of the spectrometer equal to the r.m.s. noise in the output. From equations (1) and (2)

$$B_{\lambda N} = k/(a^{1/2}.\Delta\lambda.\omega.t). \tag{3}$$

However, a must be chosen so that the desired spectral slit width is obtained. The width of the exit slit, s, is given by the equation

$$s = F.(d\theta/d\lambda).\Delta\lambda$$

where F is the focal length of the condensing lens (Fig. 1) and $d\theta/d\lambda$ is the angular dispersion of the grating.

The length of the detector, l, is equal to αF, where α is the angular length of the detector. The value of α is limited by aberrations in the optical system. From these relations one obtains the result that

$$a = F^2.\alpha.(d\theta/d\lambda).\Delta\lambda. \tag{4}$$

Combining equations (3) and (4) one obtains the final result that the noise-equivalent brightness is given by the equation

$$B_{\lambda N} = S(\Delta f/f)^{1/2}.[F.\{\alpha.(d\theta/d\lambda)\}^{1/2}.\omega t(\Delta\lambda)^{3/2}]^{-1}. \tag{5}$$

Equation (5) is useful both in the design of spectrometers and in making comparisons between existing instruments and new design proposals.

The design adopted for the balloon-borne spectrometer was checked with the help of equation (5) from which it was predicted that a signal-to-noise ratio of about 15 should be obtained for the OH bands between 2.8 and 2.95 μ. The quantities substituted into equation (5) are listed for convenience in Table I and correspond to the design described in the next section. The apparent zenith differential brightness of the sky in OH emission was calculated by constructing synthetic spectra for a rotational temperature of 220° K at spectral slit widths of 250 Å and 700 Å. These synthetic spectra, shown

*See Smith, R. A., Jones, F. E., and Chasmar, R. R. 1957. The detection and measurement of infra-red radiation (Oxford), p. 271.

TABLE I

Spectrometer constants and calculation of noise-equivalent brightness

Spectral slit width, $\Delta\lambda$	650 Å
Condenser focal length, F	6.0 cm
Condenser solid angle, ω	1.14 steradian
Angular length of detector, α	0.1 radian
Jones' factor of detector for monochromatic radiation near 3.0 μ, S	2.89×10^{-10} watt. cm^{-1}
Transmission of optics, t	0.2
Dispersion at detector, $d\theta/d\lambda$	3.07×10^{3} radian. cm^{-1}
Amplifier band width, Δf	0.8 sec^{-1}
Radiation chopping frequency, f	90 sec^{-1}
Noise-equivalent brightness, $B_{\lambda N}$	6.9×10^{-9} watt. cm^{-2}. $sterad^{-1}$. $micron^{-1}$
Predicted sky brightness ($\Delta\lambda$ = 700 Å, λ = 2.95 μ for zenith angle 75°), B_{λ}	1.0×10^{-7} watt. cm^{-2}. $sterad^{-1}$. $micron^{-1}$
$\therefore$ Signal/noise ratio expected	14.5

in Fig. 2, are similar to the one calculated by Noxon, Harrison, and Vallance Jones (1959); in the present case, however, no correction for atmospheric absorption was made. The spectra of Fig. 2 were calculated using the relative

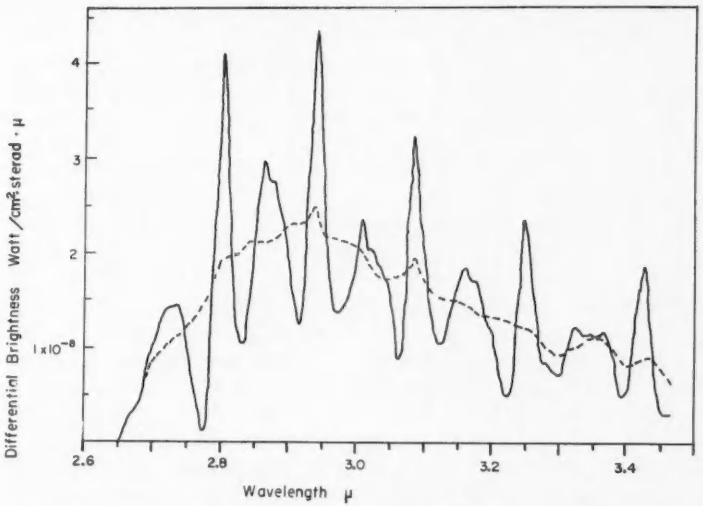

FIG. 2. Synthetic OH spectra at spectral slit widths of 700 Å (dotted line) and 250 Å (solid line). The relative brightnesses of the bands in the $\Delta v = 1$ sequence are approximately those given by Chamberlain and Smith (1959) and the brightness of the 1–0 band is chosen to be 700 kR (4.4×10^{-8} watt. cm^{-2}. $column^{-1}$).

band intensities of Chamberlain and Smith (1959), on the basis of an absolute brightness of 60 kR for the 4–2 OH band in the zenith direction. This value for the absolute brightness of the 4–2 band represents the latest measurements of the absolute brightness carried out by Shemansky and Vallance Jones (1961) and Moroz (1960) and is lower than the value used by Noxon, Harrison,

and Vallance Jones. The absolute brightnesses used for the $\Delta v = 1$ OH bands in calculating the spectra of Fig. 2 were about 30% lower than the values predicted by Chamberlain and Smith. The value of the Jones factor, S, was calculated from the test data supplied by Infrared Industries with the detector used. While there may be some uncertainty with regard to some of the values listed in Table I the results of the calculation suggested that a spectrometer of the type considered in the next section should be suitable for initial studies in the 3.0-μ region.

3. DESCRIPTION OF SPECTROMETER

The main optical and mechanical features of the spectrometer are shown in Fig. 1. Radiation from the sky enters the spectrometer through a hole in the side of the case and falls on the mirror chopper, C, from which it is reflected on to the entrance slit, S. It then falls on the spherical collimator mirror, M, from which it is reflected to the grating, G. The spectrum is focused by an arsenic trisulphide lens, L, at the detector, D, which serves also as an exit slit. The reflecting chopper, C, provides a means of comparing the radiation from the sky with the radiation from the black-body cavity, B, which is focused on the entrance slit by the spherical mirror, N. The black-body cavity is cooled by dry ice and consequently the signal obtained at the detector would, in the ideal case, become a measure of the emission from the sky. However, in practice the mirror chopper and the mirror, N, have emissivities which are between .02 and .05 and consequently they will radiate as gray bodies. To the extent that the emissivities and temperatures of the mirror chopper and the mirror, N, differ, a false signal will be contributed.

A plane, 300 line/mm, diffraction grating, blazed at 3.0 μ, was employed. This grating was rotated by the cam and lever arrangement, W, so as to scan a wavelength range between 1.6 and 3.7 μ with a repetition period of 80 seconds. Wavelengths shorter than 2.0 μ were removed by a germanium filter placed over the entrance slit. The arsenic trisulphide lens, L, had a diameter of 75 mm and a focal length of 60 mm. This lens, produced by the Fraser Glass Company, had four spherical zones giving the best approximation to an ideal plano-convex aspherical lens. The entrance slit, S, and the size of the detector, D, were chosen to provide a spectral slit width of 650 Å at 3.0 μ. Laboratory observation of the infrared helium line at 2.06 μ showed that a spectral slit width of 700 Å was attained. The detector was an Infrared Industries extended-response PbS cell. It was cooled by a hollow finger, P, projecting into the cell from a tank of liquid oxygen, T. This tank, which was insulated by 2 inches of styrofoam, contained sufficient oxygen to last for 4 hours. Since the pressure at 27 km is in the neighborhood of 14 mm Hg, an intolerable variation in the temperature of the detector would occur if the liquid-oxygen container were open to the atmosphere. Consequently the oxygen container was provided with a simple spring-loaded valve which maintained a pressure differential of about one atmosphere between the outside and the inside pressures. In this way, the variation of the boiling point of the liquid oxygen was confined to a small temperature range. The rotating chopper disk and the cam of the wavelength scanning system were driven by

miniature 400 c.p.s. synchronous geared motors. In order to keep moisture from condensing on the window of the detector the inner chamber was filled with nitrogen gas which was allowed to boil off from a second insulated container filled with liquid nitrogen.

The output from the detector was amplified by an electron tube preamplifier followed by a tuned, 90 c.p.s., transistor amplifier. Three outputs from the transistor amplifier, having relative gains of 1, 9, and 80, were fed to non-synchronous diode detectors; the outputs from the two most sensitive channels were also applied to diode-bridge phase-sensitive detectors for which the reference signals were derived from an optical pickup on the chopper, C. The outputs from these five detectors were telemetered to the ground together with information on the position of the grating, the detector temperature, and the temperature of the inside of the spectrometer case. Values of the ambient air temperature and pressure were also telemetered to the ground during the flight.

The spectrometer was mounted on the gondola so that its line of sight was inclined at a zenith distance of 75°. The azimuth angle of the line of sight was free to vary with the rotation of the balloon. It is known that variations in the inclination of the gondola during flight do not exceed 5°; the period of rotation of the gondola may be as short as 4 seconds.

The sensitivity and performance of the spectrometer were tested before flight by operating the spectrometer with the entrance hole in the outer case closed. Under these conditions the spectrometer sees radiation corresponding to an ideal black body at the temperature of the inside of the outer chamber. In this way the minimum detectable differential brightness at 3.0 μ was estimated to be 2×10^{-8} watt. cm^{-2}. sterad^{-1}. micron^{-1} at a spectral slit width of 700 Å. The difference between this observed value and the predicted design value of 0.7×10^{-8} watt. cm^{-2}. sterad^{-1}. micron^{-1} is reasonable when additional noise caused by the telemetry transmitter is considered. A check was made by inserting temporarily a thermal shield around the motor to insure that radiation from the somewhat warmer chopper motor did not contribute noticeably to the signal during this calibration.

4. RESULTS AND DISCUSSION

The spectrometer was flown from Quebec, Que., on April 27, 1960; a polyethylene balloon filled with helium was used to lift the gondola. The balloon was launched at 0245 hours E.S.T., reached a height of 7.5 km at 0305 hours, and attained a maximum height of 27.5 km at 0445 hours. It was cut down a little later and was recovered in good condition in November, 1960. Spectra were obtained up to a height of 7.5 km; above this height the spectral telemetry channels became noisy.

Figure 3*a* shows two sample scans on the intermediate sensitivity channel, one on the ground (labelled 1) and the other (labelled 2) at the maximum height of 7.5 km. The scan at 7.5 km as obtained on the highest sensitivity channel is shown as curve 1 in Fig. 3*b*. There is also shown as curve 2 on Fig. 3*b* the predicted OH spectrum scaled from Fig. 2 for a zenith angle of 75° and the measured spectrometer sensitivity.

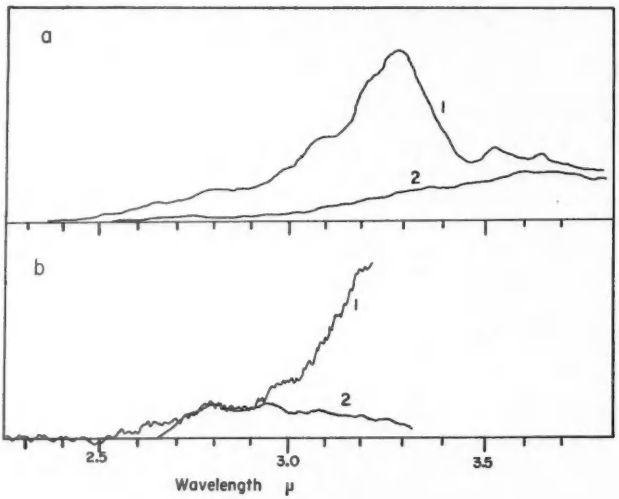

FIG. 3. Specimen spectra as recorded by telemetry.
(*a*) (1) Spectrum at ground level. (2) Spectrum from 7.5 km. The zenith angle of observation was 75° and the records were obtained on the intermediate sensitivity channel.
(*b*) (1) Spectrum at 7.5 km recorded on the highest sensitivity channel. (2) Synthetic OH spectrum scaled to match observed spectrum between 2.7 and 2.9 μ.

Most of the data required for discussing the results have been brought together in Fig. 4, which shows the spectra obtained from the ground (B) and from 7.5 km (E) plotted on a logarithmic scale. The predicted synthetic OH spectrum has been plotted on the same figure as curve F while curves A and C are calculated black-body spectra for temperatures of 280° and 250° K respectively. Curves D and G show the spectra of a gray body of emissivity 0.04 at temperatures of 290° and 250° K respectively. The relation of these curves will be discussed in the following paragraphs.

The spectrum obtained on the ground is similar to that observed by Noxon, Harrison, and Vallance Jones (1959) and explained by them as thermal emission from the lower atmosphere. The brightness at 2.7 μ is expected to be close to that from a perfect black body at the ambient air temperature; Fig. 4 shows that this is true. During the ascent, the emission at wavelengths shorter than 3.2 μ decreased in brightness, falling by a factor of 10 by the time the spectrometer reached 7.5 km. At longer wavelengths the decrease in brightness with height became progressively less until at 3.6 μ the signal was observed to be nearly as strong at 7.5 km as on the ground. It must therefore be concluded that a false thermal emission from the mirror chopper made a significant contribution to the brightness observed at these longer wavelengths. Indeed there is a possibility that a large part of the signal observed at 7.5 km may have arisen from the spurious emission from the mirror chopper since, as is shown by curve D in Fig. 4, a gray body having

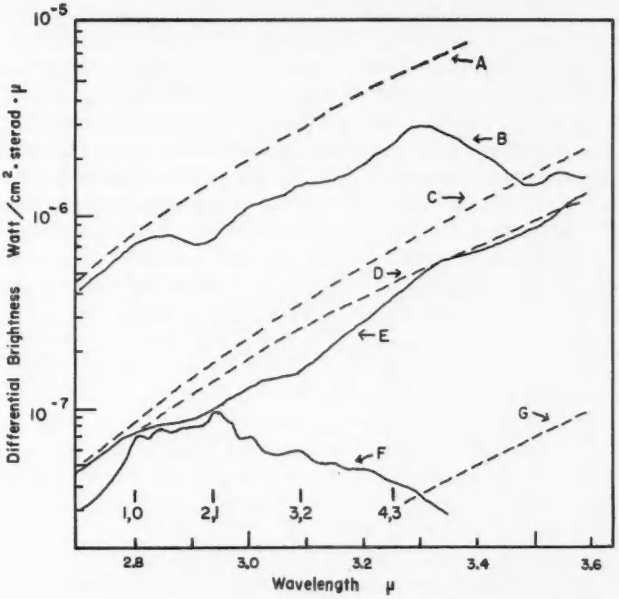

FIG. 4. Comparison between observed, synthetic, and thermal spectra. (A) Spectrum of black body at 280° K. (B) Observed night airglow spectrum from ground level. (C) Spectrum of black body at 250° K. (D) Spectrum of gray body of emissivity 0.04 at 290° K. (E) Observed night airglow spectrum at 7.5 km. (F) Predicted synthetic OH spectrum at a spectral slit width of 700 Å, replotted from Fig. 2. (G) Spectrum of gray body of emissivity of 0.04 at 250° K. The positions of the Q branches of the first four OH bands are shown.

an emissivity of .04 and a temperature of 290° K would have a spectral distribution of brightness matching the observed spectrum at 2.8 μ and from 3.3 to 3.6 μ. (The chopper was known to have a reflectivity of about 0.95 and hence an emissivity of about 0.05.)

The most interesting conclusion results from the comparison in Fig. 4 between the observed spectrum at maximum altitude, curve E, and a synthetic OH spectrum, curve F. This synthetic spectrum was scaled from the 700 Å curve in Fig. 2 by multiplying by a van Rhijn factor of 4. As will be seen from Fig. 4 the measured brightness at 7.5 km has fallen very close to the expected values of brightness for the OH emission and, consequently, one may conclude that the actual brightness of the OH bands during the flight did not in fact exceed the calculated values. Thus one may put an upper limit of approximately 4.4×10^{-3} watt. cm^{-2}. column^{-1}, or 700 kR, on the brightness of the 1–0 band.

A further result may be deduced immediately from the observed spectra concerning upper atmospheric emissions in the region between 2.3 and 2.7 μ. Since no emission features were observed in this region it may be concluded that there are present no discrete night airglow features with a brightness

greater than about 200 kR ($\sim 10^{-9}$ watt. cm^{-2}. sterad^{-1}). This unit corresponds to the brightness of a monochromatic feature which would give a detectable signal. The corresponding limit to the differential brightness of a broad feature is about 2×10^{-8} watt. cm^{-2}. sterad^{-1}. micron^{-1} ($\sim$3000 kR/micron).

As a result of the information obtained in this flight it is possible to prescribe with fair confidence the requirements for an instrument capable of making good measurements of the $\Delta v = 1$ OH bands. The observed spectrum at 7.5 km and the predicted spectrum shown in Fig. 3*b* indicate that the sensitivity of the spectrometer was adequate for the detection of the OH bands at their predicted brightness. There are still two directions in which improvements may be made. First, it would be desirable to cool the surface of the mirror chopper after the balloon has risen above 20 km. Secondly, the spectral slit width might be decreased to about 250 Å. Both of these changes would decrease the unwanted effect of stray thermal radiation from the mirror chopper. As may be seen from Fig. 4 a mirror chopper with a residual emissivity of 0.04 at 290° K produces an emission of the same order as the expected signal. If the surface of the chopper were reduced to a temperature of 250° K by means of a stream of cold dry nitrogen, the curve G in Fig. 4 shows that the thermal radiation level would be reduced well below that of the expected OH signal at 3.0 μ.

The suggested reduction of the spectral slit width would also be beneficial in reducing the signal from continuous thermal radiation and would provide more certainty in the identification of the OH bands. Figure 2 shows synthetic spectra giving the apparent differential brightness of the bands at spectral slit widths of 700 Å and 250 Å. It will be seen that the structure of the band system is much more fully developed for the smaller spectral slit width. However, if it is desired to maintain the signal-to-noise ratio at the same value obtained with the spectrometer described here then the size of the spectrometer must be increased. In equation (5) the only quantity which is altered in scaling up the spectrometer to a larger size is the focal length of the condensing system, F, since F is proportional to the linear dimensions of the instrument. An inspection of Fig. 2 shows that at the peak of the 2–1 band at 2.95 μ the apparent differential brightness is increased by nearly a factor of 2 in reducing the spectral slit width from 700 to 250 Å. The corresponding decrease in $(\Delta\lambda)^{3/2}$ in the equation (5) is therefore partially compensated for by the increase in B_λ. It is thus only necessary to double F, and hence to double the size of the instrument, in order to hold constant the signal-to-noise ratio for the peak of the 2–1 band. As was mentioned in Section 1 the experiment is soon to be repeated at CARDE using a larger spectrometer fulfilling these specifications. Consequently it is not planned to make another attempt with the instrument described in this paper.

ACKNOWLEDGMENTS

This experiment was made possible by the support of the Canadian Armament Research and Development Establishment of the Defence Research Board of Canada in undertaking to fly the spectrometer. In particular we

wish to thank Mr. R. F. Chinnick, Mr. J. Hampson, Dr. C. Cumming, Mr. R. P. Lowe, and Mr. J. C. Baril for their active interest and participation in the preparation, flight, and later recovery of the spectrometer. We are grateful to Mr. F. Rittmann, Mr. D. Flathman, and Mr. D. Strelioff for their contribution towards the design and construction of the spectrometer. We should also like to express our appreciation of the co-operation of Dr. Walter A. Fraser of the Fraser Glass Company in the production of the arsenic trisulphide lens.

REFERENCES

CHAMBERLAIN, J. W. and SMITH, C. A. 1959. J. Geophys. Research, **64**, 611.

MOROZ, V. I. 1960. Doklady Akad. Nauk S.S.S.R. **126**, 983.

NOXON, J. F., HARRISON, A. W., and VALLANCE JONES, A. 1959. J. Atmospheric and Terrest. Phys. **16**, 246.

SHEMANSKY, D. E. and VALLANCE JONES, A. 1961. J. Atmospheric and Terrest. Phys. In press.

MESURE DU TEMPS DE RELAXATION D'UNE VIBRATION DE N_2O PAR UNE MÉTHODE INFRAROUGE[1]

GERMAIN GAUTHIER ET JULES MARCOUX

RÉSUMÉ

Dans une cuve d'absorption infrarouge permettant un débit de gaz, on produit un déséquilibre thermique entre les degrés de liberté du gaz. On enregistre les changements qui apparaissent dans la courbe de transmission de la bande de N_2O à 4.55 μ en fonction de la température et du temps, sous une pression de 10 mm de mercure. On obtient deux distributions de température: une pour la vibration et une pour la translation; la température de vibration est continuellement en retard sur la température de translation. Des calculs fournissent un temps de relaxation variant entre 10^{-3} et 10^{-2} seconde, à la pression de l'expérience.

INTRODUCTION

Quand un gaz subit un changement de température, l'usage courant du terme "température" veut dire que l'énergie cinétique de translation des molécules du gaz a changé. Une nouvelle distribution statistique des vitesses s'est établie dans un temps correspondant à quelques collisions. En plus de cet échange d'énergie entre les molécules du gaz, il y a aussi échange d'énergie entre les différents degrés de liberté de la molécule: translation, vibration et rotation. L'étude de ces échanges d'énergie à l'intérieur de la molécule est intéressante à un double point de vue: compréhension du comportement des chaleurs spécifiques et influence sur les problèmes de combustion et de dynamique des gaz.

On appelle phénomène de relaxation, le retard de l'échange d'énergie entre les degrés de liberté externes (translation) et internes (vibration et rotation), ou le temps qu'une distribution énergétique des niveaux de vibration et de rotation met à s'ajuster à une nouvelle température de translation. Cet ajustement peut s'effectuer par deux processus: par émission ou absorption de radiation, ou par échange d'énergie au cours de collisions. La relaxation de translation et celle de rotation ne prennent ordinairement que quelques collisions (entre 1 et 10) correspondant à un temps de l'ordre de 10^{-9} seconde aux conditions normales de température et de pression (Herzfeld 1955). La rotation et la translation peuvent donc en pratique être considérées toutes deux comme des degrés de liberté externes.

Il a été calculé (Lukasik 1956) que le temps de relaxation de vibration pour une désactivation par radiation est constant, indépendant de la pression et relativement long, de l'ordre de 0.1 seconde. D'autre part, la désactivation par chocs demande plusieurs milliers de chocs; le temps de relaxation correspondant est inversement proportionnel à la pression et varie entre 10^{-6} et 10^{-3} seconde.

[1]Manuscrit reçu le 20 février 1961.
Contribution du Département de Physique du Collège Militaire Royal de Saint-Jean, Saint-Jean, Qué. Travail effectué avec l'aide d'un octroi du Conseil de Recherches pour la Défense (DRB 9510-22).

Une description des méthodes utilisées pour déterminer les temps de relaxation peut être trouvée facilement (par exemple, Herzfeld 1955). La méthode la plus connue vient de l'étude de la dispersion et de l'absorption des ultrasons. La méthode proposée ici repose sur l'observation des changements qui apparaissent dans le spectre infrarouge d'une vibration moléculaire isolée, quand un gaz subit un déséquilibre thermique. Elle permet des variations de pression et de température et diffère de la plupart des autres méthodes en ce qu'elle mesure le temps de relaxation d'une vibration isolée d'une molécule polyatomique. On a pu ainsi déterminer le temps de relaxation de la vibration ν_3 de la molécule N_2O à une pression relativement basse, où la désactivation par chocs est encore prépondérante.

MONTAGE EXPÉRIMENTAL

Un diagramme de l'appareil est représenté sur la figure 1. La cuve d'absorption infrarouge est constituée de deux cylindres rectangulaires d'aluminium, séparés par une bande de téflon de 13.5 mm d'épaisseur. Le cylindre a une section intérieure de 2.54 cm par 50.8 cm. On utilise du N_2O en cylindre commercial. On produit une circulation de gaz par pompage à travers la cellule

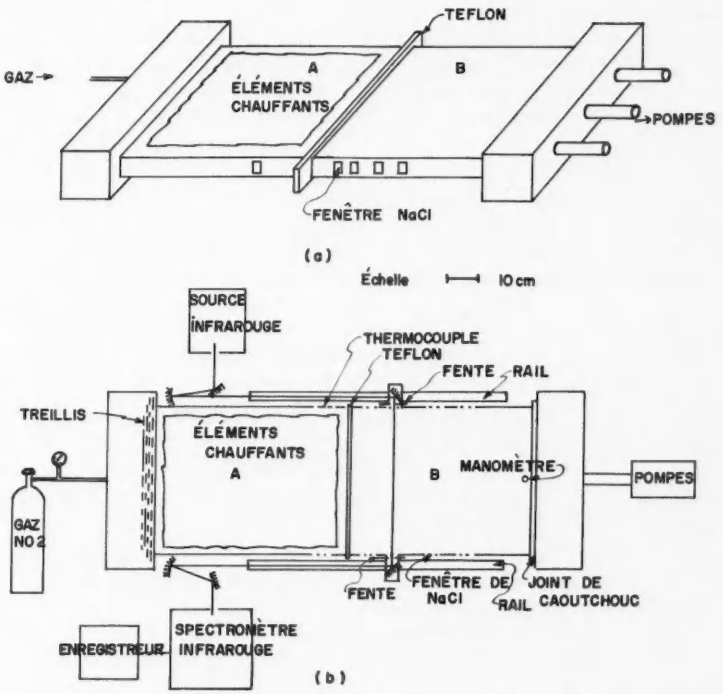

FIG. 1. (*a*) Cellule d'absorption. (*b*) Montage expérimental, vu de plan.

avec un débit d'environ 1200 litres à la minute, au moyen de trois pompes mécaniques de type Edwards S 450. On maintient facilement dans la cellule une pression de 1 cm de mercure; cette pression est mesurée à un bout de la cellule à l'aide d'un manomètre anéroïde Edwards. La vitesse d'écoulement du gaz est obtenue, en mesurant le temps d'écoulement d'une quantité connue de gaz dans les conditions de l'expérience. Dans l'expérience décrite ici, la vitesse d'écoulement est de 2.90 mètres à la seconde.

La partie B de la cuve est maintenue à la température ambiante par une circulation d'eau près du téflon. Les deux parois horizontales de la partie A peuvent être chauffées jusqu'à 200° C à l'aide de deux éléments électriques placés dans une pâte d'amiante durcie. Dans l'expérience, les sections A et B sont maintenues respectivement à 150° et 30° C, produisant un gradient de 90 degrés centigrade par centimètre dans la paroi de la cuve, à l'endroit du téflon. La température élevée (150° C) est maintenue constante par un thermostat branché sur les éléments de chauffage et constitué d'un thermocouple et d'un relai Pyr-o-Vane Honeywell-Brown, dont la réponse est de ± 5 degrés centigrade. Le gaz est préchauffé dans une chambre annexe remplie d'un treillis métallique fin, assurant ainsi une distribution uniforme du gaz. La température de la paroi chaude, mesurée à différents endroits, est uniforme à ± 2 degrés centigrade.

On examine l'état du gaz à différents points de la cuve, à travers cinq paires de fenêtres de sel gemme, une paire dans la partie A pour enregistrer le spectre à 150° C et quatre paires dans la partie B pour enregistrer le spectre à des distances connues du téflon. La source et le monochromateur d'un spectromètre Perkin-Elmer 12C sont séparés et placés de part et d'autre de la cuve. Le faisceau infrarouge est rendu parallèle à l'aide d'un miroir concave. Ce faisceau parallèle passe à travers les différentes paires de fenêtres de la cuve, au moyen de miroirs inclinés à 45° pouvant se déplacer sur des rails parallèlement à la cuve. Le faisceau est ensuite repris pour être focalisé sur la fente d'entrée du monochromateur par un miroir sphérique semblable au premier. Le faisceau est limité à l'entrée de la cellule par une fente d'environ 3 mm de largeur.

RÉSULTATS ET DISCUSSION

Les spectres de la bande de vibration ν_3 de N_2O apparaissant à 2223 cm^{-1} (4.55 μ) ont été enregistrés aux positions suivantes: (1) du côté chaud, près de la bande de téflon, donnant le spectre à 150° C; (2) du côté froid à 6.2, 13.1, 19.5, 27.1 cm du téflon; (3) à l'une quelconque de ces positions, avant le chauffage, donnant le spectre à 30° C.

Un certain nombre de spectres de la bande ν_3 ont été enregistrés dans ces conditions. La figure 2 représente la transformation des spectres au cours d'une série. Dans cette figure, les courbes expérimentales ont été transformées pour présenter la transmission ($100\ I/I_0$) en fonction de la longueur d'onde. On a mesuré sur chaque spectre la largeur de la bande ($\Delta\nu$ en unités arbitraires) à 75, 85 et 95% de transmission. Ces mesures apparaissent en graphique dans la figure 3. On y voit que la largeur de la bande diminue à mesure qu'on

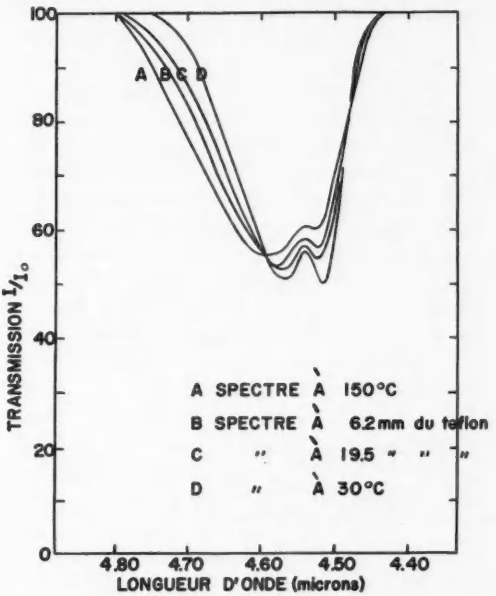

FIG. 2. Exemple de courbes de transmission.

s'éloigne de la séparation entre les sections chaude et froide de l'appareil; à quoi il fallait s'attendre puisque le gaz se refroidit continuellement. Rien n'indique cependant que la largeur de bande corresponde à une température où tous les degrés de liberté de la molécule sont en équilibre thermique, ou à une température où la vibration n'est pas en équilibre thermique avec la translation.

Il faut peut-être rappeler ici que l'absorption infrarouge est due aux changements du moment du dipole électrique au cours d'une vibration ou d'une rotation. Ces changements varient avec l'énergie ou la température de la vibration et sont indépendants de l'énergie ou de la température de la translation. Nous pouvons donc supposer (*a*) qu'un spectromètre infrarouge peut être considéré comme un thermomètre pour mesurer les températures de vibration; (*b*) que les changements de la largeur d'une bande infrarouge avec la température de vibration ne sont pas affectés par le fait que la vibration n'est pas en équilibre thermique avec la translation.

Afin de déterminer la relation qui existe entre la température de vibration et la largeur de la bande, nous avons fait une expérience où tous les degrés de liberté sont en équilibre à différentes températures connues. Les conditions expérimentales sont ici exactement les mêmes que celles décrites plus haut. La figure 4 représente graphiquement les résultats de cette expérience. Dans le domaine des températures étudiées, la largeur de la bande décroît linéairement avec la température, à 75, 85 et 95%. A des absorptions plus basses que

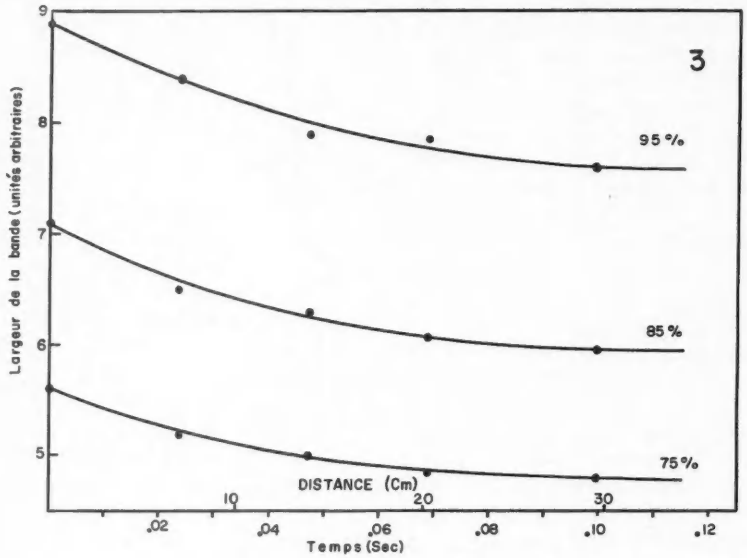

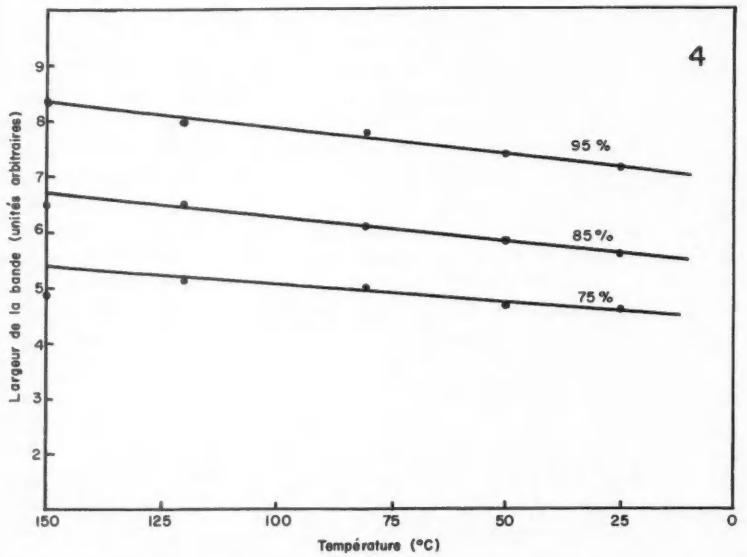

FIG. 3. Largeur de la bande à différents endroits de la section froide de la cellule d'absorption, lorsque la vibration n'est pas en équilibre thermique avec la translation.

FIG. 4. Largeur de la bande en fonction de la température du gaz, lorsque tous les degrés de liberté sont en équilibre thermique.

60% c'est le phénomène contraire qui se présente: la largeur de bande croît avec la température, alors que la largeur près de 65% d'absorption demeure constante. Dans les calculs qui suivent, nous n'avons utilisé que la largeur de la bande à 75%, très voisine de la largeur à mi-hauteur. La hauteur de la bande varie avec la température et présente deux branches d'intensités inégales. La largeur de bande est ici considérée comme une propriété variable avec la température et n'est pas comparée à la "largeur à mi-hauteur" conventionnelle.

En considérant ces résultats, il est possible de donner une température aux largeurs de bandes lorsque la vibration n'est pas en équilibre avec la translation. En effet l'expérience demande que le départ à 0 cm et la fin à 35 cm de la bande isolante de téflon, représentent des conditions d'équilibre thermique. La largeur de la bande de déséquilibre doit retrouver, dans ces deux conditions, les valeurs de la largeur de la bande d'équilibre. Ce qui permet de comparer deux points sur les courbes: le point de départ à 150° C (largeur de bande 5.60 unités) et le point d'arrivée à environ 30° C (largeur de bande 4.75 unités). On établit une relation linéaire entre les largeurs de bande et les températures de vibration entre ces deux points; ce qui permet d'étalonner en températures les largeurs de la bande de déséquilibre. La courbe des températures de vibration en fonction des distances à l'équilibre initial est tracée sur la figure 5 (courbe A).

La courbe B de la figure 5 représente la variation de la température de translation en fonction de la distance au téflon. Cette température de translation a été mesurée avec des thermocouples placés à différents endroits de

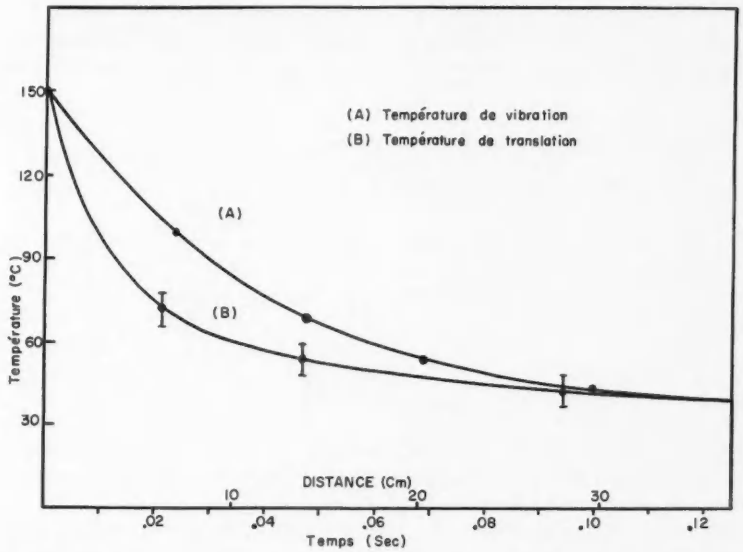

FIG. 5. Température de vibration (A) et de translation (B) à différents endroits de la cellule d'absorption.

l'appareil. Théoriquement, s'il n'y avait pas de convection, on devrait observer près du téflon une variation de température appréciable entre le centre et le haut ou le bas de l'appareil, soit sur une distance verticale de 2.54 cm. Les mesures indiquent une différence d'environ un degré centigrade: les courants de convection sont donc appréciables. Au cours de l'expérience, nous avons constaté que des variations dans le système de chauffage produisaient presque instantanément des variations dans la température du gaz.

Les températures mesurées sont limitées dans leur précision par le système régulateur de température, qui fonctionne à $\pm 5°$ C. Cette erreur est indiquée sur la courbe B de la figure 5. Cette dernière figure permet de se représenter assez bien l'allure du phénomène. Au temps $t = 0$, la vibration est en équilibre thermique avec la translation. Le gaz se déplace relativement vite (2.90 m/sec) et la température de vibration T_v ne peut suivre celle de la translation T_t. La différence $T_v - T_t$ des températures est d'abord petite, passe par un maximum après environ 0.02 seconde et devient nulle après 0.12 seconde, lorsque l'équilibre s'est rétabli.

Le temps de relaxation est défini par la relation suivante (Herzfeld et Litovitz 1959):

$$\frac{\partial T_v}{\partial t} = \frac{1}{\tau}(T_v - T_t)$$

où T_v est la température de vibration, T_t la température de translation et τ le temps de relaxation. Pour un phénomène donné déterminant $\partial T_v/\partial t$ à chaque instant, τ est proportionnel à la différence $(T_v - T_t)$. La courbe A de la figure 5 permet de déterminer le rapport $\partial T_v/\partial t$, les courbes A et B déterminent la différence $(T_v - T_t)$. Les différents temps de relaxation τ ainsi calculés sont donnés dans le Tableau I. Pour des pressions assez basses où la plupart des

TABLEAU I

Temps de relaxation calculés en partant des courbes de la figure 5

T_t (°C)	T_v (°C)	$\partial T_v/\partial t$	τ (sec) (10 mm Hg)
119	138	2.6×10^{-3}	0.007
83	115	2.1	0.016
67	97	1.7	0.018
59	82	1.4	0.016
55	70	1.0	0.015
51	62	0.7	0.015
49	56	0.6	0.012
46	51	0.4	0.011

collisions sont binaires, le temps de relaxation est inversement proportionnel à la pression. Un temps de relaxation de 0.007 seconde à 10 mm de mercure devient donc approximativement 10^{-4} seconde à l'atmosphère.

Herzfeld et Litovitz (1959) donnent plusieurs valeurs obtenues par différents chercheurs. Toutes ces valeurs sont de l'ordre de 10^{-6} seconde, soit 100 fois plus petites que celles de l'expérience présente. Il est difficile de

comparer les résultats obtenus ici et ceux donnés par l'absorption des ultrasons. Dans ce dernier phénomène, le temps de relaxation est mesuré à une température, la température moyenne du gaz, et les variations extrêmes de température se produisent dans un temps égal à la période de l'onde. Dans la présente expérience, les variations extrêmes se produisent dans un temps de l'ordre de 0.02 seconde et l'on peut pointer des températures intermédiaires.

Nous avons pu vérifier qu'entre 30° et 150° C, la surface sous les courbes, ou l'intensité intégrée de la bande d'absorption, ne varie pas lorsque tous les degrés de liberté sont en équilibre. Cependant, le déséquilibre thermique des degrés de liberté produit, dans l'expérience, une variation appréciable de la surface comprise sous les courbes d'absorption. Ces variations devraient pouvoir conduire à un calcul de la contribution de la vibration à l'intensité totale de la bande. Nous espérons continuer ces travaux et les mener dans deux directions: (1) en variant la pression, vérifier comment varie le temps de relaxation et atteindre si possible le phénomène de relaxation par émission de radiation (Lukasik 1956), (2) déterminer pour une même molécule, les différents temps de relaxation correspondant à différentes fréquences fondamentales (Massey et Burhop 1952).

BIBLIOGRAPHIE

HERZFELD, K. F. 1955. Thermodynamics and physics of matter (Princeton University Press), Section H.

HERZFELD, K. F. et LITOVITZ, T. A. 1959. Absorption and dispersion of ultrasonic waves (Academic Press), Section 10.

LUKASIK, S. J. 1956. J. Acoust. Soc. Am. **18**, 455.

MASSEY, H. S. W. et BURHOP, E. H. S. 1952. Electronic and ionic impact phenomena (Clarendon Press), Section 12.21.

NEW EMISSION BANDS OF N_2^+, $^2\Pi_g$–$A\,^2\Pi_u$[1]

Y. TANAKA, T. NAMIOKA, AND A. S. JURSA

ABSTRACT

Thirty-eight new bands of nitrogen were observed in the region 2050–3070 Å in an a-c. condensed discharge of neon mixed with a small amount of nitrogen. It was determined that these bands result from the transition $^2\Pi_g$–$A\,^2\Pi_u$ of N_2^+.

INTRODUCTION

In addition to the two well-known systems of N_2^+, $B\,^2\Sigma_u^+$–$X\,^2\Sigma_g^+$ the first negative system and $C\,^2\Sigma_u^+$–$X\,^2\Sigma_g^+$ the second negative system, Meinel (1950) discovered another system of emission bands in the night airglow and assigned them to the transition $A\,^2\Pi_u$–$X\,^2\Sigma_g^+$, the upper state being the one which Mulliken (1932) predicted at about 1 ev above the ground state of N_2^+. Shortly after Meinel's discovery, Worley (1953) studied the absorption spectrum of N_2 in the vacuum ultraviolet region and arranged a Rydberg series (he called it the third series) which converged to the $A\,^2\Pi_u$ state of N_2^+. Douglas and his co-worker (1951, 1953) have succeeded in producing the Meinel bands in the laboratory and have obtained accurate molecular constants for the related states.

Recently, Janin and d'Incan (1958, 1959) reported additional emission bands of N_2^+ in the region 2240–3070 Å and assigned them to the transition $^2\Pi_g$–$A\,^2\Pi_u$, the lower state being the upper state of the Meinel bands. Independently and at almost the same time as they reported the discovery of these bands we also observed a new system of emission bands of N_2^+ in the region 2050–3070 Å and temporarily attributed the system to the transition $^2\Pi_g$–$A\,^2\Pi_u$,* which turned out to be Janin's assignment for the bands he observed.

EXPERIMENTAL

We used a π-shaped discharge tube, 2.5 cm in diameter, 30 cm in length, with two aluminum electrodes, which was attached to a 2-meter, normal incidence type vacuum spectrograph utilizing a grating of 15,000 lines per inch. The tube was separated from the spectrograph by a thin LiF window. Tank neon, purified by passage through a charcoal trap, was introduced into the discharge tube over a pressure range of 1–20 mm Hg. A small amount of pure nitrogen was added to the neon; the amount of N_2 suitable for excitation of the present bands was about 1–5% of the neon pressure. If too much N_2 were added, strong bands, such as the Lyman–Birge–Hopfield and the fourth positive bands, interfered with the identification of the present bands.

[1]Manuscript received May 1, 1961.
Contribution from the Photochemistry Laboratory, Geophysics Research Directorate, Air Force Cambridge Research Laboratories, L. G. Hanscom Field, Bedford, Massachusetts.
*The results with an explanation were presented at the Symposium of Molecular Structure and Spectroscopy, Ohio State University, June, 1958.

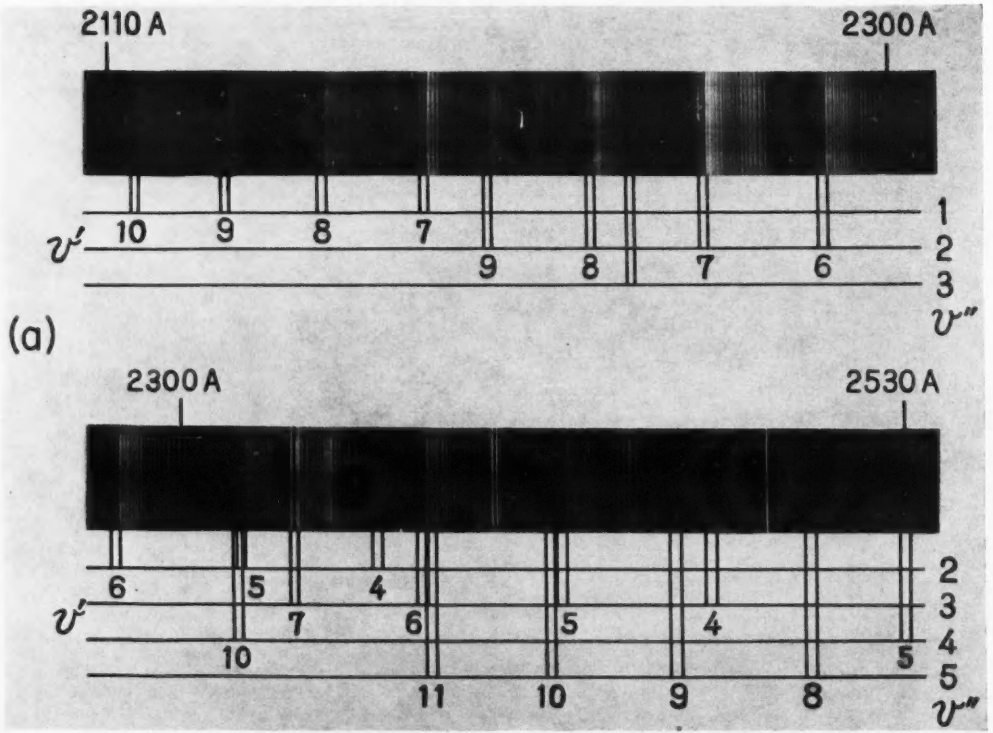

FIG. 1(*a*). The $^2\Pi_g$–$A\,^2\Pi_u$ bands of N_2^+ with the vibrational numbering as revised by Janin *et al.*

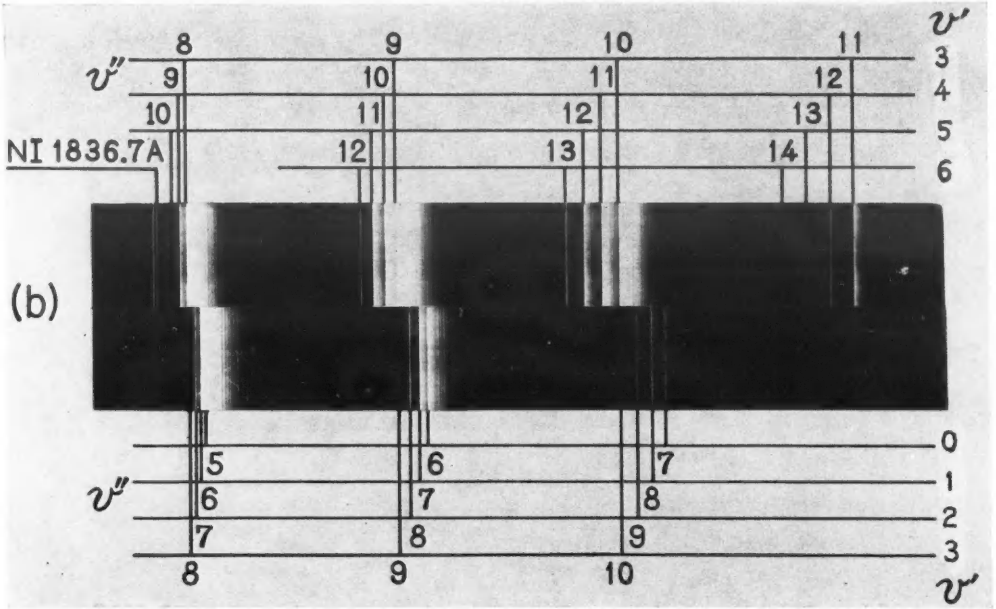

FIG. 1(*b*). Relative intensity distribution of the $C\,^2\Sigma_u^+ - X\,^2\Sigma_g^+$ bands showing the intensity shift which occurs in the two different excitation cases: with He (upper spectrum); with Ne (lower spectrum).

The mixture of Ne+N_2 was excited by an a-c. condensed discharge produced by a 15-kv, 0.96-kva transformer, combined with a laboratory-made condenser of about 0.005 μf, and an external spark gap. In most cases we used a flow method in which Ne and N_2 were suitably premixed and then pumped through the discharge tube. If one uses a closed system, then one must add nitrogen to the tube periodically in order to maintain conditions favorable for the production of the bands; this is necessary because the nitrogen disappears rapidly in the discharge in a closed system. The bands were quite strong so that a 10-minute exposure produced a reasonable density on SWR film in the first order with a spectrograph slit width of 20 μ. The use of Ne is the essential factor for the production of the bands. With helium the bands do not appear at all, but the strong C–X bands and some unidentified very weak bands in the same region as that of the present bands do appear. With argon neither the present bands nor the C–X bands are excited. The use of an a-c. condensed discharge is the other factor important in the production of the bands. In a non-condensed discharge in a mixture of Ne and N_2, band systems of N_2 such as $y\,{}^1\Pi_g$–$a'\,{}^1\Sigma_u^-$, $y\,{}^1\Pi_g$–$w\,{}^1\Delta_u$, $x\,{}^1\Sigma_g^-$–$a'\,{}^1\Sigma_u^-$, $a\,{}^1\Pi_g$–$X\,{}^1\Sigma_g^+$, and the Herman–Kaplan system were strong throughout this region, while the bands presently being considered were extremely weak.

RESULTS

The spectrum as observed in the region of 2110–2530 Å is reproduced in Fig. 1(a). As one can see, the individual bands are composed of two heads, the longer wavelength one being stronger than the other, and both are degraded toward the red with relatively coarse spacing. The measurements were carried out for the heads, and the results are listed in Table I. The values listed in Table I are the averaged ones measured from several plates which were taken under different conditions. Janin and d'Incan's values for the band origins are also listed in the same table. Recently, Janin *et al.* (Grandmontagne *et al.* 1959) revised their previous vibration assignment and raised the upper vibration number by 3 after calculating the relative intensity distribution by means of the modified "distortion" method (Pillow 1951; Grandmontagne 1957, 1958). We adopted their revised assignment in Table I and Fig. 1(a), although our original assignment was exactly the same as their old one. The intensity distribution alone cannot be considered as a reliable means of determining the vibrational numbering. However, at present, their new assignment has a plausible basis for explaining the actual band appearance, so it appears to be proper to accept their assignment until further evidence, such as isotope shift, becomes available.

For the revised numbering shown in Table I, the long wavelength heads (R_2) are well represented by the following equation calculated by the least-squares method:

$$(1)\quad \nu_{v'v''} = 43128.4+905.50(v'+\tfrac{1}{2})-11.69(v'+\tfrac{1}{2})^2+0.0114(v'+\tfrac{1}{2})^3 -1902.80(v''+\tfrac{1}{2})+14.92(v''+\tfrac{1}{2})^2.$$

TABLE I

Observed wavenumbers of the $^2\Pi_g$–$A\ ^2\Pi_u$ bands. Janin and d'Incan's values are for the band origins

v'	v''	R_1, R_2 heads (cm^{-1})	I	R_2 heads calc.	Janin and d'Incan (1958)
10	1	48598.4			
		538.5	3	48539.9	
9	1	47921.9			
		863.8	4	47864.8	
8	1	47224.4			
		166.9	5	47166.9	
7	1	46504.5			
		447.9	6	46446.3	
9	2	46077.9			
		020.8	6	46021.7	
8	2	45381.3			
		325.4	7	45323.8	45350.7[a]
10	3	44943.2			
		885.1	4	44883.5	
7	2	44661.6			
		605.0	10	44603.2	44629.9[a]
6	2	43915.9			
		857.5	7	43859.6	43886.6[a]
10	4	43161.9			
		102.1	2	43100.1	
5	2	43151.2			
		093.0	4	43092.2	43120.3[a]
7	3	42863.8			
		788.6	5	42789.9	42815.9[a]
4	2	42363.5			
		303.3	1	42303.7	42331
6	3	42105.8			
		045.4	5	42046.4	42072.7[a]
11	5	42053.7			
		41997.7	6	41998.9	
10	5	41399.3			
		343.3	1	41346.5	
5	3	41335.5			
		278.0	5	41279.9	41306.5[a]
9	5	40729.7			
		669.9	1	40671.3	40698.7[a]
4	3	40545.2			
		489.6	2	40490.4	40516.7[a]
8	5	40026.9			
		39972.0	2	39973.5	40000.0[a]
5	4	39552.4			
		495.1	2	39496.5	39524.0
7	5	39305.7			
		252.2	7	39252.8	39280.9
4	4	38768.6			
		707.2	3	38707.0	38734.6
8	6	—			
		38247.0	1	38249.7	
3	4	37947.5			
		893.3	3	37894.5	37920.2
5	5	37801.6			
		742.8	2	37742.9	
7	6	37586.5			
		528.2	6	37529.1	37557.1
4	5	—			
		36953.4	2	36953.4	36981.4
6	6	36844.9			
		786.5	6	36785.6	36813.7

TABLE I (*Concluded*)

v'	v''	R_1, R_2 heads (cm^{-1})	I	R_2 heads calc.	Janin and d'Incan (1958)
3	5	—			
		36140.5	2	36140.9	36167
5	6	36079.2			
		020.8	1	36019.1	
9	8	35649.4			
		591.0	15[b]	35589.6	
4	6	—			
		35232.5	0	35229.6	
6	7	35158.0			
		094.6	3	35091.6	35120
8	8	34951.5			
		894.0	4	34891.7	34921.0
5	7	34386.0			
		325.5	2	34325.2	
7	8	34227.9			
		170.5	10	34171.1	
7	9	32591.2			
		532.5	1	32536.8	32567

[a]Janin's unpublished data.
[b]Superimposed with another band.

For the old assignment we have the following equation:

$$(1') \quad \nu_{v'v''} = 45739.9+835.66(v'+\tfrac{1}{2})-11.60(v'+\tfrac{1}{2})^2+0.012(v'+\tfrac{1}{2})^3 -1902.81(v''+\tfrac{1}{2})+14.92(v''+\tfrac{1}{2})^2.$$

No attempt has been made to formulate the second heads (R_1) because of inaccurate measurements resulting from their weak appearance. However, the wavenumber differences of the two heads are fairly constant over the entire system, the average being $\Delta\nu = 57.8$ cm^{-1}. This indicates that the equation for the second heads will be practically identical with equation (1) or (1') except for a small difference in the electronic term.

As shown in Table II, the vibration constants for the present lower state

TABLE II

The vibrational constants of $^2\Pi_g$ and $A\,^2\Pi_u$ states. The values of Janin *et al.* are all based on the band origin, while the present values are from the head analysis

State		Present		Janin *et al.*			Douglas (1953) (cm^{-1})
		$v_0 = 0$[a] (cm^{-1})	$v_0 = 3$[b] (cm^{-1})	$v_0 = 0$[a] (1958) (cm^{-1})	$v_0 = 3$[b] (1959) (cm^{-1})	$v_0 = 3$[c] (cm^{-1})	
$^2\Pi_g$	ω_e	835.66	905.50	839.5	919.2	914.8	
	$\omega_e x_e$	11.60	11.69	12.75	13.80	13.13	
	$\omega_e y_e$	0.012	0.0114	0.116	0.117	0.083	
$A\,^2\Pi_u$	ω_e	1902.81	1902.80	1903.42	—	1903.6	1902.84
	$\omega_e x_e$	14.92	14.92	15.00	—	15.0	14.91

[a]Old assignment.
[b]Revised assignment.
[c]Janin's unpublished data.

agree very well with those of the $A\ ^2\Pi_u$ state of N_2^+. Therefore, it is certainly safe to assume that the lower state is the $A\ ^2\Pi_u$, which is the upper state of the Meinel bands. Judging from the band features the upper state is also a $^2\Pi$, and the two heads are formed by the R branches of subbands. In this type of transition, in general, the Q branch is much weaker than other main branches. With that assumption and the fact that the $A\ ^2\Pi_u$ is inverted, the upper state should be inverted also, and its spin separation turns out to be approximately 24 cm^{-1}, which is a little less than one third of the spin separation for the A-state. The ω_e of the upper state is much smaller than the ω_e of the A-state indicating that the former state is much less stable than the latter. The linear extrapolation of the $\Delta G_{v+\frac{1}{2}}$: v curve of the upper state gives 2.12 ev as a value for D_0 (1.81 ev for old assignment). Because this value results from a long extrapolation it is not necessarily an accurate one; however, interestingly enough, it gives 8.52 ev (8.54 ev for old assignment) as the dissociation limit of the upper state which is very close to the value of the dissociation energy, $D_0 = 8.66$ ev, of the ground state, $X\ ^2\Sigma_g^+$, of N_2^+.

DISCUSSION

As mentioned earlier, only a mixture of N_2 with Ne is suitable for the production of the bands. Furthermore, a condensed discharge will produce these bands with much more intensity than an uncondensed discharge will. Also, when the bands are produced, strong C–X bands of N_2^+ always appear at the same time while the N_2 bands, which usually appear in the same region, are almost gone. These observations establish quite firmly that the bands belong to N_2^+ and not to N_2.

The energy level diagram of N_2^+ is shown in Fig. 2 together with potential curves. Except for the state $^2\Pi_g$, the rest of the curves have been duplicated from Gilmore (private communication). As stated previously, the upper state, $^2\Pi_g$, of the present bands very probably dissociates at the same dissociation limit with the ground state whose dissociation products are $N(2p^3\ ^4S) + N^+(2p^2\ ^3P)$. In addition to the three known states, $X\ ^2\Sigma_g^+$, $A\ ^2\Pi_u$, $B\ ^2\Sigma_u^+$, nine more states are predicted from these products: $^2\Pi_g$, $^4\Sigma_{u,g}^+$, $^4\Pi_{u,g}$, $^6\Sigma_{u,g}^+$, and $^6\Pi_{u,g}$. However, according to Mulliken's predictions (1957) these additional states are all repulsive, although he did not mention their degree of instability. In approximately the same energy region, he also predicted two stable states $^4\Sigma_u^+$ ($T_{00} = 175{,}000\ cm^{-1} = 21.7$ ev)* and $^4\Delta_u$ ($T_{00} = 190{,}000\ cm^{-1} = 23.6$ ev),* both of which arise from the dissociation products $N(2p^3\ ^2D) + N^+(2p^2\ ^3P)$.† However, it appears obvious that neither of these two states could be the upper state of the present bands although one of them, $^4\Sigma_u^+$, has energy which is fairly close to that of the present upper state. The only possible explanation is that the upper state has to be the $^2\Pi_g$, which arises from the products, $N(^4S) + N^+(^3P)$, mentioned above. This explanation disagrees with Mulliken's prediction; however, on the other hand, the state is considerably less stable ($D_0 \simeq 2.1$ ev) than other known states.

The ionization energy of Ne is 21.47 ev, which is slightly below the energy

*The energy measured from the ground state of N_2.
†Gilmore's state $^4\Sigma_u^+$ (see Fig. 2) dissociates to $N(^4S) + N^+(^3P)$.

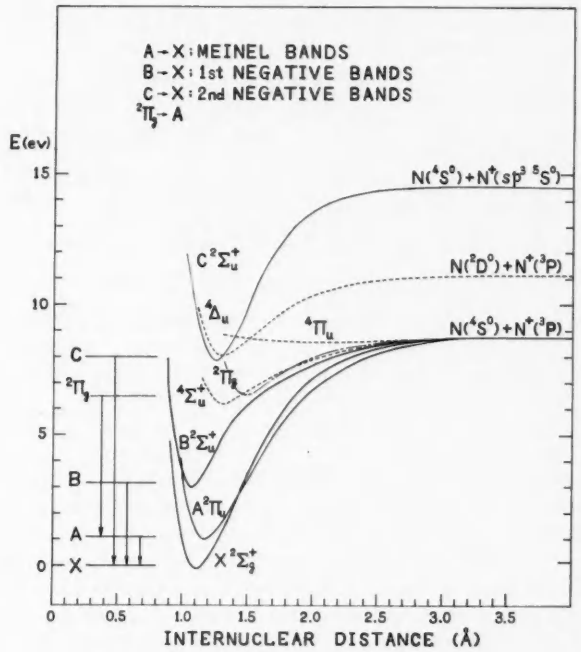

FIG. 2. Energy levels and potential curves of N_2^+.

of the present upper state. Apparently, the excitation of the bands occurs in a collision between Ne^+ and N_2. This is very similar to the process for the excitation of the C–X bands by He^+ as suggested by Watson and Koontz (1934) and Setlow (1948). The ionization energy of He, 24.580 ev, is greater than the dissociation limit, 24.24 ev, represented by the products $N(^4S)+N^+(^3P)$ and this is the reason why the present bands were not excited in a He atmosphere, although the strong C–X bands appeared with an intensity anomaly in $v' = 3$ (Douglas 1952; Tanaka 1953; Wilkinson 1956; Carroll 1959).

Janin *et al.* (Grandmontagne *et al.* 1959) stated that the absence of the $v' = 0$, 1, and 2 progressions on their plates was partly due to a selective excitation and partly due to superposition of these bands with other bands in the same system. As mentioned before, the ionization potential of Ne is slightly below the $v' = 0$ level and there is no state in Ne which may cause selective excitation of the present bands at $v' = 3$. As for their second reason, an attempt was made to identify the bands belonging to the progression of $v' = 0$, 1, and 2. Some of the bands seemed to be present (see Table III); however, they were so weak that we cannot be sure of their identification. For reference, the wavenumbers of these are listed in Table III together with some others.

TABLE III

Observed wavenumbers of uncertain band heads

v'	v''	R_1, R_2 heads (cm^{-1})	I	R_2 heads calc.
10	0	—		
		50409.3	0	50412.9
12	2	48031.9		
		47981.2	0	47979.1
12	5	—		
		42625.9	5[a]	42628.8
12	8	37605.3		
		37550.8	1	37547.0
2	5	—		
		35303.9	0	35305.2
1	5	34498.6		
		34444.2	0	34446.3
3	6	—		
		34414.6	0	34417.6
3	7	32770.1		32723.2
(or 1	6)	32718.1	0	(or 32722.6)

[a]Superimposed with another band.

It might be interesting to take note of the difference in the relative intensity distribution of the C–X bands resulting from the two methods of excitation: in a He atmosphere and in a Ne atmosphere. The two spectra are compared in Fig. 1(*b*), which shows the difference more clearly than is shown in the paper by Takamine and his co-workers (1939). According to the mechanism proposed by them, the bands which originate in the level $v' = 1$ must be abnormally strong in the case of Ne atmosphere. Actually, there is no conspicuous anomaly in the spectrum, and the distribution of intensity appeared normal to us. The C–X bands can also be excited in a condensed discharge of pure N_2. Although the bands are very weak in this case, the distribution of intensity is almost exactly the same as that when N_2 is excited in a Ne atmosphere. These observations lead us to believe that the excitation mechanism proposed by Takamine and his co-workers is actually not the case. Further work concerning this problem is now in progress and additional information will appear in the near future.

ACKNOWLEDGMENT

We wish to express our appreciation to Professor Mulliken for urging us to publish our results concerning these new emission bands of N_2^+ even though Janin and his co-workers have already published reports dealing with the same bands.

REFERENCES

CARROLL, P. K. 1959. Can. J. Phys. **37**, 880.
DALBY, F. W. and DOUGLAS, A. E. 1951. Phys. Rev. **84**, 843.
DOUGLAS, A. E. 1952. Can. J. Phys. **30**, 302.
——— 1953. Astrophys. J. **117**, 380.
GILMORE, F. R. Private communication.
GRANDMONTAGNE, R. 1957. Compt. rend. acad. sci. (Paris), **244**, 2586.
——— 1958. J. phys. radium, **19**, 151.

GRANDMONTAGNE, R., D'INCAN, J., and JANIN, J. 1959. Compt. rend. soc. franc. phys. (Paris), p. 59.
JANIN, J. and D'INCAN, J. 1958. Compt. rend. acad. sci. (Paris), **246**, 3436.
——— 1959. Rev. universelle mines, 9e Serie, **XV**, 1.
MEINEL, A. B. 1950. Astrophys. J. **112**, 562.
MULLIKEN, R. S. 1932. Revs. Modern Phys. **4**, 1.
——— 1957. The threshold of space (Pergamon Press, New York), p. 169.
PILLOW, M. E. 1951. Proc. Phys. Soc. (A), **64**, 772.
SETLOW, R. B. 1948. Phys. Rev. **74**, 153.
TAKAMINE, T., SUGA, T., and TANAKA, Y. 1939. Sci. Papers Inst. Phys. Chem. Research (Tokyo), **36**, 437.
TANAKA, Y. 1953. J. Chem. Phys. **21**, 1402.
WATSON, W. W. and KOONTZ, P. G. 1934. Phys. Rev. **46**, 32.
WILKINSON, P. G. 1956. Can. J. Phys. **34**, 250.
WORLEY, R. E. 1953. Phys. Rev. **89**, 863.

NOTE ADDED IN PROOF

Our recent study of the isotope shift in the $^2\Pi_g - A\ ^2\Pi_u$ bands substantiated the fact that the vibrational numbering as revised by Janin *et al.* is correct. An analysis of the $^2\Pi_g - A\ ^2\Pi_u$ bands of $(N_2^{16})^+$ will be presented in a separate paper.

SELF-DIFFUSION IN BODY-CENTERED CUBIC ZIRCONIUM[1]

G. KIDSON AND J. MCGURN

ABSTRACT

Self-diffusion coefficients of crystal-bar zirconium have been measured between 1500° C and 1100° C, using radioactive Zr^{95} as a tracer. The results may be represented by

$$D = 2.4\times10^{-4}\exp-\left[\frac{30{,}100}{RT}\right]\text{cm}^2/\text{sec}.$$

The pre-exponential factor is about three orders of magnitude smaller than that measured in most close-packed systems and the activation energy about one-half that anticipated from an empirical correlation with the melting point. The results, however, are similar to those of a few other recently studied body-centered cubic (BCC) systems, and agree quantitatively with work in the Soviet Union on zirconium. There is considerable evidence that the diffusion process occurs via vacant lattice sites.

1. INTRODUCTION

It is well established that the self-diffusion coefficients of pure metals have a simple Arrhenius type temperature dependence of the form

$$D = D_0\exp-\left[\frac{Q}{RT}\right], \tag{1}$$

where D_0 and Q are temperature-independent parameters characteristic of the particular system studied. It has been noted frequently that a rather good correlation exists between the activation energy Q and the absolute melting temperature for most of the metals studied. (See, for example, Kidson and Ross 1958.) It has likewise been pointed out that the values of D_0 usually lie in the range of 0.1 to 10 cm^2/sec (LeClaire 1953). These two observations have made it possible to predict values of the self-diffusion coefficients for systems in which no direct measurements are available.

Of the various models proposed to account for the fundamental diffusion process, the two most discussed are the vacancy and the ring mechanisms. The latter, proposed by Zener (1950), is a generalization of the simple interchange of two neighboring atoms to a group or ring of n atoms which move synchronously to produce the effect of a jump for any particular member of the ring. While the resulting expressions for D for the two mechanisms are similar, and lead to equations of the form (1), a fundamental difference does exist. This became significant when Smigelskas and Kirkendall (1947) showed that the different rates of interdiffusion of two chemically distinct species can give rise to a measurable mass flow in the diffusion zone. The phenomenon is readily interpretable in terms of a vacancy mechanism, but it cannot be accounted for if a ring mechanism is operative. This conclusion, plus the very

[1]Manuscript received February 2, 1961.
Contribution from the Research Metallurgy Branch, Atomic Energy of Canada Limited, Chalk River, Ontario.
Issued as A.E.C.L. No. 1271.

considerable amount of supplementary evidence accumulated during the past decade, has led to a general acceptance of the vacancy model for at least the close-packed metal systems. The situation is not quite so well defined for BCC systems, but here again the ring mechanism cannot account for the observed "Kirkendall shifts".

Zener (1951) has suggested that, regardless of the particular model chosen, the restricted range of D_0 is in keeping with the thermodynamic requirement that the associated entropy of activation must be positive. During the past two years, however, results of diffusion measurements in a number of BCC systems have been reported that appear anomalous both in the fact that a negative entropy of activation is implied by the D_0 values, and that the activation energies are about one-half those expected on the basis of the empirical correlation with the melting points. These results are summarized in Table I.

TABLE I

Self-diffusion in body-centered cubic metals

Authors	Metal	D_0 (cm^2/sec)	Q observed (kcal/mole)	Q calculated (kcal/mole)
Adda and Kirianenko (1958)	γ Uranium	1.81×10^{-3}	27.5	49
Bochvar *et al.* (1958)	γ Uranium	1.17×10^{-3}	26.6	49
Rothman *et al.* (1959)	γ Uranium	2.33×10^{-3}	28.5	49
Mortlock and Tomlin (1959)*	Tracer Cr^{51} in β titanium	5×10^{-3}	35.3	73
Paxton and Gondolf (1959)	Chromium	10^{-4}	52.0	76

*Qualitatively similar results have been obtained recently for a series of dilute solutes in β Ti (Lidiard 1960).

An attempt to account for the low D_0 values has been made recently by Pound, Bitler, and Paxton (1961). In essence, they suggest that an additional factor must be incorporated into the previous expression for D_0 derived on the basis of absolute-reaction-rate theory. This factor takes into account the requirement that not only must a migrating atom possess sufficient energy in the direction of a jump, but also that its actual movement must be in that direction or very close to it in order that a successful jump can occur. That is to say, the components of its vibration in the plane perpendicular to the jump direction must be very small or zero.

This restriction gives rise to a new factor $[1/f_v]^{2n}$ where f_v is the Einstein partition function for vibration, and n is the number of atoms involved in the jump.

For a vacancy model, n was assumed equal to unity, and the effect was not significant. For a four-atom-ring model, however, n is 4, and the additional factor is large enough to account for the observed values of D_0 in the BCC systems. On this basis, Pound *et al.* conclude that a low D_0 in a BCC system is evidence for the ring mechanism being operative. They suggest that the large chemical concentration gradients present in the Kirkendall experiments could give rise to abnormally large vacancy concentrations, and as a result, the vacancy mechanism becomes dominant in these systems. The rather

extraordinarily low activation energies tabulated in Table I were not discussed.

In view of the considerable intrinsic interest in the problem, and the technological importance in reactor metallurgy, a study of self-diffusion in the BCC β phase of high-purity zirconium has been made. During the course of the present investigation, the authors became aware of similar studies reported by three Soviet groups, Borisov *et al.* (1958), Gruzin *et al.* (1958), and Lyashenko *et al.* (1959). Their results will be compared with the present work later.

2. EXPERIMENTAL PROCEDURES AND RESULTS

Three different techniques were used to measure the diffusion coefficient of zirconium as a function of temperature. The first of these was the basic sectioning technique described below. In view of the rather surprising results so obtained, two additional methods were employed as checks on the first. One of these avoided the possibility of so-called "short-circuit" effects, while the other was a sintering experiment designed to provide information concerning the mechanism of the diffusion process.

Experimental Procedure. I

Crystal-bar zirconium was obtained from the Foote Mineral Company. The analysis is given in Table II. Buttons weighing approximately 80 grams were

TABLE II

Analysis of crystal-bar zirconium*

Si	<0.005%	Ni	<0.005%
Al	<0.005%	Ca	0.02%
Mg	<0.005%	Cu	Not detected
Fe	<0.005%	Hf/Zr	<0.05%
Ti	<0.005%		

*Received from Foote Mineral Company, Lot No. 810-8.

prepared by arc-melting sections of the crystal bar in an argon atmosphere, using a tungsten electrode.* Specimen disks ranging from $\frac{3}{8}$ in. to $\frac{1}{2}$ in. in diameter and about $\frac{3}{16}$ in. thick were machined from the buttons, cleaned in a chemical dip, and annealed at 1100° C for 4 hours in a dynamic vacuum of 3×10^{-6} mm, to remove any absorbed hydrogen. One face of each disk was carefully polished mechanically and chemically, using a 50% H_2O, 45% HNO_3, 5% HF solution.

The radioactive tracer isotope Zr^{95} was prepared by irradiating high purity zirconium wire in the NRX reactor at 1.5×10^{13} n/cm^2 sec for 14 days. The use of the Zr^{95} isotope was complicated by the presence of the radioactive daughter decay product Nb^{95}, since γ-ray energies of both species are so close as to make discrimination between the two impossible. The contribution of the Nb^{95} to the total activity measured was calculated. The results are shown graphically in Fig. 1. It was concluded that chemical separation of the Nb^{95} could be avoided justifiably provided the diffusion anneals were completed within 4 days of the removal of the irradiated zirconium from the reactor. This precaution was observed in all of the runs in this work.

*Subsequent spectral analysis gave no indication of tungsten contamination.

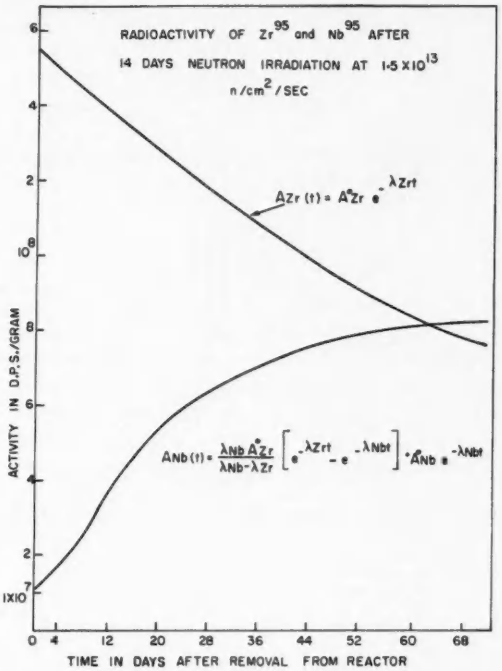

FIG. 1. Calculated curves for the radioactivity of Zr^{95} and Nb^{95} after 14 days' neutron irradiation at 1.5×10^{13} n/cm² sec.

A thin layer of the tracer metal was evaporated onto one face of each of the two disks, using the apparatus shown in Fig. 2. The diffusion specimens were annealed in pairs, in a "Globar" furnace and a dynamic vacuum of 2×10^{-6} mm of Hg. In order to avoid both contamination of the specimens and loss of the radioactive deposit by evaporation, the disks were placed with active faces close together in a pure zirconium "gettering boat". The boat was held in the cold portion of the annealing tube until the furnace was up to temperature, and then pulled into the hot zone to reduce the heating time to a minimum. The reverse procedure was followed at the end of the anneal. A typical heating and cooling curve is shown in Fig. 3 from which appropriate corrections to the annealing times were made.

Temperatures were controlled to $\pm 3°$ C and measured to $\pm 2°$ C, using a Pt – Pt Rh thermocouple.

Following the diffusion anneal, thin sections accurately parallel to the face of the specimen were removed, using a special lathe device. Surface diffusion effects were avoided in the usual way by first reducing the diameter of the specimen by 0.030 inch. The turnings from each section were collected in bottles, weighed, and dissolved in a solution of 45 parts HNO_3, 50 parts H_2O, 5 parts HF. The γ-ray activity was measured over the 0.75-Mev peak

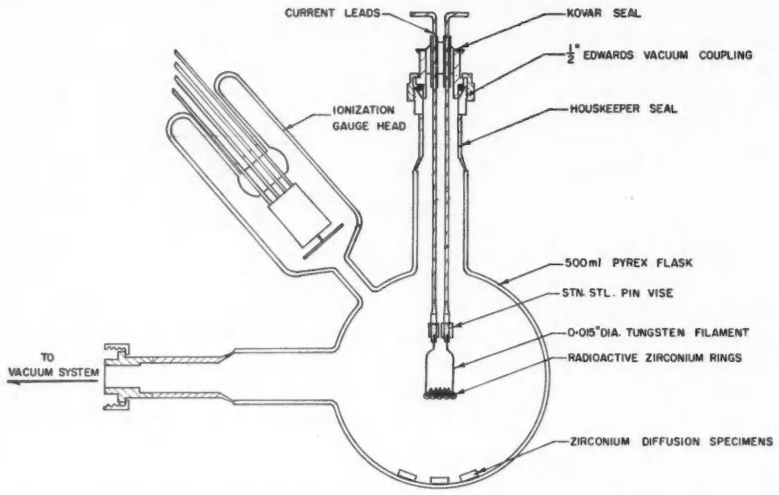

FIG. 2. A schematic drawing of the apparatus used for the evaporation of radioactive zirconium onto the diffusion specimens.

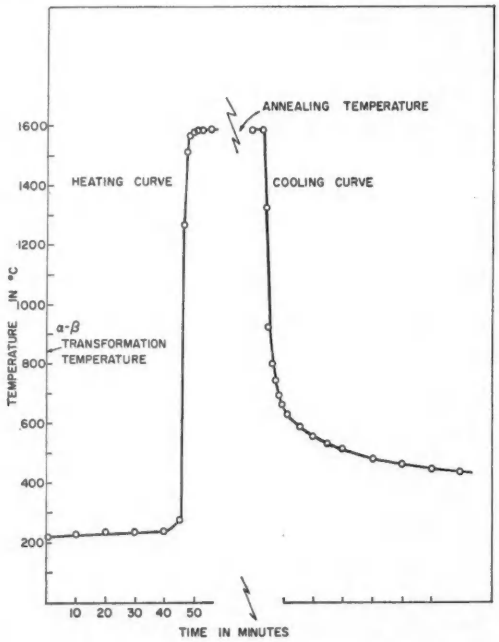

FIG. 3. A typical heating and cooling curve of the diffusion specimens.

using a well-type crystal scintillation counter and a single-channel analyzer. Appropriate corrections for background and decay were applied, and sufficient counts taken to ensure a statistical error of less than 1%.

3. RESULTS

If the diffusion paths of the atoms were through the lattice proper, as opposed to the grain boundaries, the resulting distribution should be given by

$$C(x,t) = \frac{S_0}{A\sqrt{\pi Dt}} \exp -\left[\frac{x^2}{4Dt}\right] \tag{2}$$

where C is the concentration of the diffusing species (in this case, the γ-ray activity of Zr^{95} in counts/mg), S_0 is the total Zr^{95} deposited, D the diffusion coefficient, t the annealing time, x the penetration distance, and A the specimen cross-sectional area. All of the runs carried out exhibited close linearity in a plot of log C vs. x^2, a typical example being shown in Fig. 4 for a specimen annealed at 1210° C for 3 hours.

The results are summarized in Table III, and a plot of log D vs. $1/T$° K is

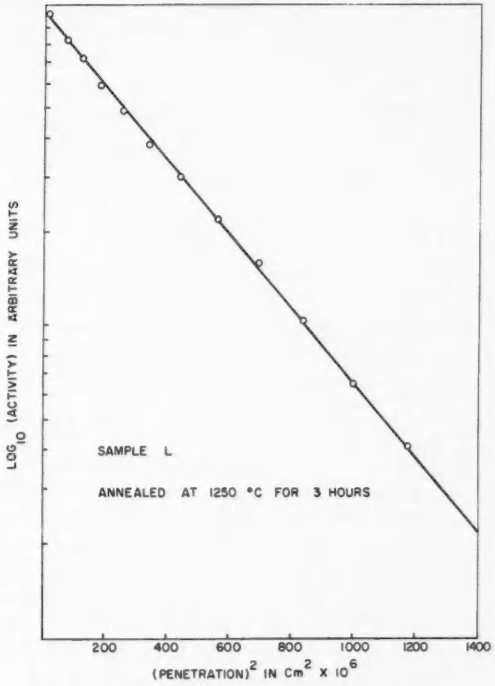

FIG. 4. A typical penetration vs. radioactivity plot.

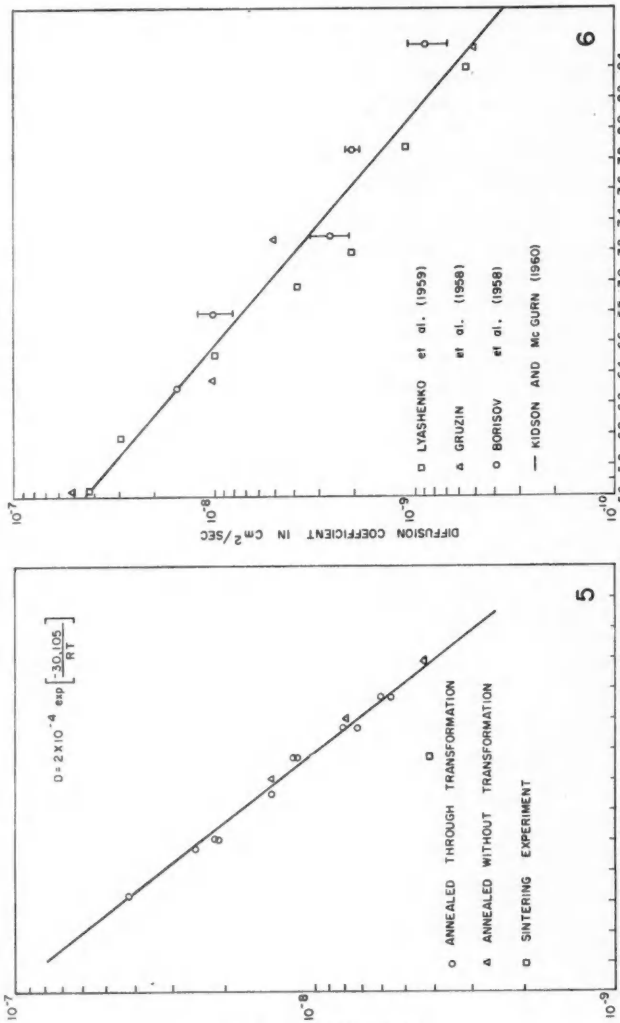

FIG. 5. A summary of all the diffusion measurements plotted as $\log_{10} D$ vs. $1/T$. Open circles denote results from the sectioning technique, triangles from measurements involving no structure transformation prior to diffusion, and the square from the sintering experiment.

FIG. 6. A comparison of results obtained by U.S.S.R. workers with those of the authors.

TABLE III

Summary of diffusion measurements

Spec. No.	Annealing temp. °K	D in cm²/sec
H	1503° C	4.2×10^{-8}
F	1410° C	2.5×10^{-8}
O	1362° C	2.2×10^{-8}
B	1362° C	2.1×10^{-8}
K	1310° C	1.4×10^{-8}
G	1251	1.1×10^{-8}
E	1251	1.2×10^{-8}
L	1210	7.3×10^{-9}
A	1210	7.3×10^{-9}
J	1168	6.1×10^{-9}
I	1168	5.7×10^{-9}

shown in Fig. 5 by the points in open circles. D_0 and Q were determined by a least-squares fit to these data giving

$$D = 2.4\times10^{-4}\exp-\left[\frac{30{,}100}{RT}\right]\text{cm}^2/\text{sec}. \tag{3}$$

It is apparent that here again D_0 lies well outside the usual range of values, and the activation energy Q is somewhat less than one-half the 70 kcal/mole anticipated on the basis of the melting-point correlation (pure zirconium melts at 2118° K).

The results are compared with those of the Soviet workers by drawing the line of best fit to the present data through the assembled points of the former. See Fig. 6. In spite of some scatter, it would appear that the anomalous D_0 and Q values are substantiated.

4. EXPERIMENTAL PROCEDURE II

Gruzin (1958) pointed out that all the zirconium specimens necessarily pass through the CPH α to BCC β phase change during the heating up to the annealing temperature. The resulting β grains could therefore contain either a high dislocation density or internal interfaces, either of which would provide short-circuit paths for the diffusion, and hence account for the observed D_0 and Q values.

To check this possibility, the apparatus shown in Fig. 7 was constructed. An inactive zirconium specimen was placed in the small tungsten-wound furnace as indicated in the offset diagram. The furnace and specimen were brought up to the annealing temperature in the β phase and held there for $\frac{1}{2}$ to 1 hour, again in a vacuum of about 2×10^{-6} mm Hg.

This promoted the growth of large perfect β grains. (In some runs, as few as two or three grains were contained in disks of about $\frac{1}{2}$ in. diameter.) The molybdenum radiation cover and zirconium specimen cover were then raised and swung out of the way, meanwhile maintaining the specimen and furnace at temperature. Finally, a layer of radioactive Zr^{95} was evaporated from the tungsten filament onto the specimen, the cover replaced, and the diffusion

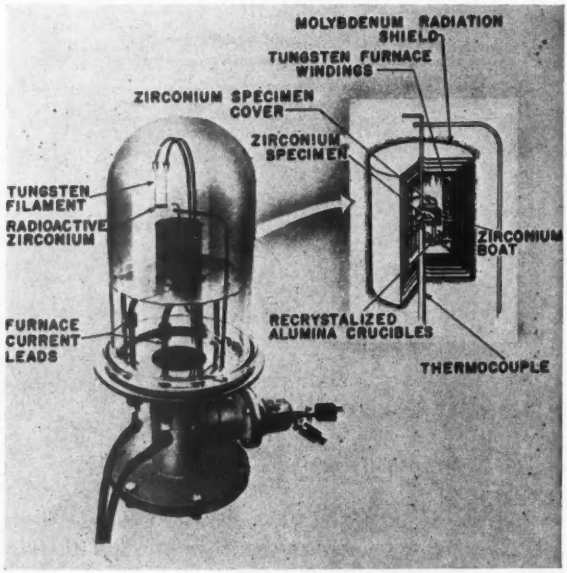

FIG. 7. The apparatus used for the measurements on samples in which no structural transformation took place prior to the diffusion anneal.

anneal completed. Three runs at temperatures between 1280° C and 1100° C were thus made, and the diffusion coefficients determined as described in Experimental Procedure I. The results are plotted in Fig. 5 as triangles. Again the previous data are confirmed.

5. DISCUSSION

From the foregoing it seems safe to conclude that there exists a real discrepancy between the measured diffusion parameters in zirconium and similar BCC systems and those anticipated from empirical correlations or theoretical models (excluding that of Pound *et al.*). The question to be answered is whether this discrepancy provides a clue to a specific mechanism as Pound *et al.* suggest, or perhaps a modification of the vacancy model, or whether there are extraneous factors common to all of these measurements leading to consistent but nevertheless not truly representative results of volume diffusion. Such a common factor, for example, could be the high reactivity of Zr, U, Ti, and Cr, which makes it difficult to prepare specimens of a purity comparable to, say, the noble metals. In the present study, the use of a zirconium "gettering" boat and high-vacuum annealing was considered necessary since zirconium can absorb up to 25 atomic per cent oxygen substitutionally. The fact that the specimens were easily machined following an anneal, whereas the gettering boats were frequently quite hard, led us to believe the contamination of the former was kept very low.

As mentioned previously, Pound and his co-workers maintain that, while the Kirkendall experiments exclude the possibility of a ring mechanism operating in BCC binary systems, this conclusion does not necessarily hold true for the pure metals. Fortunately, however, the sintering experiments described by Kuczynski (1950) provide a similar critical test of the ring mechanism for one-component systems.

Kuczynski established that the transfer of mass during carefully controlled sintering experiments on silver wires can be accounted for in terms of volume diffusion, involving the flow of vacancies. The relationship between the diffusion coefficient D, the surface energy γ, and the annealing time t is given by

$$D = \frac{3kTx^5}{80\pi a^2\delta^3\gamma t} \tag{4}$$

where x is the half width of the sintered neck between two wires of diameter a, δ is the lattice constant, T the absolute temperature, and k is Boltzmann's constant.

If the diffusion of the atoms takes place via a ring mechanism, no appreciable sintering should occur. Figure 8 shows a cross section of a bundle of 0.010 in. diameter zirconium wires wound on a zirconium thimble and sintered at 1200° C for 22 hours. Assuming a value of 1000 dynes/cm² for the surface energy γ, and averaging the neck widths over 100 measurements, one obtains a calculated value of D in order-of-magnitude agreement with the previous

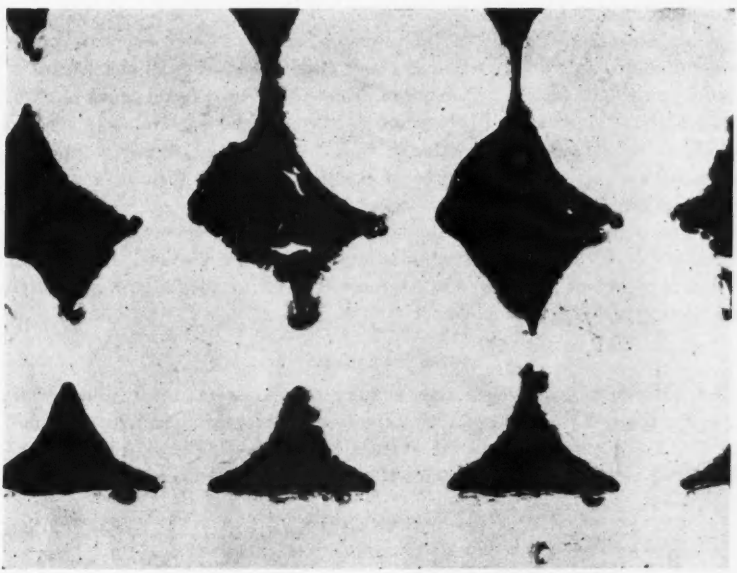

FIG. 8. A cross section of a sintered bundle of zirconium wires, indicating the considerable degree of sintering occurring.

work, as seen in Fig. 5. While this is to some extent ambiguous in view of the assumed γ, the value for the latter is not likely to be more than $\pm 30\%$ in error, as can be seen by comparing it with those of other similar metals for which γ has been measured.

This result, together with the observed Kirkendall shift in the BCC phase of U–Zr (Adda *et al.* 1959) lends strong support to the vacancy model.

A further piece of evidence again pointing toward a vacancy mechanism is given by the observation of rapid pore formation in zirconium when bombarded with monoenergetic α particles and annealed in the β phase. This effect, described in detail by Barnes (1959) and Ells and Evans (1959) for copper and aluminum, is attributed to the clustering of the injected helium atoms, with a subsequent migration of vacancies to the clusters, to form observable pores.

Dr. Ells, who made the observations on the zirconium, pointed out that the pore formation was very rapid, consistent with the low activation energy of self-diffusion found in the present work.

CONCLUSIONS

On the basis of the foregoing, it appears that the ring mechanism must be excluded as an explanation of the observed results for the BCC phase of zirconium. While there exists the possibility of impurity effects lowering both D_0 and Q, it is considered unlikely that they would be large enough to account for the observations. We conclude that the diffusion process involves vacant lattice sites as in the close-packed systems. If the parameters obtained in this study are representative of volume diffusion, it may be necessary to consider the detailed atomic configuration in the immediate vicinity of the vacant site in order to account for the departure of D_0 from the more usual range of values. In particular, the extent of relaxation of the neighboring atoms is generally thought to be considerably greater in BCC lattices than in, say, copper, and this could lead to a higher degree of co-operative motion being required to produce a jump.

Until such time as a proper calculation of Q for these systems can be made, the "abnormality" of the activation energy cannot be assessed. It is felt that this latter aspect of the results is the more interesting of the two, and further work along these lines is looked for.

ACKNOWLEDGMENTS

The authors acknowledge with thanks the co-operation and interest of many members of the Research Metallurgy and Research Chemistry Branches of A.E.C.L. In particular, we are grateful to Dr. G. R. Piercy for stimulating discussions and to Dr. J. Davies for the generous use of his counting facilities.

REFERENCES

ADDA, A. and KIRIANENKO, A. 1958. Compt. rend. **247**, 744.
BARNES, R. S. 1959. A.E.R.E.-R 3162.
BOCHVAR, A. A., KUZNETSOVA, V. G., and SERGEEV, V. S. 1958. A/Conf. 15/P/2306.
BORISOV, E. V., GODIN, YU. G., GRUZIN, P. L., EUSTYUKIN, A. I., and EMELYANOV, V. S. 1958. Metallurgy and Metallography (All Union Conf. on the Use of Isotopes and Radiation, Moscow), p. 291.

ELLS, C. E. and EVANS, W. 1959. A.E.C.L. Report No. CR Met 863.
GRUZIN, P. L., EMELYANOV, V. S., RYABOVA, G. G., and FEDOROV, G. B. 1958. A/Conf. P/2526 U.S.S.R., p. 187.
KIDSON, G. V. and ROSS, R. V. 1958. Radioisotopes in scientific research, Vol. 1, *edited by* R. C. Extermann (Pergamon Press), p. 185.
KUCZYNSKI, G. C. 1950. J. Appl. Phys. **21** (7), 632.
LECLAIRE, A. D. 1953. Progr. Metal Phys. **4**, 305.
LIDIARD, A. 1960. Private communication.
LYASHENKO, V., BIKOV, B., and PAVLINOV, L. 1959. Phys. Metals and Metallog. **7** (3), 362.
MORTLOCK, A. and TOMLIN, D. 1959. Phil. Mag. **4** (41), 628.
PAXTON, H. and GONDOLF, E. 1959. Arch. Eisenhüttenw. **30**, 55.
POUND, G., BITLER, W., and PAXTON, H. 1961. Phil. Mag. **6** (64), 473.
ROTHMAN, S., LLOYD, L. T., WEIL, R., and HARKNESS, A. L. 1959. ANL-5971.
SMIGELSKAS, A. and KIRKENDALL, E. 1947. Trans. AIME, **171**, 130.
ZENER, C. 1950. Acta Cryst. **3**, 346.
——— 1951. J. Appl. Phys. **22**, 372.

ANGULAR DISTRIBUTION OF FAST PHOTONEUTRONS[1]

R. G. Baker and K. G. McNeill

ABSTRACT

The angular distributions and the yields of the high-energy neutrons emitted in photodisintegration have been studied by silicon detectors (25 elements) and aluminum detectors (6 elements). With the silicon detectors systematic variations are apparent in the coefficient a_2 of $W(\theta) = a_0(P_0+a_2P_2)$, and these variations are interpreted in terms of the Wilkinson shell model of photonuclear reactions.

INTRODUCTION

In recent years the Wilkinson picture of the nuclear photoprocess in the region of the "giant resonance" has achieved considerable success in explaining many of the phenomena connected with this process (Wilkinson 1956, 1959).

In this picture, the absorption process is associated primarily with the excitation of levels which correspond to single-particle excitations. The disintegration process results from the decay of the excited single-particle state which proceeds either by direct emission of the particle, *or* by reabsorption of the excited particle into the nucleus and eventual de-excitation of the system by allowable competing processes. In principle, the former process is much the less complicated of the two, and definite correlations may be expected, say, between the angular distribution of the emitted nucleon and the initial single-particle state of the nucleus–photon system. On the other hand, the great internucleon interactions of the latter process, described by a statistical or evaporation model, smears out any definite angular correlations and the disintegration products would be expected to have, and do have at least for neutrons, an isotropic distribution. One also expects a differentiation of the decay mode in terms of the energy distribution of the emitted nucleons. Directly emitted nucleons leave the residual nucleus at or near the ground state and carry all or most of the available energy, while those emitted by the statistical process have a typical evaporation spectrum.

Focussing one's attention on the photoneutron cross section in the region of the maximum of the "giant resonance" at a gamma-ray energy E_m, and assuming that most of the single-particle excitations occur for those neutrons with the least binding energy (E_t), one expects the directly emitted neutrons to have an energy in the neighborhood of $E_m - E_t \simeq 6$–7 Mev, while those emitted by the evaporation process will have a Maxwellian distribution characterized by the nuclear temperature. For a typical nuclear temperature of 0.75 Mev, characteristic of the heavy elements and independent of the excitation energy (Gugelot 1951; Graves and Rosen 1953), less than 1% of the evaporation neutrons would have energies greater than 5 Mev, and in the

[1]Manuscript received February 3, 1961.
Contribution from the Physics Division, Ontario Cancer Institute, and the Physics Department, University of Toronto, Toronto, Ontario.

neighborhood of 10% would have energies greater than 3 Mev. Thus, a simple threshold detector should serve to differentiate the direct interaction spectrum from the evaporation spectrum.

While there has been a considerable amount of work already carried out in this field, the results of different workers are not in agreement. The disagreement may be attributed largely to an ill-defined detector threshold and variations in spectral sensitivity, both of which vary widely with the experimental technique. However, the experimental results obtained for the angular distribution can always be expressed in terms of an expansion in Legendre polynomials,

$$W(\theta) = a_0 \sum_{n=1}^{\infty} (1 + a_n P_n(\cos\theta))$$

where only the coefficient a_2 makes an appreciable contribution, indicating a process consistent with a mainly dipole type of interaction, although sometimes the possible addition of a significant a_1 term arises from dipole–quadrupole interference. Table I contains some of these results, with notes as to

TABLE I

Element	$-a_2$	E_0 (Mev)	$(E_n)_{min}$ (Mev)	Method	Reference
Pb	<0.07	22		ZnS	Geller *et al.* (1954)
	0.40	65	5	ZnS	Johansson (1955)
	0.05±0.05	70		ZnS	Dixon (1955)
	0.17±0.06	17		ZnS	Asada *et al.* (1958)
	0.36±0.04	22	3	Al(n,p)	Price (1954)
	0.13	23	4	Emulsion	Toms and Stephens (1957)
Bi	0.40±0.04	22	3	Al(n,p)	Price (1954)
	0.31±0.05	30	3	Al(n,p)	Ferrero *et al.* (1956)
	0.38±0.05	30	5	Si(n,p)	Ferrero *et al.* (1956)
	0.57	19	4	Emulsion	Zatsepina *et al.* (1957)
Ag	<0.07	22		ZnS	Geller *et al.* (1954)
	0.18±0.06	22	3	Al(n,p)	Price (1954)
Cu	<0.07	22		ZnS	Geller *et al.* (1954)
	0.13±0.09	70		ZnS	Dixon (1955)
	0.19±0.04	22		Al(n,p)	Price (1954)
Ta	0.37	65	5	ZnS	Johansson (1955)
Al	0.43	65	5	ZnS	Johansson (1955)
	0.19±0.15	70		ZnS	Dixon (1955)
Fe	0.06±0.17	70		ZnS	Dixon (1955)

the method used in detection of the direct (fast) photoneutrons, the maximum photon energy of the bremsstrahlung spectrum, and an estimate of the detector threshold.

The present paper reports results of measurements made using silicon and aluminum threshold detectors on a series of 25 elements in the medium- and heavy-weight parts of the periodic table. Some preliminary results of this work have been reported previously (Baker and McNeill 1960).

EXPERIMENTAL TECHNIQUE

In the present work, use has been made of Si^{28} and Al^{27} threshold detectors. For both these nuclides, the (n,p) reaction is endoergic requiring neutron energies of greater than 3.9 Mev and 1.8 Mev respectively, and for both elements the end products of the reactions are beta radioactive with half-lives of 2.3 minutes and 9.5 minutes respectively. Owing to the small cross section near threshold, effectively the silicon detector responds only to neutrons of energy greater than 5 Mev, while the aluminum detector responds to those with energies greater than 3 Mev. Thus, the response of these detectors could be expected to show the characteristics of the "direct interaction" spectrum provided it constituted an appreciable fraction of the total spectrum, e.g. more than 1% of the total for the case of the silicon detector.

The aluminum detector is also activated by the (n,γ) reaction which is exoergic, and has a cross section with a well-defined $E_n^{-1/2}$ dependence. The reaction product, Al^{28}, is beta active with a half-life of 2.3 minutes. This activity will reveal the characteristics of the low-energy or evaporation spectrum, while in the same detector the Al^{27} (n,p) Mg^{27} reaction, with a half-life of 9.5 minutes, shows the characteristics of the direct emission spectrum. Other possible competing reactions, such as (γ,n) or (n,α), which all have products with half-lives of the order of a few seconds or many hours, are easily eliminated or dealt with in the analysis of the activation data.

In the silicon detector, possible interfering activities are the (γ,p) reactions in Si^{29} and Si^{30} giving rise to half-lives of 2.3 minutes and 6.6 minutes, and the (n,α) reaction in Si^{30} giving rise to a 9.5-minute activity. Compton scattered photons from the target would have energies below the (γ,p) threshold for all practical angles of observation and the 9.5-minute Mg^{27} produced by $Si^{30}(n,\alpha)$ could in principle be distinguished by its half-life. However, in practice a pure 2.3-minute activity attributed to $Si^{28}(n,p)Al^{28}$ was found in all cases for the silicon detector.

Each detector was in the form of a cylindrical annulus of inside diameter $\frac{3}{4}$ in. designed to slip over a Victoreen 1B85 Geiger counter in a lead castle. The aluminum detectors had $\frac{1}{8}$-in. walls and were 6 cm in height. The silicon detectors were formed from powdered silicon packed in an annulus formed of 0.002-in. Mylar film to give a $\frac{1}{4}$-in. wall and 7-cm height.

A diagram of the experimental arrangement is shown in Fig. 1. The bremsstrahlung beam from the Allis-Chalmers Betatron at the Ontario Cancer Institute was collimated by lead and iron. Extraneous neutrons were moderated and absorbed by paraffin and cadmium. A jig held the target samples in the center of the beam at 120 centimeters from the bremsstrahlung source. Detectors could be placed in shielded positions at 10 centimeters from the samples and at 30°, 60°, 90°, 120°, and 150° to the direction of the incident beam.

"No sample background", due mainly to fast neutrons generated in the shielding, was always appreciable, and was sampled before, during, and after a series of runs.

Throughout the experiments, the betatron energy was maintained within limits of ±0.1 Mev of a calibrated value of 22 Mev. The absolute magnitude

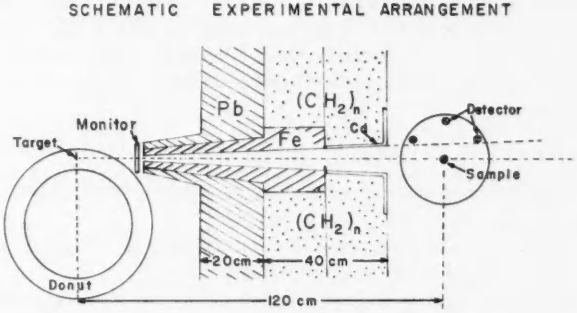

FIG. 1. Experimental arrangement for the detection of the fast photoneutrons, showing the shielding and collimation.

of the betatron energy was determined by measuring the peak voltage induced in a leg turn of the magnet at the thresholds for the (γ,n) reactions in Cu^{63} and C^{12} taken as 10.73 and 18.73 Mev respectively (Spicer 1955; Tobin *et al.* 1958). Since the relation between peak voltage and peak bremsstrahlung energy is linear (McElhinney *et al.* 1949), the two points suffice for calibration.

The γ-ray flux from the betatron was monitored by a built-in ionization chamber situated in the direct beam immediately in front of the collimator. This chamber was calibrated against a standard Victoreen chamber with a 5-cm lucite wall placed at the sample position. Corrections were made for the beam attenuation in the sample and for the angular variation of intensity of the beam.

The center of gravity for the production of neutrons, taking into account the attenuation of the beam in the target samples, was calculated and the samples so placed that this point was at the center of the angular distribution jig. For cylindrical lead and bismuth samples of 3 cm diameter, the displacement from the center of mass was 3.5 mm.

The finite sample size and consequent self-scattering of neutrons will tend to reduce the anisotropy produced by the nuclear reactions, but as this effect has been calculated to produce less than a 10% attenuation in the distribution coefficients for the worst case, no further account has been taken of it.

During a run, the samples were irradiated for a given duration at a constant exposure dose rate, and then the detectors removed immediately to a counting room. The counting data together with the irradiation data give the relative activation due to $Al(n,p)$ and $Al(n,\gamma)$ reactions or the $Si(n,p)$ reaction as a function of target material and angle of observation. After normalization to a standard sample and exposure of 100 r/minute mole, the saturated yields for each element were fitted to the Legendre polynomial $Y(\theta) = a_0[1+a_1P_1(\cos\theta) + a_2P_2(\cos\theta)]$. The average observed yield factor a_0 is related to the average absolute neutron flux produced by the sample by an efficiency factor dependent on the neutron reaction cross section and on a geometry factor. The detection efficiency factors for the two types of detectors were found using a standard

Ra–Be neutron source obtained from Atomic Energy of Canada Limited, by considering the neutron spectrum from this source (Hill 1952; Teucher 1949) and the Si(n,p) and Al(n,p) cross sections (Neutron Cross-Sections, USAEC-BNL 325). The calibration factor so obtained allowed the data to be presented in terms of

$$\int \sigma(n,p)\phi(E_n)dE = \bar{\sigma}(n,p)\Phi$$

where $\sigma(n,p)$ is the cross section of the detector nucleus in millibarns at neutron energy E_n,

$\phi(E_n)$ is the number of neutrons in the energy interval dE_n at E_n throughout the total solid angle per 100 r per mole of sample,

$\bar{\sigma}(n,p)$ is the average cross section of the detector nucleus weighted in accordance with a given neutron energy spectrum, and

Φ is the total number of neutrons per 100 r per mole of sample.

The Al(n,γ) detection efficiency could not be estimated to better than an order of magnitude since the combination of the short half-life of the reaction product and the absence of an appreciable low-energy neutron flux from the Ra–Be source gave an activation which was not statistically significant in the presence of the Al(n,p) activation.

The yields for six elements using the aluminum detectors are tabulated in Table II.

The two sets of results shown for bismuth were from runs about two months apart and are indicative of the reliability and reproducibility of the results.

While the statistics for the detection of the low-energy portion of the neutron spectrum are poor, and one would expect isotropy of emission, there does appear to be a suggestion of greater emission at the larger angles. However, without further evidence, it would be unwarranted to conclude that this is a real effect. Accordingly only the value of a_0 is shown in the table.

The angular distributions for the fast neutron component, detected by the Al(n,p) reaction, show considerable anisotropy for the neutron closed shell nuclei La, Pb, and Bi and considerably less for nuclei removed from closed shells.

Published photoneutron spectra for Pb (Toms and Stephens 1957; Dixon 1955), Ta (Cortini *et al.* 1958), and Cu (Dixon 1955) were used to calculate $\bar{\sigma}$ for the Al(n,p) reaction. Estimates of Φ at 22 Mev were taken from published data (Montalbetti *et al.* 1953; Goldemberg and Katz 1954). Table III gives the comparison of $\bar{\sigma}$(Al(n,p)) for this work and that derived from the photoneutron spectra. The agreement is good, considering that the calculations derive from material with large and uncertain correction factors and large statistical errors, and therefore gives confidence in the calculations based on the Ra–Be calibration.

The aluminum detectors have the advantage, in principle, of differentiating between the fast direct emission component and the compound nucleus emission component, and of giving information relative to the two processes simultaneously. Unfortunately, the counting statistics are subject to large standard deviations so that the angular distribution coefficients are not well defined.

TABLE II

Normalized yields for aluminum detectors

	Al(n,γ) reaction				Al(n,p) reactions						
Element	30°	90°	150°	a_0	30°	60°	90°	a_0	a_1	a_2	$(\bar{\sigma}\Phi)^*\times10^9$
Bismuth	399	567±130	620	541±85	3632	5139±290	3168	4366±185	0.06±0.06	−0.35±0.1	17.76
	478	423±130	641	484±85	2562	5353±290	2955	4144±185	−0.05±0.06	−0.53±0.1	16.87
Lead	426	312±120	725	429±77	3123	5754±260	3154	4591±166	−0.004±0.05	−0.51±0.07	18.68
Tantalum	378	367±190	688	441±122	2757	3024±425	2088	2757±275	0.14±0.14	−0.19±0.17	11.22
Lanthanum	208	222±110	330	243±70	2139	3371±250	1891	2768±160	0.05±0.07	−0.43±0.10	11.27
Arsenic	77	100±50	108	97±32	788	937±115	764	865±74	0.02±0.11	−0.16±0.14	3.52
Copper	13	65±30	70	55±20	710	748±70	569	700±45	0.11±0.08	−0.14±0.11	2.85

*$(\bar{\sigma}\Phi) = 4.07\times10^4 a_0$ millibarn-neutron.

TABLE III

Element	Φ at 22 Mev per mole/100 r	$\bar{\sigma}$ Al(n,p), millibarns		Spectrum reference
		This work	From spectra	
Pb	2.72×10^{9}	6.87	6.47	Toms and Stephens (1957)
			5.64	Dixon (1955)
Ta	2.50×10^{9}	4.49	6.1	Cortini *et al.* (1958)
Cu	0.30×10^{9}	9.50	9.02	Dixon (1955)

With the silicon detectors, the statistics were somewhat better, and the analysis was not subject to multiple regression errors since the data could be treated as merely a 2.3-minute activity associated with a background. The results are given in Table IV and are also shown graphically in Figs. 2 and 3.

Figure 2 portrays the data of Table IV, column II, showing the variation of a_0 with atomic number and also with neutron number. The values of a_1, as shown in column III, do not show any unambiguous trend with the exception that the over-all trend is to a small positive coefficient. The next section

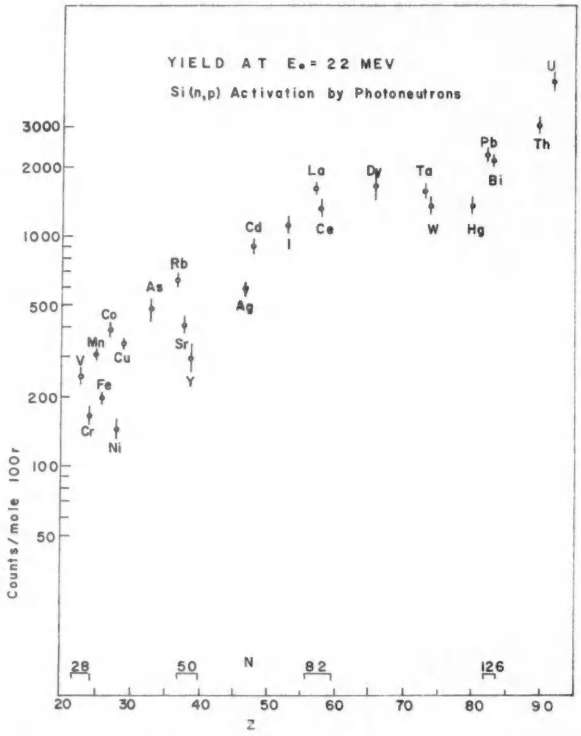

FIG. 2. The activity of the silicon detectors (proportional to the yield of fast photoneutrons) as a function of atomic number Z and neutron number N.

TABLE IV

I Element	II a_0	III a_1	IV a_2	V $(\bar{\sigma}\Phi)\times10^{9*}$	VI Φ_{total} (22 Mev)$\times10^9$	VII Φ_{fast}/Φ_{total}
Vanadium	245 (1±0.06)	0.01±0.08	−0.00±0.10	6.05	0.21	0.12
Chromium	164 (1±0.03)	0.04±0.04	−0.05±0.05	4.05	0.17	0.10
Manganese	308 (1±0.02)	0.07±0.03	−0.09±0.04	7.61	0.25	0.12
Iron	200 (1±0.03)	0.05±0.04	−0.17±0.05	4.94	0.18	0.11
Cobalt	390 (1±0.02)	0.08±0.03	−0.22±0.04	9.63	0.26	0.15
Nickel	145 (1±0.05)	0.07±0.07	−0.23±0.09	3.58	0.12	0.12
Copper	347 (1±0.02)	0.05±0.03	−0.29±0.04	8.57	0.30	0.12
Arsenic	482 (1±0.03)	0.11±0.04	−0.24±0.05	11.91	0.33	0.15
Rubidium	638 (1±0.05)	0.13±0.06	−0.14±0.08	15.76		
Strontium	409 (1±0.05)	0.10±0.06	−0.17±0.08	10.10		
Yttrium	290 (1±0.10)	0.08±0.12	−0.12±0.15	7.16		
Silver	590 (1±0.04)	0.10±0.06	−0.22±0.08	14.57	0.87	0.07
Cadmium	905 (1±0.02)	0.02±0.02	−0.26±0.03	22.35		
Iodine	1133 (1±0.03)	0.04±0.04	−0.29±0.05	27.99	1.42	0.08
Barium	1048 (1±0.04)	0.10±0.06	−0.38±0.08	25.89		
Lanthanum	1595 (1±0.02)	0.02±0.03	−0.42±0.04	39.40	1.04	0.15
Cerium	1316 (1±0.05)	0.05±0.06	−0.39±0.08	32.50		
Dysprosium	1652 (1±0.08)	0.04±0.10	−0.34±0.13	40.80		
Tantalum	1558 (1±0.02)	0.04±0.03	−0.22±0.04	38.48	2.50	0.06
Tungsten	1365 (1±0.02)	−0.07±0.03	−0.24±0.04	33.71		
Mercury	1345 (1±0.02)	0.04±0.03	−0.31±0.04	33.22		
Lead	2274 (1±0.01)	0.02±0.02	−0.42±0.03	56.17	2.72	0.08
Bismuth	2162 (1±0.02)	0.05±0.03	−0.45±0.04	53.40	3.36	0.06
Thorium	3031 (1±0.04)	0.06±0.05	−0.32±0.07	74.87		
Uranium	4630 (1±0.02)	0.05±0.03	−0.17±0.04	114.36		

*$(\bar{\sigma}\Phi) = 2.47\times10^7\, a_0$ millibarn-neutron. Errors are standard errors due to counting statistics only.

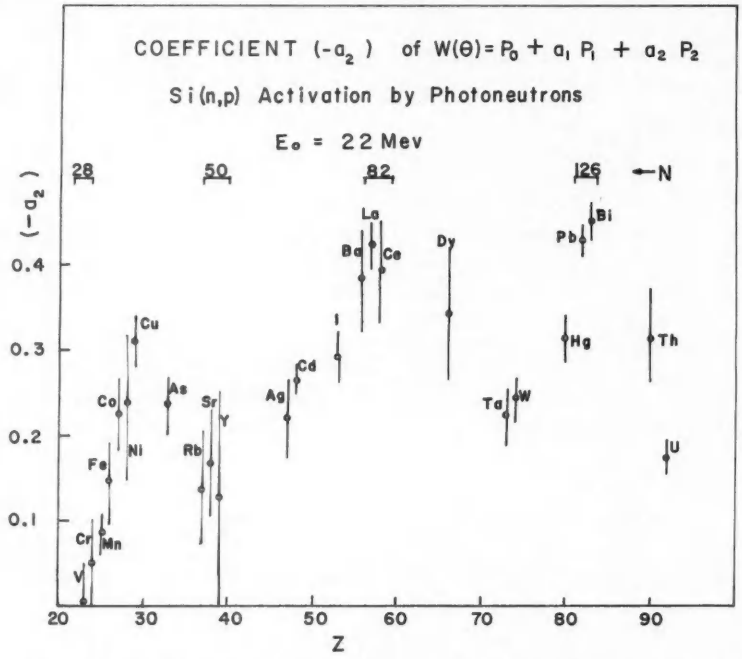

FIG. 3. The variation of the coefficient a_2 in the angular distribution $W(\theta) = P_0+a_1P_1+a_2P_2$ as a function of atomic number and neutron number.

contains the discussion of the trend and interpretation of the a_2 coefficients of column IV which are portrayed in Fig. 3 as a function of atomic number and neutron number. The values of $(\bar{\sigma}\,\mathrm{Si}(n,p)\,\Phi)$ of column V are simply related to the a_0 of column II by a detector efficiency factor obtained from the Ra–Be calibration. For our particular experimental arrangement, $(\bar{\sigma}\Phi) = 2.47\times10^7\,a_0$ millibarn-neutron. Column VI gives the number of neutrons per mole per 100 r at 22 Mev as given by Montalbetti *et al.* (1953) and Goldemberg and Katz (1954). An estimate of the ratio of the fast, direct neutron flux to the total neutron flux, as shown in column VII, was made by assuming that the fast neutrons have a Gaussian energy distribution about $E_n = 7$ Mev with a half-width of 4 Mev for which $\bar{\sigma}\,\mathrm{Si}(n,p) = 245$ millibarns. It is noted that from 6% to 15% of the photoneutrons may be interpreted as fast, direct interaction products. These rough figures are in agreement with the results of Ferrero *et al.* (1956) for Bi, and of Poss (1950) for Bi, Pb, and W.

The data of columns V and VI were used to calculate $\bar{\sigma}$, which is compared to the value of $\bar{\sigma}$ obtained by use of published spectra. The comparison is made in Table V. The agreement is satisfactory considering the statistical nature of the data.

TABLE V

Element	$\bar{\sigma}$ Si(n,p), millibarns		Spectrum reference
	This work	From spectrum	
Pb	20.8	16.25	Toms and Stephens (1957)
		17.55	Dixon (1955)
Ta	15.4	23.2	Cortini *et al.* (1958)
Cu	28.6	33.5	Dixon (1955)
Cr	23.5	17.0	Cortini *et al.* (1958)

DISCUSSION OF THE ANISOTROPY COEFFICIENT, a_2

It will be seen from Fig. 3 that although there are obvious magic number effects, they are not obviously straightforward effects; thus, whereas $|a_2|$ is a maximum for $N = 82$ and 126, it is a minimum for $N = 28$ and 50.

In the Wilkinson picture, a neutron in a shell model level may be raised by an $E1$ transition to a higher unoccupied level from which it has probability of escaping directly into the laboratory before colliding and sharing its energy with other nucleons. The relative probability of a particular $l \rightarrow l'$ transition for an individual neutron is given by (Courant 1951)

$$\frac{l+1}{2l+1} D \qquad \text{for } l' = l+1$$

and

$$\frac{l}{2l+1} D \qquad \text{for } l' = l-1$$

where

$$D = \left| \int_0^\infty R_{n'l'} R_{nl} r^3 dr \right|^2.$$

The radial overlap integrals are expected to be larger for transitions involving no change in the number of radial nodes (i.e. $l \rightarrow l+1$) than in those involving such a change (i.e. $l \rightarrow l-1$) by up to an order of magnitude. The probability of direct escape is dependent on l' and on the energy of the photon responsible for the transition minus the binding energy of the affected neutron. Values of the direct escape probability, $T_{l'}$, were taken as the transmission factor for neutrons in a square well potential (Blatt and Weisskopf 1952, Ch. VIII, Eq. (5.7)). While this is a crude approximation, it is adequate for a first-order qualitative interpretation. Other estimates, based, for example, on the empirical optical model transmission factors (Beyster *et al.* 1957) or on the overlap integral evaluated outside the nuclear radius (De Sabbata and Tomasini 1959), exhibit the same trend as the transmission probabilities for the square well for which approximate values for neutron energies of the order of 7 Mev are given below in Table VI.

Table VI assumes most of the transitions occur from the same oscillator level. Thus, 1g, 2*d*, and 3*s* neutrons occupy oscillator level number V and $E1$ transitions 1g–2*f* and 2*d*–2*f* have the same final state and the same escape

TABLE VI

Approximate values of $T_{l'}$

Transition	$T_{l'}$
$1l \rightarrow 1(l+1)$	0.0–0.2
$2l \rightarrow 2(l+1)$ $1l \rightarrow 2(l-1)$	0.3–0.5
$3l \rightarrow 3(l+1)$ $2l \rightarrow 3(l-1)$	0.7–0.9

probability. The main point to note is that for the same initial orbital angular momentum, the escape probability favors the $l \rightarrow l-1$ transition.

The angular distribution terms for the direct interaction are (Courant 1951)

$$W(\theta) = a_0\left[P_0(\cos\theta) - \frac{l+2}{2(2l+1)}P_2(\cos\theta)\right] \qquad \text{for } l \rightarrow l+1\,,$$

$$= a_0\left[P_0(\cos\theta) - \frac{l-1}{2(2l+1)}P_2(\cos\theta)\right] \qquad \text{for } l \rightarrow l-1\,.$$

The strength functions and angular distribution functions with and without spin–orbit coupling considerations are also given in terms of the Racah algebra coefficients by Fujii (1959).

It is necessary to have a knowledge of the ordering of the nuclear shells and subshells before an interpretation of the experimental results is possible. In the following discussion, an ordering based on experimental evidence is used as displayed in Fig. 4. The references to the work, pertinent to a particular region of the periodic table, are given in the caption of the figure.

Using the above ideas, and the fact that the silicon detectors will not observe neutrons of less than 5 Mev, it is possible to explain the variation of the angular distribution coefficient a_2 with neutron occupation number. The main things to note are that (1) $l \rightarrow l+1$ transitions give $-a_2 > 0.25$, while $l \rightarrow l-1$ transitions give $-a_2 < 0.25$; (2) $l \rightarrow l-1$ transitions are less probable than the $l \rightarrow l+1$ type; and (3) on the other hand, $l \rightarrow l+1$ transitions resulting in high l' will be inhibited by the angular momentum barrier from appearing as direct interactions.

The increasing anisotropy from $N \sim 28$ to $N \sim 36$, in which region the $2p_{3/2}$ and $f_{5/2}$ subshells are filling, may be attributed to the $2p \rightarrow 2d$ transitions with a small admixture of $2p \rightarrow 3s$. Considering the yields (Fig. 2) from the Z odd and Z even nuclei separately, they are noted to increase as the $2p$ shell fills. The alternation of the Z odd and Z even yields may be associated with the (γ,n) threshold energy which is higher in the Z even nuclei and results in less energy being available to the directly emitted neutron and thus, a lower barrier penetration probability and detection probability. From $N \sim 35$ to $N = 50$, decreased anisotropy reflects the angular momentum barrier effect in suppressing the $g_{9/2} \rightarrow h_{11/2}$ and $f_{5/2} \rightarrow g_{7/2}$ direct emission products and favoring the $1l \rightarrow 2(l-1)$ transitions which have $-a_2 < 0.25$. The interval from $N = 50$ to $N = 76$ marks the filling of the $2d_{5/2}$, $g_{7/2}$, and

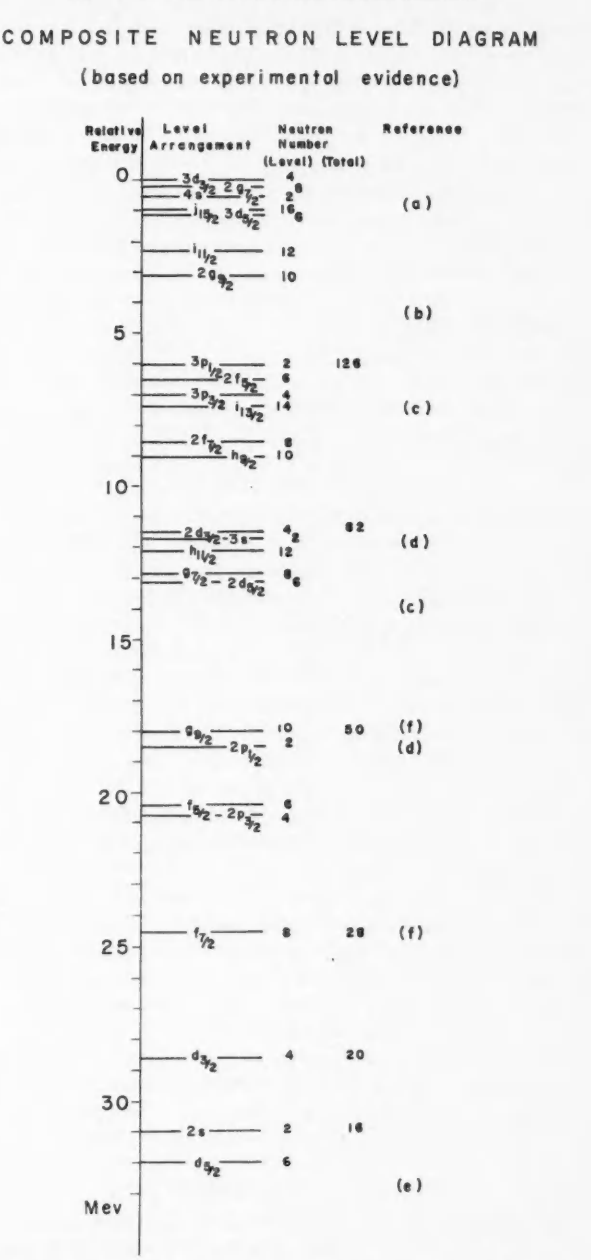

FIG. 4. The assumed ordering of nuclear levels used in the discussion. The references cited in the figure are: (*a*) Holm *et al.* (1960); (*b*) Blomquist and Wahlborn (1960); (*c*) Kurath (1960); (*d*) Zeldes (1958); (*e*) Lawson (1960); (*f*) Cohen and Price (1960).

$h_{11/2}$ subshells, with the $2d_{5/2} \rightarrow 2f_{7/2}$ transitions producing greater anisotropy. Other transitions from these subshells are rather ineffective due to either small transition strengths or suppression by the angular momentum barrier. The marked increase in anisotropy at $N = 82$ is presumably due to the $3s \rightarrow 3p$ and $2d_{3/2} \rightarrow 2f_{5/2}$ transitions. Beyond $N = 82$, subshells of higher angular momentum are filling, and only $l \rightarrow (l-1)$ transitions give an appreciable contribution, supplemented by transitions from the $N = 82$ core. The yield from the core is reduced as the subshells fill, and the yield from the $l \rightarrow (l-1)$ transitions no more than compensate for this reduction yieldwise, but in so doing gives a decreased anisotropy in the angular distribution. At $N = 126$, the $3p \rightarrow 3d$ transitions could account for the greater anisotropy if one accepts that the $3p \rightarrow 4s$ transition strength is very weak, or that the $4s$ level is depressed so that direct emission from it is at too low an energy to be detected efficiently. Thorium (25% photofission) and uranium (50% photofission) (Price and Kerst 1950) show the effect of isotropic fast photofission neutrons in their more isotropic distribution.

CONCLUSION

Comparing the results obtained here with those of other workers, it is noted that the only previous study of a variety of elements with a similar technique was by Price (1954), some of whose results were quoted earlier (Table I). The elements chosen by him happen to be such that they indicated an increase in anisotropy with increasing neutron number. While in essential agreement with the work reported herein, the significant variations of the angular distribution coefficient exhibited in Fig. 3 could not be anticipated.

The only report appearing in the literature attempting a theoretical correlation of experimental yield and angular distribution of fast photoneutrons from an element in the range of those studied here is that of Ferrero *et al.* (1956). Their results, quoted earlier, give $-a_2 = 0.38 \pm 0.05$ for bismuth for 30 Mev bremsstrahlung, which is only slightly different from the present result of 0.45 ± 0.04 for 22 Mev bremsstrahlung. They consider the total transition strength to be from allowed transitions of the shell model type $nl \rightarrow n(l+1)$, and ignore $nl \rightarrow (n+1)(l-1)$ transitions. Assuming an average energy of 7 Mev for the directly emitted neutrons and applying an appropriate transmission factor, they obtained good agreement with experiment. Although ignoring the $l \rightarrow (l-1)$ transitions does work in the region of $N = 126$, it fails for many other elements; indeed one could never get $-a_2 < 0.25$ if the $l \rightarrow (l-1)$ transition strengths are neglected.

From the correlation found here between the predictions of the Wilkinson model of photodisintegration and the experimental results, it is clear that the present results give strong evidence in favor of the independent particle model for the direct effect, at least as applied to the angular distribution phenomena.

ACKNOWLEDGMENTS

We wish to express our thanks to Dr. J. D. Prentice for many helpful discussions and to Dr. W. H. Watson for his continued encouragement. This work was supported in part by Grant BT-84 from the National Research Council of Canada.

REFERENCES

ASADA, T., MASUDA, M., OKUMURA, M., and OKUMA, J. 1958. J. Phys. Soc. Japan, **13**, 1.
BAKER, R. G. and McNEILL, K. G. 1960. Proc. Int. Conf. Nuclear Structure, Kingston, 740.
BEYSTER, J. R., SCHRANDT, R. G., WALT, M., and SALMI, E. W. 1957. USAEC-LA2099.
BLATT, J. M. and WEISSKOPF, V. F. 1952. Theoretical nuclear physics (John Wiley & Sons, Inc.).
BLOMQUIST, J. and WAHLBORN, S. 1960. Arkiv Fysik, **16**, 545.
COHEN, B. L. and PRICE, R. E. 1960. Nuclear Phys. **17**, 129.
CORTINI, G., MILONE, C., and RUBBINO, A. 1958. Nuovo Cimento, **9**, 85.
COURANT, E. D. 1951. Phys. Rev. **82**, 703.
DE SABBATA, V. and TOMASINI, A. 1959. Nuovo Cimento, **13**, 1268.
DIXON, W. R. 1955. Can. J. Phys. **33**, 785.
FERRERO, F., HANSON, A. O., MALVANO, R., and TRIBUNO, C. 1956. Nuovo Cimento, **4**, 418.
FUJII, S. 1959. Progr. Theoret. Phys. **21**, 511.
GELLER, K., HALPERN, J., and YERGIN, P. F. 1954. Phys. Rev. **95**, 659.
GOLDEMBERG, J. and KATZ, L. 1954. Can. J. Phys. **32**, 49.
GRAVES, E. R. and ROSEN, L. 1953. Phys. Rev. **89**, 343.
GUGELOT, P. C. 1951. Phys. Rev. **81**, 51.
HILL, D. L. 1952. AECD-1945.
HOLM, G. B. *et al.* 1960. Phys. Rev. **118**, 1247.
JOHANSSON, S. A. E. 1955. Phys. Rev. **97**, 434.
KURATH, D. 1960. Nuclear spectroscopy (Academic Press, New York), p. 993.
LAWSON, R. D. 1960. Nuclear spectroscopy (Academic Press, New York), p. 963.
McELHINNEY, J., HANSON, A. O., BECKER, R. A., DUFFIELD, R. B., and DIVEN, B. C. 1949. Phys. Rev. **75**, 542.
MONTALBETTI, R., KATZ, L., and GOLDEMBERG, J. 1953. Phys. Rev. **91**, 659.
POSS, H. L. 1950. Phys. Rev. **79**, 539.
PRICE, G. A. 1954. Phys. Rev. **93**, 1279.
PRICE, G. A. and KERST, D. W. 1950. Phys. Rev. **77**, 806.
SPICER, B. M. and PENFOLD, A. S. 1955. Rev. Sci. Instr. **26**, 952.
TEUCHER, M. 1949. Z. Physik, **126**, 410.
TOBIN, R., McELHINNEY, J., and COHEN, L. 1958. Phys. Rev. **110**, 1388.
TOMS, M. E. and STEPHENS, W. E. 1957. Phys. Rev. **108**, 77.
WILKINSON, D. H. 1956. Physica, **22**, 1039.
——— 1959. Ann. Rev. Nuclear Sci. **9**, 1.
ZATSEPINA, G. N., LAZAREVA, L. E., and POSPELOV, A. N. 1957. J. Exptl. Theoret. Phys. (U.S.S.R.), **5**, 21.
ZELDES, N. 1958. Nuclear Phys. **7**, 27.

CROSS SECTIONS OF (p,pxn) REACTIONS IN Au^{197} [1]

T. M. KAVANAGH AND R. E. BELL

ABSTRACT

Cross sections of (p,pn), $(p,p2n)$, and $(p,p3n)$ reactions in Au^{197} have been measured by the activation method for incident proton energies up to 86 Mev. The curves of cross section as a function of energy have similar shapes for the three reactions. They rise from apparent thresholds at about 16, 21, and 30 Mev, respectively, to peak values of 180, 145, and 150 mb at proton energies about 30 Mev higher than the apparent threshold energies. The cross sections are much larger than those predicted from the statistical and cascade-evaporation theories, and they are interpreted in terms of two-body collisions in the diffuse surface of the target nucleus. A combination of these results with measured (p,xn) cross sections yields an approximation to the total reaction cross section of a heavy nucleus.

INTRODUCTION

In an earlier paper from this laboratory Bell and Skarsgard (1956) reported the results of measurements of (p,xn) cross sections of heavy elements. This work has now been extended to (p,pxn) reactions. Cross sections of (p,pn) $(p,p2n)$, and $(p,p3n)$ reactions in Au^{197} have been measured in the proton energy range 18 to 86 Mev; the experimental method was similar to that described in the earlier paper.

Reactions of the type (p,pxn), which involve inelastic scattering of the incident proton, are inhibited by the Coulomb barrier in both the entrance and exit channels. On the basis of statistical theory such reactions in a heavy target element are expected to have negligibly small cross sections compared with (p,xn) reactions. Bell and Skarsgard found that near the peak of a particular (p,xn) curve, the $(p,p(x-1)n)$ cross section was indeed small by comparison, and they were led to expect that the sum of the (p,xn) cross sections would approximate the total reaction cross section. This sum curve, however, showed structure that could not be explained on the basis of statistical theory (Jackson 1956).

It is now well known that inelastic scattering of medium-energy protons cannot be described in terms of compound nucleus processes (Eisberg and Igo 1954; Cohen 1957). For example, Eisberg and Igo found that for 31-Mev protons incident on heavy nuclei, inelastic scattering accounts for about 15% of the total reaction cross section; furthermore the scattered protons have distributions in energy and angle that are characteristic of direct interactions. While the interpretation of these medium-energy direct interactions has been the subject of some controversy, they probably result from collisions of the incident protons with nucleons in the surface of the target nucleus (Griffiths and Eisberg 1959; Eisberg 1960).

The present experiments constitute a study of cross sections of some inelastic scattering reactions. Cross sections have been measured as a function

[1]Manuscript received May 18, 1961.
Contribution from the Radiation Laboratory, McGill University, Montreal, Que.

of proton bombarding energy over a range in which the surface mechanism is expected to predominate. The use of a heavy target nucleus makes compound nucleus contributions unimportant. At the higher energies internal direct interactions can lead to the emission of protons, but our experimental cross sections exceed those predicted by cascade-evaporation theory. The results indicate that inelastic scattering can account for the structure in the Bell and Skarsgard (p,xn) sum curve, and an addition of (p,pxn) cross sections to this curve gives an approximation to the total reaction cross section of a heavy nucleus.

Previous measurements of (p,pxn) cross sections of heavy elements are not very comprehensive. Cohen *et al.* (1954) have measured the (p,pn) cross sections of silver, palladium, and tantalum for proton energies up to 23.5 Mev. The (p,pn) cross section of gold has been measured by Sosniak (1958) for energies up to 32 Mev, and by Yule and Turkevich (1960) at 82 Mev and at several higher energies. Gusakow *et al.* (1960) have published (p,pn) and (p,$p2n$) cross sections of gold for proton energies in the range 40 to 155 Mev, with results in strong disagreement with our own. The (p,pxn) cross sections of cesium for $x = 1, 2, 3, 4$, and 6 have been reported by Fink and Wiig (1954) for proton energies of 60, 80, 100, 150, and 240 Mev.

Measurements made on medium- and light-weight elements are more extensive, but of less interest here. The $C^{12}(p,pn)C^{11}$ reaction was used, however, for monitoring the proton beam.

It should be pointed out that in the present work cross sections have been measured by the activation method. This method does not distinguish whether or not the outgoing particles are bound, and thus, for example, the measured (p,pn) cross section includes the (p,d) cross section.

EXPERIMENTAL METHOD

The experimental method was essentially that described by Bell and Skarsgard (1956). In each bombardment a gold target foil, $\frac{1}{4}$ in. wide and either 20 or 40 mg/cm^2 thick, was mounted together with a graphite beam monitoring foil in the circulating beam of the McGill synchrocyclotron. The product nuclides formed by the various (p,pxn) reactions decay primarily by orbital electron capture, and cross sections were determined by absolute counting of K X rays and gamma rays that follow decay events.

The monitor foils were sheets of pure carbon 20 mg/cm^2 thick, prepared with a surface grinder from fine-grain compressed graphite. These foils had an advantage over the teflon monitors used by Bell and Skarsgard in that they could withstand the heating caused by long bombardments. Beam monitoring was based on the reaction $C^{12}(p,pn)C^{11}$, and the monitor cross section used was that given by Aamodt *et al.* (1952) modified according to the recommendations of Whitehead and Foster (1958). Uncertainties in the energy of the proton beam limit the accuracy of carbon monitoring below about 30 Mev, since in this region the monitor cross section is a strong function of energy. Only the first few points on the (p,pn) curve are seriously affected, however, and these points are also in a region of rapidly varying cross section; thus errors

in monitoring have little effect on the appearance of the curve. Sosniak (1958) gives (p,pn) points at 18 and 21 Mev, monitored by the $F^{19}(p,pn)F^{18}$ reaction which is less energy dependent in this region, and these data define the (p,pn) cross section at energies where the present results are uncertain.

The large amounts of radioactive mercury formed in the gold foils by (p,xn) reactions were removed by vacuum distillation. Two different techniques were used. A slow method involved heating the gold foils after bombardment in an evacuated quartz tube; the mercury was driven into a liquid air trap, and at temperatures of about 800° C, separation was complete in 15 to 20 minutes. This procedure was used in initial studies of the (p,pn) and $(p,p3n)$ reactions for bombarding energies up to 60 Mev.

A more elaborate technique was required for the $(p,p2n)$ measurements since the product nuclide Au^{195} is also formed in the target foil during a slow separation by the decay of relatively short-lived Hg^{195}. Corrections for this mercury decay are difficult since the cross section for formation of Hg^{195} is not known, and more important, since an unknown amount of mercury is lost into the cyclotron vacuum during the bombardment due to heating by the proton beam. A fast separation technique was developed which involved heating the targets electrically in the cyclotron during bombardment. Gold targets 20 mg/cm² thick (half the thickness used for the slow method) were heated to 800° to 900° C by passing about 5 amperes of 100-kilocycle alternating current through them. The high frequency was necessary in order to prevent destruction of the foils in the 16-kilogauss field of the cyclotron. The target strips had a 0.01 in. wide slit cut longitudinally along the center of the strip from the base to within $\frac{1}{8}$ in. of the tip, so that both electrical terminals were at the base of the target, and the target tip could be cut to fit the monitor foil. The target's temperature was indicated by its resistance, and was controlled remotely during bombardment.

A tracer experiment was performed as a check on the above technique. A gold target of the same form as those used in the cross-section measurements was bombarded at 28 Mev, where most of the resultant radioactivity was due to mercury. Low beam current was used to prevent mercury boil-off. This sample was heated electrically in an evacuated glass vessel provided with a liquid air trap, and K X rays originating in the sample were counted with a sodium iodide counter. The counting rates before and after the heating current was turned on were recorded on a chart recorder, and the results are shown in Fig. 1. The curve indicates a "mean life" against boil-off for a mercury atom in the foil of about 40 seconds. This time is very short compared with the radioactive half-life of Hg^{195}, 9.5 hours.

A further check on the effectiveness of the fast separation was offered by a sample bombarded at about 23 Mev. The measured $(p,p2n)$ cross section (8.1 mb) is comparable with the value of 9.5 mb reported for the (p,t) reaction at this energy (Cohen and Rubin 1959). The $(p,3n)$ reaction leading to Hg^{195} probably has a cross section of about 400 millibarns at 23 Mev (Bell and Skarsgard 1956), and a decay of only 1% of the Hg^{195} before its removal from the foil would result in an apparent $(p,p2n)$ cross section at least 30% greater than the (p,t) value reported by Cohen and Rubin. It is thus concluded that

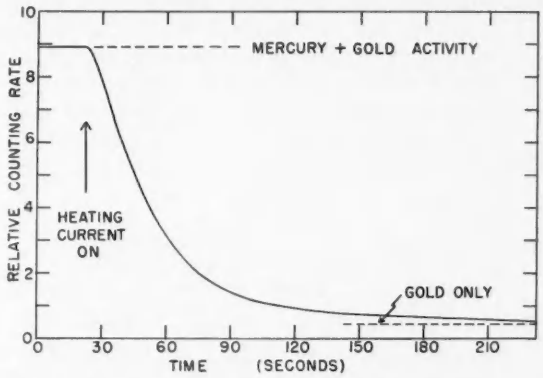

FIG. 1. Results of a radioactive tracer experiment performed as a check on the fast mercury removal technique (see text). The curve indicates the rate of vacuum distillation of mercury from a 0.0005 in. thick gold foil heated to about 800° C.

more than 99% of the mercury formed in $(p,3n)$ reactions was removed before it decayed into Au^{195}. Finally, several targets were maintained at an appreciably lower temperature (~600 degrees) during bombardment, with no significant effect on the measured $(p,p2n)$ cross section.

The fast mercury removal also facilitated the measurement of (p,pn) and $(p,p3n)$ cross sections above 60 Mev, since there was significantly less interfering activity produced in the samples by decay of the mercury isotopes formed at high energies.

X Rays and gamma rays from the active samples were counted with sodium iodide scintillation counters in conjunction with a multichannel pulse analyzer. The (p,pn) and $(p,p3n)$ reaction products (Au^{196} and Au^{194}) were counted with a single calibrated crystal; the method of determining reaction yields from counting rates for particular total energy events has been described by Bell and Skarsgard. Au^{195} activity from $(p,p2n)$ reactions was counted by sandwiching the sample foils tightly between two sodium iodide counters connected in parallel. The counter gains were made equal by adjusting the high voltages, and the assembly functioned as a single counter with about 95% geometrical efficiency. Disintegration rates were calculated from total counting rates of all detected events. This method had the advantage of being extremely insensitive to uncertainties in the Au^{195} decay scheme, and also enhanced the observed counting rates (Au^{195} has a half-life of about 6 months and thus the disintegration rates were low).

EXPERIMENTAL MEASUREMENTS AND RESULTS

(p,pn) Cross Section

Yields of the product nucleus Au^{196} were determined from the total photopeak counting rates of the 331-kev and 354-kev gamma rays that follow electron capture, and the 426-kev gamma rays that follow β^- decay. The branching ratios and conversion coefficients used were those given by Thieme and

Bleuler (1956*a*). Cross sections were calculated from counting rates after the decay of 9.5-hour Au^{196m}, and no correction was made for reactions that proceed via the isomeric state; the error introduced is negligibly small.

Decay curves of Au^{196} activity were followed for about 25 days. The measured half-lives were in good agreement with the value of 6.1 days reported by Yule and Turkevich (1960), and this value was used in the cross-section calculations.

The (p,pn) results are summarized in Table I, and are shown graphically

TABLE I

Experimental Au^{197} (p,pxn) cross-section results

Proton energy (Mev)	(p,pxn) cross sections (mb)		
	(p,pn)	$(p,p2n)$	$(p,p3n)$
18.0	23.6		
22.3	83.3		
23.2		8.1	
27.5	141		
28.3	152	26.8	
32.4	169		6
33.2	178	69	
37.3	168		18
37.9	182	116	27
	185	115	24
42.2	170		80
42.8	174	125	68
	177	138	
47.2	175		112
47.4	194	149	126
51.9	164		125
52.5	186	144	146
56.8	174		144
57.4	179	142	144
61.7	165		150
62.5	168	136	159
67.1	153	115	149
	165	130	141
72.0	153	138	133
		122	
76.9	157	135	138
		122	
81.8	146	114	136
86.0	155	120	137

by the open circles in Fig. 2. The solid curve was simply drawn freehand through the experimental points, and does not represent any theory. The standard error in the points, compounded from uncertainties in the individual quantities involved in the cross-section calculations, is about 13%; this is represented by an error bar in the figure. The crosses show (p,pn) cross sections measured by Sosniak (1958), and the triangle is the lowest-energy point from high-energy results of Yule and Turkevich (1960). The dashed curve, which disagrees strongly with the present work, is due to Gusakow *et al.* (1960).

$(p,p2n)$ Cross Section

Cross sections were calculated from the total counting rates recorded by the high-efficiency counter described above, that is, from integrated pulse height spectra. The pulse spectrum showed a strong K X-ray peak, a 99-kev gamma-

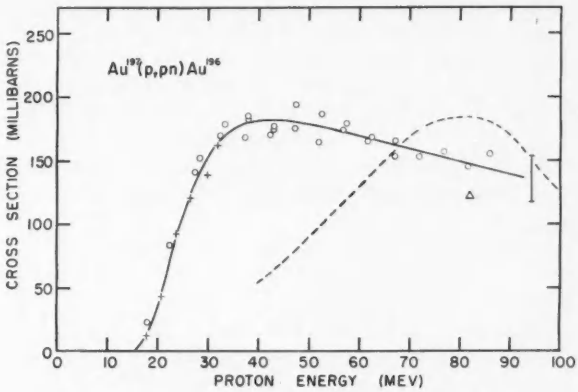

FIG. 2. Cross section of the reaction $Au^{197}(p,pn)Au^{196}$ as a function of incident proton energy. The circles are from the present work, and the error bar represents the estimated standard errors in the absolute cross-section values. The crosses are from Sosniak (1958), the triangle from Yule and Turkevich (1960), and the dashed curve was published by Gusakow *et al.* (1960).

ray peak, a strong peak at about 130 kev due primarily to $K+K$ sum events, and weaker contributions due to summing of K X-ray pulses with 99- and 130-kev gamma-ray pulses. The decay scheme parameters used were not critical; calculations were based on values published by Bisi *et al.* (1959).

The long-lived Au^{195} activity was counted for a period of from 7 to 9 months for the different samples, beginning 3 months after bombardment. The decay curves all showed a half-life of 188 ± 5 days, and this value was used in the cross-section calculations. It is in good agreement with the values of 185 ± 3 days reported by Wilkinson (1949), and 192 ± 5 days given by Bisi *et al.*

The $(p,p2n)$ cross-section results are summarized in Table I and are shown graphically in Fig. 3. The standard error in the values reported is about 13%. The dashed curve in the figure is due to Gusakow *et al.* (1960).

$(p,p3n)$ Cross Section

This reaction leads to the formation of 39-hour Au^{194}, and cross-section determinations were based on counting rates of K X rays, and 291- and 327-kev gamma rays. The gamma rays were unresolved from Au^{196} gamma rays, and their intensity, as well as that of K X rays from Au^{194}, was determined from complex decay curves. Decay scheme parameters used were due to Thieme and Bleuler (1956*b*).

At lower energies (below 45 Mev) absolute cross sections were calculated from K X-ray counting rates. At higher energies, however, there is interference from other activities, particularly 17.5-hour Au^{193}; the gamma rays were used as an indicator of relative cross sections over the whole energy range, and these relative cross sections were normalized to the absolute values obtained by K X-ray counting at low energies.

The $(p,p3n)$ results are shown in Table I and Fig. 4. The standard error in

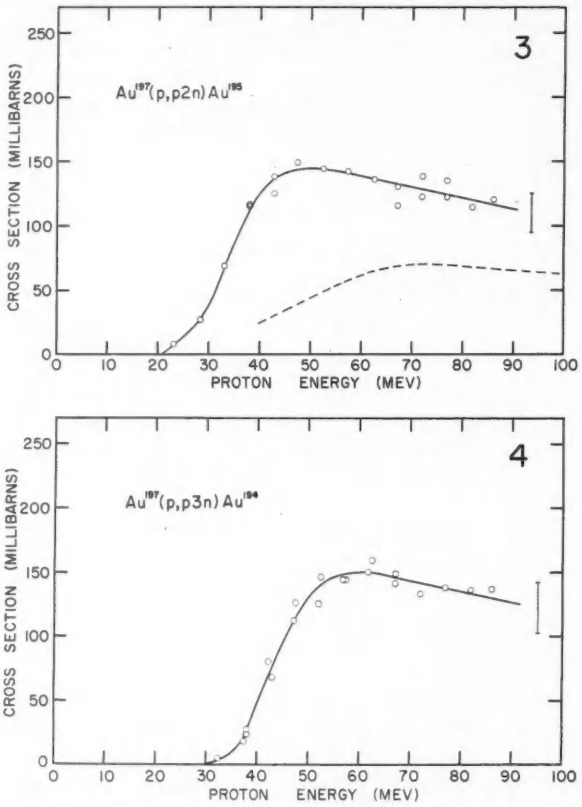

FIG. 3. Cross section of the reaction $Au^{197}(p,p2n)Au^{195}$ as a function of incident proton energy. The error bar indicates the estimated standard error in the absolute cross-section values. The dashed curve is from Gusakow *et al.* (1960).

FIG. 4. Cross section of the reaction $Au^{197}(p,p3n)Au^{194}$ as a function of incident proton energy. The error bar indicates the estimated standard error in the absolute cross-section values.

the cross-section values is somewhat larger than for the (p,pn) and $(p,p2n)$ reactions since yields were calculated from complex decay curves; the error is estimated to be about 16%.

DISCUSSION

(p,pxn) Cross Sections

The (p,pn) and $(p,p2n)$ cross-section results from the present work are in strong disagreement with the values reported by Gusakow *et al.* (1960) (see Figs. 2 and 3). Their values are, for the most part, lower than the present ones in the energy range where the two investigations overlap. It should be noted

that Gusakow *et al.* also show a $(p,3n)$ cross-section curve which does not resemble $(p,3n)$ curves for other heavy elements (Bell and Skarsgard 1956). The (p,pn) results from the present work are in very good agreement with the low-energy measurements of Sosniak (1958), and at 82 Mev they agree with the results of Yule and Turkevich (1960) to within the combined experimental errors of the two sets of measurements.

The smooth curves drawn through the experimental points in Figs. 2, 3, and 4 are presented together in Fig. 5. The two triangles in Fig. 5 represent

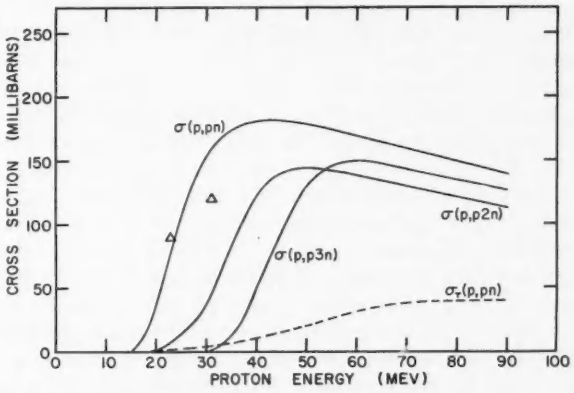

FIG. 5. The smooth curves drawn through the experimental points in Figs. 2, 3, and 4 are shown together. The triangles at 23 and 31 Mev represent (p,p') cross sections (Cohen 1959). The dashed curve is a theoretical one for the (p,pn) reaction based on cascade-evaporation calculations of Jackson (1956).

(p,p') cross sections at 23 and 31 Mev as given by Cohen (1959). (The (p,p') reaction may be regarded as a (p,pxn) reaction for $x = 0$.) Except for differences in threshold, the (p,pn), $(p,p2n)$, and $(p,p3n)$ curves are similar. The (p,pn) cross-section values are somewhat higher than the others, but they include contributions from (p,d) pickup reactions. Pickup effects are probably less important so far as the $(p,p2n)$ and $(p,p3n)$ reactions are concerned. The (p,t) reaction, which is energetically favored over true $(p,p2n)$ events by about 8.5 Mev, does, however, lead to a relative lowering of the apparent $(p,p2n)$ threshold; the effect is visible at the beginning of the $(p,p2n)$ curve in Fig. 5. Finally, it is interesting to note that a smooth curve drawn from a reasonable threshold through the two (p,p') points is similar in appearance to the other (p,pxn) curves.

The experimental (p,pxn) cross sections are an order of magnitude larger than those expected on the basis of statistical theory. These large cross sections are characteristic of proton inelastic scattering reactions in general, and as mentioned earlier, such reactions should probably be interpreted in terms of nucleon–nucleon collisions in the diffuse surface region of the target nucleus (Griffiths and Eisberg 1959), at least for energies below about 50 Mev.

In terms of the surface mechanism, (p,pxn) reactions would take place as follows. The incident proton suffers a single collision, or a small number of multiple collisions (Kikuchi 1960), near the surface of the target nucleus and the incident proton or a struck proton emerges. Prompt neutrons may accompany the prompt proton, but more likely the other nucleons involved in the initial interaction enter the nuclear core to form a compound nucleus. Finally, the compound nucleus decays by neutron evaporation.

At higher bombarding energies the nucleus as a whole becomes more transparent and direct interactions in the nuclear core can contribute to (p,pxn) events. This "cascade-evaporation" process has been treated by Monte Carlo methods (Jackson 1956; Metropolis *et al.* 1958); in these calculations the nucleus was assumed to have a sharp boundary, so the cross sections obtained indicate the importance of internal direct processes. The dashed curve in Fig. 5 represents such a cross-section curve for the (p,pn) reaction, calculated according to the results of Jackson. Direct interactions in the nuclear interior thus account for about a third of the observed cross section at 90 Mev, and at lower energies are less important. Curves for the $(p,p2n)$ and $(p,p3n)$ reactions are not shown; they are similar to the (p,pn) one but lie 10 and 20 Mev higher on the energy scale, respectively.

In a process involving prompt proton emission followed by compound nucleus formation, the residual energy of excitation following the prompt events has a distribution that is a mirror image of the energy distribution of the scattered protons. In order for a (p,pxn) reaction to occur, the residual energy of excitation must be appropriate to cause the evaporation of x neutrons; thus the relative magnitudes of the various (p,pxn) cross sections would depend in a simple way on the energy spectrum of the scattered protons. On this basis, and using neutron evaporation probabilities published by Jackson (1956), the experimental cross sections shown in Fig. 5 (including the two (p,p') points) are consistent over the whole range of bombarding energies with energy spectra that are approximately flat above the energy of the Coulomb barrier.

Comparison of (p,pxn) and (p,xn) Cross Sections

Bell and Skarsgard (1956) have published (p,xn) cross sections of several heavy nuclides, for a range of values of x. The individual curves have narrow peaks due to compound nucleus processes, followed by low tails extending to higher energies; these tails are due to direct interactions. A surprising feature of the (p,xn) results is the relatively large peak cross section for the $(p,2n)$ reaction; this has the effect of causing a minimum in the (p,xn) cross-section sum (i.e. sum for all values of x) at about 25 Mev. There are smaller ripples in this curve at higher energies, but they should probably not be taken seriously.

A comparison of the Bell and Skarsgard results for Bi^{209} with the results of the present work shows that the minimum in the (p,xn) sum curve occurs at proton energies for which (p,pxn) cross sections are becoming significant. It will be indicated in the next section (see Fig. 6) that an addition of (p,pxn) cross sections for Au^{197} (including those for $x = 0$) to the (p,xn) sum curve for

Bi^{209} yields a roughly monotonic curve, and one is led to speculate that the marked structure in the (p,xn) sum curve is due to competition from (p,pxn) reactions.

Up to about 50 Mev, incident protons that enter the nuclear core will probably lead to compound nucleus formation with subsequent neutron evaporation, or to prompt neutron emission. Competition between (p,pxn) and (p,xn) processes would be unimportant, so far as this mechanism is concerned. It is interesting, however, to consider competition between these processes for interactions in the nuclear surface. One might suppose that at low energies, say below 20 Mev, interactions in the diffuse surface also lead primarily to compound nucleus formation, or to prompt neutron emission, and hence to (p,xn) reactions. That is, the surface of the target nucleus appears relatively more dense at low energies, making direct interactions less probable, and direct interactions would be less likely to lead to proton emission due to internal reflections at the edge of the potential well. Thus at low energies surface interactions would lead to (p,xn) events, and the dip in the (p,xn) sum curve at higher energies could be attributed to an enhanced cross section for direct interactions leading to charged particle emission.

The (p,pxn) cross sections are about the same as $(p,(x+1)n)$ cross sections in the energy region of the direct interaction tail of the $(p,(x+1)n)$ cross-section curves. For example, the (p,pn) cross section of gold is approximately the same as the $(p,2n)$ cross sections of Bi^{209} and Pb^{206} at 35 Mev, and at 45 Mev the $(p,p2n)$ and $(p,3n)$ cross sections are similar. The observed $(p,2n)$ and $(p,3n)$ cross sections can be accounted for largely in terms of internal cascades (Jackson 1956), and thus, as far as the surface mechanism is concerned, (p,pxn) reactions predominate over $(p,(x+1)n)$ reactions. On the basis of an elementary surface collision model (p,pxn) cross sections are expected to be about twice as large as $(p,(x+1)n)$ cross sections (from simple statistical arguments), but the actual disparity is probably greater. Cohen (1959) has shown that at 23 and 31 Mev, (p,p') cross sections are typically 5 to 10 times larger than (p,n) cross sections. A discussion of this point in relation to the nucleon–nucleon collision mechanism is contained in a recent paper by Eisberg (1960).

The Total Reaction Cross Section

The sum of the (p,pxn) cross sections from the present work and the previously published (p,xn) cross sections gives an approximation to the total reaction cross section of a heavy nucleus. The experimental (p,pxn) cross sections include (p,d) and (p,t) cross sections, and other reactions are probably relatively unimportant. (Bell and Skarsgard have shown, for example, that at 32 Mev (p,α), $(p,\alpha n)$, and $(p,2pn)$ cross sections of lead are each less than 2 millibarns.)

The sum of the individual (p,xn) cross sections of Bi^{209} is represented by the solid curve in Fig. 6. This curve was taken from the paper of Bell and Skarsgard, and was adjusted in accordance with a more recent beam monitoring cross section (Whitehead and Foster 1958). The small circles show the smoothed

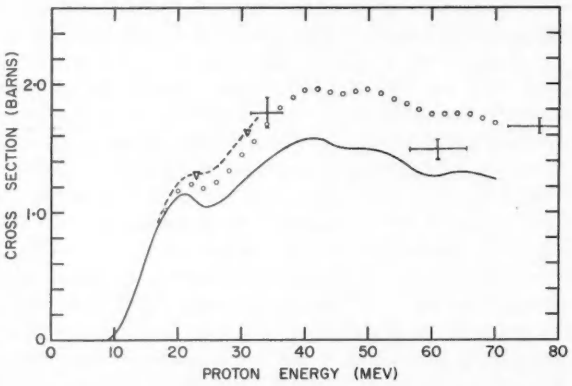

FIG. 6. The solid curve represents the sum of (p,xn) cross sections of Bi^{209} (Bell and Skarsgard 1956). The circles represent this sum plus the (p,pxn) cross sections from the present work. The triangles at 23 and 31 Mev include the (p,p') cross section (Cohen 1959), and the dashed curve drawn through these points approximates the total reaction cross section of a heavy nucleus. At higher energies the circles give a rough lower limit to the total reaction cross section. The crosses represent directly measured total reaction cross sections of lead (from Gooding 1959; Meyer *et al.* 1960; and Goloskie 1961).

(p,pxn) results from the present work added to the (p,xn) curve. The triangles include the (p,p') cross sections reported by Cohen (1959), and the dashed curve results from the addition of a reasonable (p,p') curve based on these two values. The dashed curve approximates the total reaction cross section, with a standard error of about 15%. The small circles represent a rough lower limit to the total reaction cross section at higher energies, since the (p,p') and $(p,p4n)$ cross sections are not included (the $(p,p5n)$ and $(p,p6n)$ cross sections of bismuth are contained in the sum curve presented by Bell and Skarsgard).

Three points representing directly measured total reaction cross sections of lead are shown in Fig. 6 as crossed error bars. The point at 34 Mev is due to Gooding (1959), the one at 62 Mev to Meyer *et al.* (1960), and the point at 77 Mev is from Goloskie (1961). The values at 34 and 77 Mev are in good agreement with the present work, but that at 62 Mev appears to be somewhat low.

The total reaction cross section of a heavy nucleus is, to within experimental accuracy, a monotonic function of incident proton energy. Bell and Skarsgard were led toward a different conclusion because they did not know that (p,pxn) cross sections were so large; the present work does, however, support their conclusion that near the peak of a (p,xn) cross section, the $(p,p(x-1)n)$ cross section is small by comparison.

In this section and the preceding one we have compared and combined (p,pxn) cross sections of gold with (p,xn) cross sections of bismuth and lead. This procedure is of course not strictly correct, but cross sections are not expected to vary strongly among heavy elements. In the addition of gold and bismuth cross sections, the gold results were shifted slightly toward lower

energies to account for the difference in neutron binding energies. Bismuth (p,xn) cross sections were chosen since Bi^{209}, like Au^{197}, is an odd A, odd Z nucleus. Since the total (p,pxn) contribution to the cross-section sum shown in Fig. 6 is only about 20%, the addition procedure is justified to well within the errors in the experimental measurements.

One of us (T. M. K.) wishes to thank the National Research Council for scholarships received during the course of this work.

REFERENCES

AAMODT, R. L., PETERSON, V., and PHILLIPS, R. 1952. Phys. Rev. **88**, 739.
BELL, R. E. and SKARSGARD, H. M. 1956. Can. J. Phys. **34**, 745.
BISI, A., GERMAGNOLI, E., and ZAPPA, L. 1959. Nuovo Cimento, **11**, 843.
COHEN, B. L. 1957. Phys. Rev. **105**, 1549.
——— 1959. Phys. Rev. **116**, 426.
COHEN, B. L., NEWMAN, E., CHARPIE, R. A., and HANDLEY, T. H. 1954. Phys. Rev. **94**, 620.
COHEN, B. L. and RUBIN, A. G. 1959. Phys. Rev. **114**, 1143.
EISBERG, R. M. 1960. Proceedings of the International Conference on Nuclear Structure, Kingston, Canada, *edited by* D. A. Bromley and E. W. Vogt (University of Toronto Press, Toronto, and North-Holland Pub. Co., Amsterdam).
EISBERG, R. M. and IGO, E. 1954. Phys. Rev. **93**, 1039.
FINK, R. W. and WIIG, E. O. 1954. Phys. Rev. **96**, 185.
GOLOSKIE, R. 1961. Private communication.
GOODING, T. J. 1959. Nuclear Phys. **12**, 241.
GRIFFITHS, R. J. and EISBERG, R. M. 1959. Nuclear Phys. **12**, 225.
GUSAKOW, M. M., LEGOUX, Y., and SERGOLLE, M. H. 1960. Compt. rend. **251**, 70.
JACKSON, J. D. 1956. Can. J. Phys. **34**, 767.
KIKUCHI, K. 1960. Nuclear Phys. **20**, 590.
METROPOLIS, M., BIVINS, R., STORM, M., TURKEVICH, A., MILLER, J. M., and FRIEDLANDER, G. 1958. Phys. Rev. **110**, 185, 204.
MEYER, V., EISBERG, R. M., and CARLSON, R. F. 1960. Phys. Rev. **117**, 1334.
SOSNIAK, J. 1958. Thesis, McGill University.
THIEME, M. T. and BLEULER, E. 1956*a*. Phys. Rev. **101**, 1031.
——— 1956*b*. Phys. Rev. **102**, 195.
WHITEHEAD, A. B. and FOSTER, J. S. 1958. Can. J. Phys. **36**, 1276.
WILKINSON, G. 1949. Phys. Rev. **75**, 1019.
YULE, H. P. and TURKEVICH, A. 1960. Phys. Rev. **118**, 1591.

THE RATIO OF THE RESONANCE INTEGRAL TO THE THERMAL NEUTRON CROSS SECTION FOR Sm^{152} [1]

W. H. Walker and R. E. Green

ABSTRACT

Cadmium ratio measurements have been made in similar lattice positions in ZEEP with thin foils of Sm^{152} and gold. From a comparison of these cadmium ratios we find

$$(I'/g\sigma_0)_{Sm^{152}} = 14.65 \pm 0.41.$$

If $g\sigma_0$ is assumed to be 212 ± 12 barns, then $I' = 3100 \pm 200$ barns. On the assumption that only one resonance in Sm^{152}, at 8 ev, contributes appreciably to both the resonance integral and the thermal cross section, it follows that $g = 1$ and that Γ, the width at half-maximum of the total cross section resonance, is 193 ± 5 milli-ev. Because of the appreciable disagreement between this value and one reported earlier, a new time-of-flight measurement of the resonance parameters has been made, and it is reported in the next paper (Chrien 1961).

INTRODUCTION

Although the presence of a large resonance at 8 ev in Sm^{152} was first noted in 1954 (Sailor, Landon, and Foote 1954) only recently have the parameters become generally available (Hughes *et al.* 1960). Because the neutron scattering width is unusually large for a resonance energy of the order of a few electron volts, it has not been possible to determine either width to the degree of accuracy usually associated with time-of-flight measurements in this energy region.

Even before the resonance was located, activation measurements were made of the epicadmium resonance integral (Sunyar and Goldhaber 1949) and of the ratio of the resonance integral to the thermal cross section (Harris *et al.* 1950). More recently the resonance integral and thermal cross section have been determined using the Harwell pile oscillator (Tattersall *et al.* 1960), and a crystal spectrometer has been used to measure the 2200 m/sec cross section (Pattenden 1958). The measured cross sections and values calculated from resonance parameters cover such a wide range that a further measurement of the cadmium ratio using thin foils seemed justified. A tabulation of the earlier results is included in Table III.

THEORY

The theoretical basis for relating the cadmium ratio and $I'/g\sigma_0$ has been discussed in detail elsewhere (Walker *et al.* 1960). Only an outline sufficient for the present experiment will be given here. We assume that the neutron flux can be resolved into a Maxwellian component and an epithermal component having a $1/E$ distribution, that the radiative capture cross sections of the target nuclei follow closely the $1/v$ law in the subcadmium region, and that

[1]Manuscript received May 18, 1961.
Contribution from the Reactor Physics Branch, Atomic Energy of Canada Limited, Chalk River, Ontario.
Issued as A.E.C.L. No. 1272.

the cadmium cover is sufficiently thick to eliminate all thermal neutrons. Then, for two different nuclei, A and B, irradiated in the same spectrum,

$$(1) \qquad \frac{(FR_{Cd}-1)_A}{(FR_{Cd}-1)_B} = \frac{(G_r I'/g\sigma_0)_B + \sqrt{\pi}/2K}{(G_r I'/g\sigma_0)_A + \sqrt{\pi}/2K},$$

where R_{Cd} is the measured cadmium ratio, in the present case the ratio of the activity of a detector wrapped in aluminum to that of a detector wrapped in cadmium,

σ_0 is the cross section for neutrons with a velocity of 2200 m/sec,

$g\sigma_0$ is the effective absorption cross section for a Maxwellian neutron distribution with characteristic temperature T,

I' is the "reduced" resonance integral, i.e. the usual absorption integral $\int \sigma_a(E)\,(dE/E)$ over the entire epithermal spectrum minus the contribution of the $1/v$ extrapolation of the "Maxwellian" cross section $g\sigma_0$,

F is a factor accounting for the reduction of resonance neutrons due to the high energy wing of the cadmium resonance at 0.2 ev,

G_r is the resonance self-shielding factor for detectors that are not infinitely thin, and

$1/K$ is proportional to the $1/v$ activation above the cadmium cutoff.

Since σ_0 and I' are known for gold (a summary of experimental data is given by Walker *et al.* 1960), a comparison of the cadmium ratios of gold and Sm^{152} will yield a value of $I'/g\sigma_0$ for Sm^{152} provided the other parameters can be estimated.

EXPERIMENTAL PROCEDURE

The sample material used in these measurements contained >98% samarium. The main contaminants were Cb (<0.1%), Pb (<0.1%), Zr (<0.1%), Ce (<0.5%), Pr (<0.2%), and Eu (~0.1%). The samarium was highly enriched in Sm^{152}; the relative abundances of the various samarium isotopes are shown in Table I.

TABLE I

Relative abundances of samarium isotopes

Isotope	Abundance (wt.%)
Sm^{144}	0.03
Sm^{147}	0.20
Sm^{148}	0.20
Sm^{149}	0.27
Sm^{150}	0.30
Sm^{152}	97.20
Sm^{154}	1.80

A solution of samarium nitrate in lacquer was used in the foil preparation. The samarium was deposited as samarium oxide (Sm_2O_3) on a 0.0025 cm thick sheet of spectroscopically pure aluminum by painting on a thin coat of lacquer containing about 8 $\mu g/cm^2$ of samarium and then burning off the lacquer by

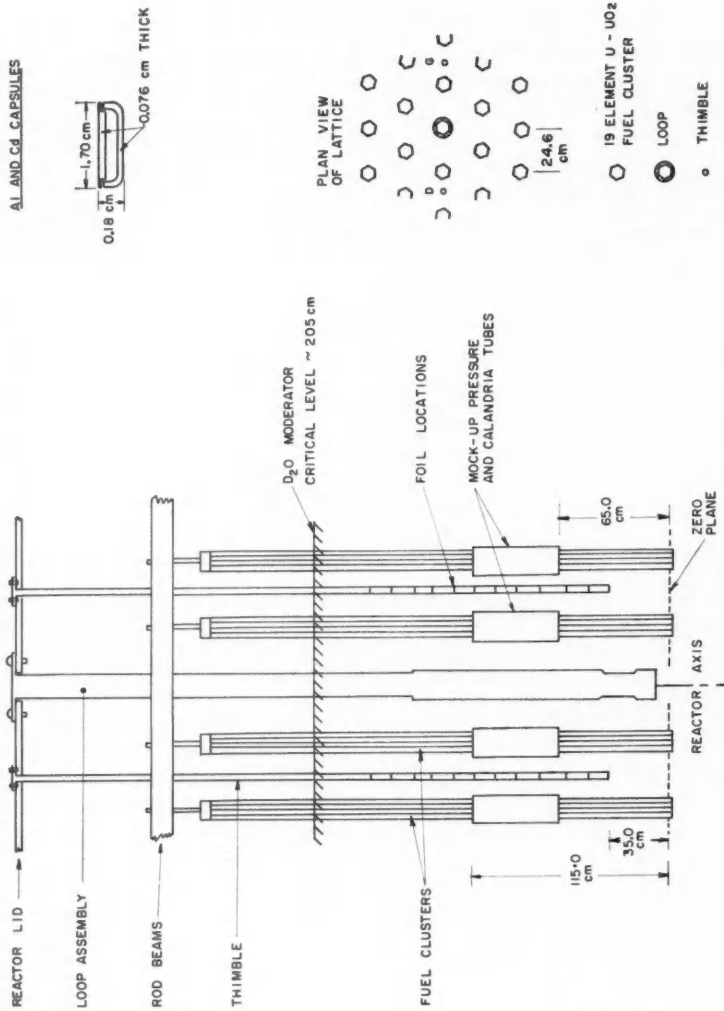

FIG. 1. Experimental arrangement in ZEEP.

"firing" in an oven at ~500° C. This process was repeated until a layer containing ~140 $\mu g/cm^2$ of Sm^{152} was built up. From this foil six 1.31 cm diameter disks were cut.

The average deposit thickness was estimated from the total amount of material used, assuming that the deposit was evenly distributed over the painted area. In a target of Pu^{240} prepared in a similar way (Walker *et al.* 1960) scanning with an α-probe showed that no local deviation exceeded 15%. The relative amounts of Sm^{152} on each of the six foils were determined, by activation, to have a standard deviation from the mean of 9%, and a maximum spread of 26% on the mean. On this basis we conclude that the mean deposit thickness, 140 $\mu g/cm^2$, is correct to $\pm 13\%$.

The gold target material was prepared by vacuum evaporation of pure gold onto spectroscopically pure aluminum foils. Average deposit thicknesses were determined by weighing the backing foil before and after deposition. Six gold targets were cut; four of these were 1 cm by 1 cm square foils, ~450 $\mu g/cm^2$ gold thickness, and the other two were disks, ~210 $\mu g/cm^2$ gold thickness and the same diameter as the samarium foils. The maximum spread in the relative amounts of gold in these foils was found to be 10% by activation. The mean deposit thicknesses are therefore assumed to be correct to $\pm 5\%$.

For the cadmium ratio measurements the foils were placed in aluminum and cadmium capsules having 0.076 cm thick walls. These capsules were mounted on thin aluminum channels which were, in turn, inserted into aluminum thimbles attached to the ZEEP reactor lid (see Fig. 1). The thimbles used in these irradiations were D and G, located at cell boundary positions in the lattice on opposite sides of the pile and equidistant from the center. They were not filled with moderator.

In addition to the central assembly, which was changed from time to time, the lattice in which these measurements were made consisted of the following: a core of eighteen 19-element U–UO_2 clusters (each cluster contained fifteen 1.32 cm diameter UO_2 elements and four 1.31 cm diameter U elements), an intermediate region of eighteen 19-element UO_2 clusters, and an outer ring of 42 ZEEP rods (3.26 cm diameter U rods) which acted as a driver region for the lattice. The cluster-type rods formed a hexagonal array with a center-to-center spacing of 24.6 cm. (For further details of these fuel elements see Hone *et al.* 1958.) The central site contained either a loop assembly (Bigham *et al.* 1961) or a normal 19-element UO_2 cluster, or was empty at various times throughout these experiments. Our measurements were always made in thimbles D and G in the U–UO_2 cluster region (see Fig. 1).

The usual procedure was to put the cadmium-covered foils in one thimble and the aluminum-covered ones in the other with the foils of a given type at the same elevation. At other times both foils of one type were mounted in the same thimble at different elevations spaced so that the cadmium capsule did not depress the thermal flux at the position of the aluminum-covered detector. Copper foils were also placed at various elevations in both thimbles to check any radial asymmetry (always $\lesssim 1\%$) and to map the axial flux distribution for the case when the foils were at different elevations.

Since the fuel rods in the U–UO_2 cluster region of the pile had 51 cm long mock-ups of pressure and calandria tubes (see Fig. 1) the epithermal fraction of the neutron density was not constant all along the axis of the pile but was higher in the region of the double-walled tubes. For most of the measurements reported here the foils were placed well away from these tubes but for the early runs some of the foils were in or near this region. The latter measurements have been corrected for the effect of the double-walled tubes using epithermal neutron densities determined from the cadmium ratios of 0.025 cm diameter gold wires placed along the axis of the pile.

The irradiated detectors were counted with a system which included two NaI(Tl) scintillation counters and an automatic sample changer and readout unit. The counters were biased to accept all pulses corresponding to γ-ray energies >30 kev. The data were recorded on typewritten sheets and on punched tape and were reduced by feeding the latter into the Burroughs-205 computer at Chalk River, which made corrections for decay, counter deadtime, and background.

The resulting cadmium ratios are listed in Table II. In order to obtain

TABLE II

Measured values of R_{Cd}. Derived values of $(G_r I'/g\sigma_0)_{Sm^{152}}$

Irradiation	$(R_{Cd})_{Sm^{152}}$	$(R_{Cd})_{Au}$	$(G_r I'/g\sigma_0)_{Sm^{152}}$
1	3.099	2.942	13.82[a]
2	3.051	3.030	13.90[a]
3	3.124	2.958	13.88[a]
4	3.162	3.061	14.32[a]
5	3.118	3.097	14.38
6	3.135	3.024	13.89[a]
7	3.096	3.041	14.12
8	3.120	3.018	13.90
9	3.130	3.023	14.07
10	3.124	3.056	14.05
11	3.150	3.009	13.84
12	3.141	3.045	13.85

Mean value of $(G_r I'/g\sigma_0)_{Sm^{152}} = 14.00 \pm 0.06$

[a]These values were corrected for differences in the epithermal fraction of the neutron density at various gold and samarium detector sites.

$G_r I'/g\sigma_0$ for Sm^{152} from the measured ratios, it is necessary to know the value of K appropriate to the irradiation conditions, values of F for both gold and Sm^{152} for the thickness of cadmium used, and the value of $G_r I'/g\sigma_0$ for gold. Values of K have been calculated for a $1/v$ detector in a $1/E$ spectrum using the known variation of the cadmium cross section with energy (Westcott *et al.* 1958). For an infinite slab (or thin foil) in an isotropic flux, and 0.076 cm (0.030 in.) of cadmium, $K = 2.20$. Values of g have been calculated for Maxwellian distributions having temperatures from 20° C up (Westcott 1960). The effective neutron temperature in the moderator of this ZEEP lattice is known to be about 10° above moderator temperature, i.e. ~30° C (Bigham and Tunnicliffe 1961), so that for these irradiations $g_{Au} = 1.006$.

The capture by cadmium of neutrons at resonance energies can be computed from the parameters of the 0.2-ev resonance, assuming that contributions

from other resonances are negligible. The cadmium capture cross section at the gold resonance energy, 4.9 ev, is 0.2 barn, and at 8.0 ev, the Sm^{152} resonance energy, it is about 0.06 barn. The corresponding F-values for 0.076-cm cadmium are 0.994 and 0.998.

For resonances in which capture predominates, as in the case of gold, resonance self-shielding can be calculated using the method described by Roe (1954). For the gold foils used here we estimate a value for $(G_r)_{Au}$ of 0.951 for the 450 $\mu g/cm^2$ foils and 0.971 for the 210 $\mu g/cm^2$ foils. Using these factors and taking $(\sigma_0)_{Au} = 98.6$ barns and $(I')_{Au} = 1525$ barns (Walker *et al.* 1960), the measured cadmium ratios can be used to derive the values of $G_rI'/g\sigma_0$ for Sm^{152} listed in the last column of Table II. Those results which required correction for differences in the value of the epithermal neutron fraction have been noted; in every case the correction was less than 3% in the ratio $(G_rI'/g\sigma_0)_{Sm^{152}}$. The mean value of $(G_rI'/g\sigma_0)_{Sm^{152}}$ for 12 irradiations is 14.00 ± 0.06; the error is based on the reproducibility of the individual measurements.

In order to derive $I'/g\sigma_0$ for Sm^{152} we require $(G_r)_{Sm^{152}}$. A straightforward calculation using Roe's method is not possible since in Sm^{152} the probability of scattering is of the same order of magnitude as that of radiative capture, and the effect of resonance scattering is not well understood. In the estimates which follow we use the recently measured values of the resonance parameters (Chrien 1961). An upper limit of 0.955 for $(G_r)_{Sm^{152}}$ is obtained if resonance scattering is assumed to have no effect; on the other hand, if scattering is considered to be just as effective as absorption then the value is 0.94. However, recent work with manganese detectors indicates that scattering is about one-quarter as effective as absorption, whence $(G_r)_{Sm^{152}} = 0.95$; this is the value we will adopt here.

A further correction is required to allow for the fact that the epithermal spectrum is not exactly $1/E$ in this energy region. Calculations of the slowing-down spectrum have been made for a fuel arrangement very similar to the one used in these experiments, namely, 19-element uranium oxide clusters in a 24.6-cm hexagonal array (Bigham and Pearce 1961). These calculations indicate an average deviation of $\lesssim 0.2\%$ per ev in the region 3–8 ev, in a direction which makes the flux smaller as E decreases. Since the resonance activation is proportional to the resonance flux times I', a correction factor of 0.994 must be applied to our result.

The average value of the ratio of the reduced resonance integral to the cross section in a Maxwellian spectrum, $(I'/g\sigma_0)_{Sm^{152}}$, will also have the following errors in addition to the one assigned in Table II to the average ratio $(G_rI'/g\sigma_0)_{Sm^{152}}$:

(i) The error in the ratio $(I'/\sigma_0)_{Au}$, 2.6%. This is due almost entirely to uncertainties in the resonance parameters, which give a calculated reduced resonance integral I' of 1525 ± 40 barns (Walker *et al.* 1960).

(ii) The error in the self-shielding factor $(G_r)_{Sm^{152}}$, 0.7%. For foils of this thickness G_r is relatively insensitive to errors in the resonance parameters or estimates of foil thickness. The 13% uncertainty in foil thickness gives rise to an error of 0.13×0.04, or 0.5% in $(G_r)_{Sm^{152}}$. The error due to uncertainty in the effect of resonance scattering is taken to be about 0.5%.

(iii) The error in the self-shielding factor $(G_r)_{Au}$, 0.3%, due to the uncertainties in the deposit thicknesses.

(iv) The uncertainty in the correction for the fact that the flux is not exactly $1/E$, 0.5%.

(v) Errors due to uncertainties in the quantities g_{Au}, F_{Au}, $F_{Sm^{152}}$, and K are all negligible.

The derived value for the ratio of the reduced resonance integral to the cross section in a Maxwellian spectrum is therefore

$$(I'/g\sigma_0)_{Sm^{152}} = 14.65 \pm 0.41.$$

This result is compared in Table III with values derived from earlier cross-section measurements.

TABLE III

Comparison of results of cross-section measurements for Sm^{152}

Source	Resonance integral I' (barns)	Thermal cross section $g\sigma_0$ (barns)	$I'/g\sigma_0$
Sunyar and Goldhaber (1949)	2400	—	—
Harris *et al.* (1950)	—	—	14[a]
Pattenden (1958)	—	200±6	—
From resonance parameters (Hughes *et al.* 1960)	2100	100	21[b]
Tattersall *et al.* (1960)	2850±300	224±7	12.7±1.4
This work	—	—	14.65±0.41

[a]The original data have been corrected for resonance self-shielding in the thick samarium detector, estimated to be a factor of 0.8.

[b]Contributions from the only known resonance, at 8 ev.

DISCUSSION

It is unlikely that any other level, virtual or bound, is contributing significantly to the cross section in the thermal region, since Sm^{152}, an even–even nucleus, is expected to have an average level spacing of several hundred electron volts. This assumption is supported by the crystal spectrometer measurements of Pattenden (1958), who found no significant deviation from a $1/v$ variation in this region. We therefore assume that $g_{Sm^{152}} = 1.0$ to better than 1%, and $(I'/\sigma_0)_{Sm^{152}} = (I'/g\sigma_0)_{Sm^{152}} = 14.65 \pm 0.41$.

Two recent measurements of the thermal cross section give $\sigma_0 = 200 \pm 6$ barns (Pattenden 1958) and $g\sigma_0 = 224 \pm 7$ barns (Tattersall *et al.* 1960). In view of the discussion above, it is unlikely that any significant part of the discrepancy can be assigned to g. Assuming a mean value $\sigma_0 = 212 \pm 12$ then, we obtain from our measured ratio a value for the reduced resonance integral of

$$I' = 3100 \pm 200 \text{ barns},$$

where the error is predominantly due to the uncertainty in the 2200 m/sec cross section.

Because the level spacing in Sm^{152} is expected to be several hundred electron volts, it is probable that the 8-ev resonance dominates the resonance integral as well as the thermal cross section. In this case it can be shown that

$$I' = \frac{\pi \sigma_r \Gamma_\gamma}{2E_r} + \text{small terms},$$

and

$$\sigma_0 = \frac{\sigma_r \Gamma \Gamma_\gamma}{4E_r^2} \sqrt{E_r/E_0} + \text{small terms},$$

hence

$$I'/\sigma_0 = \frac{2\pi \sqrt{E_0 E_r}}{\Gamma} + \text{small terms},$$

where Γ is the width at half-maximum of the total cross-section peak,
Γ_γ is the partial width for radiative capture,
$E_0 = 0.02530$ ev, the energy of 2200 m/sec neutrons,
E_r is the energy at the resonance peak, and
σ_r is the total cross section at the peak of the resonance, excluding potential scattering.

Γ, Γ_γ, and E_r are in electron volts. For the 8-ev resonance in Sm^{152} the small terms in I' and σ_0 are about 0.2% and 0.1%, respectively, of the first term, so that for the ratio I'/σ_0 the error in neglecting the small terms is about 0.1%. Thus,

$$\Gamma = 2\pi \sqrt{E_0 E_r} \frac{\sigma_0}{I'} = 193 \pm 5 \text{ milli-ev.}$$

This value for Γ disagrees appreciably with the value inferred from the compilation by Hughes *et al.* (1960). They quote $\Gamma_n = 79 \pm 8$ and $\Gamma_\gamma = 57 \pm 30$, so that $\Gamma = 136 \pm 31$ milli-ev. On the basis of this disagreement a time-of-flight measurement of the 8-ev resonance was proposed, using the BNL – Chalk River chopper facility. The results of this investigation are reported in the succeeding paper.

ACKNOWLEDGMENTS

The authors wish to thank all those who assisted in any way throughout the course of this work. In particular, they wish to thank G. T. Ewan who kindly gave us a part of his supply of Sm_2O_3 enriched in Sm^{152}, Mrs. J. S. Merritt for preparing the lacquer solution used to prepare the foils, and J. T. R. Young for preparing the Sm foils and for help in carrying out the irradiations. They also with to thank Mrs. M. Cahill and Mrs. J. Hollies who handled the Datatron programming and Miss E. Gehlert who typed the manuscript. Helpful discussions were held with R. M. Pearce and A. G. Ward.

REFERENCES

BIGHAM, C. B., CHIDLEY, B. G., and TURNER, R. B. 1961. Atomic Energy of Canada Ltd., Report CRRP-985-B.

BIGHAM, C. B. and PEARCE, R. M. 1961. Atomic Energy of Canada Ltd., Report AECL-1228.

BIGHAM, C. B. and TUNNICLIFFE, P. R. 1961. Atomic Energy of Canada Ltd., Report AECL-1186.

CHRIEN, R. E. 1961. Can. J. Phys. **39**. This issue.

HARRIS, S. P., MUEHLHAUSE, C. O., and THOMAS, G. E. 1950. Phys. Rev. **79**, 11.
HONE, D. W., CRITOPH, E., DURET, M. F., GREEN, R. E., OKAZAKI, A., PEARCE, R. M., and PEASE, L. P. 1958. Proceedings of the International Conference on the Peaceful Uses of Atomic Energy, Vol. 12, p. 351.
HUGHES, D. J., MAGURNO, B. A., and BRUSSEL, M. K. 1960. Brookhaven National Laboratory, Report BNL-325, 2nd ed., Suppl. 1.
PATTENDEN, N. J. 1958. Proceedings of the International Conference on the Peaceful Uses of Atomic Energy, Vol. 16, p. 44.
ROE, G. M. 1954. Knolls Atomic Power Laboratory, Report KAPL-1241.
SAILOR, V. L., LANDON, H. H., and FOOTE, H. L. 1954. Phys. Rev. **96**, 1014.
SUNYAR, A. W. and GOLDHABER, M. 1949. Phys. Rev. **76**, 189(A).
TATTERSALL, R. B., ROSE, H., PATTENDEN, S. K., and JOWITT, D. 1960. Reactor Sci. **12**, 32.
WALKER, W. H., WESTCOTT, C. H., and ALEXANDER, T. K. 1960. Can. J. Phys. **38**, 57.
WESTCOTT, C. H. 1960. Atomic Energy of Canada Ltd., Report AECL-1101.
WESTCOTT, C. H., WALKER, W. H., and ALEXANDER, T. K. 1958. Proceedings of the International Conference on the Peaceful Uses of Atomic Energy, Vol. 16, p. 70.

RESONANCE PARAMETERS FOR THE 8-ev LEVEL OF Sm^{152} [1]

R. E. CHRIEN

ABSTRACT

The joint BNL–AECL Fast Chopper Facility operating at the NRU reactor at Chalk River has been used to determine the resonance parameters of the 8-ev level of Sm^{152}. Using a resonance shape analysis method, the following parameters were obtained: $E_0 = 8.02 \pm 0.02$ ev, $\Gamma = 205 \pm 15$ milli-ev, and $\Gamma_n = 79 \pm 3$ milli-ev. With these values, a reduced resonance capture integral of 3090 ± 220 barns is calculated, in agreement with recent cadmium ratio measurements.

INTRODUCTION

There is considerable interest in the resonance capture properties of the nuclide Sm^{152} because of its importance as a fission product, particularly for Pu^{239} fission. Measurements of the resonance capture integral for this nuclide are in disagreement with a value calculated from previously reported resonance parameters for the 8-ev level (Hughes *et al.* 1960), a large level which dominates the resonance integral of Sm^{152}. Recent measurements at Harwell (Tattersall *et al.* 1960) and at Chalk River (Walker and Green 1961) lead to reduced resonance capture integrals of 2850 ± 300 barns and 3100 ± 200 barns, respectively, compared with 2100 barns as computed from resonance parameters. This discrepancy suggested a remeasurement of the parameters of the 8-ev level with the BNL–AECL Fast Chopper Facility at Chalk River.

EXPERIMENT

The BNL–AECL Fast Chopper Facility consists of the BNL-type fast chopper operating in conjunction with an 88.2-meter flight path at the NRU reactor. The detector is made up of an array of 384 counter elements in a common atmosphere of BF_3 gas. The time analysis of the neutron counts is done with the Brookhaven 1024-channel time analyzer. A detailed description of the Chalk River Facility will soon appear elsewhere (Zimmerman *et al.* 1961). Except for minor instrumental changes the chopper is identical with the one in operation at the Brookhaven research reactor (Seidl *et al.* 1954).

A sample of samarium enriched to 97.2% Sm^{152} was made by preparing a solution of samarium nitrate in a lacquer base and applying it to an aluminum backing according to the prescription given by Walker and Green (1961). In the present experiment 15 successive layers of Sm^{152} were built up using various brush-stroke directions. Strips of approximately 5×2 cm were cut from the center of the foil and four such strips were stacked to give a sample thickness of 4.60×10^{18} atoms/cm^2 of Sm^{152}.

The chopper was run at 2000 r.p.m. giving a repetition rate of 267 bursts/sec with the eight-armed rotor.

[1]Manuscript received May 18, 1961.
Contribution from the Brookhaven National Laboratory, Upton, N.Y.

The use of an 88-meter flight path with a rotor designed for 20-meter operation introduces the problem of "overlapping" of neutrons from successive bursts. The low-energy cutoff of the rotor is such that fast neutrons from the previous burst overtake slower neutrons before they reach the detection station. In the present experiment the use of a boron filter reduced the overlap background component to an amount much smaller than "room" background. The amount of overlap was determined by running a thick ($\frac{1}{4}$ in.) sample of U^{238} and observing the counting rate in the region of resonances, where, for a sample of this thickness, the transmission is very nearly zero.

The untreated data of this experiment are shown in Fig. 1. About 4000

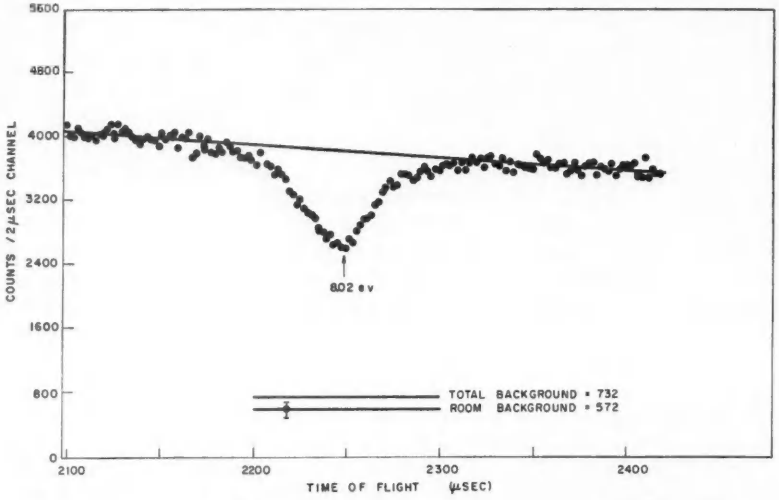

FIG. 1. The counting rate curve in the neighborhood of the 8.02-ev level of Sm^{152}. The total background indicated is the sum of the room background and the overlap components. This curve is the summation of several runs totalling 7639 minutes' duration.

counts per 2-μsec channel were recorded in the neighborhood of the resonance in several runs of 7639 minutes' total duration. The room background, that is, the beam-independent background, and overlap backgrounds are indicated in the figure. The counting rate in the "open beam" or sample out position as shown is not measured, but is computed by fitting a least-squares straight line to the counts in the neighborhood of the resonance. This line was then used for conversion of the data to transmission form.

ANALYSIS

Because of the high resolution available, a "shape" analysis of the 8-ev level was performed. The resolution function of the chopper was calculated by compounding the following contributions: a triangular chopper burst of 5.0 μsec full width at half-maximum, a time uncertainty of 4.8 μsec resulting from the flight time of an 8-ev neutron in the detector, and an analyzer channel width of 2.0 μsec. The compounding of these contributions results

in a function which is very nearly Gaussian in form with a standard deviation of 2.51 μsec. This corresponds to 52.5 milli-ev and is to be compared with a Doppler width of 74 milli-ev and a level width of about 200 milli-ev. Thus the resolution corrections on the observed shape are quite small.

The Doppler-broadened single level formula tables of Sailor (1953) were used for the shape analysis. The observed transmission curve was compared with a series of resolution-broadened, Doppler-broadened curves for various values of Γ, with the total area of the resonance held fixed to the experimentally observed value. That value of Γ was selected which corresponded to a minimum in the sum of the squares of the deviations between the observed and expected data points. The best fit was obtained for the following set of parameters:

$$\Gamma = 205 \pm 15 \text{ milli-ev},$$
$$\Gamma_n = 79 \pm 3 \text{ milli-ev},$$
$$E_0 = 8.02 \pm 0.02 \text{ ev}.$$

Figure 2 shows the fit of the curve based on these parameters to the experimental points.

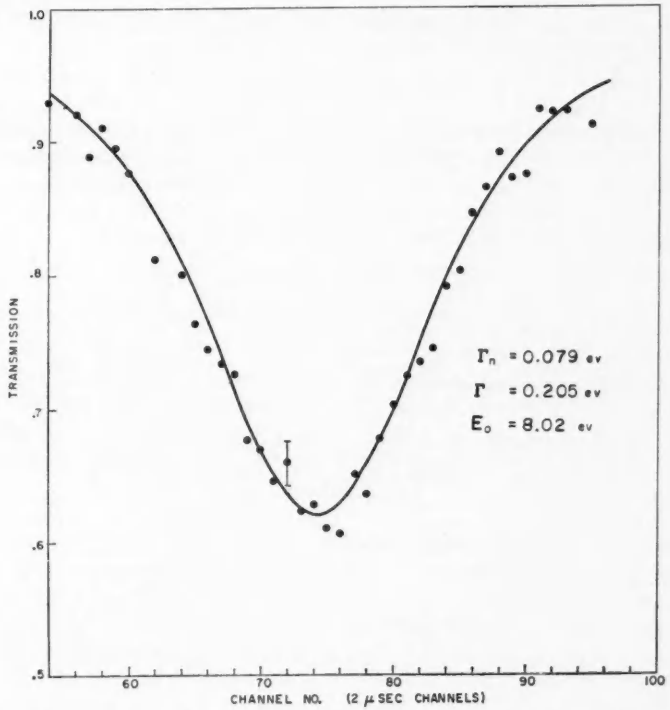

FIG. 2. The result of the shape analysis for the 8.02-ev level. The solid line is the resolution-broadened, Doppler-broadened Breit–Wigner single level curve for the set of parameters shown.

CONCLUSION

With the reasonable assumption that only the 8-ev level is important in determining the capture properties of Sm^{152}, the following quantities may be computed from the presently reported resonance parameters for comparison with experiments done with pile neutrons (for precise definitions of the following quantities refer to Walker and Green (1961)):

(1) The reduced resonance capture integral,

$$I' = 3090 \pm 220 \text{ barns.}$$

(2) The thermal capture cross section,

$$\sigma_0 = 224 \pm 18 \text{ barns.}$$

(3) The ratio of the resonance integral to the thermal neutron cross section,

$$I'/\sigma_0 = 13.8 \pm 1.0.$$

The values of parameters (1), (2), and (3) are in good agreement with recent pile neutron measurements. A detailed listing of these previously obtained parameters is given in the accompanying paper of Walker and Green.

The value of Γ_γ inferred from the present experiments is 126 ± 15 milli-ev, in disagreement with the value of 57 ± 30 quoted in the recent supplement to BNL 325 (Hughes *et al.* 1960). The value of 126 ± 15 milli-ev is significantly greater than that measured for Sm^{147}, Sm^{149}, and Sm^{151}, which all have radiation widths of about 60 milli-ev.

ACKNOWLEDGMENTS

The author is indebted to W. H. Walker and R. E. Green for their suggestion that this experiment be undertaken and for many valuable discussions concerning the interpretation of the data. Appreciation is also expressed to J. T. R. Young who prepared the sample foils, Mrs. J. Hollies who assisted in the computations, and Miss E. Gehlert who typed the manuscript.

REFERENCES

HUGHES, D. J., MAGURNO, B. A., and BRUSSEL, M. K. 1960. Brookhaven National Laboratory Report BNL 325, 2nd ed., Suppl. 1.

SAILOR, V. L. 1953. Brookhaven National Laboratory Report BNL 257 (T-40).

SEIDL, F. G. P., HUGHES, D. J., PALEVSKY, H., LEVIN, J. S., KATO, W. Y., and SJÖSTRAND, N. 1954. Phys. Rev. **95**, 476.

TATTERSALL, R. B., ROSE, H., PATTENDEN, S. K., and JOWITT, D. 1960. Reactor Sci. **12**, 32.

WALKER, W. H. and GREEN, R. E. 1961. Can. J. Phys. **39**. This issue.

ZIMMERMAN, R. L., PALEVSKY, H., CHRIEN, R. E., OLSEN, W. C., SINGH, P. P., and WESTCOTT, C. H. 1961. J. Nuclear Instr. To be published.

ALFVÉN WAVES IN PARTIALLY IONIZED GASES[1]

TOMIYA WATANABE[2]

ABSTRACT

The conditions for a wave, propagated in a partially ionized gas along an external magnetic field, to be of Alfvén type have been obtained.

1. INTRODUCTION

It is well known that hydromagnetic waves can be propagated in a good conducting medium permeated by an external magnetic field. For instance, a sinusoidal transverse wave can be propagated along the external uniform magnetic field, which is characterized by the following two properties (Alfvén 1950):

(i) The velocity of propagation of the wave is given by

$$V = H_0/\sqrt{4\pi\rho_0}\,, \tag{1.1}$$

where H_0 is the intensity of the external magnetic field and ρ_0 is the density of the fluid.

(ii) The density of the kinetic energy of the fluid is equal to that of the magnetic field energy.

These particular waves, called Alfvén waves, are the simplest kind of hydromagnetic waves.

Mathematically speaking, the preceding are inevitable results from the equation of motion of the fluid,

$$\rho_0 \frac{\partial \mathbf{u}}{\partial t} = \frac{1}{c}\mathbf{j} \wedge \mathbf{H}_0, \tag{1.2}$$

and the law of electric conduction in an infinitely good electric conductor,

$$\mathbf{E} + \frac{1}{c}\mathbf{u} \wedge \mathbf{H}_0 = 0, \tag{1.3}$$

as well as Maxwell's equations of the electromagnetic field. Equation (1.3) is the extreme case of the following ohmic law as the conductivity σ tends to infinity:

$$\frac{j}{\sigma} = \mathbf{E} + \frac{1}{c}\mathbf{u} \wedge \mathbf{H}_0. \tag{1.4}$$

It assures the condition of "freezing in" of magnetic lines of force (Cowling 1957). Any volume element of fluid which is extremely conducting cannot

[1]Manuscript received February 6, 1961.
Contribution from the Department of Physics, University of Maryland, College Park, Maryland, U.S.A.

[2]On leave from the Geophysical Institute, Faculty of Science, Tôhoku University, Sendai, Japan. Now at the Department of Physics, University of British Columbia, Vancouver 8, B.C.

move across magnetic lines of force, because no infinitely intense electromotive force may be induced. Due to this "freezing in" condition, a tube of magnetic lines of force can be simulated by a tensile string, since the Maxwell stress can be resolved into the isotropic pressure $H^2/8\pi$, and the tension $H^2/4\pi$ along a magnetic line of force. This analogy leads to the velocity of propagation given by (1.1) (Cowling 1953).

Certainly, eq. (1.3) is mathematically idealized. Actually, there is no material of infinitely good conductivity. One of the conducting fluids of particular interest is an ionized gas. For ionized gases, the equation of motion (1.2) and the law of electric conduction, eq. (1.3), do not always hold true. The condition under which Alfvén waves can exist in a completely ionized and very rarefied gas have been sought by Aström (1951), Schlüter (1952), and Ferraro (1955). Waves in slightly ionized gases have been studied by Hines (1953), and in relation to the ionosphere, by Dungey (1954*a*), Watanabe (1957), and Fejer (1960).

One of the aims of this paper is to derive the conditions for the occurrence of Alfvén waves. The approach is not to manipulate the dispersion relation as done by most of the authors, but to discover the conditions under which the equation of motion (1.2) and the ohmic law of perfect conductivity (1.3) hold true. Another aim is to find out the exact expression for the rate of dissipation of energy of Alfvén waves.

In Sections 2 and 3, the author will derive fundamental equations to describe the electrodynamical behavior of the partially ionized gas and several other useful relations. The conditions for the occurrence of Alfvén waves will be sought in Section 4, and the expression of dissipation rate of the waves in Section 5. Application to the ionosphere will be discussed in Section 6.

2. FUNDAMENTAL EQUATIONS OF WAVES IN PARTIALLY IONIZED GASES

Let us consider an ionized gas which consists of electrons, ions, and neutral particles. Ions are assumed to have been singly ionized. The number density of the electrons is assumed to be equal to that of the ions, and it is represented by N_p. Then, the equations of motion of the electrons, ions, and neutral particles are given by the following, neglecting the pressure terms (Schlüter 1951):

$$\rho_e \frac{\partial \mathbf{u}_e}{\partial t} + N_p^2 \alpha_{ie}(\mathbf{u}_e - \mathbf{u}_i) + N_p N_n \alpha_{en}(\mathbf{u}_e - \mathbf{u}_n) = -eN_p\left(\mathbf{E} + \frac{1}{c}\mathbf{u}_e \wedge \mathbf{H}_0\right), \tag{2.1}$$

$$\rho_i \frac{\partial \mathbf{u}_i}{\partial t} + N_p^2 \alpha_{ie}(\mathbf{u}_i - \mathbf{u}_e) + N_p N_n \alpha_{in}(\mathbf{u}_i - \mathbf{u}_n) = eN_p\left(\mathbf{E} + \frac{1}{c}\mathbf{u}_i \wedge \mathbf{H}_0\right), \tag{2.2}$$

$$\rho_n \frac{\partial \mathbf{u}_n}{\partial t} + N_p N_n \alpha_{in}(\mathbf{u}_n - \mathbf{u}_i) + N_p N_n \alpha_{en}(\mathbf{u}_n - \mathbf{u}_e) = 0. \tag{2.3}$$

The quantities with subscripts e, i, and n refer to the electrons, ions, and neutral particles. ρ_e, ρ_i, and ρ_n represent the mean densities of electrons, ions, and neutral particles respectively. N_n is the number density of neutral particles. $\mathbf{u}_e$, $\mathbf{u}_i$, and $\mathbf{u}_n$ represent the mean velocities of the electrons, ions, and

neutral particles. $\mathbf{H}_0$ is the intensity of the external magnetic field. $\mathbf{E}$ is the induced electric field. The coefficients α_{ie}, α_{en}, and α_{in} are defined by

$$\alpha_{ie} = \frac{\nu_{ie}}{N_p}\frac{m_i m_e}{m_i+m_e} \approx \frac{\nu_{ie} m_e}{N_p}, \tag{2.4}$$

$$\alpha_{en} = \frac{\nu_{en}}{N_n}\frac{m_e m_n}{m_e+m_n} \approx \frac{\nu_{en} m_e}{N_p}, \tag{2.5}$$

$$\alpha_{in} = \frac{\nu_{in}}{N_n}\frac{m_i m_n}{m_i+m_n} \approx \frac{\nu'_{in} m_i}{N_n}, \tag{2.6}$$

$$\nu'_{in} = \tfrac{1}{2}\nu_{in}. \tag{2.7}$$

ν_{ie} is the collision frequency of an ion with electrons; ν_{en} and ν_{in} have similar meanings. m_e, m_i, and m_n are the masses of an electron, ion, and a neutral particle. The ion mass is assumed to be equal to that of a neutral particle, i.e. $m_i = m_n$. The mass of an electron is assumed much smaller than the ion mass. The second and third terms of each equation from (2.1) to (2.3) represent the forces due to collisions between the different kinds of particles. Since we are considering only the case of transverse waves, we may obviously omit the pressure terms. The amplitudes of waves are assumed to be so small that all the quantities may be linearized.

From eqs. (2.1), (2.2), and (2.3), we can derive the following equations (cf. Schlüter 1951):

$$\rho_n \frac{\partial \mathbf{u}_n}{\partial t} = -\frac{H_0}{c}\frac{\nu_1}{\omega_e}\mathbf{j} - \rho_p \nu_2 (\mathbf{u}_n - \mathbf{u}_p), \tag{2.8}$$

$$\rho_p \frac{\partial \mathbf{u}_p}{\partial t} = \frac{H_0}{c}\frac{\nu_1}{\omega_e}\mathbf{j} - \rho_p \nu_2 (\mathbf{u}_p - \mathbf{u}_n) + \frac{H_0}{c}\mathbf{j}\wedge\mathbf{1}, \tag{2.9}$$

where $\mathbf{1}$ is the unit vector parallel to the external magnetic field. ρ_p and $\mathbf{u}_p$ are the density and the mean velocity of the ionized part of the gas, which we shall call here the plasma gas:

$$\rho_p = \rho_i + \rho_e, \tag{2.10}$$

$$\mathbf{u}_p = \frac{\rho_i \mathbf{u}_i + \rho_e \mathbf{u}_e}{\rho_p}. \tag{2.11}$$

The electric current density is given by

$$\mathbf{j} = eN_p(\mathbf{u}_i - \mathbf{u}_e). \tag{2.12}$$

$\mathbf{u}_i$ and $\mathbf{u}_e$ are related to $\mathbf{j}$ and $\mathbf{u}_p$ as follows:

$$\mathbf{u}_i = \mathbf{u}_p + \frac{1}{eN_p}\frac{\rho_e}{\rho_p}\mathbf{j}, \tag{2.13}$$

$$\mathbf{u}_e = \mathbf{u}_p - \frac{1}{eN_p}\frac{\rho_i}{\rho_p}\mathbf{j}. \tag{2.14}$$

The third term on the right-hand side (abbreviated herein as r.h.s.) of eq. (2.9) represents the ampère force, which of course acts on the plasma gas only. The second term of each equation (2.8) and (2.9) may be considered as an internal friction force between the plasma gas and the neutral particle gas. Writing the equations of motion in the forms of (2.8) and (2.9) implies that the behavior of a partially ionized gas can be described by a model of two kinds of fluids, the plasma gas and the neutral particle gas, with the mutual interactions between them due to both collisions and electromagnetic field (Schlüter 1951).

By defining the density and the mean velocity of the whole gas, ρ and $\mathbf{u}$, as follows,

$$\rho = \rho_p + \rho_n, \tag{2.15}$$

$$\mathbf{u} = \frac{\rho_p \mathbf{u}_p + \rho_n \mathbf{u}_n}{\rho}, \tag{2.16}$$

the equation of the whole gas becomes

$$\rho \frac{\partial \mathbf{u}}{\partial t} = \frac{1}{c} \mathbf{j} \wedge \mathbf{H}_0. \tag{2.17}$$

One can also derive the following equation, which may be called the generalized ohmic law (cf. Schlüter 1951):

$$\frac{4\pi}{\omega_p^2}\left(\frac{\partial \mathbf{j}}{\partial t} + \nu_3 \mathbf{j} + \omega_e \mathbf{j} \wedge \mathbf{1}\right) = \mathbf{E} + \frac{H_0}{c} \mathbf{u}_p \wedge \mathbf{1} + \frac{H_0}{c} \frac{\nu_1}{\omega_e} (\mathbf{u}_p - \mathbf{u}_n). \tag{2.18}$$

The coefficients involved are defined by

$$\omega_p^2 = \frac{4\pi N_p e^2}{m_e}, \qquad \omega_p = \text{plasma frequency}, \tag{2.19}$$

$$\omega_e = \frac{eH_0}{m_e c}, \qquad \omega_e = \text{electron gyro-frequency}, \tag{2.20}$$

$$\omega_1 = \frac{eH_0}{m_1 c}, \qquad \omega_1 = \text{ion gyro-frequency}, \tag{2.21}$$

$$\nu_1 = \nu_{en} - \nu'_{in}, \tag{2.22}$$

$$\nu_2 = \nu'_{in} + \frac{m_e}{m_1} \nu_{en}, \tag{2.23}$$

$$\nu_3 = \nu_{1e} + \nu_{en} + \frac{m_e}{m_1} \nu'_{in}. \tag{2.24}$$

The terms of eq. (2.18) are defined as follows. The first term in the left-hand side (abbreviated herein as l.h.s.) may be called the term of plasma oscillation, i.e., the plasma oscillations come from this term. The second and third terms in l.h.s. are the terms of ohmic and Hall electric fields. The second term in r.h.s. is called the dynamo field. The last term in r.h.s. is called here the term of friction electromotive force (abbreviated as the friction e.m.f.).

3. SOME USEFUL RELATIONS

Let us consider sinusoidal transverse plane waves propagated along the external and uniform magnetic field. Wave quantities of the first degree may be assumed to depend on time and space by only one factor

$$e^{i(\omega t+\mathbf{k}\cdot\mathbf{r})}. \tag{3.1}$$

Therefore, the operator $\partial/\partial t$ on the wave quantities of the first degree may be replaced by $i\omega$. Hence, the following result:

$$\mathbf{u}_p = \frac{H_0}{c}\frac{\rho_n}{\rho_p}\frac{1}{\rho\nu_2+i\rho_n\omega}\left[\frac{\nu_1}{\omega_e}\mathbf{j}+\left(1-i\frac{\rho_p}{\rho_n}\frac{\nu_2}{\omega}\right)\mathbf{j}\wedge\mathbf{1}\right], \tag{3.2}$$

$$\mathbf{u}_n = -\frac{H_0}{c}\frac{1}{\rho\nu_2+i\rho_n\omega}\left[\frac{\nu_1}{\omega_e}\mathbf{j}+i\frac{\nu_2}{\omega}\mathbf{j}\wedge\mathbf{1}\right], \tag{3.3}$$

by making use of eqs. (2.8) and (2.9). Then, by use of eq. (2.18), the following are derived:

$$\mathbf{u}_p = \frac{\rho\nu_2}{\rho\nu_2+i\rho_n\omega}\left[\left(1+i\frac{\rho_n}{\rho_p}\frac{\omega}{\nu_2}\right)\mathbf{u}-i\frac{\rho_n}{\rho_p}\frac{\nu_1}{\omega_e}\frac{\omega}{\nu_2}(\mathbf{u}\wedge\mathbf{1})\right], \tag{3.4}$$

$$\mathbf{u}_n = \frac{\rho\nu_2}{\rho\nu_2+i\rho_n\omega}\left[\mathbf{u}+i\frac{\nu_1}{\omega_e}\frac{\omega}{\nu_2}(\mathbf{u}\wedge\mathbf{1})\right]. \tag{3.5}$$

Using eqs. (3.2) and (3.3) or eqs. (3.4) and (3.5), we have

$$\mathbf{u}_p-\mathbf{u}_n = \frac{H_0}{c}\frac{\rho}{\rho_p}\frac{1}{\rho\nu_2+i\rho_n\omega}\left[\frac{\nu_1}{\omega_e}\mathbf{j}+\frac{\rho_n}{\rho}(\mathbf{j}\wedge\mathbf{1})\right], \tag{3.6}$$

or

$$\mathbf{u}_p-\mathbf{u}_n = i\frac{\rho}{\rho_p}\frac{\rho\nu_2}{\rho\nu_2+i\rho_n\omega}\frac{\omega}{\nu_2}\left[\frac{\rho_n}{\rho}\mathbf{u}-\frac{\nu_1}{\omega_e}(\mathbf{u}\wedge\mathbf{1})\right]. \tag{3.7}$$

With eqs. (3.6), (2.18), and Maxwell's fundamental equations, we can show that $\mathbf{j}$ must satisfy the relation

$$\alpha\mathbf{j} = \beta\mathbf{j}\wedge\mathbf{1}, \tag{3.8}$$

where

$$\alpha = -(i\omega+\nu_3)+i\frac{\omega_p^2}{\omega}\frac{1}{1-c^2/V^2}+\frac{\rho\omega_1\omega_e}{\rho\nu_2+i\rho_n\omega}\left\{\left(\frac{\nu_1}{\omega_e}\right)^2-\frac{\rho_n}{\rho}+i\frac{\rho_p}{\rho}\frac{\nu_2}{\omega}\right\} \tag{3.9}$$

and

$$\beta = \omega_e-\frac{2\rho_n\omega_1\nu_1}{\rho\nu_2+i\rho_n\omega}. \tag{3.10}$$

In order that $\mathbf{j}$ may not vanish identically, the following relations should be satisfied:

$$\beta = \pm i\alpha \tag{3.11}$$

and accordingly we have

$$\mathbf{j} = \mp i\mathbf{j} \wedge \mathbf{1}. \tag{3.12}$$

This shows us that there are two kinds of circularly polarized waves. In one of them, eq. (3.12) with + sign, all the field vectors rotate in the same sense that the electrons gyrate. This kind of wave is called the extraordinary wave; the other kind is the ordinary wave.

4. CONDITIONS FOR ALFVÉN WAVES

Equation (3.11) is the dispersion relation. One could examine the characteristics of the waves with this relation as done in Hines' work (1953), and further seek the condition under which waves may become Alfvén waves. In this paper, however, the author will seek the conditions in a way so as to reduce the equation of motion and the equation of the generalized ohmic law to eqs. (1.2) and (1.3) respectively.

A. Slightly Ionized Gases; $\kappa_p = \rho_p/\rho \ll 1$, $\rho_n \approx \rho$

A(*a*) *Strong Magnetic Field*, $\omega_e \gg \nu_1$

In this case, eqs. (3.2) and (3.3) or eqs. (3.4) and (3.5) tell us that

$$|\mathbf{u}_p| \gg |\mathbf{u}_n|, \qquad \text{if } \omega \gg \kappa_p\nu_2,$$

and

$$|\mathbf{u}_p| \ll |\mathbf{u}_n|, \qquad \text{if } \omega \ll \kappa_p\nu_2.$$

A(*a*)i. $\omega \gg \kappa_p\nu_2$

In the frequency range $\omega \gg \kappa_p\nu_2$, the importance of the friction e.m.f. relative to the dynamo field is of the order of ν_1/ω_e, which is always smaller than 1 in this case. In the equation of motion of the plasma gas (2.9), the first term of l.h.s. is always negligible compared with the third term. The friction force is negligible compared with the ampère force only if

$$\omega \gg \nu_2. \tag{4.1}$$

Under these conditions, the equation of motion of the plasma gas is reduced to

$$\rho_p \frac{\partial \mathbf{u}_p}{\partial t} = \frac{H_0}{c}\mathbf{j} \wedge \mathbf{1}, \tag{4.2}$$

and with this relation we easily find that the relative importance of the plasma oscillation term, the ohmic electric field, and the Hall electric field term to the term of the dynamo electric field becomes $\omega^2/\omega_1\omega_e$, $\omega\nu_3/\omega_1\omega_e$, and ω/ω_1, respectively. Therefore, if the following conditions as well as condition (4.1) are satisfied,

$$\omega \ll \sqrt{\omega_1\omega_e}, \tag{4.3}$$

$$\omega \ll \omega_1\omega_e/\nu_3, \tag{4.4}$$

$$\omega \ll \omega_1, \tag{4.5}$$

the dynamo field predominates over the other fields, and thus, we have the relation

$$\mathbf{E}+\frac{1}{c}\mathbf{u}_p \wedge \mathbf{H}_0 = 0. \tag{4.6}$$

Since $\omega_1 < \omega_e$, condition (4.3) is automatically satisfied if condition (4.5) is satisfied. Conclusively, we can say that both eqs. (4.2) and (4.6) hold true for the frequency range

$$\nu_2 \ll \omega \ll \min\,[\omega_1, \omega_1\omega_e/\nu_3], \tag{4.7}$$

and, therefore, Alfvén waves will be propagated along the external magnetic field with the velocity (cf. Fejer 1960)

$$V_1 = \frac{H_0}{\sqrt{4\pi\rho_p}}. \tag{4.8}$$

A(*a*)ii. $\omega \ll \kappa_p\nu_2$

In this case, we have

$$\mathbf{u}_p \approx \mathbf{u}_n \approx \mathbf{u}.$$

Replacing $\mathbf{u}_p$ in the dynamo field term of the generalized ohmic law by $\mathbf{u}$ given by (2.17), we find that the relative importance of the friction e.m.f. to the dynamo field is given by $\nu_1/\omega_e \cdot \omega/\kappa_p\nu_2$, which is smaller than 1 in our case. With the following conditions satisfied, the dynamo field term will predominate over the other terms (plasma oscillation, ohmic electric, and Hall electric fields):

$$\omega \ll \sqrt{\kappa_p\omega_1\omega_e}\,, \qquad \omega \ll \kappa_p\frac{\omega_1\omega_e}{\nu_3}\,, \qquad \omega \ll \kappa_p\omega_1. \tag{4.9}$$

In this case, the generalized ohmic law is reduced to

$$\mathbf{E}+\frac{H_0}{c}\mathbf{u} \wedge \mathbf{1} = 0, \tag{4.10}$$

where $\mathbf{u}$ is the mean velocity of the whole gas. Therefore, in the frequency range

$$\omega \ll \min\left[\kappa_p\nu_2,\ \kappa_p\omega_1,\ \kappa_p\frac{\omega_1\omega_e}{\nu_3}\,,\ \sqrt{\kappa_p\omega_1\omega_e}\right], \tag{4.11}$$

we have Alfvén waves propagated with the velocity

$$V_2 = \frac{H_0}{\sqrt{4\pi\rho}} = \sqrt{\kappa_p}\cdot V_1, \tag{4.12}$$

which is smaller than V_1 given by eq. (4.8) (cf. Fejer 1960).

A(*b*) *Weak Magnetic Field*, $\omega_e \ll \nu_1$

In the frequency range where

$$\omega \gg \kappa_p\nu_2\cdot\frac{\omega_e}{\nu_1}\ (\ll \nu_2)$$

we have $|\mathbf{u}_p| \gg |\mathbf{u}_n|$, and thus, the term representing the friction e.m.f. predominates over the dynamo field.

When

$$\omega \ll \kappa_p \nu_2 \cdot \frac{\omega_e}{\nu_1}, \tag{4.13}$$

we have $\mathbf{u}_p \approx \mathbf{u}_n \approx \mathbf{u}$, and the dynamo field term predominates over the terms representing the plasma oscillation field, the ohmic electric field, the Hall electric field, and the friction e.m.f., if condition (4.9) and the following are satisfied:

$$\omega \ll \kappa_p \nu_2 \left(\frac{\omega_e}{\nu_1}\right)^2. \tag{4.14}$$

Then, we have Alfvén waves propagated with the velocity V_2, in the frequency range

$$\omega \ll \min\left[\kappa_p \nu_2 \left(\frac{\omega_e}{\nu_1}\right)^2, \sqrt{\kappa_p \omega_1 \omega_e}, \kappa_p \frac{\omega_1 \omega_e}{\nu_3}, \kappa_p \omega_1\right]. \tag{4.15}$$

B. Highly Ionized Gases; $\kappa_n = \rho_n/\rho \ll 1$, $\rho_p \approx \rho$

B(a) *Strong Magnetic Field*, $\nu_1 \ll \omega_e$

In this case, the friction force term and the first term in r.h.s. of the equation of motion of the plasma gas is always negligible compared with the ampère force term. Therefore, the equation of motion is reduced to eq. (4.2) and the conditions that the terms of the plasma oscillation, the ohmic electric field, and the Hall electric field are negligible compared with the dynamo electric field term are again given by (4.4) and (4.5).

The importance of the friction e.m.f. relative to the dynamo electric field is conveniently discussed case by case.

B(a)i. *Very Strong Magnetic Field*, $\nu_1/\omega_e \ll \kappa_n \ll 1$

In this case, the friction e.m.f. is always negligible compared with the dynamo electric field. In addition, it can be seen that $\mathbf{u}_p \approx \mathbf{u}_n$ if $\omega \ll \nu_2/\kappa_n$, and $|\mathbf{u}_p| \gg |\mathbf{u}_n|$ if $\omega \gg \nu_2/\kappa_n$. Therefore, we have the following conclusions: If

$$\frac{\nu_2}{\kappa_n} \ll \min\left[\omega_1, \frac{\omega_1 \omega_e}{\nu_3}\right],$$

the Alfvén waves are propagated with the velocity V_1 in the frequency range

$$\frac{\nu_2}{\kappa_n} \ll \omega \ll \min\left[\omega_1, \frac{\omega_1 \omega_e}{\nu_3}\right], \tag{4.16}$$

and with the velocity V_2 in the frequency range

$$\omega \ll \nu_2/\kappa_n. \tag{4.17}$$

If

$$\frac{\nu_2}{\kappa_n} \gg \min\left[\omega_1, \frac{\omega_1 \omega_e}{\nu_3}\right],$$

they are propagated with the velocity V_2, in the frequency range

$$\omega \ll \min\left[\omega_1, \frac{\omega_1\omega_e}{\nu_3}\right]. \tag{4.18}$$

B(a)ii. $\kappa_n \ll \nu_1/\omega_e \ll 1$

In this case, it can be seen that $\mathbf{u}_p \approx \mathbf{u}_n$ if $\omega \ll \nu_2 . \omega_e/\nu_1$ and that $|\mathbf{u}_n| \gg |\mathbf{u}_p|$ if $\omega \gg \nu_2(\omega_e/\nu_1)$.

The friction e.m.f. is always negligible compared with the dynamo electric field if $(\nu_1/\omega_e)^2 \ll \kappa_n$. When $(\nu_1/\omega_e)^2 \gg \kappa_n$, it is negligible only if $\omega \ll \nu_2(\omega_e/\nu_1)^2$. Therefore, we have the following results.

(α) *Moderately Strong Magnetic Field*, $(\nu_1/\omega_e)^2 \ll \kappa_n \ll (\nu_1/\omega_e) \ll 1$

If

$$\nu_2 \frac{\omega_e}{\nu_1} \ll \min\left[\omega_1, \frac{\omega_1\omega_e}{\nu_3}\right],$$

the Alfvén waves are propagated with the velocity V_1 in the frequency range

$$\nu_2 \frac{\omega_e}{\nu_1} \ll \omega \ll \min\left[\omega_1, \frac{\omega_1\omega_e}{\nu_3}\right] \tag{4.19}$$

and with the velocity V_2 in the frequency range

$$\omega \ll \nu_2 . \frac{\omega_e}{\nu_1} . \tag{4.20}$$

If

$$\nu_2 \frac{\omega_e}{\nu_1} \gg \min\left[\omega_1, \frac{\omega_1\omega_e}{\nu_3}\right],$$

the waves are propagated with the velocity V_2, in the frequency range,

$$\omega \ll \min\left[\omega_1, \frac{\omega_1\omega_e}{\nu_3}\right]. \tag{4.21}$$

(β) *Fairly Strong Magnetic Field*, $\kappa_n \ll (\nu_1/\omega_e)^2 \ll \frac{\nu_1}{\omega_e} \ll 1$

If

$$\min\left[\omega_1, \frac{\omega_1\omega_e}{\nu_3}\right] \ll \nu_2 \frac{\omega_e}{\nu_1},$$

the Alfvén waves are propagated with the velocity V_2 in the frequency range

$$\omega \ll \min\left[\omega_1, \frac{\omega_1\omega_e}{\nu_3}\right]. \tag{4.22}$$

If

$$\nu_2 \frac{\omega_e}{\nu_1} \ll \min\left[\omega_1, \frac{\omega_1\omega_e}{\nu_3}\right],$$

the Alfvén waves are propagated with the velocity V_1 in the frequency range

$$\nu_2 \frac{\omega_e}{\nu_1} \ll \omega \ll \min\left[\omega_1, \frac{\omega_1\omega_e}{\nu_3}, \nu_2\left(\frac{\omega_e}{\nu_1}\right)^2\right] \tag{4.23}$$

and with the velocity in the frequency range

$$\omega \ll \nu_2 \frac{\omega_e}{\nu_1}. \tag{4.24}$$

B(*b*) *Weak Magnetic Field*, $\omega_e \ll \nu_1$

In the frequency range where $\omega \ll \nu_2(\omega_e/\nu_1)$, we have $\mathbf{u}_p \approx \mathbf{u}_n \approx \mathbf{u}$ and we find that the relative importance of the friction e.m.f. to the dynamo electric field is of the order of $(\omega/\nu_2).(\nu_1/\omega_e)^2$. It is much smaller than 1 if $\omega \ll \nu_2(\omega_e/\nu_1)^2$. The conditions under which the terms representing the plasma oscillation field, the ohmic field, and the Hall field are negligible compared with the dynamo field are given by (4.9). Conditions in (4.9), however, are practically the same as in (4.4) and (4.5), since κ_p is almost equal to 1 in this case. Therefore, we have Alfvén waves propagated with the velocity V_2, which is almost equal to V_1 in highly ionized gases, for the frequency range

$$\omega \ll \min\left[\omega_1, \frac{\omega_1\omega_e}{\nu_3}, \nu_2\left(\frac{\omega_e}{\nu_1}\right)^2\right]. \tag{4.25}$$

If $\omega \gg \nu_2(\omega_e/\nu_1)$, we have $|\mathbf{u}_n| \gg |\mathbf{u}_p|$, and we find that the friction e.m.f. term predominates over the dynamo field term.

The frequency ranges where Alfvén waves can exist are shown schematically in Table I.

5. RATE OF DISSIPATION OF WAVE ENERGY

It is important to deduce the exact formula of the rate of dissipation of wave energy in problems of damping of waves and heating of ionized gases.

Scalar multiplying both sides of equations (2.1), (2.2), and (2.3) by $\mathbf{u}_e$, $\mathbf{u}_i$, and $\mathbf{u}_n$, we can derive the following equation:

$$-\frac{\partial}{\partial t}\left(\tfrac{1}{2}\rho_e u_e^2 + \tfrac{1}{2}\rho_i u_i^2 + \tfrac{1}{2}\rho_n u_n^2\right) = -(\mathbf{j}\cdot\mathbf{E}) + Q, \tag{5.1}$$

where

$$Q = \nu_{ie} m_e N_p (\mathbf{u}_i - \mathbf{u}_e)^2 + \nu_{en} m_e N_p (\mathbf{u}_e - \mathbf{u}_n)^2 + \nu'_{in} m_i N_p (\mathbf{u}_i - \mathbf{u}_n)^2. \tag{5.2}$$

On the other hand, one can also derive the following equation from Maxwell's equations:

$$(\mathbf{j}\cdot\mathbf{E}) = -\frac{\partial}{\partial t}\left(\frac{E^2}{8\pi} + \frac{h^2}{8\pi}\right) - \operatorname{div}\mathbf{S} \tag{5.3}$$

where Poynting's vector $\mathbf{S}$ is defined by

$$\mathbf{S} = \frac{c}{4\pi}\mathbf{E} \wedge \mathbf{h}. \tag{5.4}$$

Then, we have

TABLE I

Frequency ranges where Alfvén waves can exist

Ionization	Magnetic field		Frequency range	Propagation velocity
Slight	Strong	$\omega_e \gg \nu_1$	$\nu_2 \ll \omega \ll \min\left[\omega_1, \frac{\omega_1\omega_e}{\nu_3}\right]$	V_1
			$\omega \ll \min\left[\kappa_p\nu_2, \kappa_p\omega_1, \kappa_p\frac{\omega_1\omega_e}{\nu_3}, \sqrt{\kappa_p\omega_1\omega_e}\right]$	V_2
	Weak	$\omega_e \ll \nu_1$	$\omega \ll \min\left[\kappa_p\nu_2\left(\frac{\omega_e}{\nu_1}\right)^2, \kappa_p\omega_1, \kappa_p\frac{\omega_1\omega_e}{\nu_3}, \sqrt{\kappa_p\omega_1\omega_e}\right]$	V_2
High	Very strong	$\frac{\nu_1}{\omega_e} \ll \kappa_n \ll 1$	$\frac{\nu_2}{\kappa_n} \ll \omega \ll \min\left[\omega_1, \frac{\omega_1\omega_e}{\nu_3}\right]$	V_1
			$\omega \ll \frac{\nu_2}{\kappa_n}$	V_2
			$\omega \ll \min\left[\omega_1, \frac{\omega_1\omega_e}{\nu_3}\right] \ll \frac{\nu_2}{\kappa_n}$	V_2
	Moderately strong	$\left(\frac{\nu_1}{\omega_e}\right)^2 \ll \kappa_n \ll \frac{\nu_1}{\omega_e} \ll 1$	$\nu_2\frac{\omega_e}{\nu_1} \ll \omega \ll \min\left[\omega_1, \frac{\omega_1\omega_e}{\nu_3}\right]$	V_1
			$\omega \ll \nu_2\frac{\omega_e}{\nu_1}$	V_2
			$\omega \ll \min\left[\omega_1, \frac{\omega_1\omega_e}{\nu_3}\right] \ll \nu_2\frac{\omega_e}{\nu_1}$	V_2
	Fairly strong	$\kappa_n \ll \left(\frac{\nu_1}{\omega_e}\right)^2 \ll \frac{\nu_1}{\omega_e} \ll 1$	$\nu_2\frac{\omega_e}{\nu_1} \ll \omega \ll \min\left[\omega_1, \frac{\omega_1\omega_e}{\nu_3}, \nu_2\left(\frac{\omega_e}{\nu_1}\right)^2\right]$	V_1
			$\omega \ll \nu_2\frac{\omega_e}{\nu_1}$	V_2
			$\omega \ll \min\left[\omega_1, \frac{\omega_1\omega_e}{\nu_3}\right] \ll \nu_2\frac{\omega_e}{\nu_1}$	V_2
	Weak	$\omega_e \ll \nu_1$	$\omega \ll \min\left[\omega_1, \frac{\omega_1\omega_e}{\nu_3}, \nu_2\left(\frac{\omega_e}{\nu_1}\right)^2\right]$	V_2

$$-\frac{\partial}{\partial t}\left(\tfrac{1}{2}\rho_e u_e^2+\tfrac{1}{2}\rho_i u_i^2+\tfrac{1}{2}\rho_n u_n^2\right)-\frac{\partial}{\partial t}\left(\frac{E^2}{8\pi}+\frac{h^2}{8\pi}\right)=\operatorname{div}\mathbf{S}+Q. \tag{5.5}$$

Equation (5.5) is the extended Poynting's theorem. Q gives the accurate rate of dissipation of wave energy. Every term in Q involves a collision frequency in its coefficient, suggesting that the energy of the systematic motion of the gas particles is changed into the thermal energy through collisions. It is to be noticed that the quantity $(\mathbf{j}\cdot\mathbf{E})$ does not give the rate of dissipation in our case.

By making use of eqs. (2.13), (2.14), and (3.6), we have†

$$\bar{Q}=\frac{1}{2}\left(\frac{1}{\sigma_3}+\frac{1}{\sigma_2}\chi\right)\mathbf{j}\cdot\mathbf{j}^*+\frac{2}{\sigma_1}\psi\mathscr{I}(j_x j_y^*), \tag{5.6}$$

where σ_1, σ_2, σ_3, χ, and ψ are given as follows:

$$\frac{1}{\sigma_1}=\frac{m_e\nu_1}{N_p e^2},\qquad \frac{1}{\sigma_2}=\frac{m_i\nu_2}{N_p e^2},\qquad \frac{1}{\sigma_3}=\frac{m_e\nu_3}{N_p e^2}, \tag{5.7}$$

$$\chi=\frac{\rho_n^2\omega_i^2-\rho^2\nu_1^2(m_e/m_i)^2}{\rho^2\nu_2^2+\rho_n^2\omega^2}=\omega_i^2\frac{\rho_n^2-\rho^2(\nu_1/\omega_e)^2}{\rho^2\nu_2^2+\rho_n^2\omega^2}, \tag{5.8}$$

and

$$\psi=\frac{\rho_n^2\omega_i\omega}{\rho^2\nu_2^2+\rho_n^2\omega^2}. \tag{5.9}$$

$\mathbf{j}^*$ represents the complex conjugate of $\mathbf{j}$; hence

$$\mathbf{j}\cdot\mathbf{j}^*=j_x j_x^*+j_y j_y^*. \tag{5.10}$$

In circularly polarized waves, we have

$$\mathscr{I}(j_x j_y^*)=\pm j_x j_x^*=\pm j_y j_y^*=\pm\tfrac{1}{2}\mathbf{j}\cdot\mathbf{j}^*, \tag{5.11}$$

where the + sign corresponds to the extraordinary waves, and thus, $\bar{Q}$ becomes

$$\bar{Q}=\frac{1}{2}\left(\frac{1}{\sigma_3}+\frac{1}{\sigma_2}\chi\pm 2\frac{1}{\sigma_1}\psi\right)\mathbf{j}\cdot\mathbf{j}^*. \tag{5.12}$$

The energy of the magnetic field averaged over one period is given by $(\pi/\omega^2)(V^2/c^2)\mathbf{j}\cdot\mathbf{j}^*$, with the condition that the propagation velocity of the wave is much smaller than the velocity of light. Under this condition, the amount of energy of the electric field becomes negligible compared with that of the magnetic field. In Alfvén waves, this condition is tacitly assumed to be satisfied. Besides, in Alfvén waves the amount of the kinetic energy of the gas particles is equal to that of the magnetic field as mentioned in Section 1. Therefore, the density of the total wave energy averaged over one cycle is $(2\pi/\omega^2)(V^2/c^2)\mathbf{j}\cdot\mathbf{j}^*$. The equation of the extended Poynting's theorem shows that dissipation of the wave energy becomes negligible if the amount of the energy dissipated in a time interval $1/\omega=(1/2\pi)\times$(one period) is negligible

†$\bar{Q}$ is the dissipation rate averaged over one period.

compared with the amount of the total wave energy, which we have calculated above. One can show that the condition is satisfied in the cases mentioned in Section 4.

6. APPLICATION TO THE IONOSPHERE

The ionosphere is slightly ionized; thus the discussions in case A in Section 3 are appropriate.

Table II shows the values of ω_i, ω_e, and ν_{in}, and ν_{en} in the ionosphere

TABLE II

Ionospheric data due to Francis and Karplus (1960). ω_i = ion gyro-frequency, and ω_e = electron gyro-frequency at the geomagnetic latitude 45°. ν_{in} = the collision frequency of an ion with neutral particles. ν_{en} = the collision frequency of an electron with neutral particles. The meanings of T_1 and T_2 are given in Section 6

Altitude, km	ω_i	ω_e	ν_{in}	ν_{en}	T_1	T_2
80	1.60^2	8.47^6	2.05^5	3.29^6	3.92^{-2}	6.14^{-5}
90	1.60^2	8.43^6	3.24^4	5.42^5	3.92^{-2}	3.88^{-4}
100	1.62^2	8.39^6	5.37^3	1.00^5	3.88^{-2}	2.34^{-3}
120	1.71^2	8.32^6	3.12^2	7.93^3	3.68^{-2}	4.03^{-2}
140	1.76^2	8.24^6	7.44^1	2.66^3	3.57^{-2}	1.69^{-1}
160	1.81^2	8.16^6	2.83^1	1.37^3	3.47^{-2}	4.44^{-1}
180	1.87^2	8.09^6	1.33^1	8.86^2	3.36^{-2}	9.46^{-1}
200	1.91^2	8.02^6	6.94^0	6.46^2	3.29^{-2}	1.81^0
250	2.04^2	7.84^6	2.01^0	3.97^2	3.08^{-2}	6.25^0
300	2.16^2	7.66^6	8.25^{-1}	3.83^2	2.91^{-2}	1.53^1
350	2.23^2	7.49^6	3.91^{-1}	4.20^2	2.82^{-2}	3.21^1
400	2.31^2	7.33^6	1.94^{-1}	4.43^2	2.72^{-2}	6.48^1
450	2.34^2	7.17^6	1.00^{-1}	4.32^2	2.68^{-2}	1.26^2
500	2.37^2	7.01^6	5.26^{-2}	4.14^2	2.65^{-2}	2.48^2
550	2.34^2	6.86^6	2.86^{-2}	3.73^2	2.68^{-2}	4.40^2

(Francis and Karplus 1960). One can see that $\nu_1 \approx \nu_{en}$ and $\nu_2 \approx \nu'_{in}$. ν_{ie} is at most of the order of 10^2, and thus we also have, approximately, $\nu_3 \approx \nu_{en}$. Therefore, we have $\omega_i\omega_e/\nu_3 \approx \omega_i\omega_e/\nu_{en}$ and the lower limit of this is of the order of 4×10^2 sec, which is larger than ω_i throughout the ionosphere. And thus, Alfvén waves propagated with the velocity V_1 can occur in the frequency range

$$\nu'_{in} \ll \omega \ll \omega_i, \tag{6.1}$$

or in the period range

$$(T_1 =) \frac{2\pi}{\omega_i} \ll T \ll \frac{2\pi}{\nu_{in}} (= T_2). \tag{6.2}$$

As shown in the table, $\nu'_{in} \gg \omega_i$ ($T_2 \ll T_1$), below an altitude of 100 km. Therefore, no Alfvén wave can appear below this altitude. The lower and upper limits in the period range are also shown in the table. Waves whose periods are shorter than about 3×10^{-2} second cannot be of Alfvén (V_1) type. The upper limit increases with altitude. It has been suggested that Alfvén waves can occur in the exosphere (Dungey 1954*b*) or in the lower ionosphere (Watanabe 1959). For instance, a wave of period 1 second can

penetrate to an altitude of 180 km as an Alfvén wave. Below that it is transformed into an electromagnetic wave as in metallic substances (Watanabe 1957; Piddington 1959). On the other hand, a wave of period 15 seconds can occur only above 300 km.

The rate of dissipation of wave energy is simplified as follows in the ionosphere: $(m_e/m_i)\nu'_{in} \ll \nu_{en}$ and $\nu'_{in} \approx \nu_2$, so that we have

$$\chi = \omega_i^2 \frac{1}{\nu_{in}'^2+\omega^2},$$

$$\psi = \frac{\omega_i \omega}{\nu_{in}'^2+\omega^2},$$

and thus

$$\bar{Q} = \frac{1}{2}\frac{m_e}{N_p e^2}\left\{\left(\nu_{en}+\frac{m_i}{m_e}\frac{\nu'_{in}\omega_i^2}{\nu_{in}'^2+\omega^2}\right)\mathbf{j}\cdot\mathbf{j}^* + 4\nu_{en}\frac{\omega\omega_i}{\nu_{in}'^2+\omega^2}\mathscr{I}(j_z j_y^*)\right\}. \tag{6.3}$$

7. CONCLUSIONS

In a slightly ionized gas, there appear two types of Alfvén waves if the external magnetic field is strong. One type, in which only charged particles partake of the wave propagation (V_1), appears in a higher-frequency range. The other, in which neutral particles also partake of the wave propagation (V_2), appears in a low-frequency limit. If the magnetic field is weak, only the latter type of low-frequency wave appears.

In a highly ionized gas, the situation is more complicated, as shown in Table I. Practically speaking, however, there is little difference between the two kinds of propagation velocities, V_1 and V_2. And, if we do not distinguish between them, the Alfvén waves can be always propagated in a frequency range limited by ω_0,

$$0 < \omega \ll \omega_0. \tag{7.1}$$

The upper limit ω_0 is given by

$$\omega_0 = \min\left[\omega_i, \frac{\omega_i\omega_e}{\nu_3}\right], \tag{7.2}$$

if the conditions $\omega_e \gg \nu_1$ and $(\nu_1/\omega_e)^2 \ll \kappa_n$ are satisfied. In the other cases (fairly strong or weak magnetic fields), ω_0 is given by

$$\omega_0 = \min\left[\omega_i, \frac{\omega_i\omega_e}{\nu_3}, \nu_2\left(\frac{\omega_e}{\nu_1}\right)^2\right]. \tag{7.3}$$

REFERENCES

ALFVÉN, H. 1950. Cosmical electrodynamics (Clarendon Press, Oxford).
ASTRÖM, E. 1951. Arkiv Fysik, **2**, 443.
COWLING, T. G. 1953. The sun, *edited by* G. P. Kuiper (University of Chicago Press).
——— 1957. Magnetohydrodynamics (Interscience Publishers, Inc., New York).
DUNGEY, J. W. 1954*a*. Sci. Rept. No. 57, Ionosph. Research Lab., The Pennsylvania State Univ.
——— 1954*b*. Sci. Rept. No. 69, Ionosph. Research Lab., The Pennsylvania State Univ.

FEJER, J. A. 1960. J. Atmospheric and Terrest. Phys. **18**, 135.
FERRARO, V. C. A. 1955. Proc. Roy. Soc. (London), A, **233**, 310.
FRANCIS, W. E. and KARPLUS, R. 1960. J. Geophys. Research, **65**, 3593.
HINES, C. O. 1953. Proc. Cambridge Phil. Soc. **49**, 299.
PIDDINGTON, J. H. 1959. Geophys. J. **2**, 173.
SCHLÜTER, A. 1951. Z. Naturforsch. **6A**, 73.
——— 1952. Ann. Physik, 6, **10**, 418.
WATANABE, T. 1957. Sci. Repts. Tôhoku Univ. Ser. 5, **9**, 81.
——— 1959. J. Geomag. Geoelectr. **10**, 195.

ANGULAR CORRELATION OF BETA–GAMMA COINCIDENCES IN THE COMPTON EFFECT[1]

F. W. Van Name, Jr. and John W. Koch

INTRODUCTION

In the theory of Compton scattering of photons it is well known that the relation between the angle θ of the scattered photon and the angle Φ of the recoil electron is as follows:

$$\cot \Phi = (1+\alpha) \tan(\theta/2), \tag{1}$$

where α represents the energy of the incident photon in Mev divided by 0.511. Shankland (1937) verified equation (1) to within $\pm 20°$. Cross and Ramsey (1950) verified equation (1) to within $\pm 1°$ using a single target and a single pair of angles. In view of the improved detection and coincidence circuits now available, it was decided to verify equation (1) for a variety of angles and with two different scattering targets.

APPARATUS AND EXPERIMENTAL PROCEDURE

The source was a 10-millicurie interstitial needle of Co^{60} which was placed in a brass rod for ease in centering and for elimination of unwanted beta-rays. A hole $\frac{1}{4}$ in. in diameter was drilled through three lead bricks, thus providing a collimating tube 5.5 in. long. The targets were beryllium, 0.028 in. thick, and carbon, 0.050 in. thick. Each target, in turn, was mounted at one end of a steel pipe 13.5 in. long, which had three Mylar windows each 0.001 in. thick. A vacuum of 15 microns was maintained in this pipe, so that recoil electrons would not be appreciably scattered in their passage from the target to the beta-counter. The large Mylar window behind the target allowed the escape of photons traveling at small angles to the initial direction. The arrangement of the apparatus is shown in Fig. 1.

The recoil electrons were detected by an anthracene crystal and the scattered photons by a NaI(Tl) crystal. The pulses from the two photomultipliers were amplified and sent to a coincidence circuit similar to that described by Garvin (1953), which has a resolving time of 4×10^{-9} second. The coincidences were recorded after passing through a scaler.

The position of the gamma-counter was set at some particular angle and coincidences were measured for 1-hour periods for each position of the beta-counter. The beta-counter was moved in 2° steps up to 6° on each side of the expected angle of maximum coincidences. The data are shown in Table I.

[1]Abstracted from a thesis submitted by John W. Koch in partial fulfillment of the requirements for the M.S. degree in physics at the University of Delaware.

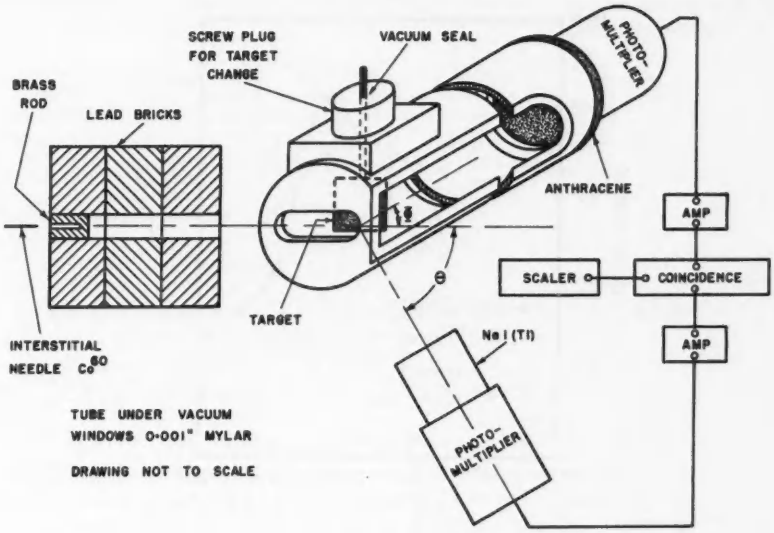

FIG. 1. Diagram of the apparatus.

TABLE I

Angular correlations in the Compton effect

θ, angle of scattered photon	Φ, angle of recoil electron	θ, angle of scattered photon	Φ, angle of recoil electron
Carbon		Beryllium	
100°	14°±2°	90°	16°±1°
80°	18°±2°	70°	22°±1°
65°	24°±2°	60°	27°±2°
57°	28°±2°	53°	30°±2°
46.5°	34°±2°		

DISCUSSION OF RESULTS

The two runs yielding the narrowest and widest peaks about the expected angle are shown in Fig. 2. The estimated uncertainties in locating the centers of these peaks are ±1° and ±2° respectively. A plot of the angle of the scattered photon, θ, versus the angle of maximum coincidences of the recoil electron, Φ, is shown in Fig. 3. The estimated uncertainties in the values of Φ are shown by vertical lines. Since the beryllium target was about half as thick as the carbon target, the beryllium target provided more accurate points.

Although Co^{60} emits gamma rays of energy 1.17 and 1.33 Mev, an average value of 1.25 Mev was used in computing the theoretical curve shown in Fig. 3.

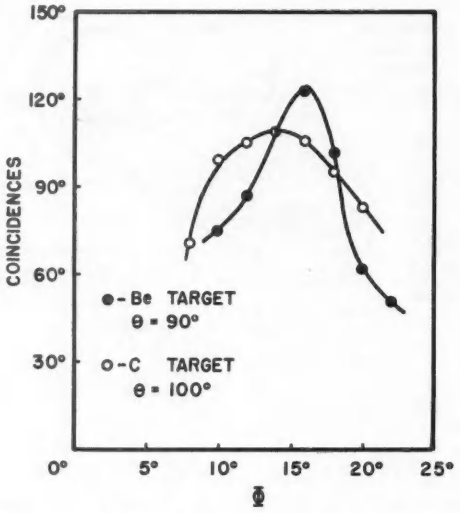

FIG. 2. Coincidences plotted as a function of Φ for the narrowest and widest peaks.

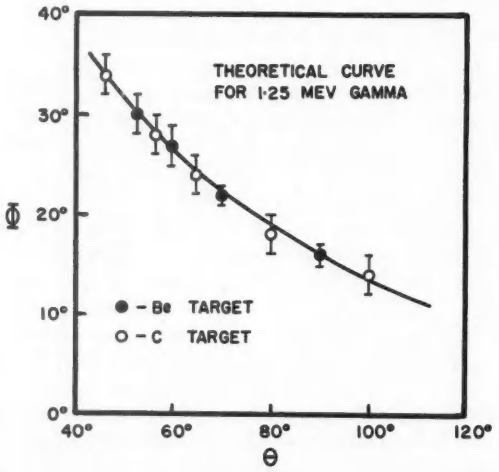

FIG. 3. Plot of Φ, the recoil angle of the electron, versus θ, the angle of the scattered photon.

Since the difference in energy of the two gamma rays should produce a change in Φ slightly less than 2° on the average, the use of the average energy appears to be consistent with the accuracy of the measurements. All of the configurations used agreed with equation (1) within ±2° or better for both targets.

Our thanks are due to Mr. Melvin Weaver for his help in the mechanical construction and to Mrs. John W. Koch for her help in taking measurements.

CROSS, W. G. and RAMSEY, N. F. 1950. Phys. Rev. **80**, 929.
GARVIN, R. L. 1953. Rev. Sci. Instr. **24**, 618.
SHANKLAND, R. S. 1937. Phys. Rev. **52**, 414.

RECEIVED MAY 15, 1961.
DEPARTMENT OF PHYSICS,
UNIVERSITY OF DELAWARE,
NEWARK, DELAWARE, U.S.A.

FRANCK–CONDON FACTORS AND *r*-CENTROIDS FOR SOME BANDS OF THE SiO $A^1\Pi$–$X^1\Sigma^+$ BAND SYSTEM

A. T. MCGREGOR, R. W. NICHOLLS, AND W. R. JARMAIN

A partial ($v'+v'' \leqslant 8$) array of Franck–Condon factors $q_{v'v''}$ for the SiO ($A^1\Pi$–$X^1\Sigma^+$) band system was computed to assist the interpretation of spectra of shock-excited powdered SiO_2. Private requests for Franck–Condon factor arrays of this and other band systems of diatomic inorganic oxides which we have studied prompts us to report Franck–Condon factors, *r*-centroids, and wavelengths for SiO ($A^1\Pi$–$X^1\Sigma^+$) in Table I.

TABLE I

Franck–Condon factors $q_{v'v''}$, *r*-centroids $\bar{r}_{v'v''}$, and wavelengths $\lambda_{v'v''}$ for the SiO $A^1\Pi$–$X^1\Sigma^+$ band system

	v''					
v'	0	1	2	3	4	5
0	0.14_2 1.563 2344.3	*0.27*$_8$ 1.597 2413.8	*0.27*$_3$ 1.630 2486.8	*0.17*$_7$ 1.66_1 2563.8	0.08_8 1.69_3 2644.8	0.03_2 1.724 2703.1
1	*0.26*$_6$ 1.539 2298.9	0.12_7 1.575 2365.7	0.00_0 1.605 2436.3	0.09_8 1.639 2509.9	*0.19*$_1$ 1.671 2587.1	*0.16*$_8$ 1.702 2669.0
2	0.25_7 1.516 2255.9	0.00_0 1.550 2321.4*	*0.12*$_6$ 1.584 2387.9	0.09_1 1.618 2459.0	0.00_0 1.645 2534.3*	0.07_6 1.680 2611.3
3	0.17_6 1.492 2215.4	0.07_2 1.525 2277.2	0.09_4 1.564 2342.4	0.00_7 1.591 2410.2	*0.11*$_2$ 1.627 2481.9	0.05_6 1.655 2559.0*
4	0.09_5 1.467 2176.6	0.15_6 1.503 2236.3	0.00_3 1.538 3000.1*	*0.10*$_1$ 1.573 2364.5		
5	0.04_3 1.385 2141.4*	*0.15*$_7$ 1.479 2197.4	0.03_8 1.518 2259.7*	0.06_8 1.550 2323.0*		

LEGEND: $q_{v'v''}$, $\bar{r}_{v'v''}$(A), $\lambda_{v'v''}$(A).
*Band wavelength calculated.

The wavelengths are mainly those of Jevons (1924); wavelengths of weak bands which he does not report have been calculated. The r-centroids were evaluated by methods discussed by Nicholls and Jarmain (1956) and the Franck–Condon factors were calculated by the method of Fraser and Jarmain (Fraser and Jarmain 1953; Jarmain and Fraser 1953; Fraser 1954) for Morse molecules using the basic data for the transition tabulated by Herzberg (1950).

The band system involves a moderately large change in internuclear separation ($\Delta r_e = 0.11$ Å) and exhibits primary and secondary Condon 'parabolae' in the Franck–Condon factor array. The entries for bands through which they pass are italicized. The eye estimate intensity distribution reported in Pearse and Gaydon's (1950) compilation agrees well with the Franck–Condon factor array.

The work has been supported in part by research grants from the National Research Council and the Ontario Research Foundation, and in part by contracts with the Air Force Cambridge Research Center, The Air Force Office of Scientific Research, and the Office of Naval Research.

Fraser, P. A. 1954. Proc. Phys. Soc. A, **67**, 939.
Fraser, P. A. and Jarmain, W. R. 1953. Proc. Phys. Soc. A, **66**, 1145.
Herzberg, G. 1950. Spectra of diatomic molecules (D. Van Nostrand, New York).
Jarmain, W. R. and Fraser, P. A. 1953. Proc. Phys. Soc. A, **66**, 1153.
Jevons, W. 1924. Proc. Roy. Soc. **106**, 174.
Nicholls, R. W. and Jarmain, W. R. 1956. Proc. Phys. Soc. **69**, 253.
Pearse, R. W. B. and Gaydon, A. G. 1950. The identification of molecular spectra, 2nd ed. (Chapman and Hall Ltd., London).

Received May 8, 1961.
Department of Physics,
University of Western Ontario,
London, Ontario.

THE HALF-LIFE OF Sm^{153}*

R. E. Green and W. H. Walker

During the course of some measurements to determine the resonance integral of Sm^{152} (Walker and Green 1961) it was observed, when correcting the product activity, Sm^{153}, for decay, that best results were obtained using a half-life for Sm^{153} which was smaller by 2% than the best published value of 47.1 ± 0.1 hours (Cork *et al.* 1958). Since we were concerned about the presence of impurities which would affect our resonance integral results we decided to investigate more fully the decay of Sm^{153}.

The target material used consisted of a layer of Sm_2O_3 ($\sim$140 $\mu g/cm^2$ of Sm^{152}) baked onto 0.0025 cm thick superpure aluminum foil (see Walker

*Issued as A.E.C.L. No. 1280.

and Green (1961) for details of foil preparation). The original sample material contained >98% Sm, the main impurities being Ce (<0.5%), Pr (<0.2%), and Eu (~0.1%). The samarium was highly enriched in Sm^{152} (97.2%), so that radiations from the other samarium isotopes could be neglected.

The foils were irradiated either in the ZEEP reactor or in the thermal column of the NRU reactor for an integrated flux of $\sim 10^9$ neutrons/cm^2. After activation the targets were counted in a system which included two NaI(Tl) scintillation counters and an automatic sample changer and readout unit. The counters were biased to accept all pulses corresponding to γ-ray energies >30 kev. To check on counter stability, a source of long-lived Am^{241} ($T_{1/2}$ = 470 years) was also counted throughout each experiment. The readout unit recorded on punched tape the sample number, the counts in the two detector scalers, the counting time interval, and the time of day. The timing unit was a tuning fork oscillator with a frequency of 1000 c.p.s. This information was fed to a Burroughs-205 "Datatron" computer where each sample count was corrected for background and counter dead time (~3.0 μsec).

The counting was continued until the Sm^{153} activity had decayed to a few times background. The results of one run are shown in Fig. 1. Here the corrected activities of the Sm^{153} and Am^{241} are plotted as a function of time. The constancy of the Am^{241} results indicates the stability of the system. In all, four separate measurements of the Sm^{153} decay were made. In each case more than 200 individual counts were obtained and in the least-squares fits 200–215 points were used. In fitting the data it is important to correct for the presence of any contaminant activity. The main interfering activity is expected to come from the ~0.1% europium impurity since Eu^{151} has a large thermal neutron capture cross section (~1400 barns) leading to a 9.35-hour isomeric state in Eu^{152}. In order to correct for this impurity the counting results were fitted by the method of least squares to a double exponential function of the form

$$A(t) = A_1(0)e^{-\lambda_1 t} + A_2(0)e^{-\lambda_2 t}, \tag{1}$$

where $A(t)$ is the corrected activity at time t,

$A_1(0)$, $A_2(0)$ are the Sm^{153} and Eu^{152} activities at zero time, respectively,

and λ_1, λ_2 are the corresponding decay constants.

For the fitting λ_2 was fixed at the value corresponding to the Eu^{152} half-life of 9.35±0.02 hours obtained by Guében and Govaerts (1958), and $A_1(0)$, $A_2(0)$, and λ_1 were allowed to vary. The results of the least-squares fits are given in Table I for the four experiments. The table lists the Sm^{153} half-lives obtained using both double (eq. (1)) and single exponential decay ($A_2(0) = 0$). The run labelled Sm^{153}/Am^{241} is a fit of run 4 with each Sm^{153} activity point normalized to the nearest Am^{241} activity. This procedure should correct at least partially for any long-term drift in the counting system.

The errors shown for the individual values of the half-lives are based on the "goodness-of-fit" of the results to the function assumed, while the errors given for the mean values of $T_{1/2}$ are based on the reproducibility of the individual results.

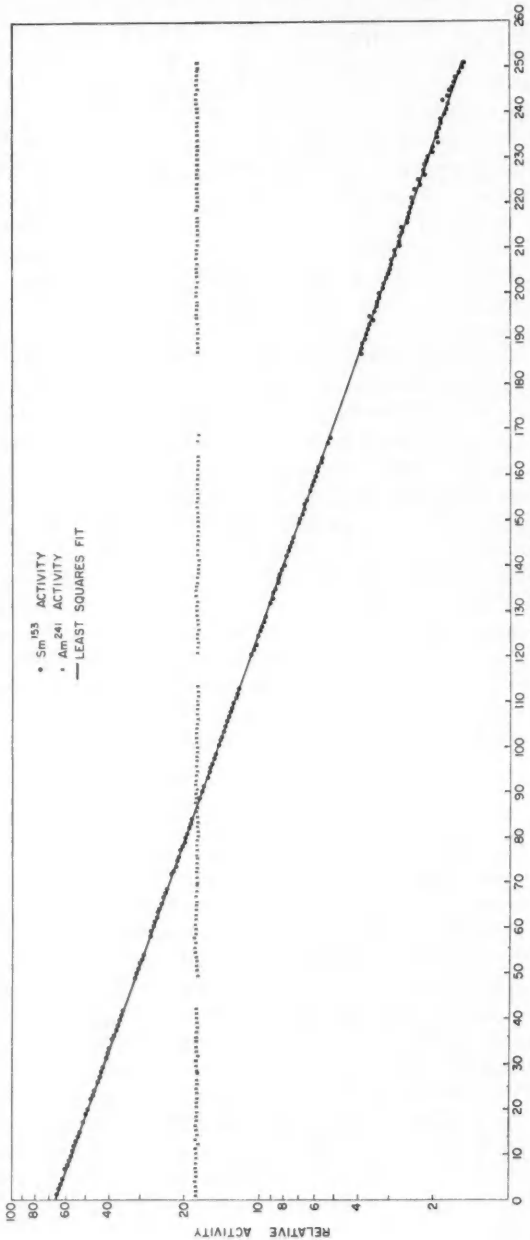

FIG. 1. Decay curve for samarium foil.

TABLE I

Sm^{153} half-life results from least-squares fitting

Run	Number of points in fit	Half-life, hours	
		Double exponential	Single exponential
1	215	46.14±0.09	45.97±0.06
2	212	46.22±0.18	46.33±0.13
3	212	46.27±0.03	46.19±0.02
4	200	46.34±0.08	46.20±0.06
		Mean 46.24±0.04	46.17±0.08
Sm^{153}/Am^{241}	200	46.16±0.09	

The value obtained for $A_2(0)/A_1(0)$ varied somewhat because of the different irradiation and counting conditions but was always <0.02, in agreement with that expected on the basis of the amount of europium impurity present. This fact was verified by a γ-ray spectrum study made with a 100-channel kick-sorter; using γ-ray spectra taken at intervals for several days it was found that all resolvable lines decayed with the Sm^{153} half-life. It was concluded therefore that any contaminant activity present was initially $<2\%$ of the initial Sm^{153} activity. The close agreement between the half-lives obtained using either single or double exponential decay functions supports this conclusion.

TABLE II

Summary of Sm^{153} half-life measurements

Reference	$T_{1/2}$, hours
Kurbatov *et al.* (1942)	47±1
Miller and Curtiss (1946)	46 (no error quoted)
Rutledge *et al.* (1952)	46.5±1
Cork *et al.* (1958)	47.1±0.1
Wille and Fink (1958)	45±3
Guében and Govaerts (1958)	46.7±1.6
Present work	46.2±0.1

In addition to counting statistics, the main sources of error in these measurements are: (1) the error in the absolute frequency of the tuning fork, (2) the variation of tuning fork frequency with temperature, (3) the uncertainty in the counter dead time, (4) non-statistical variations in the background, and (5) a long-term variation in the efficiency of the counting system. Errors (2), (4), and (5) have already been dealt with satisfactorily since they affect the reproducibility of the individual results. Also, error (2) is small since the frequency temperature coefficient is $-0.015\%/°C$ and the maximum temperature variation in the air-conditioned counting room was 4° C. We have calibrated the fork against a quartz crystal controlled oscillator and found it to be within 0.02% of the rated frequency of 1000 c.p.s. This will produce an uncertainty in $T_{1/2}$ of $\pm 0.02\%$. The maximum dead-time correction applied in these experiments was $\sim 0.1\%$; if we assume that the dead time is known only to $\pm 30\%$ this will lead to a maximum error in $T_{1/2}$ of $\pm 0.03\%$.

As a result we take the total error in $T_{1/2}$ to be $\sim 0.2\%$ so that the value we obtain for the half-life of Sm^{153} is 46.2 ± 0.1 hours. This result is $\sim 2\%$ less than that found by Cork *et al.* (1958), who also quoted about the same error. These and other values are listed in Table II. Except for the disagreement noted above, for which we have no explanation, the measurements all agree within experimental error.

CORK, J. M., BRICE, M. K., HELMER, R. G., and WOODS, R. M., Jr. 1958. Phys. Rev. **110**, 526.
GUÉBEN, G. and GOVAERTS, J. 1958. Inst. Interuniversitaire Sci. Nucléaires (Bruxelles), Monographie No. 2.
KURBATOV, J. D., MACDONALD, D. C., POOL, M. L., and QUILL, L. L. 1942. Phys. Rev. **61**, 106A.
MILLER, L. C. and CURTISS, L. F. 1946. Phys. Rev. **70**, 983.
RUTLEDGE, W. C., CORK, J. M., and BURSON, S. B. 1952. Phys. Rev. **86**, 775.
WALKER, W. H. and GREEN, R. E. 1961. Can. J. Phys. **39**. This issue.
WILLE, R. G. and FINK, R. W. 1958. Phys. Rev. **112**, 1950.

RECEIVED MAY 29, 1961.
REACTOR PHYSICS BRANCH,
ATOMIC ENERGY OF CANADA LIMITED,
CHALK RIVER, ONTARIO.

CALCULATION OF THE ν_2 AND INVERSION ENERGY LEVELS FOR AMMONIA AND SOME OF ITS ISOTOPICALLY SUBSTITUTED SPECIES

T. P. NORRIS AND J. M. DOWLING

In 1935, Manning used a potential function with a double minimum proposed by Morse and Stueckelberg (1931) to calculate energy levels for ammonia (NH_3) and deuterated ammonia (ND_3). The results were in good agreement with the available experimental data.

Since then more and better data have been obtained from high resolution studies of the infrared (Plyler and Benedict 1957) and microwave (summarized by Townes and Schawlow 1955) spectra of these molecules. The purpose of this investigation was to refine Manning's calculations in order to obtain better parameters for the potential function, and to calculate the energy levels for some isotopically substituted species, namely NH_2D, ND_2H, and NT_3.

The potential function used by Manning was

$$(1) \qquad V(r) = -\frac{1}{k\rho^2}\left\{\left[\frac{\beta}{2}\left(\frac{\beta}{2}+\frac{1}{2}\right)+D\right]\operatorname{sech}^2\left(\frac{r}{2\rho}\right)-D\operatorname{sech}^4\left(\frac{r}{2\rho}\right)\right\}$$

where ρ, β, and D are parameters to be determined, r is the co-ordinate describing the motion, and

$$(2) \qquad k = \frac{8\pi^2 c}{h}\mu$$

where c is the velocity of light, h is Planck's constant, and μ is the reduced mass. The potential energy function has a double minimum at $r = \pm r_0$, where

$$\text{sech}^2\left(\frac{r_0}{2\rho}\right) = \left[\frac{\beta}{2}\left(\frac{\beta}{2}+\frac{1}{2}\right)+D\right] \Big/ 2D. \tag{3}$$

The Schrodinger wave equation has been solved (Morse and Stueckelberg 1931) and the energy levels are given in terms of the roots of a continued fraction, which is a function of β, D, and $k\rho^2$. Since the potential energy function must remain invariant under isotopic substitution, it is seen that the parameters $\frac{1}{2}\beta(\frac{1}{2}\beta+\frac{1}{2})$, and D must increase or decrease in the same ratio the reduced mass increases or decreases.

In the first set of calculations r_0 was taken as the equilibrium value of the height of the NH_3 pyramid (0.3810 Å, Plyler and Benedict 1957) and the angle between a N—H bond and the plane formed by the three hydrogen nuclei was taken as 22.1°. Essentially this reduced the number of parameters in the potential function from three to two by means of eq. (3). Computations were carried out to fit the inversion transition ($0_a \leftarrow 0_s$) and the higher transitions ($3_s \leftarrow 0_s$, and $3_a \leftarrow 0_s$) for ammonia and deuterated ammonia. A wide range of parameters were investigated, but the calculated values were always in poor agreement with the experimental values. In particular it was found that when the inversion transitions were fitted closely, the calculated values for the higher transitions were considerably lower than the experimental values.

Because of this difficulty calculations were carried out to find the three parameters β, D, and $k\rho^2$ without using eq. (3). The best set of results is summarized in Table I and the parameters obtained are given in Table II. The over-all agreement is somewhat better than that obtained by Manning. In order to require eq. (3) to hold for $r_0 = 0.3810$ Å it was necessary to treat the reduced mass as unknown. The reduced mass is a function of the geometry and under these conditions it was found that the angle between a N—H bond and the plane of the three hydrogen nuclei is reduced by 8° from its equilibrium value. This is not unusual in view of the large amplitude of this vibration. The value of the reduced mass obtained in this manner should be considered as some sort of average reduced mass for this kind of vibration.

The parameters from Table II give the following potential energy expression

$$v = \left\{-111{,}432\ \text{sech}^2\left(\frac{r}{2\rho}\right)+67{,}587\ \text{sech}^4\left(\frac{r}{2\rho}\right)\right\}\ \text{cm}^{-1},$$

which for $r_0 = 0.3810$ Å yields $\rho = 0.4262$ Å, and a barrier-hindering inversion of 2085 cm^{-1}.

With all the parameters determined, the energy levels of NH_2D, ND_2H, and NT_3 were calculated. The results are summarized in Tables I and II.

From this investigation it has become apparent that if better results are to be obtained, with this type of potential function, at least two modifications will have to be made. They are: (1) the reduced mass should be considered as a

TABLE I

The double minimum potential energy levels in cm^{-1} for ammonia and some of its isotopic species

Level	NH_3		NH_2D		ND_2H		ND_3		NT_3
	Calc.	Obs.	Calc.	Obs.	Calc.	Obs.	Calc.	Obs.	Calc.
3_a	2881	2895.5	2489		2247		2079	2106.6	1791
3_s	2389	2383.5	2106		1945		1843	1830	1684
2_a	1887	1910	1662		1521		1420	1429	1236
2_s	1624	1597.6	1515		1438		1374	1359	1227
1_a	971	968.3	864	894†	796	818†	742	749.4	642.3
1_s	939	932.5	853	874†	789	808†	740	745.7	642.0
0_a	0.794	0.793	0.350	0.406	0.172	0.170	0.058	0.053	0.00
0_s	0	0	0	0	0	0	0	0	0
E_0*	512.5		454		416.6		388		333

*E_0 is the height, in cm^{-1}, of the level 0_a above the bottom of the double-well minimum.
†Migeotte and Barker (1936).

TABLE II

Parameters of the double minimum potential function for ammonia and some of its isotopically substituted species*

Parameter	NH_3	NH_2D	ND_2H	ND_3	NT_3
$k\rho^2$	2.83554×10^{-2}†	3.63657×10^{-2}	4.37355×10^{-2}	5.06937×10^{-2}	6.93332×10^{-2}
β	70.021	79.364	87.082	93.792	109.772
D	1916.5	2457.8	2955.9	3426.2	4686.0

*The parameters are expressed in units such that the potential energy function has the unit of cm^{-1}.
†This number of significant figures is not justified but they were carried to secure internal consistency in the calculations.

variable, because of the large amplitude of vibration, and (2) the interaction with the symmetric N—H stretching mode ν_1 should be included, since this vibration is mixed to a fair degree with the ν_2 mode. This may alleviate to a large extent the difficulty mentioned previously, namely the fitting of the upper- and lower-energy levels, since a term describing the N—H stretching vibration would increase the slope of the potential energy functions for $r > r_0$ and thus raise the upper levels.

The authors would like to acknowledge the assistance of Mr. David Deglar and the staff of the General Electric Computor Center of Arizona State University for their assistance in the programming and computations involved in this investigation. They would also like to thank the National Science Foundation for financial assistance during the period this investigation was being carried out.

MANNING, M. F. 1935. J. Chem. Phys. **3**, 136.
MIGEOTTE, M. V. and BARKER, E. F. 1936. Phys. Rev. **50**, 418.
MORSE, P. M. and STUECKELBERG, E. C. G. 1931. Helv. Phys. Acta, **4**, 337.
PLYLER, E. K. and BENEDICT, W. S. 1957. Can. J. Phys. **35**, 1235.
TOWNES, C. H. and SCHAWLOW, A. L. 1955. Microwave spectroscopy (McGraw-Hill Book Co., Inc.).

RECEIVED MAY 1, 1961.
DEPARTMENT OF PHYSICS,
ARIZONA STATE UNIVERSITY,
TEMPE, ARIZONA.

EFFECT OF SOLUTE ATOMS ON GRAIN BOUNDARY MIGRATION IN PURE METALS

E. L. HOLMES AND W. C. WINEGARD

INTRODUCTION

It has been suggested by Lücke and Detert (1957) in a theory of grain boundary migration in the presence of solute atoms that, if the interaction between the impurity atoms and the boundary is sufficiently large, the rate

of boundary migration will be controlled by the speed at which solute atoms can diffuse along with the boundary. The measured activation energy in this case would be approximately equal to Q_D, the activation energy for diffusion of solute atoms in the solvent matrix. Lücke and Detert also suggested that at high temperature or low concentrations, the boundary might "break away" from the solute atoms and the measured apparent activation energy would be greater than the value Q_D.

This theory did not appear to be supported by the investigations on the effect of solute atoms on the rate of migration of a single boundary by Aust and Rutter (1959, 1960), or by those on grain growth by Bolling and Winegard (1958) and Holmes and Winegard (1960). Recent work, however, using concentrations of solute higher than those used previously, may be interpreted, at least in part, by the theory of Lücke and Detert.

THE EFFECT OF LEAD ON GRAIN GROWTH IN ZONE-REFINED TIN

Grain growth experiments on alloys of lead in zone-refined tin have been performed using the technique of Bolling and Winegard (1958). Figure 1 shows the results of these experiments and the activation energies obtained. The activation energy for grain growth increases, with increase in lead concen-

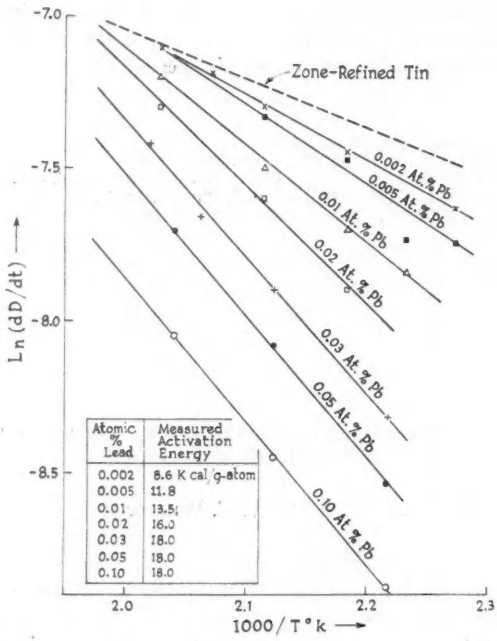

FIG. 1. Logarithmic rate of grain growth at 100 seconds plotted against $1000/T$ °K for zone-refined tin with various concentrations of lead added.

tration, to a value of 18±2 kcal/g-atom before the effect of solute on the rate of growth close to the melting temperature becomes markedly evident. Further additions of solute do not affect the measured activation energy but do decrease the rate of grain growth at the melting temperature. The activation energies measured for the various concentrations are plotted in Fig. 2.

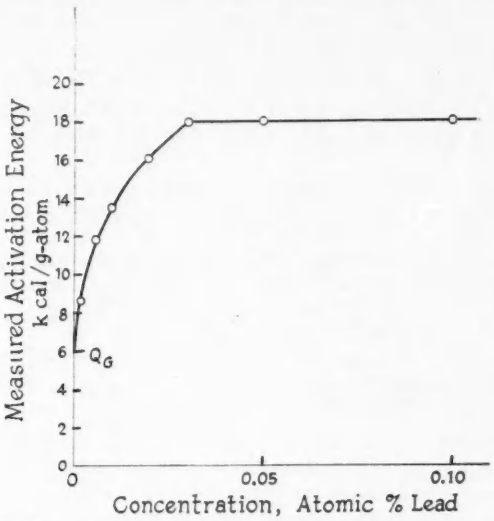

FIG. 2. Graph of activation energy plotted against concentration for grain growth in zone-refined tin with lead added.

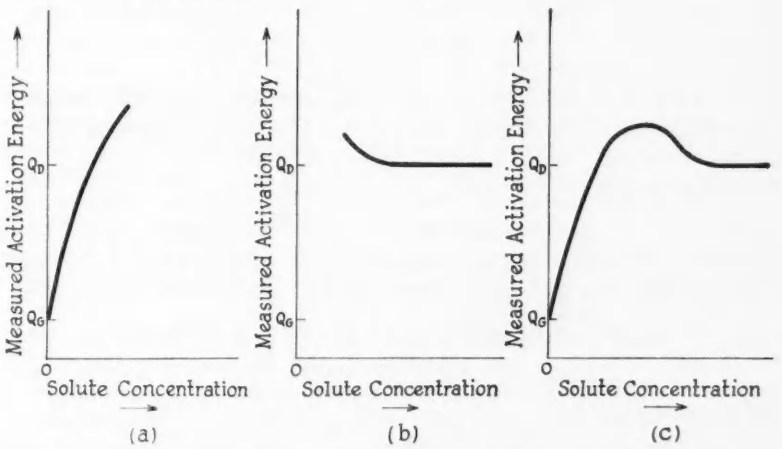

FIG. 3. Schematic representation of graph of activation energy plotted against concentration for (*a*) single boundary migration, (*b*) Lücke and Detert theory, and (*c*) a possible combination.

DISCUSSION

Shown schematically in Fig. 3 are: (*a*) the results of Aust and Rutter on the effect of solute atoms on single boundary migration in zone-refined lead; (*b*) what might be expected from the theory of Lücke and Detert; and (*c*) a possible plot of activation energy versus concentration if both (*a*) and (*b*) are correct. At high concentrations of solute, the experimental results shown in Fig. 2 are in agreement with the theory of Lücke and Detert. At low concentrations, the value of the activation energy varies with concentration in a similar manner to that in the Aust and Rutter work, up to the value Q_D. The difference between Fig. 2 and Fig. 3*c* may be due to the fact that the grain growth experiments may not be sufficiently sensitive to determine the "breakaway".

The authors gratefully acknowledge the support of the National Research Council of Canada (grant No. BT-48) and the University of Toronto.

AUST, K. T. and RUTTER, J. W. 1959. Trans. Am. Inst. Mining Met. Engrs. **215**, 820.
——— 1960. Trans. Am. Inst. Mining Met. Engrs. **218**, 682.
BOLLING, G. F. and WINEGARD, W. C. 1958. Acta Met. **6**, 283.
HOLMES, E. L. and WINEGARD, W. C. 1960. J. Inst. Metals, **88**, 468.
LÜCKE, K. and DETERT, K. 1957. Acta Met. **11**, 628.

RECEIVED NOVEMBER 18, 1960.
DEPARTMENT OF METALLURGICAL ENGINEERING,
UNIVERSITY OF TORONTO,
TORONTO, ONTARIO.

A NOTE ON SOME PROPERTIES OF HAMILTONIANS INVOLVING SPIN MATRICES FOR HALF-INTEGRAL VALUES OF *I*

G. M. VOLKOFF

In discussions of problems of nuclear magnetic and quadrupole resonance a prominent role is played by the expressions for the magnetic dipole (Zeeman) interaction of the nuclear magnetic moment $\boldsymbol{\mu} = \gamma\hbar\mathbf{I}$ with a given uniform external magnetic field $\mathbf{H} = H\mathbf{P}$

$$\mathcal{H}_Z = -\boldsymbol{\mu}\cdot\mathbf{H} = -\gamma\hbar H\mathbf{P}\cdot\mathbf{I} \tag{1}$$

and for the electric quadrupole interaction of the nuclear electric quadrupole moment tensor $e\tilde{\mathbf{Q}}$ with a given external electric field gradient $\nabla\mathbf{E} = -\nabla\nabla\phi$

$$\begin{aligned}\mathcal{H}_Q &= -\tilde{\mathbf{Q}}\cdot\nabla\mathbf{E} = C_1[\phi_{zz}(3I_z^2-\mathbf{I}^2)+(\phi_{xx}-\phi_{yy})(I_x^2-I_y^2)] \\ &= C[(3I_z^2-\mathbf{I}^2)+\eta(I_x^2-I_y^2)]\end{aligned} \tag{2}$$

with

$$C_1\phi_{zz} \equiv C \equiv \frac{eQ\phi_{zz}}{4I(2I-1)}, \qquad \eta \equiv \frac{\phi_{xx}-\phi_{yy}}{\phi_{zz}}. \tag{3}$$

Here I, γ, eQ are the nuclear spin, gyromagnetic ratio, and electric quadrupole moment, H is the magnitude, and $\mathbf{P}$ the polarization vector of the external magnetic field (constant or time dependent, and representing a linearly, circularly, or elliptically polarized field), x, y, z are the principal axes of the electric field gradient tensor $\phi_{ij} = \partial^2\phi/\partial x_i \partial x_j$ (defined by $\phi_{xy} = \phi_{yz} = \phi_{zx} = 0$), η is its asymmetry parameter, and $\mathbf{I}$ is the usual spin operator.

Expressions (1) and (2) are simple examples of spin-Hamiltonians involving odd or even powers of the components I_ξ of the spin operator $\mathbf{I}$. Hamiltonians involving homogeneous polynomials in the I_ξ of degree higher than the second can also be written down to express the interaction of higher nuclear moments with higher order inhomogeneities of given external electric or magnetic fields. However, in this note we shall be particularly concerned with (1) and (2).

Since $\mathbf{I}^2$ commutes with any polynomial in the I_ξ the eigenvectors ψ of (1), (2), etc., can always be chosen as eigenvectors of $\mathbf{I}^2$ describing nuclei of definite spin I. If T is the time-reversal operator (cf., for example, Heine 1960, or Wigner 1959) it may be shown that for any such eigenvector

$$T^2\psi = (-1)^{2I}\psi. \tag{4}$$

Any spin-Hamiltonian which is a polynomial with real coefficients containing only terms of even degree in the I_ξ, in particular $\mathfrak{H}_Q$ defined by (2), may be shown to be invariant under time reversal. From this it follows that if ψ_{L_n} is one of its eigenvectors belonging to the eigenvalue E_n, then $\psi_{M_n} \equiv T\psi_{L_n}$ is also an eigenvector belonging to the same eigenvalue. It follows from (4) and from the invariance of the Hamiltonian under time reversal that when I is an odd half-integer (giving a minus sign in (4)) then $\psi_{M_n} \equiv T\psi_{L_n}$ must be linearly independent of ψ_{L_n}, and that $T\psi_{M_n} = T^2\psi_{L_n} = -\psi_{L_n}$. In other words, for half-integral I the eigenstates of (2) must necessarily be degenerate in pairs. This is an example of Kramers' theorem (cf. Heine 1960; Wigner 1959).

Therefore, it is known that for odd half-integral I the $2I+1$ eigenvectors of (2) split up into two sets ψ_{L_n} and ψ_{M_n} of $(I+\frac{1}{2})$ eigenvectors each with one set being obtainable from the other set by time reversal. To demonstrate this explicitly, and to prepare the way for later theorems we have found it convenient to introduce a special representation of the operators I_ξ for half-integral values of I.

The $(2I+1)$-rowed Hermitian matrices representing the components of spin angular momentum $\mathbf{I}$ have their familiar form in the representation in which I_z is diagonal and the order of the rows and columns of the matrices is chosen so as to exhibit the eigenvalues m of I_z in the standard order $m = I, I-1, \ldots, -(I-1), -I$ down the principal diagonal. In this representation non-zero elements of I_x and I_y appear only in positions one row or one column away from the principal diagonal.

In discussing half-integral values of I we introduce a different representation which leaves $\mathbf{I}^2$ and I_z in diagonal form, and which is obtained by separating the $2I+1$ eigenvectors $\chi_{\pm m}$ of I_z (and also of I_z^2) into two equal sets L and M of $I+\frac{1}{2}$ elements each (which go over into each other by time reversal) by means of the definition

$$m_{L_n} = -m_{M_n} = I-2n, \qquad n = 0, 1, \ldots (I-\tfrac{1}{2}).$$

After rearranging the order of rows and columns so as to obtain a representation in which the set of m_L values is followed by the set of m_M values down the principal diagonal of I_z, we can write

$$I_x = X\,\Sigma_x, \qquad I_y = Y\,\Sigma_y, \qquad I_z = Z\,\Sigma_z. \tag{5}$$

Here Σ_x, Σ_y, Σ_z are $(2I+1)$-rowed generalized Pauli matrices

$$\Sigma_x \equiv \left(\begin{array}{c|c} 0 & \hat{1} \\ \hline \hat{1} & 0 \end{array}\right), \qquad \Sigma_y \equiv e^{i\pi I}\left(\begin{array}{c|c} 0 & -\hat{1} \\ \hline \hat{1} & 0 \end{array}\right), \qquad \Sigma_z \equiv \left(\begin{array}{c|c} \hat{1} & 0 \\ \hline 0 & -\hat{1} \end{array}\right), \tag{6}$$

in which $\hat{1}$ stands for the $(I+\frac{1}{2})$-dimensional identity matrix and the phase of Σ_y has been chosen to agree with the ordinary Pauli matrices for $I = \frac{1}{2}$ and to make the traces of X, Y, Z all positive for all I. The Σ_ξ satisfy the generalized Pauli relations:

$$\Sigma_x\Sigma_y = -\Sigma_y\Sigma_x = e^{i\pi I}\Sigma_z, \text{ etc.}, \quad \Sigma_x^2 = \Sigma_y^2 = \Sigma_z^2 = \left(\begin{array}{c|c} \hat{1} & 0 \\ \hline 0 & \hat{1} \end{array}\right). \tag{7}$$

X, Y, Z are "block-diagonal" matrices defined by

$$X \equiv \left(\begin{array}{c|c} \hat{I}_x & 0 \\ \hline 0 & \hat{I}_x \end{array}\right), \qquad Y \equiv \left(\begin{array}{c|c} \hat{I}_y & 0 \\ \hline 0 & \hat{I}_y \end{array}\right), \qquad Z \equiv \left(\begin{array}{c|c} \hat{I}_z & 0 \\ \hline 0 & \hat{I}_z \end{array}\right), \tag{8}$$

in terms of the "half-matrices" $\hat{I}_x$, $\hat{I}_y$, $\hat{I}_z$ which are $(I+\frac{1}{2})$-rowed real symmetric matrices ($\hat{I}_z$ diagonal), all with the same eigenvalues $m_L = I-2n$, $n = 0, 1, \ldots (I-\frac{1}{2})$, and with positive traces $\frac{1}{2}(I+\frac{1}{2})$, whose matrix elements (for m, m' both belonging to the m_L set) are defined in terms of the matrix elements of the usual spin operators I_ξ by:

$$(\hat{I}_x)_{m,m'} \equiv (I_x)_{m,-m'}; \qquad (\hat{I}_y)_{m,m'} \equiv e^{i\pi I}(I_y)_{m,-m'}; \qquad (\hat{I}_z)_{m,m'} \equiv (I_z)_{m,m'}. \tag{9}$$

In virtue of the properties of the I_ξ matrices for half-integral values of I the matrix elements of the X, Y, Z matrices in the (lower) M subspace are identical with those in the (upper) L subspace. As a result of this X, Y, Z commute with the Σ_ξ. Examples of $\hat{I}_x$, $\hat{I}_y$, $\hat{I}_z$ are given for $I = 3/2$ and $I = 5/2$:

$$\hat{I}_x = \frac{1}{2}\begin{pmatrix} 0 & \sqrt{3} \\ \sqrt{3} & 2 \end{pmatrix}, \quad \hat{I}_y = \frac{1}{2}\begin{pmatrix} 0 & -\sqrt{3} \\ -\sqrt{3} & 2 \end{pmatrix}, \quad \hat{I}_z = \frac{1}{2}\begin{pmatrix} 3 & 0 \\ 0 & -1 \end{pmatrix}, \quad I = \frac{3}{2}, \tag{10}$$

$$\hat{I}_x = \frac{1}{2}\begin{pmatrix} 0 & 0 & \sqrt{5} \\ 0 & 3 & 2\sqrt{2} \\ \sqrt{5} & 2\sqrt{2} & 0 \end{pmatrix}, \quad \hat{I}_y = \frac{1}{2}\begin{pmatrix} 0 & 0 & \sqrt{5} \\ 0 & 3 & -2\sqrt{2} \\ \sqrt{5} & -2\sqrt{2} & 0 \end{pmatrix},$$

$$\hat{I}_z = \frac{1}{2}\begin{pmatrix} 5 & 0 & 0 \\ 0 & 1 & 0 \\ 0 & 0 & -3 \end{pmatrix}, \quad I = \frac{5}{2}.$$

The commutation relations for the Σ_ξ and the I_ξ lead to:

$$\hat{I}_x\hat{I}_y + \hat{I}_y\hat{I}_x = (-1)^{I-\frac{1}{2}}\hat{I}_z \text{ etc.}, \quad \hat{I}_x^2 + \hat{I}_y^2 + \hat{I}_z^2 = I(I+1)\hat{1}. \tag{11}$$

Expressed in terms of these matrices the nuclear quadrupole coupling Hamiltonian is given by

$$\mathfrak{H}_Q = C[3Z^2 - I(I+1)1 + \eta(X^2 - Y^2)] = C\left(\begin{array}{c|c} \hat{H}_0 & 0 \\ \hline 0 & \hat{H}_0 \end{array}\right) \tag{12}$$

where the $(I+\frac{1}{2})$-rowed real matrix

$$\hat{H}_0 \equiv 3\hat{I}_z^2 - I(I+1)\hat{1} + \eta(\hat{I}_x^2 - \hat{I}_y^2) \tag{13}$$

has exactly the same form both in the L and the M subspaces. This is an explicit demonstration of the result embodied in Kramers' theorem that for half-integral I the eigenvalues of $\mathfrak{H}_Q$ are all doubly degenerate, and that the pairs of degenerate eigenfunctions ψ_L and ψ_M in this representation consist of pairs of linear combinations (connected by time reversal) of class L or class M eigenfunctions χ_m of I_z with exactly the same real coefficients. In other words the real unitary transformation D which diagonalizes $\mathfrak{H}_Q$ can be written in "block-diagonal" form with the elements in the M subspace being identical with those in the L subspace:

$$C\left(\begin{array}{c|c} \hat{D} & 0 \\ \hline 0 & \hat{D} \end{array}\right)\left(\begin{array}{c|c} \hat{H}_0 & 0 \\ \hline 0 & \hat{H}_0 \end{array}\right)\left(\begin{array}{c|c} \hat{D}^{-1} & 0 \\ \hline 0 & \hat{D}^{-1} \end{array}\right) = C\left(\begin{array}{c|c} \hat{D}\hat{H}_0\hat{D}^{-1} & 0 \\ \hline 0 & \hat{D}\hat{H}_0\hat{D}^{-1} \end{array}\right) = \left(\begin{array}{c|c} \hat{E} & 0 \\ \hline 0 & \hat{E} \end{array}\right) \tag{14}$$

where $\hat{E}$ is a $(I+\frac{1}{2})$-rowed diagonal matrix with real diagonal elements $E_i (i = 1, 2, \ldots, I+\frac{1}{2})$ which in the cases considered so far have always been found to be distinct.

The magnetic dipole coupling Hamiltonian (1) is given in terms of the representation (5) by:

$$\mathfrak{H}_Z = -\gamma\hbar H\mathbf{P}\cdot\mathbf{I} = -\gamma\hbar H(P_x X\,\Sigma_x + P_y Y\,\Sigma_y + P_z Z\,\Sigma_z). \tag{15}$$

The transformation D which diagonalizes $\mathfrak{H}_Q$, being in "block-diagonal" form with the same "half-matrix" $\hat{D}$ in both the L and M subspaces, commutes with the Σ_ξ, and therefore puts $\mathfrak{H}_Z$ in the form

$$D\mathfrak{H}_Z D^{-1} = -\gamma\hbar H(P_x DXD^{-1}\,\Sigma_x + P_y DYD^{-1}\,\Sigma_y + P_z DZD^{-1}\,\Sigma_z). \tag{16}$$

Here

$$DXD^{-1} = \left(\begin{array}{c|c} \hat{D}\hat{I}_x\hat{D}^{-1} & 0 \\ \hline 0 & \hat{D}\hat{I}_x\hat{D}^{-1} \end{array}\right) \text{etc.}, \tag{17}$$

are still in "block-diagonal" form, and $\hat{D}\hat{I}_\xi\hat{D}^{-1}$ are still real symmetric matrices but with many more non-zero elements than the $\hat{I}_\xi$. Whereas (12) does not involve the Σ_ξ, and is therefore "block-diagonal", both (15) and (16) do involve the Σ_ξ and are therefore, in general, neither "block-diagonal" nor "block-antidiagonal" in this representation.

For perturbation theory calculations in which $\mathfrak{H}_Z$ given by (1) is treated as a small time-dependent perturbation on $\mathfrak{H}_Q$ defined by (2) it is useful to classify the eigenstates of $\mathfrak{H}_Q$ into those which are connected by zero and by non-zero elements of $D\mathfrak{H}_Z D^{-1}$ as this determines the selection rules. Also

in connection with an investigation by Volkoff and Jog (to be published) of the generalized Bloch equations we were interested in the conditions under which $D\mathfrak{H}_z D^{-1}$ could be put into "block-diagonal" or "block-antidiagonal" form (with zero matrix elements in two quadrants of the matrix, as in (6) or (8)) without upsetting the diagonal form of $D\mathfrak{H}_Q D^{-1}$. Since the only transformations which will not upset the diagonal form of $D\mathfrak{H}_Q D^{-1}$ are unitary transformations in the two-dimensional subspaces defined by each doubly degenerate eigenvalue E_i we find it convenient to rearrange once again the rows and columns by putting them in the order $L_1, M_1, L_2, M_2, \ldots L_i, M_i, \ldots$, each pair L_i, M_i belonging to the appropriate eigenvalue E_i. In this representation the $(2I+1)$-rowed matrices $D\mathfrak{H}_Q D^{-1}$ and $D\mathfrak{H}_z D^{-1}$ now take on the "mosaic" form of $(I+\frac{1}{2})$-rowed square arrays $(i, j = 1, 2, \ldots I+\frac{1}{2})$ of two-rowed matrices defined by

$$(D\mathfrak{H}_Q D^{-1})_{ij} = \delta_{ij} E_i 1,$$

$$(18)\quad (D\mathfrak{H}_z D^{-1})_{ij} = -\gamma\hbar H[P_x(\hat{D}\hat{I}_x\hat{D}^{-1})_{ij}\sigma_x + (-1)^{I-\frac{1}{2}} P_y(\hat{D}\hat{I}_y\hat{D}^{-1})_{ij}\sigma_y + P_z(\hat{D}\hat{I}_z\hat{D}^{-1})_{ij}\sigma_z]$$

$$= -\gamma\hbar H(a_{ij}\sigma_x + b_{ij}\sigma_y + c_{ij}\sigma_z).$$

Here $(\hat{D}\hat{I}_\xi\hat{D}^{-1})_{ij}$ are one-dimensional matrix elements of $\hat{I}_\xi$ between either the L_i, L_j or the M_i, M_j states, $1, \sigma_x, \sigma_y, \sigma_z$ are two-rowed unit and ordinary Pauli matrices for $I = \frac{1}{2}$, and a_{ij}, b_{ij}, c_{ij} are constant or time-dependent scalars.

The transformations which leave $D\mathfrak{H}_Q D^{-1}$ diagonal are those unitary transformations in $2I+1$ dimensions, which in the "mosaic" representation consist of two-dimensional unitary matrices U_i along the principal diagonal of the "mosaic" array, and zero elsewhere. Application of such a transformation to $D\mathfrak{H}_z D^{-1}$ yields for the two-dimensional i,j element of the "mosaic":

$$(19)\quad U_i(D\mathfrak{H}_z D^{-1})_{ij}U_j^{-1} = -\gamma\hbar H(a_{ij}U_i\sigma_x U_j^{-1} + b_{ij}U_i\sigma_y U_j^{-1} + c_{ij}U_i\sigma_z U_j^{-1})$$

$$= -\gamma\hbar H[P_x(\hat{D}\hat{I}_x\hat{D}^{-1})_{ij}U_i\sigma_x U_j^{-1} + (-1)^{I-\frac{1}{2}} P_y(\hat{D}\hat{I}_y\hat{D}^{-1})_{ij}U_i\sigma_y U_j^{-1} + P_z(\hat{D}\hat{I}_z\hat{D}^{-1})_{ij}U_i\sigma_z U_j^{-1}].$$

In order for the whole $D\mathfrak{H}_z D^{-1}$ to be either "block-diagonal" or "block-antidiagonal" each two-dimensional element of the "mosaic" representation must be either diagonal or antidiagonal. We consider the case when $U_i = U_j = U$ is independent of i. It is known that of the three Pauli matrices $\sigma_x, \sigma_y, \sigma_z$ only *one* at a time can be made diagonal, and only *two* at a time antidiagonal by a unitary transformation. This means that we can bring $(D\mathfrak{H}_z D^{-1})_{ij}$ into diagonal form simultaneously for all values of i,j by the same transformation U if, and only if, any two of P_x, P_y, P_z vanish (magnetic field along one of the principal axes of the electric field gradient tensor), and we can bring it into antidiagonal form if, and only if, at least one of P_x, P_y, P_z vanishes (magnetic field in one of the principal planes, but not necessarily along a principal axis of the electric field gradient tensor).

If none of the three P_x, P_y, P_z vanishes then, in general, we can diagonalize or antidiagonalize $(D\mathfrak{H}_z D^{-1})_{ij}$ only in a particular i,j position (and its transpose) in the "mosaic" array. In this two-dimensional subspace it has the form:

$$(D\mathfrak{H}_z D^{-1})_{ij} = -\gamma\hbar H\begin{pmatrix} c & a-ib \\ a+ib & -c \end{pmatrix} \tag{20}$$

with real values of

$$a \equiv P_x(\hat{D}\hat{I}_x\hat{D}^{-1})_{ij}, \qquad b \equiv (-1)^{I-\frac{1}{2}}P_y(\hat{D}\hat{I}_y\hat{D}^{-1})_{ij}, \qquad c \equiv P_z(\hat{D}\hat{I}_z\hat{D}^{-1})_{ij}. \tag{21}$$

Diagonalization of (20) yields:

$$\begin{vmatrix} c-\lambda & a-ib \\ a+ib & -c-\lambda \end{vmatrix} = \lambda^2-c^2-a^2-b^2 = 0 \qquad \lambda = \pm(a^2+b^2+c^2)^{\frac{1}{2}}. \tag{22}$$

The square of such a diagonal matrix element λ^2 appears in the calculations by Volkoff and Lamarche (1954) of the intensity of nuclear magnetic and quadrupole resonance absorption lines in spodumene. The linear combinations $\psi^{(\pm)}$ of the ψ_{L_i}, ψ_{M_i} (and of the ψ_{L_j}, ψ_{M_j}) states corresponding to the eigenvalues $\pm\lambda$ are:

$$\begin{aligned} \psi^{(+)} &= \frac{1}{\sqrt{2}}(K^{(+)}\psi_L + e^{i\epsilon}K^{(-)}\psi_M) \\ \psi^{(-)} &= \frac{1}{\sqrt{2}}(e^{-i\epsilon}K^{(-)}\psi_L - K^{(+)}\psi_M) \end{aligned} \tag{23}$$

with

$$\epsilon \equiv \tan^{-1}(b/a), \qquad K^{(\pm)} \equiv [1 \pm c/(a^2+b^2+c^2)^{\frac{1}{2}}]^{\frac{1}{2}}. \tag{24}$$

$\psi^{(+)} = T\psi^{(-)}$, and $\psi^{(-)} = -T\psi^{(+)}$ are connected by time reversal.

Antidiagonalization of (20) yields

$$U(D\mathfrak{H}_z D^{-1})_{ij}U^{-1} = -\gamma\hbar H\begin{pmatrix} 0 & |\lambda|e^{-i(\delta-2\mu+\epsilon)} \\ |\lambda|e^{i(\delta-2\mu+\epsilon)} & 0 \end{pmatrix} \tag{25}$$

with δ, μ arbitrary and

$$\begin{aligned} \psi_A &= \frac{e^{-i\mu}}{\sqrt{2}}[\psi^{(+)}+e^{i(\delta+\epsilon)}\psi^{(-)}] = \frac{e^{-i\mu}}{2}[(K^{(+)}+e^{i\delta}K^{(-)})\psi_L \\ &\qquad -e^{i(\delta+\epsilon)}(K^{(+)}-e^{-i\delta}K^{(-)})\psi_M], \\ \psi_B &= \frac{e^{i\mu}}{\sqrt{2}}[e^{-i(\delta+\epsilon)}\psi^{(+)}-\psi^{(-)}] = \frac{e^{i\mu}}{2}[(K^{(+)}-e^{-i\delta})e^{-i(\delta+\epsilon)}\psi_L \\ &\qquad +(K^{(+)}+e^{-i\delta}K^{(-)})\psi_M]. \end{aligned} \tag{26}$$

ψ_A and ψ_B are connected by time reversal.

$(D\mathfrak{H}_z D^{-1})_{ij}$ can be diagonalized in all the i,j subspaces by the same transformation U defined by (23) only if ϵ, $K^{(\pm)}$ are all independent of i,j, i.e., only if the ratios a/c, b/c are independent of i,j. As noted earlier, this happens if any two of P_x, P_y, P_z are zero. This cannot happen if any two of the P_ξ

(say, P_x, P_y) are different from zero, for this would imply that the corresponding $\hat{I}_\xi$ (say, $\hat{I}_x$, $\hat{I}_y$) are multiples of each other, and this is not the case.

$(D\mathfrak{H}_Z D^{-1})_{ij}$ can be antidiagonalized in all the i,j subspaces by the same transformation U defined by (26) only if either ϵ is independent of i,j (which implies that either P_x or P_y is zero, since $\hat{I}_x$ is not a multiple of $\hat{I}_y$) and we take $\delta = \pi/2$ and $\mu = \tan^{-1}(K^{(-)}/K^{(+)})$, or $P_z = 0$ (so that $K^{(\pm)} = 1$) and we take $\delta = 0$, $\mu = 0$.

Thus, for a nucleus of half-integral spin I in the general case a magnetic dipole interaction (15) can interconnect by non-zero matrix elements all eigenfunctions of the nuclear quadrupole interaction (12). But for special orientations of the magnetic field (confined to one of the principal planes of the electric field gradient tensor) linear combinations (26) of the doubly degenerate eigenfunctions ψ_{L_i}, ψ_{M_i} of the quadrupole Hamiltonian (12) can always be found such that all the states can be divided into two equal classes ψ_{A_i}, ψ_{B_i} defined by (26) and having the property that the magnetic dipole interaction (15) has only zero matrix elements between states of the same (A or B) class, i.e. that $\mathfrak{H}_Z$ is "block-antidiagonal" in this representation. If the magnetic field not only lies in a principal plane but is also parallel to one of the principal axes, a recombination of all the states into two other equal classes $\psi_i^{(+)}$ and $\psi_i^{(-)}$ defined by (23) is always possible, which makes the dipole interaction (15) "block-diagonal", i.e. having zero elements between states of opposite class (+ and −).

In the general case of a magnetic field oriented in an arbitrary manner with respect to the principal axes of the electric field gradient tensor, $\mathfrak{H}_Z$ given by (15) can always be diagonalized or antidiagonalized with respect to the eigenstates of $\mathfrak{H}_Q$ only in one particular two-dimensional subspace at a time defined by any two arbitrarily selected doubly degenerate levels E_i and E_j of the quadrupole Hamiltonian $\mathfrak{H}_Q$ given by (12). If $\eta = 0$ in (12) several, but not all, such subspaces of $\mathfrak{H}_Z$ can be diagonalized or antidiagonalized simultaneously.

The author is grateful to Prof. W. Opechowski for valuable discussions and is indebted to the National Research Council for grants-in-aid of the experimental program which gave rise to these calculations.

HEINE, V. 1960. Group theory in quantum mechanics (Pergamon Press, New York).
VOLKOFF, G. M. and LAMARCHE, G. 1954. Can. J. Phys. **32**, 493.
WIGNER, E. P. 1959. Group theory and its application to the quantum mechanics of atomic spectra (Academic Press, New York).

RECEIVED MAY 9, 1961.
PHYSICS DEPARTMENT,
UNIVERSITY OF BRITISH COLUMBIA,
VANCOUVER, BRITISH COLUMBIA.

SOME REMARKS ON THE SPECTROSCOPIC STATE OF PARAMAGNETIC IONS IN DILUTE ALLOYS EXHIBITING RESISTIVE ANOMALIES

E. W. COLLINGS,* F. T. HEDGCOCK,† AND T. SAKUDO‡

Recent experimental investigations of the spectroscopic state of manganese in a weakly magnetic solvent reported by Collings and Hedgcock (1961) have led to the suggestion that the manganese ion is not in an S state as previously suggested by Owen *et al.* (1956, 1957). In fact appreciable crystal field splitting of the paramagnetic ions may be present. The immediate interest in the spectroscopic state of paramagnetic ions in dilute metallic solution is the fact that these alloys exhibit anomalous electron transport properties at low temperatures (see Gerritsen 1959). The purpose of the present note is to report recent electron spin resonance experiments carried out on Au–Fe, Cu–Fe, and Cu–Co alloys, all of which exhibit so-called "resistive minima" at low temperatures. Table I contains the results of the present investigation where A/B is a measure of the symmetry of the resonance absorption curve and S/N is the signal-to-noise ratio of the absorption. The resistance ratios of the samples given in Table I indicate that the alloys contain appreciable paramagnetic ions in solution. The sensitivity and resolution of the electron spin resonance spectrometer used is such that 5×10^{15} spins could be detected in a resonance line of width over 300 oersted. Although both specimens of Cu–Fe exhibited a resonance at room temperature the symmetry of the resonance absorption, the temperature dependence of the absorption, and the g value observed all indicate that the resonance was *not* due to paramagnetic iron in solution in copper but to precipitated agglomerates of ferromagnetic iron. It can be concluded therefore that no detectable resonance could be found for paramagnetic ions in solution in the dilute alloys studied.

Included in Table I are values of the effective magneton number for the paramagnetic ions in the appropriate solvent. It can be seen that the effective magneton number is a marked function of concentration in most of these systems and seldom takes the limiting value corresponding to the magneton number calculated from the spin value of the isolated ion. In the previously mentioned publication of Collings and Hedgcock (1961), it was suggested that mixtures of spectroscopic states of the manganese ion would be consistent with the experimental results in the Mg–Mn system, where a mixture of states could result if either:

(*a*) crystalline field splitting of the d state is sufficiently large to put the doubly degenerate state close to the conduction band Fermi level, or if the ionization energy for a $3d$ electron is too great to permit this, then

(*b*) the exchange energy could place the ground level of the next filled state

*Department of Physics, Victoria University of Wellington, Wellington, New Zealand.
†Present address: Franklin Institute, Philadelphia 3, Pennsylvania.
‡National Research Council Postdoctoral Fellow. On leave from Electrotechnical Laboratory, Nagatacho, Tokyo, Japan.

TABLE I

Magnetic and electrical properties of some dilute copper and gold alloys. The data on Cu–Mn has been included for comparison purposes. The effective magneton number is calculated from magnetic susceptibility data and comes from the following sources. Au–Fe, Krongvist (1952); Cu–Fe, Bitter *et al.* (1950), Hedgcock (1956); Cu–Co, Jacobs and Schmitt (1959); Cu–Mn, Owen *et al.* (1956, 1957)

Alloy	Cu–Mn	Au–Fe	Cu–Fe	Cu–Co
Atomic per cent	1.14 Mn	7.06 Fe	4.55 and 0.55 Fe	0.57 Co
P (Ω cm)	3.4×10^{-6}	1.76×10^{-5}	4.03×10^{-6}	4.38×10^{-6}
Resistance ratio $R_{4.2}/R_{2.73}$	—	0.847	0.59	0.575
No. of paramagnetic ions in r-f. field	2.6×10^{17}	1.7×10^{18}	7.7×10^{17}	1.0×10^{17}
Electron spin resonance	$A/B\sim2.6$ $g\sim2.0$ $\Delta H\sim330$ oe $S/N\sim20$ at 77° K	No resonance at 293° K at 77° K at 4.2° K	$A/B\sim1.0$ $g\sim2.16$–2.07 $\Delta H\sim250$ to 170 oe $S/N\sim6$–5 at 293° K no signal at lower temp.	No resonance at 293° K at 77° K
P_B (units of Bohr magneton)	4.9	~3.9 at low conc. ~4.9 at high conc.	~1.9 at low conc. ~4.9 at high conc.	~2 at low conc. ~4.2 at high conc.
S	2	$\sim3/2$ at low conc. ~2 at high conc.	$\frac{1}{2}$–1 at low conc. ~2 at high conc.	$\frac{1}{2}$–1 at low conc. ~2 at high conc.
No. of d electrons	4 or 6	3 or 7 at low conc. 4 or 6 at high conc.	2 or 8 at low conc. 4 or 6 at high conc.	2 or 8 at low conc. 4 or 6 at high conc.

near the Fermi level of the conduction band. If a similar mechanism is suggested for the dilute alloys considered in Table I, then the following mixtures of states could be suggested:

Fe in Cu or Au, $(3d)^6$ and $(3d)^8$ (a),
or $(3d)^6$ and $(3d)^7$ (b),
Co in Cu, $(3d)^7$ and $(3d)^9$ (a),
or $(3d)^7$ and $(3d)^8$ (b),
Mn in Cu, $(3d)^3$ and $(3d)^5$ (a),
$(3d)^5$ and $(3d)^6$ (b).

It should be noted that none of the suggested mixtures of states results in the presence of an S state for Fe in Cu or Au or for Co in Cu. However, either mechanism (a) or (b) results in the presence of some manganese ions in a $(3d)^5$ state when dissolved in either Cu or Mg. The fact that there are no ions in a $(3d)^5$ state could result in the non observance of a resonance in the alloys Cu–Fe, Au–Fe, and Cu–Co.

An interesting speculation exists that if process (*b*) is chosen then the mixture of ions will always result in the presence of some ions in the $(3d)^6$ or $(3d)^7$ configuration. Due to the Jahn-Teller effect both of these ions show zero-field splitting when present in insulating solids. If a splitting of a similar nature persists in a conducting solid, then the ground state degeneracy is removed in zero applied field and the resulting levels would be available for the Schmitt (1956) scattering mechanism to operate at low temperatures.

BITTER, F. *et al.* 1950. Phys. Rev. **60**, 134.
COLLINGS, E. W. and HEDGCOCK, F. T. 1961. Phys. Rev. To be published.
HEDGCOCK, F. T. 1956. Phys. Rev. **104**, 1564.
GERRITSEN, A. N. 1959. Physica, **25**, 489. See Appendix.
JACOBS, I. S. and SCHMITT, R. W. 1959. Phys. Rev. **113**, 459.
KRONGVIST, E. 1952. Arkiv Fysik, **5**, 453.
OWEN, J. *et al.* 1956. Phys. Rev. **102**, 1501.
——— 1957. Phys. and Chem. Solids, **2**, 85.
SCHMITT, R. W. 1956. Phys. Rev. **103**, 83.

RECEIVED MAY 11, 1961.
DEPARTMENT OF PHYSICS,
UNIVERSITY OF OTTAWA,
OTTAWA, CANADA.

DIRECTIONAL CORRELATION OF THE 769–609 KEV GAMMA-RAY CASCADE IN Po^{214}

H. W. TAYLOR AND R. MCPHERSON

The level structure of ${}_{84}Po^{214}_{130}$ (RaC′) excited by the beta-decay of ${}_{83}Bi^{214}_{131}$ (RaC) has been the subject of many experimental studies (Mayer-Böricke 1959). As many as 58 gamma rays have been reported in the literature. In addition the conversion coefficients and K/L ratios have been measured for a number of the most intense transitions, and spins and parities assigned to many of the levels involved. A consequence of this work has been the identification of some levels as collective excited states and others as single particle excitations. Since Po^{214} is an even–even nucleus only slightly displaced in Z and N from doubly magic Pb^{208}, the collective levels are expected to arise from simple phonon excitations of a spherical nuclear shape.

The first excited state of Po^{214} at 609 kev has a spin 2+, and the multipolarity of the associated ground state gamma transition is $E2$ (Mladjenovic and Slätis 1954). A 0+ level at 1416 kev has been identified with certainty from α-particle measurements, internal conversion work, and directional correlation measurements with the 807–609 kev cascade which de-excites this level. If this level is part of the expected collective triplet state with spins 0+, 2+, 4+ the other members of the set are less firmly established. Levels at 1281 (Van Patter 1959) and 1378 kev (Alder *et al.* 1956; Bishop 1958) have been identified as the second 2+ state in the decay scheme. The second of these appears the more

likely since the existence of a 769–609 kev cascade and a 1378-kev crossover transition have been firmly established. Measurement of the K/L ratio by Mladjenovic and Slätis (1954) ($K/L = 3.9$) indicates a pure $E2$ multipolarity for the 769-kev gamma ray. The measurement of Nielson, Nielson, and Waggoner (1956) ($K/L = 4.6 \pm 1.2$) would permit a considerable $M1$ mixture in the transition. The present directional correlation study was undertaken to check the 2+ spin assignment for the 1378-kev level and to determine the mixing ratio (if any) for the 769-kev gamma ray. This information would also extend our knowledge of 2 – 2 – 0 spin sequences near magic nuclei.

The coincidence spectrometer used for the experiment has been described in some detail elsewhere (Taylor and McPherson 1960*a*). About 30 microcuries of $RaCl_2$ in HCl in equilibrium with its decay products was used as source material. All the gamma rays with energies greater than 500 kev emitted by such a source belong to the Bi^{214} decay. The material was confined to a cylindrical cavity (2 mm diameter×2 mm high) in a cylindrical piece of plastic with 5 mm thick walls.

The pulse-height spectrum of the gamma radiations in coincidence with the 609-kev ground state transition from the first excited state of Po^{214} is shown in Fig. 1. The data were obtained with two 3.75 cm diameter×2.5 cm NaI

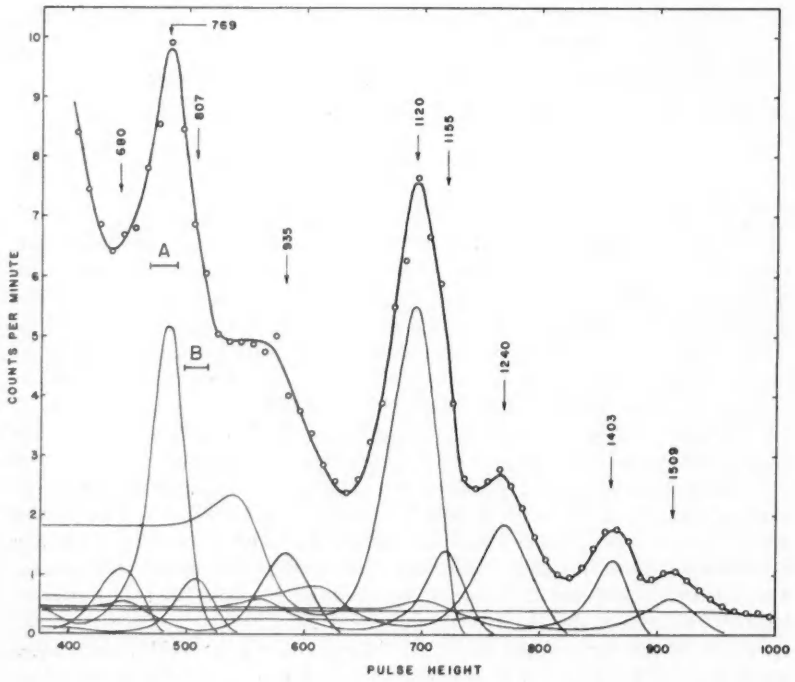

FIG. 1. Gamma-ray spectrum seen in coincidence with the 609-kev ground state transition. Crystal size: 3.75 cm diameter×2.5 cm long; source-to-crystal distance 5 cm; angle between counter axes 90°.

crystals located 5 centimeters from the source with an angle of 90° between their axes. The two gate positions A and B were used for the moveable counter in the directional correlation measurements. Gate A was chosen to include most of the 769-kev photopeak and B to include most of the 807-kev photopeak. By analyzing the spectrum using standard line shapes and the energies of the more intense gamma rays as reported in the literature, the contributions to the counting rates of gates A and B due to the gamma rays involved were determined. The Compton continuum of gamma rays with energies above 935 kev remains relatively flat through these two gate positions.

For the directional correlation work, the two counters were placed at the afore-mentioned source-to-crystal distance in a horizontal plane with the counter axes passing through the source center. The dependence of the singles rate of the moveable counter on the angle θ between the counter axes was constant to better than 1%. Two experiments were performed: (1) the gate of the fixed counter was positioned on the central portion of the 609-kev photopeak, the gate of the moveable counter at position A; the coincidence rate was measured every 10° over the interval $90° \leqslant \theta \leqslant 180°$; (2) the gate of the moveable counter was located at position B and the experiment repeated. More than 10^5 coincidences, of which about 2% were accidental, were recorded in each of the experiments. The coincidence rates for both experiments were least squares fitted to the correlation function $W(\theta) = 1+A_2P_2(\cos\theta)+A_4P_4(\cos\theta)$. To obtain the directional correlation of the 769–609 kev cascade, the correlation of the Compton continuum was subtracted from the result obtained with gate position A. The continuum correlation was calculated by correcting the results obtained with gate position B for the presence of the correlations of the 935–609 kev (3 – 2 – 0) and 807–609 kev (0 – 2 – 0) cascades. The results for gate A were also corrected for small contributions from these cascades. After a further correction for the finite angular resolution of the counters, the correlation coefficients for the 769–609 kev cascade were found to be $A_2 = -0.220\pm0.065$, $A_4 = +0.378\pm0.125$. Most of the error in each coefficient arises from the uncertainty of the spectral analysis. Additional contributions come from the counting rates and the experimental errors of the directional correlation results of Bishop (1958).

A plot of A_4 vs. A_2 using the mixing ratio δ of the 769-kev transition as a parameter is shown in Fig. 2 for the spin sequences 4(2,3)2(2)0, 3(1,2)2(2)0, 2(1,2)2(2)0, 1(1,2)2(2)0, and 0(2)2(2)0 (Taylor and McPherson 1960*b*). The experimental result is shown as a point with the appropriate error bars. The $\delta = \infty$ point gives the coefficients appropriate to a pure quadrupole 769-kev transition. Assuming that the pure $E2$ character of the 609-kev transition is correct, a spin assignment of 2 for the 1378-kev level would appear to be unambiguous. The value of δ determined from the value of A_2 only is $-4.3^{+1.8}_{-4.5}$, corresponding to a mixture of 95% quadrupole and 5% dipole radiation for the 769-kev gamma ray.

The information concerning the 1378-kev level may now be summarized: the energy ratio E_2/E_1 for the second and first 2+ levels is 2.26, the intensity

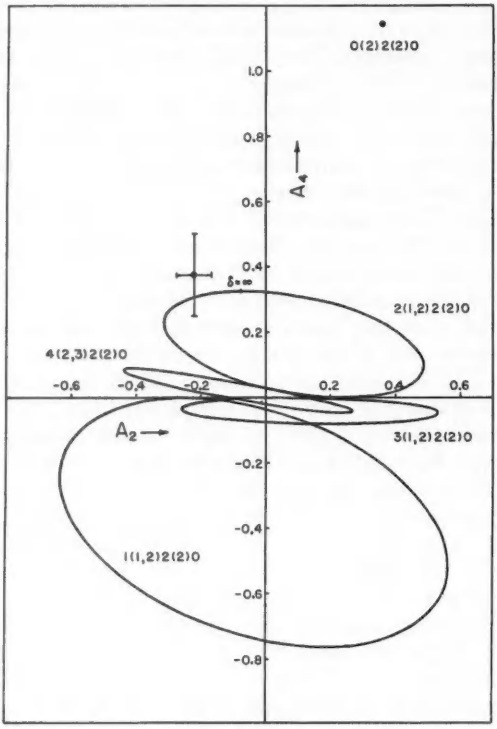

FIG. 2. Plot of A_4 against A_2 using the mixing ratio δ as a parameter for the spin sequences shown.

of the 1378-kev crossover transition relative to the 769-kev stopover transition is about unity, the spin of the level is certainly 2+ with the multipole order of the 769-kev gamma ray being predominantly $E2$. These data would appear to confirm the suggestion that this level is the second 2+ level of Po^{214}.

The nature of the level at 1281 kev is left somewhat uncertain by this result. It could be another component of the predicted triplet state in which case its spin would be 4+, or a single particle state. Bishop (1958) has suggested 0+ and Mayer-Böricke (1959) 2+ as the spin of the level but these assignments are quite uncertain as yet.

The work has been supported by the Atomic Energy Control Board, the National Research Council of Canada, and Queen's University.

ALDER, K., BOHR, A., HUUS, T., MOTTELSON, B., and WINTHER, A. 1956. Revs. Modern Phys. **28**, 432.
BISHOP, G. R. 1958. Nuclear Phys. **5**, 358.
MAYER-BÖRICKE, C. 1959. Z. Naturforsch. **14a**, 609.
MLADJENOVIC, M. and SLÄTIS, H. 1954. Arkiv Fysik, **8**, 65.
NIELSON, K. O., NIELSON, O. B., and WAGGONER, M. A. 1956. Nuclear Phys. **2**, 476.
TAYLOR, H. W. and MCPHERSON, R. 1960*a*. Nuclear Instr. and Methods, **7**, 315.
——— 1960*b*. Directional correlation coefficients A_2 and A_4 as functions of the mixing ratio. Privately circulated tables.
VAN PATTER, D. M. 1959. Nuclear Phys. **14**, 42.

RECEIVED FEBRUARY 28, 1961.
DEPARTMENT OF PHYSICS,
QUEEN'S UNIVERSITY,
KINGSTON, ONTARIO.

LETTERS TO THE EDITOR

Under this heading brief reports of important discoveries in physics may be published. These reports should not exceed 600 words and, for any issue, should be submitted not later than six weeks previous to the first day of the month of issue. No proof will be sent to the authors.

The Identification of Vibrational Levels in H_2^+

Using an electrostatic electron selector (Clarke 1954; Marmet and Kerwin 1960) we have measured the energy intervals between several of the vibrational levels in H_2^+ (Marmet and Kerwin 1960*b*). It has recently been pointed out by Stevenson (1960) that difficulties in the interpretation of appearance potential curves are implied by our results. To be complete, these required the establishment of the ionization potential of H_2 as an additive constant to the vibrational intervals. It was not possible to obtain this in our case without mass analysis.

A selector has now been installed in the mass spectrometer at Saint Francis Xavier University, and further data have been obtained from the Laval instrument. The ionization potential of H_2 has been obtained by comparison with He, and has been measured as 15.37 ± 0.05 ev. This is the additive constant required to establish that the first vibrational interval measured corresponded indeed to the difference between the $\nu' = 0$ and $\nu' = 1$ levels of the $^2\Sigma_g$ state of H_2^+. Two other intervals have been measured, and our results are now as follows:

	Vibrational interval ($\nu'_a - \nu'_b$), ev ±0.01					
Experiment	0–1	1–2	2–3	3–4	4–5	5–6
No mass analysis	0.276	0.258	0.230	0.230	0.214	—
Mass analysis	*0.268*	*0.266*	*0.235*	*0.245*	*0.20*	*0.20*
Average	0.272	0.262	0.233	0.237	0.21 ±2	0.20 ±2
Reference (Richardson 1934)	0.269	0.254	0.238	0.223	0.208	0.192

The relative probabilities of ionization from the molecular ground state to the various vibrational levels of the ionic state may be calculated from the slopes of the various parts of the ionization curve. The probabilities are, for succeeding states: 0.45, 0.77, *1.00*, 0.55, 0.35. Krauss and Kropf (1957) have given theoretical values for these probabilities as: 0.44, 0.87, *1.00*, 0.91, 0.72. Our low values for the higher states may be due to the unfavorable geometric conditions under which they are measured (Marmet 1960) and we hope to conduct experiments to investigate this point.

All of these data appear to constitute evidence favoring the Franck–Condon principle as applied to the hydrogen molecule. The experimental evidence offered by Stevenson to the contrary seems to suffer from two ills: first, as Stevenson points out, the interpretation of ionization curves is open to question, the more so because of the recent observance of structure in the curves that have been traditionally used as references (Fineman and Bouffard 1960; Kerwin, Marmet, and Clarke 1961); secondly, there is some question in our minds as to whether the potential curve for the $^2\Sigma_u$ state of H_2^+ used by him may be in slight error, and in fact should not be a trifle lower, as required by his data.

Clarke, E. M. 1954. Can. J. Phys. **32**, 764.
Fineman, M. A. and Bouffard, R. 1960. Bull. Am. Phys. Soc. Ser. II, **5**, 15.
Kerwin, L., Marmet, P., and Clarke, E. 1961. Proc. of the Conference on Mass Spectrometry, Institute of Petroleum, London.
Krauss, M. and Kropf, A. 1957. J. Chem. Phys. **26**, 1776.
Marmet, P. 1960. Thèse de Doctorat, Université Laval.
Marmet, P. and Kerwin, L. 1960*a*. Can. J. Phys. **38**, 787.
——— 1960*b*. Can. J. Phys. **38**, 2071.
Richardson, O. W. 1934. Molecular hydrogen and its spectrum (Yale University Press, N.Y.).
Stevenson, D. P. 1960. J. Am. Chem. Soc. **82**, 5961.

Received June 15, 1961.

Faculty of Sciences,
Laval University,
Quebec, Que.
and
Saint Francis Xavier University,
Antigonish, Nova Scotia.

Larkin Kerwin*
Paul Marmet*
Ernest Clarke†

*Laval University, Quebec, Que.
†Saint Francis Xavier University, Antigonish, Nova Scotia.

Lifetimes of the Low-lying Levels in Ne^{20}†

We have measured the lifetimes of the 1.63-, 4.25-, and 4.97-Mev levels in Ne^{20} by the Doppler shift attenuation method (Devons *et al.* 1955; Litherland *et al.* 1961).

Triply charged carbon ions of energies near 18 Mev produced by the Chalk River tandem accelerator were directed upon unbacked carbon targets and carbon targets evaporated on thin magnesium, aluminum, and copper foils. The energies of gamma rays emitted from Ne^{20*} following the $C^{12}(C^{12},\alpha)Ne^{20*}$ reaction were observed in gamma–alpha coincidences between a movable 5 in.×6 in. NaI crystal gamma-ray detector and a p–n silicon junction alpha-particle detector placed at zero degrees to the ion beam (Gove *et al.* 1961*a*).

Since the neon ions associated with the coincidences were moving forward with velocities near 4×10^9 cm/sec, Doppler shifts in the gamma-ray energies would be expected with maximum values for the unbacked target of about $v/c \sim 1.3\%$. The gamma-ray energy as a function of angle is given by $E = E_0(1+F(v/c)\cos\theta)$ where F is an attenuation factor which takes into account the slowing down of the neon ions before gamma-ray emission.

Measurements of dE/dx for heavy ions in various materials made at Manchester (K. Ramavataram, private communication) were used to derive slowing down times for the target backings. For neon ions of initial velocity near 4×10^9 cm/sec, the velocity decreases almost exponentially with time in many materials. Consequently the attenuation F of the Doppler shifts is given simply by $F = \alpha/(\alpha+\tau)$ where α is the mean slowing down time and τ is the mean life of the gamma-ray emitting system (Devons *et al.* 1955).

Coincidence gamma-ray spectra (Gove *et al.* 1961*a*, Fig. 1(*b*)) were measured at a number of angles in order to determine the small shifts of energy with angle. Gain changes in the gamma-ray detection system were monitored by simultaneous observation of the 1.28-Mev gamma rays from a Na^{22} source. Least-squares fits were made to the gamma-ray energies as a function of $\cos\theta$ in order to determine $F(v/c)$ for both the backed and unbacked targets (see Fig. 1 for an example of these results). The experimental value of F for a given material

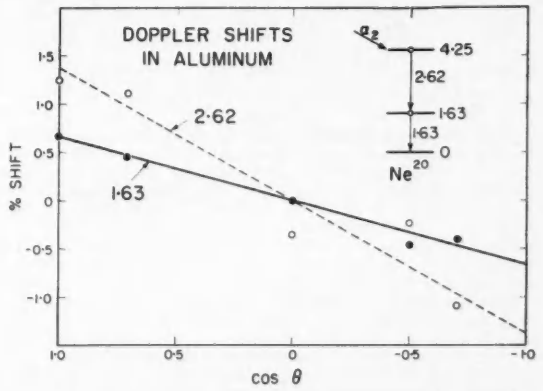

FIG. 1. Doppler shifts in gamma-ray energy as a function of the angle of emission, θ, relative to the direction of motion of the emitting nucleus, which travels in aluminum. The shifts associated with population of the 4.25-Mev level in Ne^{20} are shown. Note that the shift is smaller (though finite) for the second gamma-ray in the cascade, which shows directly that the 1.63-Mev level has a lifetime near the slowing down time for neon ions in aluminum.

was obtained from the ratio of two such results, one for the unbacked and one for the backed target. Figure 2 shows the determination of the lifetime of the 4.97-Mev level from the value of F measured in magnesium. The errors in the lifetimes are asymmetrical as one can see from this figure, and in particular the result for the 4.97-Mev level is four standard deviations away from zero lifetime.

In Table I are listed the lifetimes obtained for the 1.63-Mev, 4.25-Mev, and 4.97-Mev levels in Ne^{20}. The slowing down time, α, is given for each material used.

The lifetime value $5.6^{+1.1}_{-1.2}\times10^{-13}$ sec, obtained for the 1.63-Mev level, is in agreement with the previous work of Devons *et al.* (1955) and Lemberg *et al.* (1950).

†Issued as A.E.C.L. No. 1282.

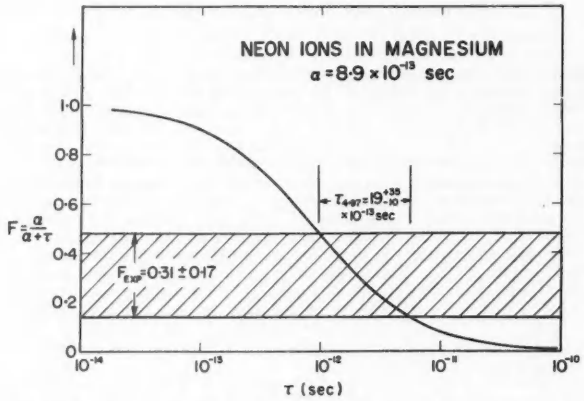

FIG. 2. The relation $F = \alpha/(\alpha+\tau)$ is plotted against τ for neon ions in magnesium. Also shown is the measured value of F for the 4.97-Mev level in Ne^{20}. The band encloses one standard deviation in either direction.

TABLE I

Level (Mev)	1.63	4.25	4.97
E_γ(Mev)	1.63	2.62	3.34
Slowing materials	Mg, Al	Al, Cu	Mg, Al
$\alpha(10^{-13}$ sec)	8.9, 5.9	5.9, 2.9	8.9, 5.9
τ_{exp} $(10^{-13}$ sec)	$5.6^{+2.8}_{-1.2}$	$0.76^{+.72}_{-.32}$	$19^{+3.5}_{-1.0}$
Assumed multipolarity	$E2$	$E2$	$M1$, $E2$ $E1$, $M2$
$\lvert M\rvert^2$	38	26	4.4×10^{-4}, 1.6×10^{-3}, 1.6×10^{-5}, 3.3×10^{-2}

Table I also gives, for certain assumed multipolarities, the ratio $|M|^2$ of the measured gamma-ray transition probabilities to the Weisskopf estimate which is equal to the ratio $B(E2)\downarrow/B(E2)\downarrow_{S.P.}$ for the $E2$ transitions. The values of $|M|^2$ for the transitions from the 1.63-Mev and 4.25-Mev levels, which have spin and parity values $2+$, $4+$ respectively (Broude and Gove 1961; Gove *et al.* 1961*a*), are seen to be typical of those for known $E2$ transitions in light nuclei (Wilkinson 1960).

The most striking result is the long $(19^{+3.5}_{-1.0}\times10^{-13}$ sec) lifetime of the 4.97-Mev level. The 3.34-Mev gamma ray from this level has a dipole-to-quadrupole amplitude ratio equal to about 0.1 (Broude and Gove 1961; Gove *et al.* 1961*a*). From Table I it appears that the values of $|M|^2$ for this transition are reasonable (Wilkinson 1960) except that for the $E2$ component which is present if the 4.97-Mev level has positive parity. The small value of $|M|^2$, 3×10^{-3}, would make this the most retarded $E2$ transition yet observed in light nuclei despite the presence of two strongly enhanced $E2$ transitions in the same nucleus. This result for the 4.97-Mev level suggested a measurement of the polarization of the 3.34-Mev gamma ray in the Ne^{20} $(pp'\gamma)$ reaction. This measurement has been made, with the result that the 4.97-Mev level has been found to have negative parity (Gove *et al.* 1961*b*). This latter result has been confirmed in alpha-particle angular distribution measurements by Almqvist *et al.* (1961), and in alpha–gamma angular correlation measurements (Gove *et al.* 1961*a*).

ALMQVIST, E., BROMLEY, D. A., KUEHNER, J. A., and WHALEN, B. 1961. To be published.
BROUDE, C. and GOVE, H. E. 1961. Bull. Am. Phys. Soc. Ser. II, **6**, 37.
DEVONS, S., MANNING, G., and BUNBURY, D. ST. P. 1955. Proc. Phys. Soc. A, **68**, 18.
DEVONS, S., MANNING, G., and TOWLE, J. H. 1956. Proc. Phys. Soc. A, **69**, 173.
GOVE, H. E., LITHERLAND, A. E., and CLARK, M. A. 1961*a*. Can. J. Phys. **39**. This issue.
——— 1961*b*. To be published.
LEMBERG, I. Kh. 1960. Proc. 2nd Conf. on Reactions between Complex Nuclei, Gatlinburg, May 1960 (Wiley & Sons).
LITHERLAND, A. E., ADAMS, B., ECCLESHALL, D., and YATES, M. 1961. Bull. Am. Phys. Soc. Ser. II, **6**, 248.
WILKINSON, D. H. 1960. Nuclear spectroscopy, Part B, *edited by* F. Ajzenberg-Selove (Academic Press), p. 852ff.

RECEIVED JUNE 20, 1961.
ATOMIC ENERGY OF CANADA LIMITED,
CHALK RIVER, ONTARIO.

M. A. CLARK
H. E. GOVE
A. E. LITHERLAND

Alpha–Gamma Angular Correlations in the Reaction $C^{12}(C^{12},\alpha)Ne^{20}$*

Angular correlations between gamma rays and alpha particles detected at 0° have been measured in the reaction $C^{12}(C^{12},\alpha)Ne^{20}$ using beams of 17- and 18-Mev triply charged carbon ions from the Chalk River tandem accelerator. The geometry employed was the same as that for the lifetime measurements (Clark, Gove, and Litherland 1961) and is shown in an inset on Fig. 2. The detectors employed were p–n silicon junction counters from 5 to 15 mm^2 in area and of resistivity 10,000 ohm cm,† located about 1 centimeter from the target. Two NaI(Tl) detectors were employed, each 5 in. in diameter and 6 in. long, 6.25 inches from the target. Sufficient aluminum absorber was inserted between target and detector to stop the carbon ions. One gamma-ray detector was moved in angle with respect to the beam direction and the other was fixed at 90° to the beam and served as a monitor. The spectra of gamma rays from each detector, in coincidence with a particular alpha group, were displayed on two 100-channel pulse-height analyzers.

The upper half of Fig. 1 shows the alpha-particle spectrum measured directly by the zero-degree alpha counter. The inset level diagram shows the levels in Ne^{20}; the present experiment

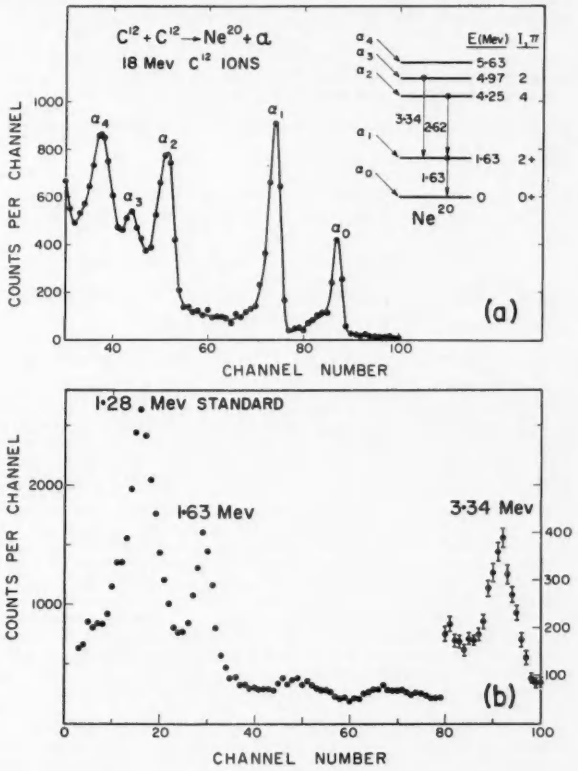

FIG. 1. (*a*) Alpha-particle groups from the reaction $C^{12}(C^{12},\alpha)Ne^{20}$ as observed in silicon p–n junction detector at zero degrees to the carbon ion beam. Gates were set on individual groups for the coincidence measurements. A partial level scheme for Ne^{20} is also shown.
(*b*) The gamma-ray spectrum in coincidence with the alpha-particle group α_3 leading to the 4.97-Mev level in Ne^{20}. The 1.28-Mev gamma ray from Na^{23} which was used for calibration in lifetime measurements is also present in the spectrum.

*Issued as A.E.C.L. No. 1281.
†These were obtained from both the General Physics Branch, Atomic Energy of Canada Limited, and R.C.A. Victor, Montreal.

involved measuring the angular distributions of 3.34- and 1.63-Mev gamma rays in coincidence with the alpha group α_2, the 2.62- and 1.63-Mev gamma rays in coincidence with α_2, and the 1.63-Mev gamma rays in coincidence with α_1. A coincidence spectrum for the first of the above cases is shown in the lower half of Fig. 1. In addition to the 1.63- and 3.34-Mev gamma rays a 1.28-Mev peak from Na^{22} is shown which was employed in lifetime measurements.

Because the incident particles (C^{12}), the target (C^{12}), and the outgoing particles (He^4) all have zero spin and positive parity the coincident gamma-ray angular correlations measured with the alpha detector at 0° are particularly easy to interpret (Litherland and McCallum 1960; Litherland and Ferguson 1961) since only the $m = 0$ substate of the residual nucleus is populated. However, if the state of the residual nucleus is $0-$ it will not be fed in this reaction and if it has spin and parity $1+$, $2-$, $3+$, $4-$, etc. the alpha particles cannot be emitted at zero degrees (Litherland 1961). This latter condition is modified because of the finite size of the alpha detector and, in these particular cases, only the $m = \pm 1$ magnetic substates of the level in the residual nucleus are populated. This provides a method for measuring not only the spin of a level but also its parity (Litherland 1961).

The spin of both the 4.97-Mev and the 4.25-Mev levels in Ne^{20} as well as the dipole–quadrupole mixing in the 3.34-Mev radiation had been previously measured (Broude and Gove 1961) and the present work was undertaken to check these assignments. The results are summarized in Table I where values of a_2/a_0 and a_4/a_0 obtained both experimentally and theoretically are

TABLE I

Experimental and theoretical coefficients in the angular correlation of gamma rays in coincidence with alpha particles measured at 0° in the $C^{12}(C^{12},\alpha)Ne^{20}$ reaction fitted to $W(\theta) = 1+(a_2/a_0)P_2(\cos\theta)+(a_4/a_0)P_4(\cos\theta)$

Level (Mev)	γ-ray (Mev)	a_2/a_0	a_4/a_0	
4.97	1.63	0.23±0.04	−0.77±0.06	Experiment
		0.18	−0.76	Theory
	3.34	0.15±0.04	−0.09±0.06	Experiment
		0.19	0	Theory
4.25	1.63	0.39±0.04	−0.45±0.05	Experiment
		0.51	−0.37	Theory
	2.62	0.59±0.02	−0.62±0.03	Experiment
		0.51	−0.37	Theory
1.63	1.63	0.58±0.05	−1.40±0.07	Experiment
		0.71	−1.71	Theory

compared. The experimental points were fitted by a least-squares computer program to a Legendre polynomial expansion and the theoretical coefficients in Table I have been corrected for the finite size of the gamma-ray detector. In the case of the 3.34-Mev radiation the quadrupole–dipole amplitude ratio of +0.08 obtained by Broude and Gove (1961) was employed.

The results for 1.63-Mev gamma rays measured in coincidence with alpha particles feeding the 4.97-Mev level in Ne^{20} are shown in Fig. 2. The results of this correlation and of the 3.34-

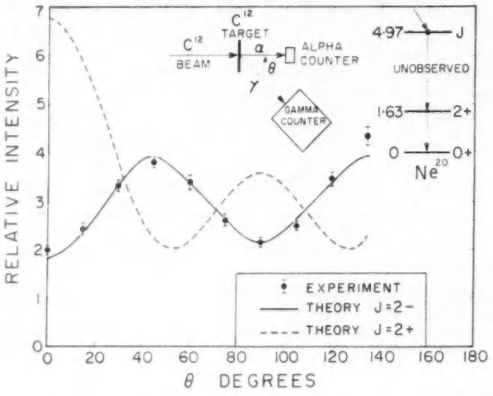

FIG. 2. The angular correlation of 1.63-Mev gamma rays in coincidence with alpha particles, feeding the 4.97-Mev level in Ne^{20}, observed at zero degrees as shown in the inset diagram. The dashed and solid curves are the theoretical ones for $J\pi = 2+$ and $2-$ respectively for the level. Note that in this coincidence measurement of a triple correlation, the 3.34-Mev gamma ray was the "unobserved" intermediate radiation.

Mev gamma correlation not only confirm the spin assignment and multipole mixing (assuming no $E3$ radiation) of Broude and Gove (1961) but also establish negative parity for the level. The parity has also been established by measurements of the linear polarization of the 3.34-Mev gamma ray (Gove *et al.* 1961) and by direct measurement of the alpha-particle angular distributions (Almqvist *et al.* 1961).

Although the agreement with theory is not as good the results for the 4.25- and 1.63-Mev levels establish unambiguously spin and parity values of 4+ and 2+ respectively for these levels. The errors shown on the experimental coefficients do not include any systematic errors and are therefore probably underestimates.

When the gate on the alpha counter was set on the alpha group feeding the 5.63-Mev level a weak 4.00-Mev gamma ray was observed in the coincident spectrum. From this measurement a value of $\Gamma_\gamma/\Gamma = .04 \pm .02$ was obtained and proved that the 5.63 level decays by alpha emission. Recent measurements of this ratio give a value of 0.07 ± 0.01 (Kuehner and Almqvist 1961).

ALMQVIST, E., BROMLEY, D. A., KUEHNER, J. A., and WHALEN, B. 1961. To be published.
BROUDE, C. and GOVE, H. E. 1961. Bull. Am. Phys. Soc. Ser. II, **6**, 37.
CLARK, M. A., GOVE, H. E., and LITHERLAND, A. E. 1961. Can. J. Phys. **39**. This issue.
GOVE, H. E., LITHERLAND, A. E., and CLARK, M. A. 1961. To be published.
KUEHNER, J. A. and ALMQVIST, E. 1961. To be published.
LITHERLAND, A. E. 1961. Can. J. Phys. **39**. This issue.
LITHERLAND, A. E. and FERGUSON, A. J. 1961. Can. J. Phys. **39**, 788.
LITHERLAND, A. E. and MCCALLUM, G. J. 1960. Can. J. Phys. **38**, 927.

RECEIVED JUNE 20, 1961.
ATOMIC ENERGY OF CANADA LIMITED,
CHALK RIVER, ONTARIO.

H. E. GOVE
A. E. LITHERLAND
M. A. CLARK

The Interpretation of Angular Distributions and Angular Correlations from the Reaction $C^{12}(C^{12},\alpha\gamma)Ne^{20}$†

In recent studies of the $C^{12}(C^{12},\alpha\gamma)Ne^{20}$ reaction (Gove *et al.* 1961) it was found that the angular correlations of the gamma rays in coincidence with alpha particles, detected in a small axially symmetrical counter at zero degrees to the beam of C^{12} ions, agreed with the theory given by Litherland and Ferguson (1961) with one exception. It was found that the angular correlation of the 1.63-Mev gamma ray following the 3.34-Mev unobserved cascade gamma ray from the 4.97-Mev state in Ne^{20} was in complete disagreement with theory. This disagreement has now been explained and has led to an increased understanding of the angular distributions of the alpha particles from the $C^{12}(C^{12},\alpha)Ne^{20}$ and similar reactions.

In the paper by Litherland and Ferguson (1961, hereinafter referred to as LF) it was proved that in reactions of the type $X(h_1,h_2)Y^*$, in which the particle h_2 is detected in a small counter at 0° or 180° to the beam of h_1 particles, the magnetic quantum numbers of the substates of Y^* do not exceed the sum of the spins of X, h_1, and h_2. In the case of the $C^{12}(C^{12},\alpha)Ne^{20}$ reaction one might expect that only the $\gamma = 0$ magnetic substate, of a state of spin c in the residual Ne^{20}, would be populated. However, the element of the density matrix corresponding to the $\gamma = 0$ magnetic substate, given by equations (21), (28), and (29) of LF, is identically zero if the parity of the state of spin c is $(-1)^{c+1}$. This result is a consequence of vanishing Clebsch–Gordan coefficients‡ and is independent of the size of the axially symmetrical counter detecting the alpha particle and the complexity of the situation in the compound nucleus.

Two important conclusions relating to angular correlations and angular distributions follow from this result.

(1) In the case of the $C^{12}(C^{12},\alpha\gamma)Ne^{20}$ reaction and similar reactions, the angular correlations of gamma rays observed in coincidence with an axially symmetrical counter of finite but small size situated at zero degrees to the incident beam have no contribution from the $\gamma = 0$

†Issued as A.E.C.L. No. 1294.

‡The relevant Clebsch–Gordan coefficient is $(c\gamma,l\lambda|b\beta)$, where c is the spin of state in Ne^{20}, l is the angular momentum of the alpha particle, and b is the spin of the state in the compound nucleus Mg^{24}. γ, λ, and β are the projections of the angular momenta c, l, and b along the quantization axis which in this case is the accelerated beam of C^{12} ions. Because both the target nucleus and bombarding particle have zero spin β is zero. Consequently if γ is zero then λ must also be zero and the sum $c+l+b$ must be even otherwise the Clebsch–Gordan coefficient vanishes. Because both the alpha particle and C^{12} have even parity and parity is conserved in the reaction it is clear that if the state c has parity $(-1)^{c+1}$ then the Clebsch–Gordan coefficient is zero.

magnetic substate if the residual of state of spin c has parity $(-1)^{c+1}$. The main contribution to the angular correlation will be from the $\gamma = \pm 1$ magnetic substates. The contribution from the $\gamma = \pm 2$ substates will usually be much smaller and be given by an equation similar to equation (29) of LF.

(2) In the study of the angular distributions of alpha particles from such reactions as the $C^{12}(C^{12},\alpha)Ne^{20}$ reaction no alpha particles will be observed at zero degrees to the beam if the state in the residual nucleus of spin c has parity $(-1)^{c+1}$. Conversely if alpha particles are observed at zero degrees to the beam the parity of the state of spin c is $(-1)^c$. It should be noted in this case that it is possible for no alpha particles to be emitted at zero degrees to the beam due to interference between states in the compound nucleus. This situation is unlikely and extremely unlikely to persist at different excitations in the compound nucleus.

The effects on angular correlations and angular distributions of the above considerations have been observed recently. The $C^{12}(C^{12},\alpha\gamma)Ne^{20}$ angular correlations from the 2− third excited state of Ne^{20} measured by Gove *et al.* (1961) show that the $m = 0$ substate of the 2− excited state is not populated. The angular correlations can be fitted if only the $m = \pm 1$ substates are populated.

The angular distributions of the alpha particles leading to the ground, first and second excited states of Ne^{20} from the $C^{12}(C^{12},\alpha)Ne^{20}$ reaction are in agreement with the known positive parity of these states (Almqvist *et al.* 1961 and Clark *et al.* 1961). The third excited state of Ne^{20} is now known to be a 2− state (Gove *et al.* 1961) and in this case the angular distributions measured as a function of C^{12} energy by Almqvist *et al.* (1961) show a pronounced minimum in the differential cross section at zero degrees to the beam and at all bombarding energies. The small but non-zero yield at zero degrees is attributed by Almqvist *et al.* (1961) to the finite size of the counter detecting the alpha particles and to background.

It is worth emphasizing in conclusion that measurements on heavy ion reactions such as those described above or from inelastic alpha scattering from even–even nuclei can decide the parity of states whose angular momenta have been determined. For example, the 6.44-Mev state in Mg^{24} which has been assigned spin zero (Broude and Gove 1961) was observed in the $C^{12}(O^{16},\alpha)Mg^{24}$ reaction (Hinds *et al.* 1961). In this case the observation of the alpha-particle group at any angle in the reaction is sufficient to assign positive parity to the state at 6.44 Mev in Mg^{24} since the reaction cannot populate 0− levels.

I would like to acknowledge my thanks to Dr. J. A. Kuehner for a stimulating discussion.

ALMQVIST, E., BROMLEY, D. A., KUEHNER, J. A., and WHALEN, B. 1960. Proceedings of the Kingston Conference on Nuclear Structure (University of Toronto Press), p. 922, and private communication. See also GOVE, H. E. 1961. Nucl. Instr. and Methods, **11**, 79.

BROUDE, C. and GOVE, H. E. 1960. Proceedings of the Kingston Conference on Nuclear Structure (University of Toronto Press), p. 457. See also BROUDE, C. and GOVE, H. E. 1961. Bull. Am. Phys. Soc. Ser. II, **6**, 37.

CLARK, M. A., GOVE, H. E., and LITHERLAND, A. E. 1961. Can. J. Phys. **39**. This issue.

GOVE, H. E., LITHERLAND, A. E., and CLARK, M. A. 1961. Can. J. Phys. **39**. This issue.

HINDS, S., LITHERLAND, A. E., and MIDDLETON, R. 1961. To be published.

LITHERLAND, A. E. and FERGUSON, A. J. 1961. Can. J. Phys. **39**, 788.

RECEIVED JUNE 20, 1961.

A. E. LITHERLAND
ATOMIC ENERGY OF CANADA LIMITED,
CHALK RIVER, ONTARIO.

Magnetic Spectrometer Measurements of Levels of Ne^{20}*

In connection with recent experiments (see accompanying letters) on the levels of Ne^{20}, spectra of alpha particles from $C^{12}(C^{12},\alpha)Ne^{20}$ have been measured using a magnetic spectrometer (Enge 1958). Figure 1 contains spectra measured at 0°, 10°, and 50° in the laboratory system and Table I summarizes the excitation energies in Ne^{20} obtained; the numbers in the left-hand column identify the corresponding peaks. The energy resolution obtained was $\Delta E/E \sim 1\%$ and was limited by the target thickness. The spectrometer energy calibration was obtained assuming the excitation corresponding to group 2 to be 4.25 Mev. In general probable errors of 0.02 Mev are estimated; however, energy differences are given somewhat more accurately. In particular the difference in excitation energy corresponding to groups 4 and 5 is obtained as 0.17 ± 0.01 Mev.

These spectra confirm the existence of a level at 5.81 Mev, first observed in the $Na^{23}(p,\alpha)Ne^{20}$ reaction (Temmer 1961). Additional measurements have established spin 1− for the new 5.80-Mev level as well as 3− for that known at 5.64 Mev (Kuehner 1961) and values of the ratio Γ_γ/Γ of $0.003(\pm 0.003)$ and $0.07(\pm 0.01)$ respectively (Kuehner and Almqvist 1961).

*Issued as A.E.C.L. No. 1283.

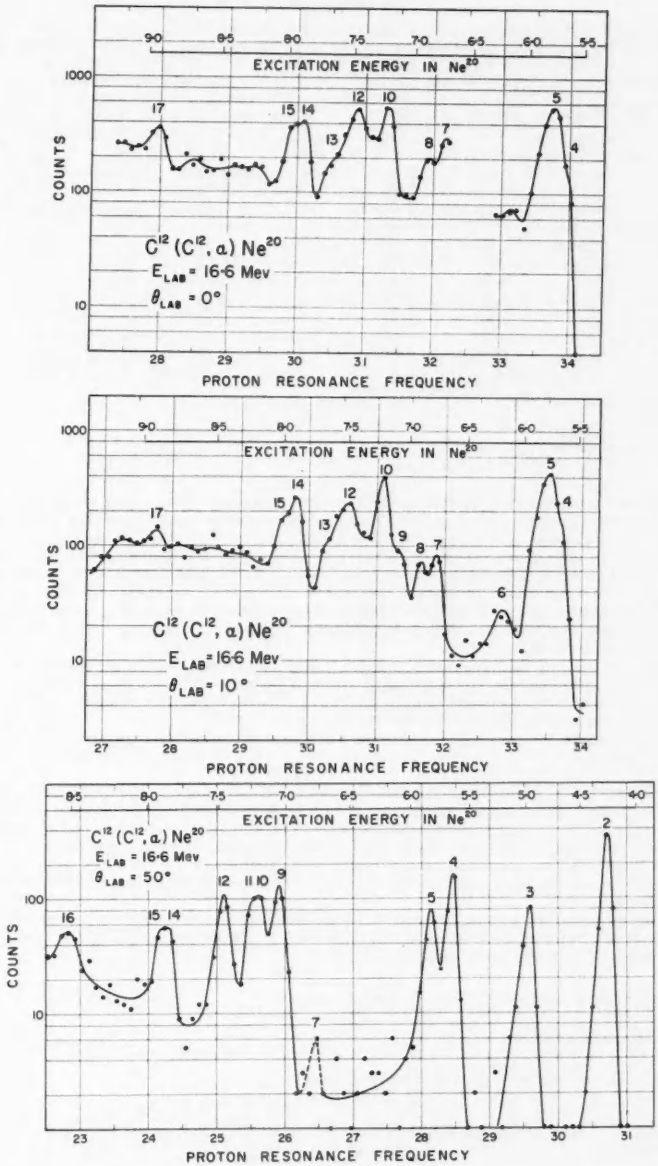

FIG. 1. Spectra of alpha particles from the reaction $C^{12}(C^{13},\alpha)Ne^{20}$ measured with a magnetic spectrometer are presented for angles of 0°, 10°, and 50° in the laboratory system. Included in each spectrum is a scale giving the excitation energy in Ne^{20}. The numbers on the peaks identify them with entries in Table I. A region of the spectrum at 0° was obscured due to the presence at the detector of a portion of the transmitted beam.

TABLE I

Summary of Ne^{20} level energies in Mev obtained from spectrometer measurements of Fig. 1. The corresponding alpha-particle groups are identified by the numbers in the left-hand column. Values of the level spins and parities, where known, are given in the right-hand column

Peak identification	0°	10°	50°	Weighted average	Previous value†	$J\pi$
2			4.25*	4.25*	4.25	$4+$[a]
3			4.97	4.97	4.97	$2-$[a,b]
4	5.64	5.64	5.64	5.64	5.63	$3-$[c]
5	5.77	5.80	5.83	5.81		$1-$[c]
6		6.17		6.17		
7	6.72	6.75		6.74	6.75	$0+$[d]
8	6.85	6.88		6.87		
9		7.05	7.05	7.05		$(4-)$[e]
10	7.20	7.19	7.19	7.19	7.19	$3-$[d]
11			7.25	7.25	7.23	$0+$[d]
12	7.45	7.47	7.47	7.46	7.46	$2+$[d]
13	7.67	7.63		7.65		$(6+)$[e]
14	7.86	7.88	7.85	7.86	7.86	$2+$[d]
15	7.96	8.00	7.92	7.93		
16			8.52	8.52		
17	8.92	8.91		8.92		

*Energy scale normalization point.
†Taken from Ajzenberg and Lauritsen (1959).
[a]Broude and Gove (1961).
[b]Gove *et al.* (1961).
[c]Kuehner (1961).
[d]Cameron (1953).
[e]Litherland *et al.* (1961).

Preliminary evidence for several new levels is presented. The group of alpha particles labelled 9 corresponds to a level at 7.05-Mev excitation and is identified with a level observed in earlier (α,γ) coincidence studies as 7.02($\pm$0.02)-Mev excitation (Litherland *et al.* 1961). The absence of this group in the 0° spectrum suggests a spin–parity combination of $\pi = (-1)^{J+1}$ for this level because, as was pointed out by Litherland (1961), only levels of Ne^{20} with $\pi = (-1)^J$ can show yield at 0° in the $C^{12}(C^{12},\alpha)Ne^{20}$ reaction. In this connection additional spectra taken at 0° but not illustrated have shown α_0, α_1, and α_2 to be present thus confirming these levels all to have + parity since their spins $J = 0$, 2, and 4 (Broude and Gove 1961) respectively.

A shoulder, 13, on the low-energy side of group 12 corresponds to an excitation in Ne^{20} of $\sim$7.7 Mev and may be identified with a new level near this excitation suggested by γ,γ coincidence measurements (Litherland *et al.* 1961). The fact that this shoulder is strong at 0° requires the corresponding level in Ne^{20} to have parity $(-1)^J$.

A possible additional new level in Ne^{20} at 7.93-Mev excitation is suggested by the appearance of a group at all three angles. Its appearance in the 0° spectrum requires the parity to be $(-1)^J$.

Further work will be required on these levels as well as others suggested by these spectra to establish their identities. In particular, groups 6, 8, 16, and 17 may be from contaminant reactions. It is interesting to note that if a rotational band is associated with the 1− (5.81 Mev) and 3− (7.19 Mev) levels (Litherland *et al.* 1961*a*) the spectra show no evidence for a 2− member near 6.3 Mev of comparable strength. The absence of 2− and 4− members of this band requires a K quantum number of 0 and implies an octupole shape deformation or vibration of the nucleus.

Further measurements using this reaction and the $Na^{23}(p,\alpha)Ne^{20}$ reaction are planned using the instrument in its broad range spectrograph mode of operation instead of the spectrometer mode used in this preliminary survey.

AJZENBERG, F. and LAURITSEN, T. 1959. Nuclear Phys. **11**, 1.
BROUDE, C. and GOVE, H. E. 1961. Bull. Am. Phys. Soc. Ser. II, **6**, 37.
CAMERON, J. R. 1953. Phys. Rev. **90**, 839.
ENGE, H. A. 1958. Rev. Sci. Instr. **29**, 885.
GOVE, H. E., LITHERLAND, A. E., and CLARK, M. A. 1961. Can. J. Phys. **39**. This issue.
KUEHNER, J. A. 1961. To be published.
KUEHNER, J. A. and ALMQVIST, E. 1961. To be published.
LITHERLAND, A. E. 1961. Can. J. Phys. **39**. This issue.
LITHERLAND, A. E., CLARK, M. A., and GOVE, H. E. 1961. Can. J. Phys. **39**. This issue.
LITHERLAND, A. E., KUEHNER, J. A., GOVE, H. E., CLARK, M. A., and ALMQVIST, E. 1961*a*. To be published.
TEMMER, G. M. 1961. Private communication. See also ADAMS, H. S., FOX, J. D., HEYDENBURG, N. P., and TEMMER, G. M. 1961. Bull. Am. Phys. Soc. Ser. II, **6**, 250.

RECEIVED JUNE 20, 1961.
ATOMIC ENERGY OF CANADA LIMITED,
CHALK RIVER, ONTARIO.

E. ALMQVIST
J. A. KUEHNER

A 7.02-Mev Level in Ne^{20}*

A new level in Ne^{20} at 7.02-Mev excitation energy has been observed in a study of coincidences between alpha particles and gamma rays from the reaction $C^{12}(C^{12},\alpha\gamma)Ne^{20}$. The new level was sought deliberately as a result of a prediction based upon the collective model. Recently it has been shown by Clark *et al.* (1961) that the cascade electric quadruple transitions from the 4.25-Mev (4+) and the 1.63-Mev (2+) levels are both considerably enhanced over the single particle estimate. Also the levels at 4.97 and 5.63 Mev have been shown to have spins and parities of 2− and 3− respectively (Gove *et al.* 1961 and Kuehner 1961). The presence of a 5− level at 8.84 Mev (McDermott *et al.* 1960) suggests that, as the collective model may be relevant for Ne^{20}, there should be a level in Ne^{20} near 7-Mev excitation with spin and parity 4−. Such a level cannot decay by alpha-particle emission to O^{16} because of parity conservation and should consequently decay entirely by gamma-ray emission.

A level at 7.02 Mev has now been located and it has some of the properties expected for a 4− rotational level based on the 2− level in Ne^{20} at 4.97 Mev. The level was located by observing the spectrum of alpha particles, in a 10,000 ohm cm silicon p–n solid state counter, in coincidence with the gamma rays from the low-lying levels of Ne^{20}. The alpha-particle counter was situated at 0° to the incident beam of C^{12} ions which bombarded a 50-$\mu g/cm^2$ carbon foil. Three 0.4-mg/cm² aluminum foils were used to prevent the C^{12} ions from hitting the alpha-particle counter. The gamma rays were observed with the aid of a 5 in. diameter by 6 in. long NaI(Tl) crystal.

Figure 1(*a*) shows the spectrum of alpha particles in coincidence with gamma rays in three

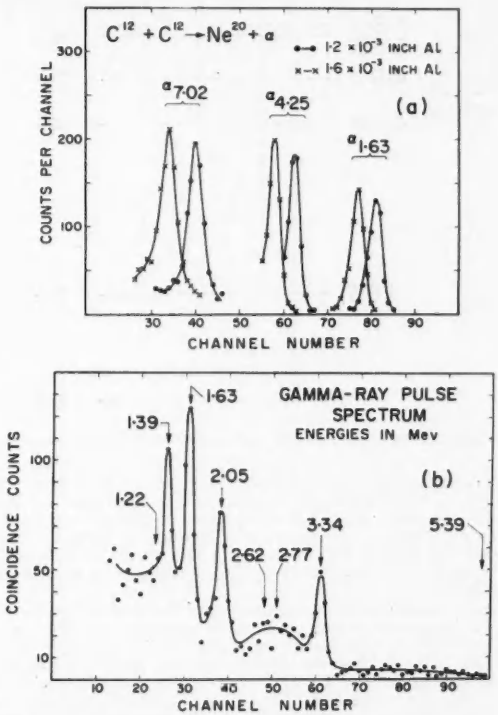

FIG. 1. (*a*) Portions of the spectrum of alpha particles from the reaction $C^{12}(C^{12},\alpha)Ne^{20}$ are shown taken in coincidence with gamma rays. The effect of introducing an extra 0.4×10^{-2} inches of aluminum absorber is shown. The groups are labelled by the excitation energy in Mev of the level in the residual nucleus which they leave excited.

(*b*) The gamma-ray pulse spectrum taken in coincidence with the alpha-particle group exciting the 7.02-Mev level in Ne^{20} is shown. The energies of possible cascade gamma rays from the 7.02-Mev level are shown in Mev.

*Issued as A.E.C.L. No. 1284.

regions of the pulse spectrum. The shift of the peak positions upon insertion of an additional 0.4-mil aluminum foil in front of the counter proves that the groups are alpha-particle groups. The group designated $\alpha_{7.02}$ corresponds to the formation of Ne^{20} in a new level at 7.02 Mev. Figure 1(*b*) shows the gamma-ray spectrum in coincidence with the alpha-particle group corresponding to $\alpha_{7.02}$ taken at 90° to the incident C^{12} beam and Fig. 2 summarizes the results of the analysis of gamma-ray spectra taken at 30°, 60°, and 90°. The energies in Mev shown in Fig. 2 correspond to possible transitions from the new level at 7.02 Mev to lower levels in

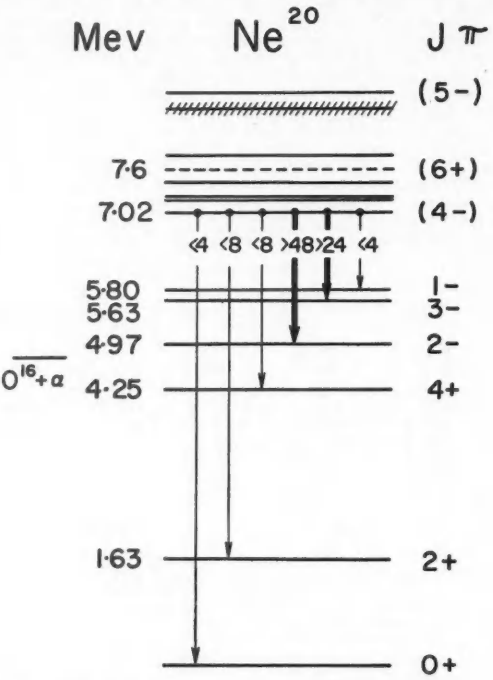

FIG. 2. The energy level diagram of Ne^{20} is shown together with the percentage branching of the new level at 7.02 Mev.

Ne^{20}. The absence of cascade gamma rays from the 5.63-Mev (3−) level, which is fed by the 1.39-Mev gamma ray of Fig. 1(*b*), is due to predominant alpha-particle emission (Gove *et al.* 1961; Kuehner and Almqvist 1961). The most recent excitation energy of the new level is 7.02±.02 Mev. In a subsidiary gamma–gamma coincidence experiment evidence has been obtained for another new level in Ne^{20} at about 7.6 Mev which has some of the expected properties for a 6+ level in Ne^{20}. Because the evidence is not conclusive the level is shown by a dashed line in Fig. 2.

At present there are no conclusive measurements of the spin and parity of the new level at 7.02 Mev though the intensities of the gamma rays observed at 30°, 60°, and 90° are consistent with the assignment of 4−. Also recent measurements by Almqvist and Kuehner (1961) suggest a parity of $(-1)^{J+1}$. However, the gamma-ray branching ratios shown in Fig. 2 strongly support the assignment of 4− and the assignment of the level to a rotational band based on the 4.97-Mev level. The lack of evidence for an electric dipole transition from the new level to the 4.25-Mev level is expected because of the strong inhibition of electric dipole radiation in Ne^{20} and the observed strong enhancement of interband electric quadrupole transitions (Clark *et al.* 1961). It is hoped to measure the spin directly in the near future by alpha–gamma correlations (Gove *et al.* 1961*a*) and to determine the lifetime of the new state by the Doppler shift attenuation method (Devons *et al.* 1954; Litherland *et al.* 1961).

ALMQVIST, E. and KUEHNER, J. A. 1961. Can. J. Phys. **39**. This issue.
CLARK, M. A., GOVE, H. E., and LITHERLAND, A. E. 1961. Can. J. Phys. **39**. This issue.
DEVONS, S., MANNING, G., and BUNBURY, D. ST. P. 1955. Proc. Phys. Soc. A, **68**, 18.

GOVE, H. E., LITHERLAND, A. E., and CLARK, M. A. 1961. To be published.
——— 1961*a*. Can. J. Phys. **39**. This issue.
KUEHNER, J. A. 1961. To be published.
KUEHNER, J. A. and ALMQVIST, E. 1961. To be published.
LITHERLAND, A. E., ADAMS, B., ECCLESHALL, D., and YATES, M. 1961. Bull. Am. Phys. Soc. Ser. II, **6**, 248.
MCDERMOTT, L. C., JONES, K. W., SMOTRICH, H., and BENENSON, R. E. 1960. Phys. Rev. **118**, 175.

RECEIVED JUNE 20, 1961.
ATOMIC ENERGY OF CANADA LIMITED,
CHALK RIVER, ONTARIO.

A. E. LITHERLAND
M. A. CLARK
H. E. GOVE

ANNOUNCEMENTS

Frequency Measurement of Standard Frequency Transmissions[1,2]

Measurements are made at Ottawa, Canada, using N.R.C. caesium-beam frequency resonator as reference standard (with an assumed frequency of 9 192 631 770 c.p.s.). Frequency deviations from nominal are quoted in parts per 10^{10}. A negative sign indicates that the frequency is below nominal.

Date, May 1961	MSF, 60 kc/s	GBR, 16 kc/s		WWVB, 60 kc/s
		8-hour average*	24-hour average†	
1	−151	−151	−140	−148
2	−169	−156	−150	−146
3	−159	−154	−153	−149
4	−153	−155	−150	−151
5	−149	−145	−148	−139
6	−141	−137	−138	−139
7	−139	−135	−137	−144
8	−152	−147	−136	−142
9	−145	−146	−134	−149
10	−152	−149	−147	−151
11	−149	−150	−147	−154
12	−159	−156	−149	−146
13	−155	−155	−152	−156
14	N.M.	N.M.	N.M.	N.M.
15	N.M.	N.M.	N.M.	N.M.
16	N.M.	N.M.	N.M.	N.M.
17	N.M.	N.M.	N.M.	N.M.
18	N.M.	N.M.	N.M.	−147
19	−151	−154	N.M.	−152
20	−149	−152	−154	−149
21	N.M.	−151	−150	N.M.
22	N.M.	−155	−155	N.M.
23	−151	−153	−154	−154
24	−153	−150	−154	−149
25	−153	−152	−150	−149
26	−155	−153	−150	−150
27	N.M.	−153	−152	N.M.
28	N.M.	−154	−152	−151
29	N.M.	N.M.	N.M.	−153
30	−157	−154	−154	−151
31	N.M.	−155	−153	−148
Average	−152	−151	−148	−149
Midmonthly mean of WWV	−148			

NOTE: N.M., no measurement.
*Time of observations: 10:30 to 18:30 U.T.
†Time of observations: 15 to 15 hours U.T.

These measurements will no longer appear regularly in the Canadian Journal of Physics. However, individuals or organizations interested may obtain this information on a monthly basis by requesting it from the Director, Applied Physics Division, National Research Council, Ottawa, Canada.

RECEIVED JUNE 9, 1961.
DIVISION OF APPLIED PHYSICS,
NATIONAL RESEARCH COUNCIL,
OTTAWA, CANADA.

S. N. KALRA

[1]Issued as N.R.C. No. 6395.
[2]Cf. Kalra, S. N. 1959. Can. J. Phys. **37**, 1328.

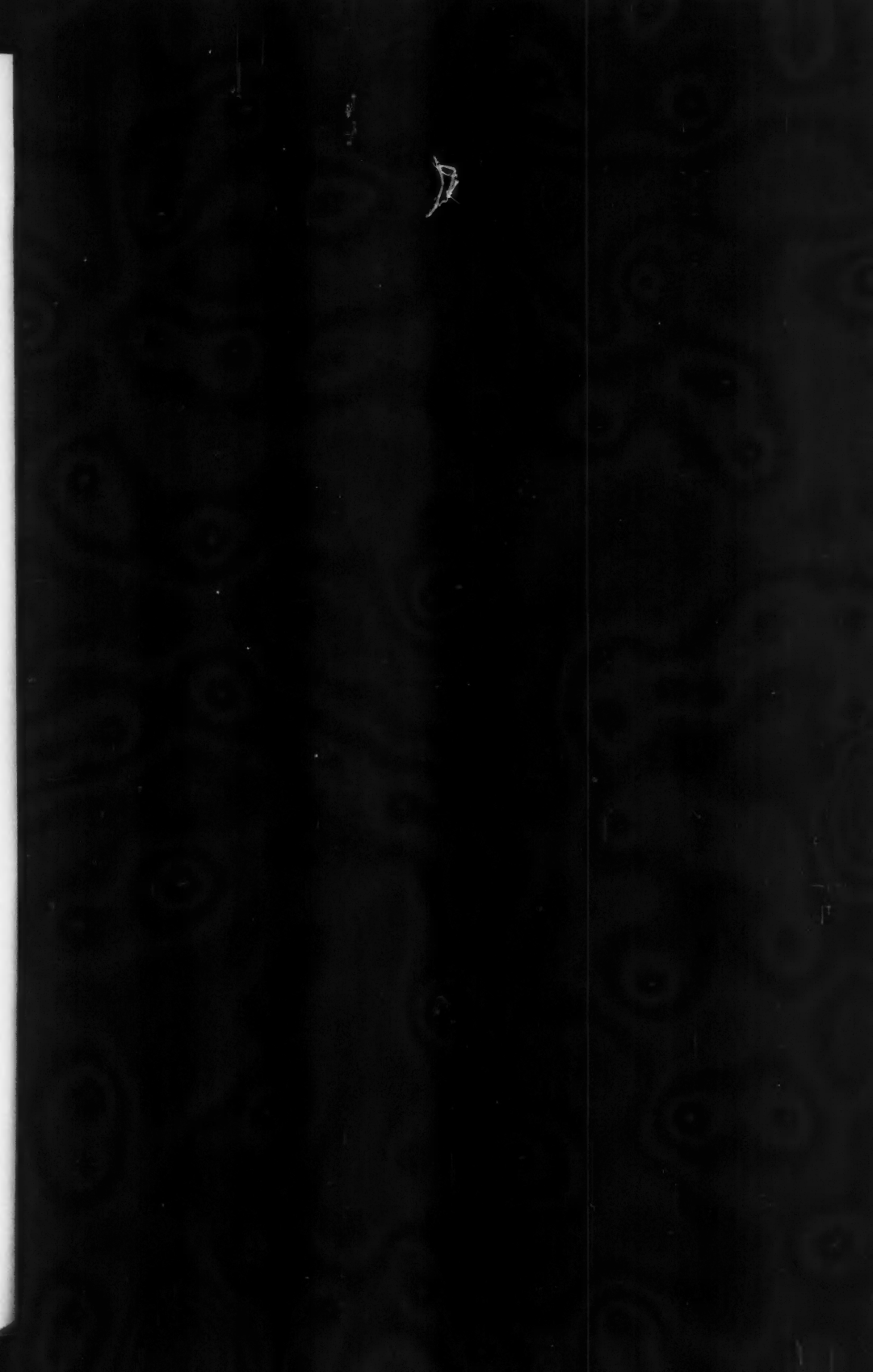

NOTES TO CONTRIBUTORS

Canadian Journal of Physics

MANUSCRIPTS

General.—Manuscripts, in English or French, should be typewritten, double spaced, on paper 8½×11 in. **The original and one copy are to be submitted.** Tables and captions for the figures should be placed at the end of the manuscript. Every sheet of the manuscript should be numbered. Style, arrangement, spelling, and abbreviations should conform to the usage of recent numbers of this journal. Greek letters or unusual signs should be written plainly or explained by marginal notes. Characters to be set in boldface type should be indicated by a wavy line below each character. Superscripts and subscripts must be legible and carefully placed. Manuscripts and illustrations should be carefully checked before they are submitted. Authors will be charged for unnecessary deviations from the usual format and for changes made in the proof that are considered excessive or unnecessary.

Abstract.—An abstract of not more than about 200 words, indicating the scope of the work and the principal findings, is required, except in Notes.

References.—References should be listed **alphabetically by authors' names,** unnumbered, and typed after the text. The form of the citations should be that used in current issues of this journal; in references to papers in periodicals, titles should not be given and only initial page numbers are required. The names of periodicals should be abbreviated in the form given in the most recent *List of Periodicals Abstracted by Chemical Abstracts.* All citations should be checked with the original articles and each one referred to in the text by the authors' names and the year.

Tables.—Tables should be numbered in roman numerals and each table referred to in the text. Titles should always be given but should be brief; column headings should be brief and descriptive matter in the tables confined to a minimum. Vertical rules should not be used. Numerous small tables should be avoided.

ILLUSTRATIONS

General.—All figures (including each figure of the plates) should be numbered consecutively from 1 up, in arabic numerals, and each figure referred to in the text. The author's name, title of the paper, and figure number should be written in the lower left corner of the sheets on which the illustrations appear. Captions should not be written on the illustrations.

Line drawings.—Drawings should be carefully made with India ink on white drawing paper, blue tracing linen, or co-ordinate paper ruled in blue only; any co-ordinate lines that are to appear in the reproduction should be ruled in black ink. Paper ruled in green, yellow, or red should not be used. All lines must be of sufficient thickness to reproduce well. Decimal points, periods, and stippled dots must be solid black circles large enough to be reduced if necessary. Letters and numerals should be neatly made, preferably with a stencil (**do NOT use typewriting**) and be of such size that the smallest lettering will be not less than 1 mm high when the figure is reduced to a suitable size. Many drawings are made too large; originals should not be more than 2 or 3 times the size of the desired reproduction. Whenever possible two or more drawings should be grouped to reduce the number of cuts required. In such groups of drawings, or in large drawings, full use of the space available should be made; the ratio of height to width should conform to that of a journal page (4¾×7½ in.), but allowance must be made for the captions. **The original drawings and one set of clear copies (e.g. small photographs) are to be submitted.**

Photographs.—Prints should be made on glossy paper, with strong contrasts. They should be trimmed so that essential features only are shown and mounted carefully, with rubber cement, on white cardboard, with no space between those arranged in groups. In mounting, full use of the space available should be made. **Photographs are to be submitted in duplicate;** if they are to be reproduced in groups one set should be mounted, the duplicate set unmounted.

REPRINTS

A total of 100 reprints of each paper, without covers, are supplied free. Additional reprints, with or without covers, may be purchased at the time of publication.

Charges for reprints are based on the number of printed pages, which may be calculated approximately by multiplying by 0.6 the number of manuscript pages (double-spaced typewritten sheets, 8½×11 in.) and including the space occupied by illustrations. Prices and instructions for ordering reprints are sent out with the galley proof.

Contents

Notes:

Letters to the Editor:

Announcements:

Printed in Canada *by* University of Toronto Press